



FLUXNET-CH₄: a global, multi-ecosystem dataset and analysis of methane seasonality from freshwater wetlands

Kyle B. Delwiche¹, Sara Helen Knox², Avni Malhotra¹, Etienne Fluet-Chouinard¹, Gavin McNicol¹, Sarah Feron^{1,3}, Zutao Ouyang¹, Dario Papale^{4,5}, Carlo Trotta⁵, Eleonora Canfora⁵, You-Wei Cheah⁶, Danielle Christianson⁶, Ma. Carmelita R. Alberto⁷, Pavel Alekseychik⁸, Mika Aurela⁹, Dennis Baldocchi¹⁰, Sheel Bansal¹¹, David P. Billesbach¹², Gil Bohrer¹³, Rosvel Bracho¹⁴, Nina Buchmann¹⁵, David I. Campbell¹⁶, Gerardo Celis¹⁷, Jiquan Chen¹⁸, Weinan Chen¹⁹, Housen Chu²⁰, Higo J. Dalmagro²¹, Sigrid Dengel⁶, Ankur R. Desai²², Matteo Detto²³, Han Dolman²⁴, Elke Eichelmann²⁵, Eugenie Euskirchen²⁶, Daniela Famulari²⁷, Kathrin Fuchs²⁸, Mathias Goeckede²⁹, Sébastien Gogo³⁰, Mangaliso J. Gondwe³¹, Jordan P. Goodrich¹⁶, Pia Gottschalk³², Scott L. Graham³³, Martin Heimann²⁹, Manuel Helbig^{34,35}, Carole Helfter³⁶, Kyle S. Hemes^{1,37}, Takashi Hirano³⁸, David Hollinger³⁹, Lukas Hörtnagl¹⁵, Hiroki Iwata⁴⁰, Adrien Jacotot³⁰, Gerald Jurasinski⁴¹, Minseok Kang⁴², Kuno Kasak⁴³, John King⁴⁴, Janina Klatt⁴⁵, Franziska Koebsch⁴¹, Ken W. Krauss⁴⁶, Derrick Y. F. Lai⁴⁷, Annalea Lohila^{9,48}, Ivan Mammarella⁴⁸, Luca Beilelli Marchesini⁵⁰, Giovanni Manca⁴⁹, Jaclyn Hatala Matthes⁵¹, Trofim Maximov⁵², Lutz Merbold⁵³, Bhaskar Mitra⁵⁴, Timothy H. Morin⁵⁵, Eiko Nemitz³⁶, Mats B. Nilsson⁵⁶, Shuli Niu¹⁹, Walter C. Oechel⁵⁷, Patricia Y. Oikawa⁵⁸, Keisuke Ono⁵⁹, Matthias Pechl⁵⁶, Olli Peltola⁹, Michele L. Reba⁶⁰, Andrew D. Richardson^{61,62}, William Riley⁶, Benjamin R. K. Runkle⁶³, Youngryel Ryu⁶⁴, Torsten Sachs³², Ayaka Sakabe⁶⁵, Camilo Rey Sanchez¹⁰, Edward A. Schuur⁶⁶, Karina V. R. Schäfer⁶⁷, Oliver Sonntag⁶⁸, Jed P. Sparks⁶⁹, Ellen Stuart-Haëntjens⁷⁰, Cove Sturtevant⁷¹, Ryan C. Sullivan⁷², Daphne J. Szutu¹⁰, Jonathan E. Thom⁷³, Margaret S. Torn⁶, Eeva-Stiina Tuittila⁷⁴, Jessica Turner⁷⁵, Masahito Ueyama⁷⁶, Alex C. Valach¹⁰, Rodrigo Vargas⁷⁷, Andrej Varlagin⁷⁸, Alma Vazquez-Lule⁷⁷, Joseph G. Verfaillie¹⁰, Timo Vesala^{48,79}, George L. Vourlitis⁸⁰, Eric J. Ward⁴⁶, Christian Wille³², Georg Wohlfahrt⁸¹, Guan Xhuan Wong⁸², Zhen Zhang⁸³, Donatella Zona^{57,84}, Lisamarie Windham-Myers⁸⁵, Benjamin Poulter⁸⁶, and Robert B. Jackson^{1,37,87}

¹Department of Earth System Science, Stanford University, Stanford, California, USA

²Department of Geography, The University of British Columbia, Vancouver, British Columbia, Canada

³Department of Physics, University of Santiago de Chile, Santiago, Chile

⁴Dipartimento per la Innovazione nei Sistemi Biologici, Agroalimentari e Forestali, Università degli Studi della Tuscia, Largo dell'Università, Viterbo, Italy

⁵Euro-Mediterranean Center on Climate Change CMCC, Lecce, Italy

⁶Earth and Environmental Sciences Area, Lawrence Berkeley National Lab, Berkeley, California, USA

⁷International Rice Research Institute, Los Baños, Laguna, Philippines

⁸Natural Resources Institute Finland (LUKE), Helsinki, Finland

⁹Finnish Meteorological Institute, P.O. Box 501, 00101 Helsinki, Finland

¹⁰Department of Environmental Science, Policy and Management, University of California, Berkeley, CA, USA

¹¹Northern Prairie Wildlife Research Center, US Geological Survey, 8711 37th St Southeast, Jamestown, ND 58401, USA

¹²Department of Biological Systems Engineering, University of Nebraska-Lincoln, Lincoln, NE 68583, USA

¹³Department of Civil, Environmental and Geodetic Engineering, Ohio State University, Columbus, OH, USA

¹⁴School of Forest Resources and Conservation, University of Florida, Gainesville, FL 32611, USA

¹⁵Department of Environmental Systems Science, Institute of Agricultural Sciences, ETH Zurich, 8092 Zurich, Switzerland

- ¹⁶School of Science, University of Waikato, Hamilton, New Zealand
- ¹⁷Agronomy Department, University of Florida, Gainesville, FL 32601, USA
- ¹⁸Department of Geography, Environment, and Spatial Sciences, Michigan State University, East Lansing, MI 48823, USA
- ¹⁹Institute of Geographic Sciences and Natural Resources Research, Chinese Academy of Sciences, Beijing 100101, PR China
- ²⁰Climate and Ecosystem Sciences Division, Lawrence Berkeley National Lab, Berkeley, CA 94702, USA
- ²¹Environmental Sciences Graduate Program, University of Cuiabá, Cuiabá, Mato Grosso, Brazil
- ²²Department of Atmospheric and Oceanic Sciences, University of Wisconsin-Madison, Madison, WI 53706, USA
- ²³Department of Ecology and Evolutionary Biology, Princeton University, Princeton, NJ, USA
- ²⁴Department of Earth Sciences, Vrije Universiteit, Amsterdam, the Netherlands
- ²⁵School of Biology and Environmental Science, University College Dublin, Dublin, Ireland
- ²⁶Institute of Arctic Biology, University of Alaska Fairbanks, Fairbanks, AK, USA
- ²⁷CNR – Institute for Agricultural and Forestry Systems in the Mediterranean, Piazzale Enrico Fermi, 1 Portici, Napoli, Italy
- ²⁸Institute of Meteorology and Climate Research – Atmospheric Environmental Research, Karlsruhe Institute of Technology (KIT Campus Alpin), 82467 Garmisch-Partenkirchen, Germany
- ²⁹Max Planck Institute for Biogeochemistry, Jena, Germany
- ³⁰ISTO, Université d'Orléans, CNRS, BRGM, UMR 7327, 45071, Orléans, France
- ³¹Okavango Research Institute, University of Botswana, Maun, Botswana
- ³²GFZ German Research Centre for Geosciences, Telegrafenberg, 14473 Potsdam, Germany
- ³³Manaaki Whenua – Landcare Research, Lincoln, New Zealand
- ³⁴Département de géographie, Université de Montréal, Montréal, QC H2V 0B3, Canada
- ³⁵Department of Physics and Atmospheric Science, Dalhousie University, Halifax, NS B2Y 1P3, Canada
- ³⁶UK Centre for Ecology and Hydrology, Edinburgh, UK
- ³⁷Woods Institute for the Environment, Stanford University, Stanford, California
- ³⁸Research Faculty of Agriculture, Hokkaido University, Sapporo, Japan
- ³⁹Northern Research Station, USDA Forest Service, Durham, NH 03824, USA
- ⁴⁰Department of Environmental Science, Faculty of Science, Shinshu University, Matsumoto, Japan
- ⁴¹Landscape Ecology, University of Rostock, Rostock, Germany
- ⁴²National Center for AgroMeteorology, Seoul, South Korea
- ⁴³Department of Geography, University of Tartu, Vanemuise st 46, Tartu, 51410, Estonia
- ⁴⁴Department of Forestry and Environmental Resources, North Carolina State University, Raleigh, NC, USA
- ⁴⁵Chair of Vegetation Ecology, Institute of Ecology and Landscape, University of Applied Sciences Weihenstephan-Triesdorf, Am Hofgarten 1, 85354 Freising, Germany
- ⁴⁶Wetland and Aquatic Research Center, US Geological Survey, Lafayette, LA, USA
- ⁴⁷Department of Geography and Resource Management, The Chinese University of Hong Kong, Shatin, New Territories, Hong Kong SAR, China
- ⁴⁸Institute for Atmospheric and Earth System Research/Physics, Faculty of Science, University of Helsinki, Helsinki, Finland
- ⁴⁹Joint Research Centre (JRC), European Commission, Ispra, Italy
- ⁵⁰Department of Sustainable Agro-Ecosystems and Bioresources, Research and Innovation Centre, Fondazione Edmund Mach, San Michele all'Adige, Italy
- ⁵¹Department of Biological Sciences, Wellesley College, Wellesley, MA 02481, USA
- ⁵²Institute for Biological Problems of the Cryolithozone, RAS, Yakutsk, Russia
- ⁵³International Livestock Research Institute (ILRI), Mazingira Centre, Old Naivasha Road, P.O. Box 30709, 00100 Nairobi, Kenya
- ⁵⁴School of Informatics, Computing and Cyber Systems, Northern Arizona University, Flagstaff, AZ, USA
- ⁵⁵Environmental Resources Engineering, SUNY College of Environmental Science and Forestry, Syracuse, NY, USA
- ⁵⁶Department of Forest Ecology and Management, Swedish University of Agricultural Sciences, 901 83 Umeå, Sweden

- ⁵⁷Department of Biology, San Diego State University, San Diego, CA 92182, USA
- ⁵⁸Department of Earth and Environmental Sciences, Cal State East Bay, Hayward, CA 94542, USA
- ⁵⁹National Agriculture and Food Research Organization, Tsukuba, Japan
- ⁶⁰USDA-ARS Delta Water Management Research Unit, Jonesboro, Arkansas 72401, USA
- ⁶¹School of Informatics, Computing and Cyber Systems, Northern Arizona University, Flagstaff, AZ 86011, USA
- ⁶²Center for Ecosystem Science and Society, Northern Arizona University, Flagstaff, AZ 86011, USA
- ⁶³Department of Biological and Agricultural Engineering, University of Arkansas, Fayetteville, AR 72701, USA
- ⁶⁴Department of Landscape Architecture and Rural Systems Engineering, Seoul National University, Seoul, South Korea
- ⁶⁵Hakubi Center, Kyoto University, Kyoto, Japan
- ⁶⁶Department of Biological Sciences, Northern Arizona University, Flagstaff, AZ, USA
- ⁶⁷Department of Earth and Environmental Science, Rutgers University Newark, NJ, USA
- ⁶⁸Département de géographie, Université de Montréal, Montréal, QC H2V 0B3, Canada
- ⁶⁹Department of Ecology and Evolution, Cornell, Ithaca, NY, USA
- ⁷⁰California Water Science Center, US Geological Survey, 6000 J Street, Placer Hall, Sacramento, CA 95819, USA
- ⁷¹National Ecological Observatory Network, Battelle, 1685 38th St Ste 100, Boulder, Colorado 80301, USA
- ⁷²Environmental Science Division, Argonne National Laboratory, Lemont, IL, USA
- ⁷³Space Sciences and Engineering Center, University of Wisconsin-Madison, Madison, WI 53706, USA
- ⁷⁴School of Forest Sciences, University of Eastern Finland, Joesnuu, Finland
- ⁷⁵Freshwater and Marine Science, University of Wisconsin-Madison, Madison, WI 53706, USA
- ⁷⁶Graduate School of Life and Environmental Sciences, Osaka Prefecture University, Osaka, Japan
- ⁷⁷Department of Plant and Soil Sciences, University of Delaware, Newark, DE, USA
- ⁷⁸A.N. Severtsov Institute of Ecology and Evolution, Russian Academy of Sciences, Moscow, Russia
- ⁷⁹Yugra State University, 628012, Khanty-Mansiysk, Russia
- ⁸⁰Biological Sciences Department, California State University San Marcos, San Marcos, CA, USA
- ⁸¹Department of Ecology, University of Innsbruck, Sternwartestr. 15, 6020 Innsbruck, Austria
- ⁸²Sarawak Tropical Peat Research Institute, Sarawak, Malaysia
- ⁸³Department of Geographical Sciences, University of Maryland, College Park, MD 20740, USA
- ⁸⁴Department of Animal and Plant Sciences, University of Sheffield, Western Bank, Sheffield, S10 2TN, United Kingdom
- ⁸⁵Water Mission Area, US Geological Survey, 345 Middlefield Road, Menlo Park, CA 94025, USA
- ⁸⁶Biospheric Sciences Laboratory, NASA Goddard Space Flight Center, Greenbelt, Maryland, USA
- ⁸⁷Precourt Institute for Energy, Stanford University, Stanford, California, USA

Correspondence: Kyle B. Delwiche (delwiche@stanford.edu)

Received: 15 October 2020 – Discussion started: 18 January 2021

Revised: 27 April 2021 – Accepted: 28 April 2021 – Published: 29 July 2021

Abstract. Methane (CH₄) emissions from natural landscapes constitute roughly half of global CH₄ contributions to the atmosphere, yet large uncertainties remain in the absolute magnitude and the seasonality of emission quantities and drivers. Eddy covariance (EC) measurements of CH₄ flux are ideal for constraining ecosystem-scale CH₄ emissions due to quasi-continuous and high-temporal-resolution CH₄ flux measurements, coincident carbon dioxide, water, and energy flux measurements, lack of ecosystem disturbance, and increased availability of datasets over the last decade. Here, we (1) describe the newly published dataset, FLUXNET-CH₄ Version 1.0, the first open-source global dataset of CH₄ EC measurements (available at <https://fluxnet.org/data/fluxnet-ch4-community-product/>, last access: 7 April 2021). FLUXNET-CH₄ includes half-hourly and daily gap-filled and non-gap-filled aggregated CH₄ fluxes and meteorological data from 79 sites globally: 42 freshwater wetlands, 6 brackish and saline wetlands, 7 formerly drained ecosystems, 7 rice paddy sites, 2 lakes, and 15 uplands. Then, we (2) evaluate FLUXNET-CH₄ representativeness for freshwater wetland coverage globally because the majority of sites in FLUXNET-CH₄ Version 1.0 are freshwater wetlands which are a substantial source of total atmospheric CH₄ emissions; and (3) we provide the first global estimates of the seasonal variability and seasonality predictors of freshwater wetland CH₄ fluxes. Our representativeness analysis

suggests that the freshwater wetland sites in the dataset cover global wetland bioclimatic attributes (encompassing energy, moisture, and vegetation-related parameters) in arctic, boreal, and temperate regions but only sparsely cover humid tropical regions. Seasonality metrics of wetland CH₄ emissions vary considerably across latitudinal bands. In freshwater wetlands (except those between 20° S to 20° N) the spring onset of elevated CH₄ emissions starts 3 d earlier, and the CH₄ emission season lasts 4 d longer, for each degree Celsius increase in mean annual air temperature. On average, the spring onset of increasing CH₄ emissions lags behind soil warming by 1 month, with very few sites experiencing increased CH₄ emissions prior to the onset of soil warming. In contrast, roughly half of these sites experience the spring onset of rising CH₄ emissions prior to the spring increase in gross primary productivity (GPP). The timing of peak summer CH₄ emissions does not correlate with the timing for either peak summer temperature or peak GPP. Our results provide seasonality parameters for CH₄ modeling and highlight seasonality metrics that cannot be predicted by temperature or GPP (i.e., seasonality of CH₄ peak). FLUXNET-CH₄ is a powerful new resource for diagnosing and understanding the role of terrestrial ecosystems and climate drivers in the global CH₄ cycle, and future additions of sites in tropical ecosystems and site years of data collection will provide added value to this database. All seasonality parameters are available at <https://doi.org/10.5281/zenodo.4672601> (Delwiche et al., 2021). Additionally, raw FLUXNET-CH₄ data used to extract seasonality parameters can be downloaded from <https://fluxnet.org/data/fluxnet-ch4-community-product/> (last access: 7 April 2021), and a complete list of the 79 individual site data DOIs is provided in Table 2 of this paper.

1 Introduction

Methane (CH₄) has a global warming potential that is 28 times larger than carbon dioxide (CO₂) on a 100-year timescale (Myhre et al., 2013), and its atmospheric concentration has increased by > 1000 ppb since 1800 (Etheridge et al., 1998). While atmospheric CH₄ concentrations are substantially lower than those of CO₂, CH₄ has contributed 20 %–25 % as much radiative forcing as CO₂ since 1750 (Etminan et al., 2016). Despite its importance to global climate change, natural CH₄ sources and sinks remain poorly constrained and with uncertain attribution to the various biogenic and anthropogenic sources (Saunio et al., 2016, 2020). Bottom-up and top-down estimates differ by 154 Tg yr⁻¹ (745 versus 591 Tg yr⁻¹, respectively); much of this difference arises from natural sources (Saunio et al., 2020). Vegetated wetlands and inland water bodies account for most natural CH₄ emissions, as well as the majority of uncertainty in bottom-up emission estimates (Saunio et al., 2016). Better diagnosis and prediction of terrestrial CH₄ sources to the atmosphere requires high frequency and continuous measurements of CH₄ exchange across a continuum of time (hours to years) and space (meters to kilometers) scales.

Tower-based eddy covariance (EC) measurements providing ecosystem-scale CH₄ fluxes at high temporal resolution across years are coupled with measurements of key CH₄ drivers such as temperature, water, and recent substrate input (inferred from CO₂ flux) and thus help constrain bottom-up CH₄ budgets and improve CH₄ predictions. Although EC towers began measuring CO₂ fluxes in the late 1970s (Desjardins, 1974; Anderson et al., 1984), and some towers began measuring CH₄ in the 1990s (Verma et al., 1992), most CH₄ flux EC measurements began within the last decade (2010s).

Given that many EC CH₄ sites are relatively new, the flux community has only recently compiled them for global synthesis efforts (e.g., Chang et al., 2021) and is still working to standardize CH₄ flux measurements and establish gap-filling protocols (Nemitz et al., 2018; Knox et al., 2019). Furthermore, the growth of EC networks for CH₄ fluxes has sometimes taken place in a relatively ad hoc fashion, often at sites that were already measuring CO₂ fluxes or where higher CH₄ fluxes were expected, potentially introducing bias. The representativeness and spatial distribution of CO₂ flux tower networks have been assessed to evaluate their ability to up-scale fluxes regionally (Hargrove et al., 2003; Hoffman et al., 2013; Papale et al., 2015; Villarreal et al., 2018, 2019) and globally (Jung et al., 2009, 2020). However, a relatively sparse coverage of CH₄ flux towers prompts the question of how well the current observation network provides a sufficient sampling of global or ecosystem-specific bioclimatic conditions.

Broad-scale wetland CH₄ seasonality estimates, such as when fluxes increase, peak, and decrease and the predictors of seasonality, remain relatively unconstrained across wetlands globally. These key seasonality metrics vary considerably across high-emitting systems such as wetlands and other aquatic systems (Desjardins, 1974; Dise, 1992; Melloh and Crill, 1996; Wik et al., 2013; Zona et al., 2016; Treat et al., 2018). The few continuous CH₄ flux datasets across representative site years make it difficult to establish trends in seasonal dynamics, though monthly or annually aggregated estimates of CH₄ fluxes from different seasons do exist for high latitudes (Zona et al., 2016; Treat et al., 2018). Seasonal variability in freshwater wetland CH₄ fluxes is expected to be driven by changes in air (TA) and soil temperature (ST), soil moisture (including water table dynamics), and recent carbon

substrate availability, which influence the rates of CH₄ production and consumption (Lai, 2009; Bridgham et al., 2013; Dean et al., 2018). Temperature has widely been found to strongly affect CH₄ flux (Chu et al., 2014; Yvon-Durocher et al., 2014; Sturtevant et al., 2016), but the relationship is complex (Chang et al., 2020) and varies seasonally (Koebsch et al., 2015; Helbig et al., 2017). CH₄ flux is also driven by inundation depth since anoxic conditions are typically necessary for methanogenesis (Lai, 2009; Bridgham et al., 2013), though CH₄ production under bulk-oxic conditions has been observed (Angle et al., 2017). Substrate availability influences CH₄ production potential and is linked with gross primary productivity (GPP) because recent photosynthate fuels methanogenesis, though this relationship can vary by ecosystem type, plant functional type, and biome (Meronigal et al., 1999; Chanton et al., 2008; Hatala et al., 2012; Lai et al., 2014; Malhotra and Roulet, 2015; Sturtevant et al., 2016). In process models, the seasonality of CH₄ emissions from wetlands globally is primarily constrained by inundation (Poulter et al., 2017) with secondary within-wetland influences from temperature and availability of carbon (C) substrates (Melton et al., 2013; Castro-Morales et al., 2018). Bottom-up and top-down global CH₄ estimates continue to disagree on total CH₄ flux magnitudes and seasonality, including the timing of annual peak emissions (Spahni et al., 2011; Saunois et al., 2020). Thus, the variability in and predictors of wetland CH₄ seasonality globally remain a knowledge gap that high-frequency and long-term EC data can help fill.

Here, we first describe version 1.0 of the FLUXNET-CH₄ dataset (available at <https://fluxnet.org/data/fluxnet-ch4-community-product/>, last access: 7 April 2021). Version 1.0 of the dataset expands and formalizes the publication of data scattered among regional flux networks as described previously in Knox et al. (2019). FLUXNET-CH₄ includes half-hourly and daily gap-filled and non-gap-filled aggregated CH₄ fluxes and meteorological data from 79 sites globally: 42 freshwater wetlands, 6 brackish and saline wetlands, 7 formerly drained ecosystems, 7 rice paddy sites, 2 lakes, and 15 upland ecosystems. FLUXNET-CH₄ includes an additional two wetland sites (RU-Vrk and SE-St1), but they are not available under the CC BY 4.0 data policy and thus are excluded from this analysis. Since the majority of sites in FLUXNET-CH₄ Version 1.0 (hereafter referred to solely as “FLUXNET-CH₄”) are freshwater wetlands, which are a substantial source of total atmospheric CH₄ emissions, we use the subset of data from freshwater wetlands to evaluate the representativeness of freshwater wetland coverage in the FLUXNET-CH₄ dataset relative to wetlands globally, and we provide the first assessment of global variability in and predictors of freshwater wetland CH₄ flux seasonality. We quantify a suite of CH₄ seasonality metrics and evaluate temperature and GPP (a proxy for recent substrate input) as predictors of seasonality across four latitudinal bands (northern, temperate, subtropical, and tropical). Due to a lack of high-temporal-resolution water table data at all sites,

our analyses are unable to evaluate the critical role of water table on CH₄ seasonality. Here we provide parameters for better understanding and modeling seasonal variability in freshwater wetland CH₄ fluxes and generate new hypotheses and data resources for future syntheses.

2 Methods

2.1 FLUXNET-CH₄ dataset

2.1.1 History and data description

The FLUXNET-CH₄ dataset was initiated by the Global Carbon Project (GCP) in 2017 to better constrain the global CH₄ budget (<https://www.globalcarbonproject.org/methanebudget/index.htm>, last access: 6 July 2021). Beginning with a kick-off meeting in May 2018 in Washington DC, hosted by Stanford University, we coordinated with the AmeriFlux Management Project, the European Ecosystem Fluxes Database, and the Integrated Carbon Observation System Ecosystem Thematic Centre (ICOS-ETC) to avoid duplication of efforts as most sites are part of different regional networks (albeit with different data products). We collected and standardized data for FLUXNET-CH₄ with assistance from the regional flux networks, AmeriFlux’s “Year of Methane”, FLUXNET, the EU’s Readiness of ICOS for Necessities of Integrated Global Observations (RINGO) project, and a US Geological Survey Powell Center working group. FLUXNET-CH₄ is a community-led project, so while we developed it with assistance from FLUXNET, we do not necessarily use standard FLUXNET data variables, formats, or methods.

FLUXNET-CH₄ includes gap-filled half-hourly CH₄ fluxes and meteorological variables. Gaps in meteorological variables (TA – air temperature; SW_IN – incoming shortwave radiation; LW_IN – incoming longwave radiation; VPD – vapor pressure deficient; PA – pressure; *P* – precipitation; WS – wind speed) were filled with the ERA-Interim (ERA-I) reanalysis product (Vuichard and Papale, 2015). We used the REdDyProc package (Wutzler et al., 2018) to filter flux values with low friction velocity (u_*) based on relating nighttime u_* to fill gaps in CO₂, latent heat, and sensible heat fluxes and to partition net CO₂ fluxes into gross primary production (GPP) and ecosystem respiration (RECO) using both the daytime (Lasslop et al., 2010) and nighttime (Reichstein et al., 2005) approaches. Data gaps of CH₄ flux were filled using artificial neural network (ANN) methods first described in Knox et al. (2015, 2019) and summarized here in Sect. 2.1.2. Gap-filled data for gaps exceeding 2 months are provided and flagged for quality. Please see Table B1 for variable description and units, as well as quality flag information. For the seasonality analysis in this paper we excluded data from gaps exceeding 2 months, and we encourage future users of FLUXNET-CH₄ to critically evaluate gap-filled

values from long data gaps before including them in analyses (Dengel et al., 2013; Kim et al., 2020).

In addition to half-hourly data, the FLUXNET-CH₄ Version 1.0 release also contains a full set of daily mean values for all parameters except wind direction and precipitation. Daily precipitation is included as the daily sum of the half-hourly data, and daily average wind direction is not included.

2.1.2 Gap-filling methods and uncertainty estimates

As described in Knox et al. (2015, 2019), the ANN routine used to gap-fill the CH₄ data was optimized for generalizability and representativeness. To avoid biasing the ANN toward environmental conditions with typically better data coverage (e.g., summertime and daytime measurements), the explanatory data were divided into a maximum of 15 clusters using a *k*-means clustering algorithm. Data used to train, test, and validate the ANN were proportionally sampled from these clusters. For generalizability, the simplest ANN architecture with good performance (< 5 % gain in model accuracy for additional increases in architecture complexity) was selected for 20 extractions of the training, test, and validation data. Within each extraction, each tested ANN architecture was reinitialized 10 times, and the initialization with the lowest root-mean-square error was selected to avoid local minima. The median of the 20 predictions was used to fill each gap. A standard set of variables available across all sites was used to gap-fill CH₄ fluxes (Dengel et al., 2013), which included the previously mentioned meteorological variables TA, SW_IN, WS, and PA and sine and cosine functions to represent seasonality. These meteorological variables were selected for their relevance to CH₄ exchange and were gap-filled using the ERA-I reanalysis data. Other variables related to CH₄ flux (e.g., water table depth, WTD, and soil temperature, TS) were not included as explanatory variables as they were not available across all sites or had large gaps that could not be filled using the ERA-I reanalysis data (Knox et al., 2019). The ANN gap-filling was performed using MATLAB (Mathworks 2018a, version 9.4.0).

While the median of the 20 predictions was used to fill each gap, the spread of the predictions was used to provide a measure of uncertainty resulting from the ANN gap-filling procedure. Specifically, the combined annual gap-filling and random uncertainty was calculated from the variance of the cumulative sums of the 20 ANN predictions (Knox et al., 2015; Anderson et al., 2016; Oikawa et al., 2017). The (non-cumulative) variance of the 20 ANN predictions was also used to provide gap-filling uncertainty for each half-hourly gap-filled value. While this output is useful for data–model comparisons, it cannot be used to estimate cumulative annual gap-filling error because gap-filling error is not random, which is why the cumulative sums of the 20 ANN predictions are used to estimate annual gap-filling error.

Random errors in EC fluxes follow a double exponential (Laplace) distribution with the standard deviation vary-

ing with flux magnitude (Richardson et al., 2006, 2012). For half-hourly CH₄ flux measurements, random error was estimated using the residuals of the median ANN predictions, providing a conservative “upper limit” estimate of the random flux uncertainty (Moffat et al., 2007; Richardson et al., 2008). The annual cumulative uncertainty at 95 % confidence was estimated by adding the cumulative gap-filling and random measurement uncertainties in quadrature (Richardson and Hollinger, 2007; Anderson et al., 2016). Annual uncertainties in CH₄ flux for individual site years are provided in Table B2. Throughout this paper, we include uncertainties on individual site years when discussing single years of data. In sites with multiple years of data, we report the standard deviation of the multiple years.

2.1.3 Dataset structure and site metadata

FLUXNET-CH₄ contains two comma-separated data files per site at half-hourly and daily resolutions which are available for download at <https://fluxnet.org/data/fluxnet-ch4-community-product/> (last access: 7 April 2021), along with a file containing select site metadata. Each site has a unique FLUXNET-CH₄ DOI. All data from the 79 sites used in this analysis are available under CC BY 4.0 (<https://creativecommons.org/licenses/by/4.0/>, last access: 6 July 2021) copyright license (FLUXNET-CH₄ has an additional two sites available under the FLUXNET Tier 2 license (<https://fluxnet.org/data/data-policy/>, last access: 6 July 2021), though these sites are not included in our analysis).

Metadata (Table B3) include site coordinates, ecosystem classification based on site literature, presence/absence and dominance for specific vegetation types, and DOI link, as well as calculated data such as annual and quarterly CH₄ flux values. FLUXNET-CH₄ Version 1.0 sites were classified based on site-specific literature as fen, bog, swamp, marsh, salt marsh, lake, mangrove, rice paddy field, wet tundra, upland, or drained ecosystems that previously could have been wetlands, seasonally flooded pastures, or agricultural areas. To the extent possible, we followed classification systems of previous wetland CH₄ syntheses (Olefeldt et al., 2013; Turetsky et al., 2014; Treat et al., 2018). Drained systems are former wetlands that have subsequently been drained but may maintain a relatively shallow water table, which can contribute to occasional methane emissions, although we do not have specific water table depth information at all drained sites. Upland ecosystems are further divided into alpine meadows, grasslands, needleleaf forests, mixed forest, crops, tundra, and urban. Freshwater wetland classifications follow hydrological definitions of bog (ombrotrophic), fen (minerotrophic), wet tundra, marshes, and swamps and were designated as per the primary literature on the site. For all sites, vegetation was classified for the presence or absence of brown mosses (all species from the division Bryophyta except those in the class Sphagnopsida), *Sphagnum* mosses

(any species from class Sphagnopsida), ericaceous shrubs, trees (of any height), and aerenchymatous species (mostly order Poales but includes exceptions). These categories closely follow Treat et al. (2018) except that aerenchymatous species had to be expanded beyond Cyperaceae to incorporate wetlands globally. Presence/absence of vegetation groups was designated based on species lists in primary literature from the site. Out of the vegetation groups present, the dominant (most abundant) group is also reported and is based on information provided by lead site investigators.

In addition to the variable description table (Table B1) and the site metadata (Table B3), we provide several more tables to complement our analysis. Table B4 includes the climatic data used in the representativeness analysis. Table B5 provides seasonality parameters for CH₄ flux, air temperature, soil temperature (from the probe closest to the ground surface), and GPP. For sites with multiple soil temperature probes, the full set of soil temperature parameters are in Table B6. Table B7 contains the soil temperature probe depths. Table B2 contains the annual CH₄ flux and uncertainty. All Appendix B tables are also available at <https://doi.org/10.5281/zenodo.4672601> (Delwiche et al., 2021).

2.1.4 Annual CH₄ fluxes

Annual CH₄ fluxes were calculated from gap-filled data for site years with data gaps shorter than 2 consecutive months or for sites above 20° N where > 2-month data gaps occurred outside of the highest CH₄-emission months of 1 May through 31 October. Since we did not sum gap-filled values for > 2 month-gaps during the winter, annual sums from these years will be an underestimate since winter fluxes can be important (Zona et al., 2016; Treat et al., 2018). Several sites had less than 1 year of data, and we report gap-filled CH₄ flux annual sums for sites with between 6 months and 1 year of data (BW-Gum = 228 d, CH-Oe2 = 200 d, JP-Swl = 210 d, and US-EDN = 182 d). While these sums will be an underestimate of annual CH₄ flux since they do not span a full year (and we therefore do not use them in the seasonality analysis), their relative magnitude can still be informative. For example, site JP-SWL is a lake site, and even with less than 1 year of data the summed CH₄ flux of 66 g C m⁻² is relatively high (Taoka et al., 2020). In addition to sites with short time series, the annual CH₄ sum for site ID-Pag represents 365 d spanning June 2016 to June 2017.

2.1.5 Subset analysis on freshwater wetland CH₄ flux

In addition to the FLUXNET-CH₄-wide description of site class distributions and annual CH₄ fluxes, we also include a subset analysis on freshwater wetlands given that it is the dominant ecosystem type in our dataset and an important global CH₄ source (Saunio et al., 2016). First, we analyze freshwater wetland representativeness and sub-

sequently the seasonality of their CH₄ emissions. Freshwater wetlands included in the seasonality and representativeness analysis are indicated in Table B3, column “IN_SEASONALITY_ANALYSIS”.

2.2 Wetland representativeness

2.2.1 Principal component analysis

To compare the FLUXNET-CH₄ site distribution to the global wetland distribution, we evaluated their representativeness in the entire global wetland cover along four bioclimatic gradients. Only freshwater wetland sites were included in this analysis. Coastal sites were excluded because salinity, an important control on CH₄ production, could not be evaluated across the tower network due to a lack of global gridded salinity data (Bartlett et al., 1987; Poffenbarger et al., 2011). The four bioclimatic variables used were mean annual air temperature (MAT), latent heat flux (LE), enhanced vegetation index (EVI), and simple ratio water index (SRWI; data sources in Table B4). We use EVI because it is a more direct measurement than GPP from global gridded products and is considered a reasonable proxy for GPP (Sims et al., 2006). Together, these environmental variables account for, or are, proxies for key controls of CH₄ production, oxidation at the surface, and transport (Bridgham et al., 2013). We use a principal components analysis (PCA) to visualize the site distribution across the four environmental drivers at once. For this analysis, we consider the annual average bioclimatic conditions over 2003–2015. In the PCA output, we evaluate the coverage of the 42 freshwater sites over 0.25° grid cells containing > 5 % wetland mean cover in Wetland Area and Dynamics for Methane Modeling (WAD2M; Zhang et al., 2020, 2021) for the same time period.

2.2.2 Global dissimilarity and constituency analysis

To further identify geographical gaps in the coverage of the FLUXNET-CH₄ Version 1.0 network, we quantified the dissimilarity of global wetlands from the tower network, using a similar approach to that taken for CO₂ flux towers (Meyer and Pebesma, 2020). We calculated the 4-dimensional Euclidean distance from the four bioclimatic variables between every point at the land surface to every tower location at the FLUXNET-CH₄ network. We then divided these distances by the average distance between towers to produce a dissimilarity index. Dissimilarity scores < 1 represent areas whose nearest tower is closer than the average distance among towers, while areas with scores > 1 are more distant. Lastly, we identified the importance of an individual tower in the network by estimating the geographical area to which it is most analogous in bioclimate space. We divided the world's land surface according to closest towers in bioclimatic space. The area to which each tower is nearest is defined as the tower's constituency.

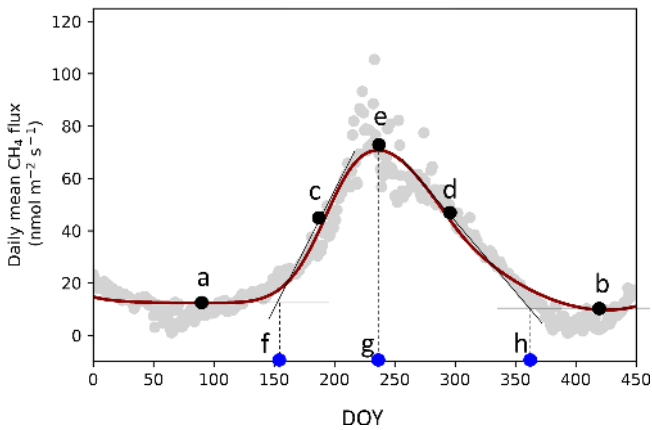


Figure 1. TIMESAT parameter description. (a, b) Base values (TIMESAT reports the average of these two values), (c, d) slopes of seasonal curves (lines drawn between 20 % and 80 % of the amplitude), (e) peak value, and day of year (DOY) for the start (f), peak (g), and end (h) of the elevated methane (CH₄) emission season. Data points are the mean daily gap-filled CH₄ fluxes from site JP-Bby in 2015.

2.3 Wetland CH₄ seasonality

To examine freshwater wetland CH₄ seasonality across the global range of sites in FLUXNET-CH₄, we extracted seasonality parameters for CH₄, temperature, and GPP using TIMESAT, a software package designed to analyze seasonality of environmental systems (Jönsson and Eklundh, 2002, 2004; Eklundh and Jönsson, 2015). TIMESAT calculates several seasonality parameters, including baseline flux, peak flux, and the slope of spring flux increase and fall decrease (Fig. 1). We also calculate parameters such as amplitude (peak flux minus baseline, which is the average of spring and fall baselines; “e” – ((“a” + “b”)/2) in Fig. 1) and relative peak timing ((“g” – “f”)/ (“h” – “f”) in Fig. 1). TIMESAT uses a double-logistic fitting function to create a series of localized fits centered on data minima and maxima. Localized fits are determined by minimizing a merit function with the Levenberg–Marquardt method (Madsen et al., 2004; Nielsen, 1999). These localized fits are then merged using a global function to create a smooth fit over the full time interval. To fit CH₄ time series in TIMESAT, we used gap-filled data after removing gaps exceeding 2 months. We do not report TIMESAT parameters when large gaps occur during the spring CH₄ emissions’ increase, peak, or fall decrease.

We estimate “start of elevated emission season” when CH₄ emissions begin to increase in the spring (“f” in Fig. 1), and “end of elevated emission season” when the period of elevated CH₄ flux ends in the fall (“h” in Fig. 1), as the intercept between the TIMESAT fitted baseline parameter and shoulder-season slope (similar to Gu et al., 2009). To extract seasonality parameters with TIMESAT, sites need a sufficiently pronounced seasonality, a sufficiently long time period, and minimal data gaps (we note that while TIMESAT is

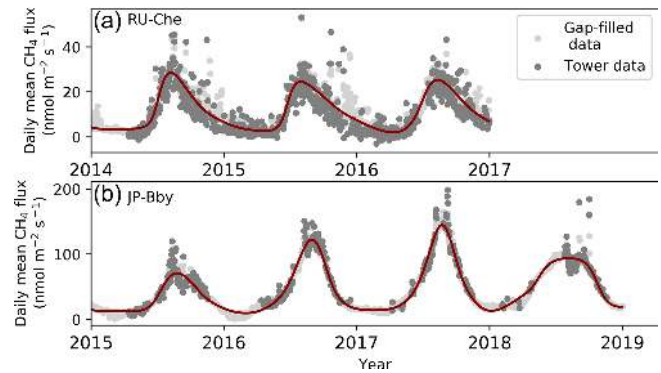


Figure 2. Examples of TIMESAT fits for two FLUXNET-CH₄ sites, (a) RU-Che and (b) JP-Bby. Methane (CH₄) flux data showing daily average flux tower data, with several high outliers excluded to improve the plot (dark gray), gap-filled values (light gray), and TIMESAT-fitted curve (dark red line) for sites JP-Bby and RU-Che. TIMESAT captures the size and shape of peaks (note different scale on y axes). CH₄ = methane.

capable of fitting two peaks per year, all the freshwater wetland sites have a single annual peak). We excluded site years in restored wetlands when wetlands were still under construction. Of the 42 freshwater wetland sites in FLUXNET-CH₄ Version 1.0, 36 had sufficient data series to extract seasonality parameters. These 36 wetlands had 141 site years of data in total, which we fit with the double-logistic fitting method which followed site data well (representative examples in Fig. 2). For extratropical sites in the Southern Hemisphere, we shifted all data by 182 d so that maximum solar insolation seasonality would be congruent across the globe.

We also used TIMESAT to extract seasonality metrics for GPP, partitioned using the daytime-based approach (Lasslop et al., 2010) (GPP_DT), air temperature (TA), and soil temperature (TS_1, TS_2, etc). For sites where winter soil temperatures fall significantly below 0 °C, TIMESAT fits a soil temperature “start of elevated season” date to periods when the soil is still frozen. In order for TIMESAT to define the soil temperature seasonality within the thawed season, we converted all negative soil temperatures to zero (simply removing these values results in too many missing values for TIMESAT to fit). Many sites have more than one soil temperature probe, so we extracted separate seasonality metrics from each individual probe (although we used the metrics from the shallowest temperature probe in our analysis). Table B4 contain the TIMESAT seasonality parameters used in the seasonality analysis. We did not include water table depth in the seasonality analysis because many sites either lack water table depth measurements or have sparse data.

We regressed the CH₄ seasonality parameters from TIMESAT against annual temperature, annual water table depth, and TIMESAT seasonality parameters for air temperature, soil temperature, and GPP (proxy for recent carbon input available as substrate) using linear mixed-effect modeling

with the *lmer* command (with site as a random effect) from the R (R Core Team, 2018, version 3.6.2) package *lmerTest* (Kuznetsova et al., 2017). For these regressions we present the marginal R^2 outputs from *lmer*, which represent the variance explained only by the fixed effects. Mixed-effect modeling was necessary to account for the non-independence between measurements taken at the same site during different years (Zona et al., 2016; Treat et al., 2018). We also compared how seasonality metrics varied across latitudinal bands by dividing sites into northern ($> 60^\circ$ N), temperate (between 40 and 60° N), subtropical (absolute value between 20 and 40° N latitude, with site NZ-KOP being the only Southern Hemisphere site), and tropical (absolute value below 20° N). Site-year totals for the northern, temperate, subtropical, and tropical bands were $n = 57, 36, 39,$ and $9,$ respectively. We used the Kruskal–Wallis test to establish whether groups (either across quarters or across latitudes) were from similar distributions and the post hoc multiple comparison “Dwass, Steel, Critchlow, and Fligner” procedure for inter-group comparisons. Kruskal–Wallis and post hoc tests were implemented in Python Version 3.7.4, using stats from *scipy* for Kruskal–Wallis and *posthoc_dscf* from *scikit_posthocs*.

We also compared quarterly CH₄ flux sums by dividing data into quarterly periods: January–February–March (JFM), April–May–June (AMJ), July–August–September (JAS), and October–November–December (OND). For the sake of simplicity, we chose to compare quarterly periods rather than site-specific growing/non-growing season periods so that all time periods would be the same length. Quarterly sums were computed from the gap-filled CH₄ fluxes when the longest continuous data gap within the quarter did not exceed 30 d, leading to site-year counts of 67, 92, 95, and 72 for JFM, AMJ, JAS, and OND, respectively. We compared quarterly CH₄ fluxes across latitudinal bands both for the total CH₄ flux and for the quarterly percentage of the annual CH₄ flux. Quarterly statistics were also conducted with the Kruskal–Wallis test and the post hoc multiple comparison “Dwass, Steel, Critchlow, and Fligner” procedure implemented in Python. Quarterly values are provided in Table B3, and the sum of mean quarterly CH₄ flux does not always equal mean annual CH₄ flux because some quarters either do not have data or have data gaps that exceed 30 d.

3 Results and discussion

3.1 FLUXNET-CH₄ dataset

3.1.1 Dataset description

Version 1.0 of the FLUXNET-CH₄ dataset contains 79 unique sites, 293 total site years of data, and 201 site years with sufficient data to estimate annual CH₄ emissions. A synthesis paper, published prior to the public data release of FLUXNET-CH₄ Version 1.0, had 60 unique sites and 139 site years with annual CH₄ emission estimates (Knox

et al., 2019). Freshwater wetlands make up the majority of sites ($n = 42$), and the dataset also includes five salt marshes and one mangrove wetland. Notable additions to FLUXNET-CH₄ from the previous unpublished dataset used in Knox et al. (2019) include six tropical sites (between 20° S and 20° N), including one site in South America, two sites in southern Africa, and three sites in Southeast Asia. The 15 upland sites include six needleleaf forests, three crop sites (excluding rice), two alpine meadows, one grassland, one mixed forest, one tundra, and one urban site. The drained sites represent former wetlands that have been artificially drained for use as grasslands ($n = 3$) or croplands ($n = 3$). FLUXNET-CH₄ sites span the globe, though they are concentrated in North America and Europe (Fig. 3). Table B3 includes characteristics of all sites in the dataset.

Sites represent a range of ecosystem types, latitudes, median fluxes, and seasonality patterns (Table 1). Across all FLUXNET-CH₄ sites (including non-wetland sites), mean average annual CH₄ flux is positively skewed with a median flux of $9.5 \text{ g C m}^{-2} \text{ yr}^{-1}$, a mean flux of $16.9 \text{ g C m}^{-2} \text{ yr}^{-1}$, and numerous annual CH₄ fluxes exceeding $60 \text{ g C m}^{-2} \text{ yr}^{-1}$. Marshes and swamps have the highest median flux, and upland, salt marsh, and tundra sites have the lowest (Fig. 4). Lake emissions are highly variable due to one high-flux lake site (JP-SWL). Flux data at many sites show strong seasonality in CH₄ emissions, but data coverage is also lower outside the growing season (Table 1). Data coverage is lowest during the JFM quarter (on average 20 % of half-hourly time periods contain flux data), reflecting the predominance of Northern Hemisphere sites and the practical difficulties in maintaining EC tower sites during colder winter months (Table 1). Bogs, fens, and marshes have pronounced seasonality, with fluxes being highest in the AMJ and JAS quarters. In contrast, CH₄ fluxes from uplands, drained sites, and salt marshes are more uniform and low year-round.

3.1.2 Freshwater wetland CH₄ characteristics

The FLUXNET-CH₄ Version 1.0 dataset contains 42 freshwater wetlands that span 37° S to 69° N, including bogs, fens, wet tundra, marshes, and swamps, and a range of annual CH₄ emission rates (Fig. 4). The majority of freshwater wetlands in our dataset emit 0 – $20 \text{ g C m}^{-2} \text{ yr}^{-1}$, with 10 emitting 20 – $60 \text{ g C m}^{-2} \text{ yr}^{-1}$, and one more than $60 \text{ g C m}^{-2} \text{ yr}^{-1}$. Differences in annual CH₄ flux among wetland types is partially driven by temperature (which is often linked to site type), with mean annual air temperature explaining 51 % of the variance between sites (Fig. 5, exponential relationship). The global relationship between annual methane emissions and temperature can be described using a Q_{10} relationship where $Q_{10} = R2/R1^{((T2-T1)/10)}$, with $R2$ and $R1$ being the CH₄ emission rates at temperatures $T2$ and $T1$, respectively (temperature in $^\circ\text{C}$). The Q_{10} based on Fig. 5 data is 2.57. We also note that annual CH₄ flux from individual biomes may have different relationships with temperature, as previ-

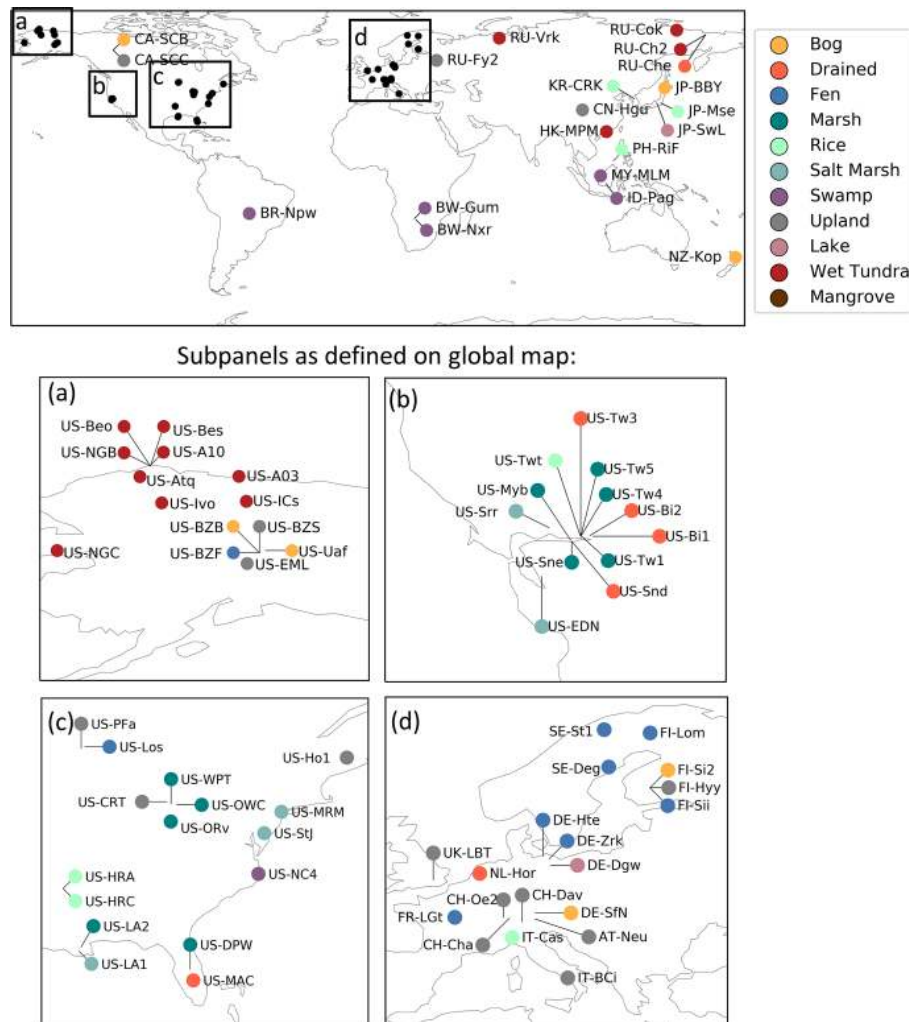


Figure 3. Global map of FLUXNET-CH₄ Version 1.0 site locations colored by site type. Panels (a)–(d) show sites that were too closely located to distinguish in the global map.

ous work has shown biome-specific trends in CH₄ flux with environmental drivers (Abdalla et al., 2016). However, there currently are not enough data points in each biome category to compare relationships between mean annual CH₄ flux and temperature. Annual CH₄ flux is not correlated with mean annual water table depth in FLUXNET-CH₄, unlike in Knox et al. (2019), which used a subset of the FLUXNET-CH₄ sites in which CH₄ flux was correlated with water table depth only for sites with water table below ground for 90 % of measured days ($r^2 = 0.31$, $p < 0.05$, $n = 27$ site years). Freshwater wetland seasonality is further described in Sect. 3.3.

3.1.3 Upland, rice, and urban CH₄ characteristics

Upland agricultural sites are characterized by a lack of seasonal pattern in CH₄ emissions, relatively low flux, and sometimes negative daily flux (i.e., CH₄ uptake) averages. All of the upland non-agricultural sites in FLUXNET-CH₄

Version 1.0 are net (albeit weak) CH₄ sources except for the needleleaf forest site US-Ho1, which has a mean annual CH₄ flux of $-0.1 \pm 0.1 \text{ g C m}^{-2} \text{ yr}^{-1}$ (see Table B3 for site acronyms and metadata). The average agricultural site emissions are $1.3 \pm 0.8 \text{ g C m}^{-2} \text{ yr}^{-1}$, and non-agricultural site emissions are $1.6 \pm 1.2 \text{ g C m}^{-2} \text{ yr}^{-1}$ across sites.

Rice sites ($n = 7$) have average annual emissions across all sites of $16.7 \pm 7.7 \text{ g C m}^{-2} \text{ yr}^{-1}$ and are characterized by strong seasonal patterns, with either one or more CH₄ emission peaks per year depending on the number of rice seasons and field water management. One peak is typically observed during the reproductive period for the continuously flooded sites with one rice season (i.e., US-HRC, JP-MSE) (Iwata et al., 2018; Runkle et al., 2019; Hwang et al., 2020). For sites with only one rice season but with single or multiple drainage and re-flooding periods, a secondary peak may appear before the reproductive peak (i.e., KR-CRK, IT-Cas, and US-HRA; Meijide et al., 2011; Runkle et al., 2019; Hwang et al., 2020).

Table 1. Summary table of sites grouped by ecosystem class reporting annual mean flux (Ann_Flux) and standard deviation from interannual variability (Ann_Flux_SD), site years of data, percent data cover per quarter, and median (med.) flux across site class. JFM signifies January–February–March, AMJ April–May–June, JAS July–August–September, and OND October–November–December.

| | No. of sites | No. of site years | Ann_Flux (g C m ⁻² yr ⁻¹) | Ann_Flux_SD (g C m ⁻² yr ⁻¹) | JFM cover -age (%) | AMJ cover -age (%) | JAS cover -age (%) | OND cover -age (%) | JFM flux (med.) | AMJ flux (med.) | JAS flux (med.) | OND flux (med.) |
|------------|--------------|-------------------|--|---|--------------------|--------------------|--------------------|--------------------|-----------------|-----------------|-----------------|-----------------|
| Salt marsh | 5 | 10 | 2.9 | 4.7 | 7 | 42 | 50 | 37 | 1.5 | 1.7 | 2.1 | 1.6 |
| Wet tundra | 11 | 39 | 3.8 | 1.8 | 8 | 28 | 40 | 18 | 0.4 | 2.6 | 8.1 | 3.2 |
| Upland | 15 | 47 | 4.0 | 10.5 | 23 | 35 | 39 | 28 | 1.2 | 0.5 | 1.4 | 0.8 |
| Drained | 7 | 20 | 6.3 | 7.1 | 22 | 39 | 39 | 29 | 4.6 | 3.6 | 5.1 | 3.6 |
| Bog | 7 | 32 | 10.5 | 6.4 | 8 | 27 | 37 | 18 | 7.2 | 11.0 | 24.8 | 9.5 |
| Mangrove | 1 | 3 | 11.1 | 0.5 | 46 | 28 | 30 | 41 | 3.2 | 7.2 | 22.5 | 14.1 |
| Rice | 7 | 20 | 14.4 | 8.8 | 16 | 37 | 45 | 27 | 3.2 | 11.9 | 43.1 | 4.2 |
| Fen | 8 | 40 | 20.5 | 16.0 | 29 | 43 | 40 | 30 | 2.8 | 14.2 | 26.0 | 6.4 |
| Swamp | 6 | 15 | 26.4 | 19.9 | 24 | 34 | 29 | 19 | 14.7 | 24.9 | 31.0 | 24.4 |
| Lake | 2 | 4 | 28.2 | 33.4 | 15 | 13 | 27 | 36 | 0.2 | 47.6 | 90.2 | 40.3 |
| Marsh | 10 | 42 | 40.8 | 20.7 | 22 | 43 | 53 | 30 | 13.5 | 55.0 | 85.8 | 36.1 |

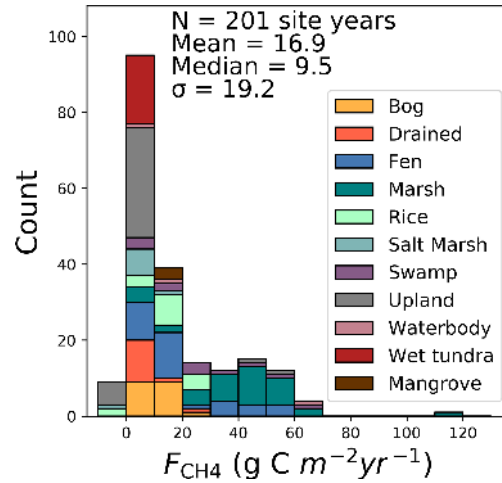


Figure 4. Histogram of annual methane fluxes (F_{CH_4} , g C m⁻² yr⁻¹) grouped by site type.

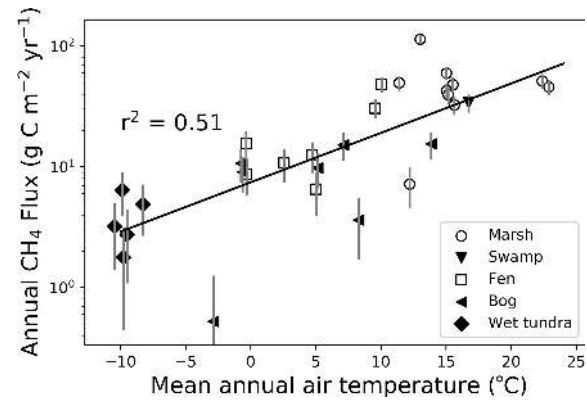


Figure 5. Relationship between mean annual wetland methane (CH₄) flux (g C m⁻² yr⁻¹, logarithmic scale) and mean annual air temperature (°C) for each freshwater wetland site, with wetland type indicated by symbol. Markers represent individual site means, with vertical error bars representing the standard deviation of interannual variability.

Two reproductive peaks appear for sites with two rice seasons (i.e., PH-RiF), and each reproductive peak may be accompanied by a secondary peak due to drainage events (Alberto et al., 2015). Even sites with one continuously flooded rice season may experience a second peak if the field is flooded during the fallow season to provide habitat for migrating birds (e.g., US-Twt; Knox et al., 2016).

The dataset has 1 year of urban data from site UK-LBT in London, England. UK-LBT observes CH₄ fluxes from a 190 m tall communications tower in the center of London and has a mean annual CH₄ flux of 46.5 ± 5.6 g C m⁻² yr⁻¹. This flux is more than twice as high as the mean annual CH₄ flux across all FLUXNET-CH₄ sites, 16.9 g C m⁻² yr⁻¹. The London site has higher CH₄ emissions in the winter com-

pared to summer, which is attributed to a seasonal increase in natural gas usage (Helfter et al., 2016.)

3.1.4 Saltwater and mangrove wetland CH₄ characteristics

Three of the five saltwater wetlands in FLUXNET-CH₄ (US-Edn, US-MRM, and US-Srr) have a very low mean annual CH₄ flux (see Table B2 for individual site-year CH₄ flux sums and associated uncertainty) and minimal seasonality. Two other FLUXNET-CH₄ saltwater sites (US-La1 and US-StJ) have significantly higher fluxes, with annual sums of 12.6 ± 0.6 and 9.6 ± 1.0 g C m⁻² yr⁻¹, respectively, while the mangrove site HK-MPM has annual mean fluxes of 11.1 ± 0.5 g C m⁻² yr⁻¹. This range of CH₄ fluxes across different saltwater ecosystems could be valuable for exploring the effect of salinity and different biogeochemical pathways of CH₄ production, oxidation, and transport of CH₄ (Bartlett et al., 1987; Poffenbarger et al., 2011). Saltwater wetlands along the coast have unique CH₄ dynamics attributable to the presence of abundant electron acceptors, most importantly sulfates which inhibit methanogenesis (Pattnaik et al., 2000; Mishra et al., 2003; Weston et al., 2006) but at low concentrations can have no effect (Chambers et al., 2011) or even increase methanogenesis (Weston et al., 2011). In fact, estuarine wetlands with moderate salinity can still be significant sources of CH₄ (Liu et al., 2020). Even under sulfate-rich conditions, high CH₄ production can be found via methylotrophic methanogenesis (Dalcin Martins et al., 2017; Seyferth et al., 2020,) or because the processes of sulfate reduction and methanogenesis are spatially separated (Koebsch et al., 2019). Consequently, representing the biophysical drivers of ecosystem-scale CH₄ fluxes in non-freshwater wetlands is challenging and may represent a combination of competing or confounding effects (Vazquez-Lule and Vargas, 2021).

3.2 Freshwater wetland representativeness

We evaluated the representativeness of freshwater wetland sites in the FLUXNET-CH₄ Version 1.0 dataset against wetlands globally, based on bioclimatic conditions of our sites. When evaluating bioclimatic variables individually, the distribution of freshwater wetlands across the network was significantly different from the global distribution ($\alpha > 0.05$; two-tailed Kolmogorov–Smirnov tests; see Table B4). We exclude wetlands classified as “salt marsh” in this representativeness analysis and the seasonality analysis below because of the unique CH₄ flux dynamics in saltwater ecosystems (as discussed in Sect. 3.1.4), though we note that some of the coastal wetlands included in the freshwater analysis periodically experience brackish water (i.e., US-Myb, US-Sne).

When considering the four bioclimatic variables, MAT, LE, EVI, and SRWI in a PCA, we found that our tower network generally samples the bioclimatic conditions of global

wetland cover, but some noticeable gaps remain (Fig. 6). Three clusters of the world’s wetland-dense regions are identified but are not equally sampled by the network. A cluster of low-temperature wetlands is sampled by a large number of high-latitude sites. The other two wetland clusters are not as well sampled: a high-temperature and LE cluster is represented only by two towers (ID-Pag and MY-MLM), while drier and temperate and subtropical wetlands including large swathes of the Sahel in Africa only have a site in Botswana (BW-Npw) as their closest analog tower.

Evaluating the bioclimatic dissimilarity of global wetlands to the FLUXNET-CH₄ network shows the least captured regions are in the tropics (Fig. 7a). Sparse coverage in the tropics also means that the few existing towers occupy a critical place in the network, particularly as tropical wetlands are the largest CH₄ emitters (Bloom et al., 2017; Poulter et al., 2017). Highly dissimilar wetlands are limited in extent and distributed across all latitudes, but the average dissimilarity is higher in north temperate (55 to 65°) and tropical (−5 to 5°) latitudes (Fig. 7b). To evaluate the importance of individual towers in the network, we estimated the geographical area to which it is most analogous in bioclimate space (Fig. 7c). We found that some towers have disproportionately large constituencies (i.e., wetland areas that share the same closest bioclimatic analog tower). Towers in Indonesia (ID-Pag), Brazilian Pantanal (BR-Npw), and Botswana floodplains (BW-Nxr) represent the closest climate analog for much of the tropics (678 000, 300 000, and 284 000 km², respectively), while CA-SCB represents a vast swath (291 000 km²) of boreal and arctic regions (Fig. 7d).

Our assessment of wetland CH₄ tower coverage determines the ability of our dataset to represent global wetland distributions and highlights some clear representation gaps in the network, particularly in tropical and humid regions. Other geographic regions such India, China, and Australia, where towers exist but are not included in the current network, should be prioritized when expanding the network even though they are not among the most distant areas to the current network. Similar representativeness assessments have been developed for CO₂ tower networks to identify gaps and priorities for expansion (Jung et al., 2009). To improve the geographic coverage of the network for representing global-scale fluxes, locations for new tower sites can be targeted to cover bio-climatically distant areas from the current network (Villarreal et al., 2019). Candidate regions for expansion that are both high CH₄ emitting (Saunio et al., 2020) and located in under-sampled climates are the following: African Sahel, Amazon Basin, Congo Basin, and Southeast Asia. Climatic conditions over boreal and arctic biomes are generally better represented (primarily at lower elevations), but there is scope to expand the network in wetland-dense regions like the Hudson Bay Lowlands and North Siberian Lowlands. Moreover, establishing sites in other ecosystem types, especially lakes and reservoirs (see Deemer et al., 2016; Bastviken et al., 2011; Matthews et al.,

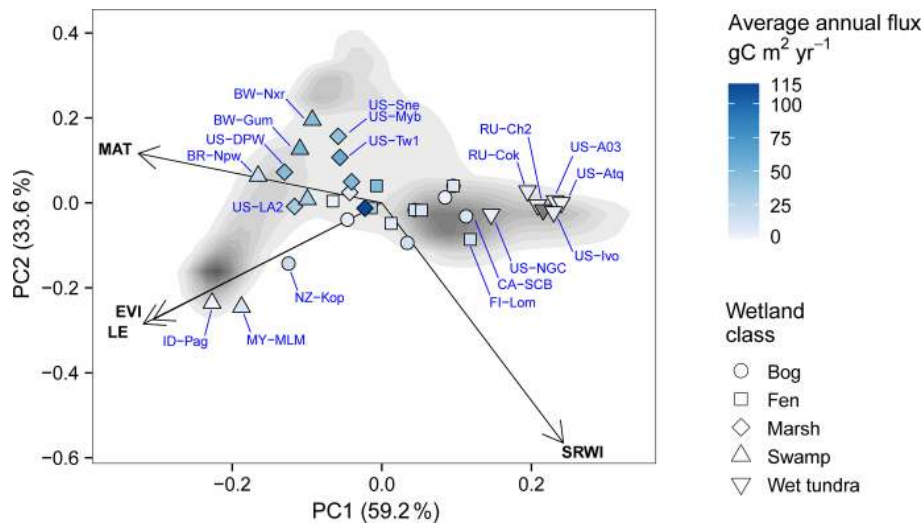


Figure 6. Principal component analysis displaying the distribution of freshwater wetland sites (points) along the two main principal components together accounting for 91.9% of variance. Tower sites are represented as points with shapes indicating their wetland type and color shade representing the annual methane (CH₄) flux (gray points represent sites for which < 6 months of flux data were available to estimate annual budget). Sites codes are labeled in blue text for selected sites deviating from average conditions. Loading variables are represented by the arrows: mean annual temperature (MAT), simple ratio water index (SRWI), latent heat flux (LE), and enhanced vegetation index (EVI). The background shades of gray are a qualitative representation of the density of global wetland pixels and their distribution in the PCA climate space, with darker color representing higher densities (excluding Greenland and Antarctica). Only grid cells with > 5% average wetland fraction according to the WAD2M over 2000–2018 are included (Zhang et al., 2020).

2020) in most climatic zones would help capture CH₄ fluxes from these ecosystems.

Understanding the representativeness of the network is essential when inferring general patterns of flux magnitude, seasonality, and drivers from the tower data (Villarreal et al., 2018). We produced a first-order representativeness of average bioclimatic conditions, but temporal representativeness (across seasons, climate anomalies, and extreme events) is particularly needed given the episodic nature of CH₄ fluxes (Chu et al., 2017; Mahecha et al., 2017; Göckede et al., 2019).

Assessing representation of wetland CH₄ sites is complicated by the fact that wetlands occupy only a fraction of most landscapes (except wetland-dense regions such as North Siberian Lowlands, Hudson Bay Lowlands, Congo Basin, etc.) and that not all relevant factors affecting CH₄ production and consumption could be considered in our analysis. For instance, our assessment of representation did not consider wetland types as such maps are limited by the inherent difficulties in remotely sensing wetland features (Gallant, 2015). The attribution of representativeness is further complicated by the fact that many EC tower locations are subject to small-scale variability within the field of view, or footprint, of the sensor. Consequently, the individual time steps within EC flux time series may represent a mixture of different wetland types or different fractions of wetland contribution to the total CH₄ flux, varying with wind direction, atmospheric stability, or season (Chu et al., 2021). This further compli-

cates upscaling efforts. Additionally, this representativeness analysis did not apply weights to the drivers to reflect their varying influence on CH₄ flux. Such weights can be included in future versions as they are generated by a cross-validated machine learning approach (Jung et al., 2020). Future efforts could include the dissimilarity index from this analysis as a metric of extrapolation in a CH₄ flux upscaling effort.

3.3 Freshwater wetland flux seasonality

3.3.1 Seasonal flux comparisons by latitudinal bands

CH₄ flux and seasonality varied substantially across latitudinal bands (northern, temperate, subtropical, and tropical) (Fig. 8). Annual CH₄ fluxes for temperate, and subtropical sites were significantly higher than for northern sites (8.7 ± 5.0 , 29.7 ± 25.2 , 40.1 ± 14.6 , and 24.5 ± 20.7 g C m⁻² yr⁻¹ for northern, temperate, subtropical, and tropical, respectively, and $p < 0.0001$ using Kruskal–Wallis and post hoc comparisons; Fig. 8a), and tropical sites were similar to all other latitudinal bands likely because of their small sample size. The ratio of seasonal amplitude to peak flux provides a measure of the relative seasonal increase in emissions compared with baseline, in which a ratio of 0 indicates no seasonal change in amplitude, a ratio of 1 indicates the off-season flux is zero, and values over 1 mean the off-season baseline CH₄ fluxes were negative (i.e., uptake). Average amplitude to peak flux ratios were similar across all latitudinal bands (0.9 ± 0.1 , 0.9 ± 0.1 , 0.9 ± 0.1 ,

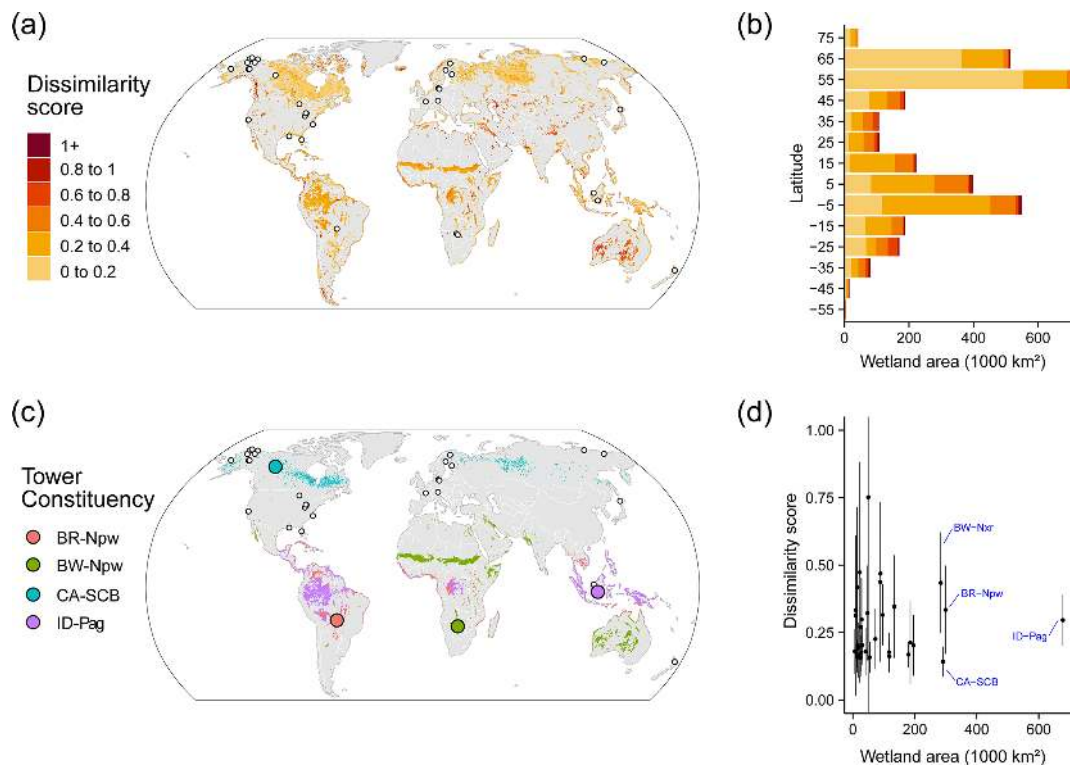


Figure 7. (a) Distance in bioclimatic space between global land surface and the FLUXNET-CH₄ Version 1.0 tower network (gray areas indicate no mapped wetlands). The Euclidean distance was computed on the four bioclimatic variables and was then standardized by the average distance within the network. Most of the land surface has a dissimilarity score lower than 1, meaning these areas are closer than the average tower distance (lower dissimilarity score means a similar bioclimate to that represented by towers in the network). However, this pattern reflects more the sparsity of the tower network than a similarity of the land surface to the network. Areas with < 5% coverage by wetlands were excluded to focus on wetland-dense regions. (b) Latitudinal distribution of dissimilarity score, (c) map of the four largest tower constituencies, and (d) scatterplot of wetland area in each tower constituency plotted against the average dissimilarity score (point) and \pm standard deviation (error bar).

and 1.0 ± 0.7 for northern, temperate, subtropical, and tropical, respectively; Fig. 8b). The spring increase in CH₄ emissions began later in northern sites compared with temperate and subtropical sites (end of May versus April, respectively, and $p = 0.001$; Fig. 8c), while tropical sites vary widely in elevated emission season start date. Northern sites also had shorter elevated CH₄ flux season lengths (138 ± 24 d) compared to temperate sites (162 ± 32 d), and both were shorter than subtropical sites (209 ± 43 d; $p < 0.0001$; Fig. 8e). On average, CH₄ flux peaked earlier for temperate sites compared to northern ($p = 0.008$) and subtropical sites ($p = 0.02$; middle to late July compared with early August; Fig. 8f), while tropical sites again vary widely. Given their unique seasonality and low number of site years ($n = 9$), tropical systems are discussed separately in Sect. 3.3.3 and are not included in the comparisons in the remainder of this section. While our results on CH₄ seasonality corroborate expected trends for these latitudinal bands, they provide some of the first estimates of CH₄ seasonality parameters and ranges across a global distribution of sites.

We found that latitudinal groups showed strong differences in absolute CH₄ flux across quarters and narrower differences in percentage of annual CH₄ flux (Fig. 9a versus 9b). Thus, the AMJ quarter had a similar relative contribution to the annual CH₄ flux across latitudes regardless of the absolute annual CH₄ flux. CH₄ fluxes (Fig. 9a) were highest during JAS for northern, temperate, and subtropical sites and highest in AMJ and JAS for temperate sites ($p < 0.01$). Though CH₄ fluxes in northern sites are most commonly measured during warm summer months (Sachs et al., 2010; Parmentier et al., 2011), fluxes in JFM and OND (50% of the yearly duration) on average make up $18.1 \pm 3.6\%$, $15.3 \pm 0.1\%$, and $31.2 \pm 0.1\%$ (northern, temperate, and subtropical, respectively) of annual emissions. This pattern indicates that a substantial fraction of annual CH₄ fluxes occur during cooler months. The contribution of non-growing season CH₄ emissions to annual CH₄ fluxes has previously been described for arctic and boreal regions (Zona et al., 2016; Treat et al., 2018), and our analysis suggests comparable contributions in temperate and subtropical systems for the same quarterly periods.

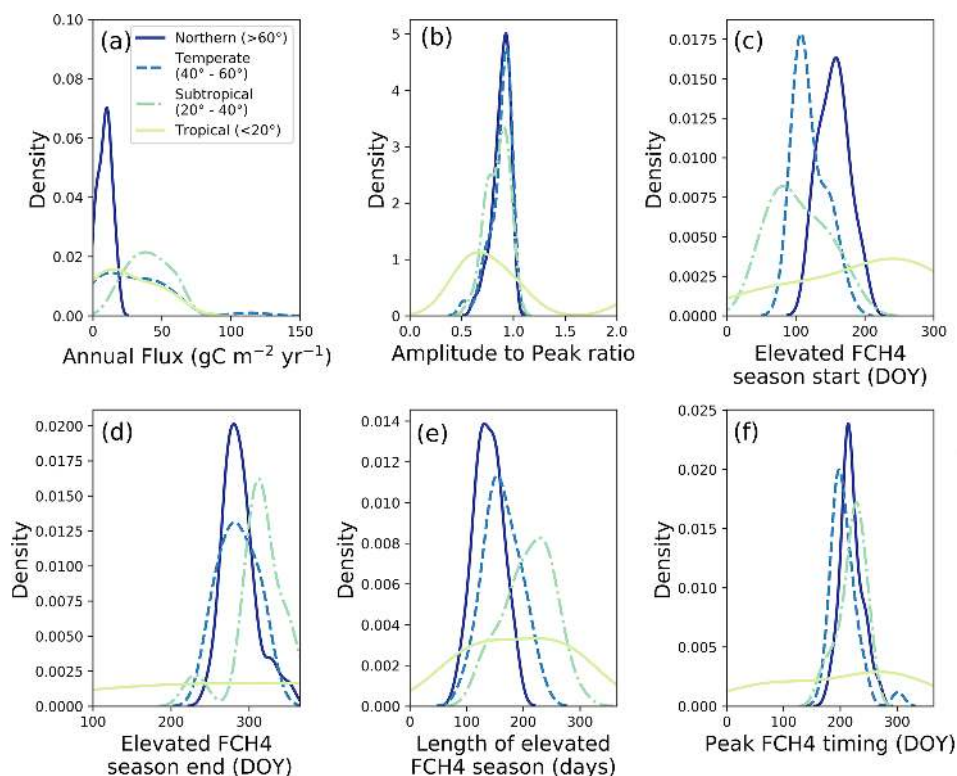


Figure 8. (a) Annual methane (CH₄) flux ($\text{gC m}^{-2} \text{yr}^{-1}$), (b) ratio of seasonal amplitude to seasonal peak, where values of 0 indicate uniform annual CH₄ flux, values of 1 indicate zero off-season fluxes, and values exceeding 1 indicate negative off-season fluxes, (c) CH₄ flux (FCH₄) elevated emission season start by day of year (DOY), (d) FCH₄ elevated emission season end by DOY, (e) length of elevated CH₄ flux season (days), and (f) DOY of peak FCH₄. Northern (dark blue, solid line), temperate (blue, dashed line), sub-tropical (green, dot-dash line), and tropical (light green, solid line) wetlands plotted using the kernel density function. Each panel has lines that represent latitudinal bands as follows: northern ($> 60^\circ$), temperate (between 40 and 60°), subtropical (between 20 and 40°), and tropical ($< 20^\circ$), though the site-year totals vary between these groups ($n = 57$, $n = 36$, $n = 39$, and $n = 9$ respectively). All total CH₄ flux values and elevated season start values are positive, and the apparent continuation of the data distribution into negative values is an artifact of the kernel density function. Southern Hemisphere sites below 20°S were shifted by 182 d to make summer the middle of the year for comparability with Northern Hemisphere sites.

3.3.2 Predictors of CH₄ flux phenology

The start of the elevated CH₄ flux season, and how long the elevated flux season lasts, correlated strongly with mean annual air temperature (Fig. 10; $p < 0.0001$ for each). Methane flux began to increase roughly 2 months earlier in the warmest systems (mean annual temperature $> 20^\circ \text{C}$) compared to the coldest (mean annual temperature near -10°C), though several of the warmer sites had high variability. Our data suggest that the CH₄ season started $2.8 \pm 0.5 \text{ d}$ earlier for every degree Celsius increase in mean annual temperature (Fig. 10a). In contrast, the end of the CH₄ emission season was not correlated with mean annual temperature, but a positive trend existed despite high variability at the warmest and coldest sites (Fig. 10b). The high variability seen in the end of the CH₄ season at northern sites is important to note and would likely be better resolved by incorporating other seasonality or phenological characteristics, such as moisture, active layer depth, and plant community composition (e.g.,

Kittler et al., 2017). Plants with aerenchymatous tissue, for example, influence the timing of plant-mediated CH₄ flux and are a key source of uncertainty when predicting CH₄ seasonality for northern wetlands (Xu et al., 2016; Kwon et al., 2017). Despite the relative lack of trend with season end date, the season length was still positively correlated with mean annual temperature, with the warmest sites having roughly 3 more months of seasonally elevated CH₄ emissions than the coldest sites (Fig. 10c). CH₄ season length increased $3.6 \pm 0.6 \text{ d}$ for every degree Celsius increase in mean annual temperature (note that these relationships are correlations, and we cannot disentangle causality with this analysis). Temperature is highly correlated with other parameters (i.e., radiation, days of snow cover, etc.), so CH₄ flux is also likely to correlate with other environmental parameters.

Although the spring onset of increasing CH₄ emissions correlated with mean annual air temperature, on average it lagged behind the spring increase in the shallowest soil temperatures by $31 \pm 40 \text{ d}$ (Fig. 11; lag is significantly different

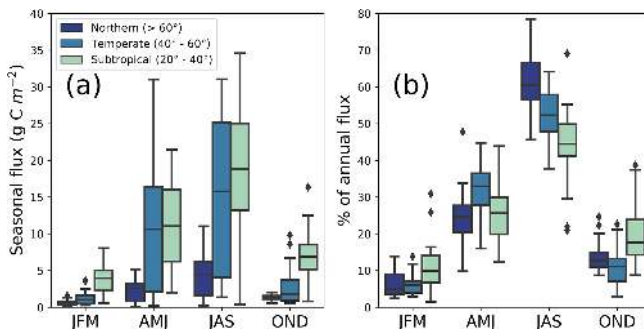


Figure 9. (a) Quarterly contribution to total annual CH₄ flux (in g C m⁻²) and (b) percentage of annual CH₄ flux. Sites were divided into northern (> 60° N), temperate (40°–60° N), and subtropical (20°–40° N). Quarters with continuous data gaps exceeding 30 d were excluded. We used the following quarterly periods: January–February–March (JFM), April–May–June (AMJ), July–August–September (JAS), and October–November–December (OND). Tropical sites are discussed separately in Sect. 3.3.3 because of their unique seasonality and low number of sites.

than zero, and $p < 0.001$), with very few instances of CH₄ emissions beginning before seasonal soil temperatures increase (and by 20 ± 50 d for the deepest temperature probes). In contrast, for roughly half of the sites, CH₄ emission increased prior to seasonal GPP (a proxy for fresh substrate availability) increases. This suggests that the initiation of increased CH₄ fluxes at the beginning of the season was not limited by availability of substrate derived from recent photosynthates. Additionally, the onset of CH₄ fluxes tended to occur closer to the onset of soil temperature increase for cooler temperature sites (sites with later start dates tend to be cooler; Fig. 11a). This result is likely attributable to the direct influence of increased temperature on microbial processes (Chadburn et al., 2020), as well as the indirect influences of snowmelt, both via release of CH₄ from the snowpack and a higher water table leading to more CH₄ production (Hargreaves et al., 2001; Tagesson et al., 2012; Mastepanov et al., 2013; Helbig et al., 2017). These observed trends hold for the entire temperature or GPP range of freshwater wetland sites but are not necessarily applicable within individual latitudinal bands.

In contrast with the CH₄ season start timing, the timing of the CH₄ peak did not correlate with the timing of either the soil temperature peak or the GPP peak (Fig. A1). For 63 % of the sites, the average timing of peak CH₄ emissions lagged behind the soil temperature peak, and at 83 % of the sites average peak CH₄ lagged behind peak GPP (Fig. A1). Although there was no simple relationship between absolute CH₄ peak timing and the environmental drivers we investigated, there was a correlation ($p = 0.0005$) between the relative timing of peak CH₄ compared to season onset (calculated as described in Sect. 2.3) and mean annual air temperature (Fig. 12a). For cooler sites, the peak of sea-

sonal CH₄ emissions occurred closer to the onset of the CH₄ emission season than the end of the season, resulting in an asymmetrical seasonal CH₄ flux shape that is illustrated in Fig. 2a. Soil temperature also peaked earlier in the season for cooler wetlands, though the relationship is not as pronounced ($p = 0.009$; Fig. 12b). In contrast, GPP peaked later in the season for cooler wetlands ($p = 0.009$, Fig. 12c). Previous work on Arctic sites (sites US-Ivo, US-Beo, US-Atq, US-Bes, and RU-CH2) highlighted the asymmetrical annual CH₄ peak, with higher fall emissions being attributed to the “zero curtain” period when soil below the surface remains thawed for an extended period of time due to snow insulation (Zona et al., 2016; Kittler et al., 2017). Furthermore, soils can stay above the “zero curtain” range for an extended time into the fall and winter (Helbig et al., 2017), which may also be caused by snow insulation. The rapid onset of emissions in the spring following snowmelt could be attributed to the release of accumulated CH₄ (Friborg et al., 1997), and other high latitude sites have seen similarly sharp increases in CH₄ emissions at snowmelt (Dise, 1992; Windsor, 1992). However, not all studies in high latitudes have observed asymmetrical CH₄ emission peaks, pointing to the inherent complexity of these ecosystems (Rinne et al., 2007; Tagesson et al., 2012).

3.3.3 Uniqueness of tropical wetlands

Tropical wetlands typically do not experience the large swings in temperature and GPP that contribute to CH₄ flux seasonality in temperate and northern sites. Indeed, the relatively constant high temperatures and high GPP in tropical ecosystems may lead to the lower ratio between seasonal amplitude and peak CH₄ flux compared with temperate and northern sites (Fig. 8b). Tropical flux sites have historically been under-studied, leading to a lack of synthesized information about these ecosystems. FLUXNET-CH₄ has five tropical wetland sites (latitudes between 20° S and 20° N) and one tropical rice site, representing 13 site years of data. These sites are especially insightful as they provide the first estimates of CH₄ fluxes from large, tropical, seasonal floodplain systems.

We found a broad range of annual CH₄ fluxes across tropical sites in FLUXNET-CH₄ Version 1.0. Annual CH₄ flux emissions from two Southeast Asian flooded peat forests were relatively low, 0.01 ± 0.1 and 9.5 ± 0.6 g C m⁻² yr⁻¹ for ID-PAG and MY-MLM, respectively, which is consistent with annual CH₄ fluxes measured at another peat forest in Indonesia (Deshmukh et al., 2020). In contrast, mean annual CH₄ flux for a seasonally flooded swamp in the Brazilian Pantanal region (BR-NPW) was over twice as high as MY-MLM, at 19.2 ± 2.5 g C m⁻² yr⁻¹. Similarly high annual CH₄ fluxes were observed at the two Botswana swamp sites in the Okavango Delta (51.7 ± 10.6 and 47.3 ± 3.7 g C m⁻² yr⁻¹ for BW-GUM and BW-NXR, respectively), one of which is seasonally inundated and sur-

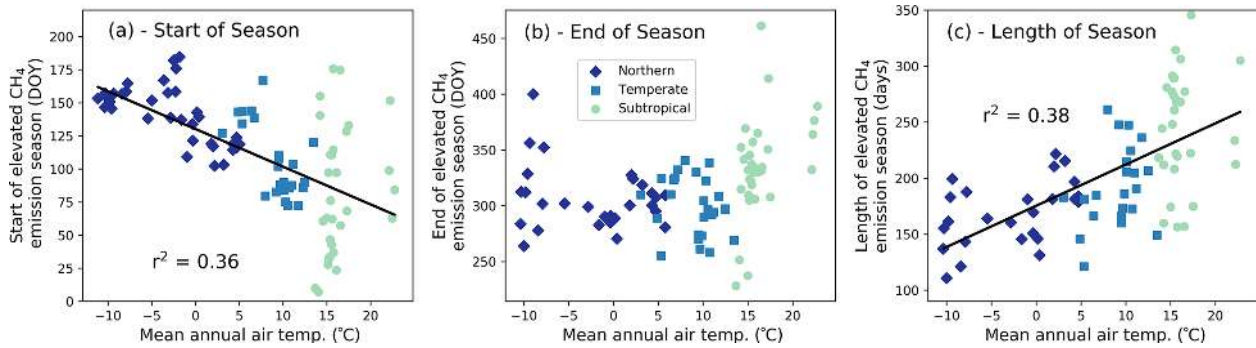


Figure 10. The (a) start of the elevated methane (CH₄) emission season ($y = -2.8x + 130$, with “ x ” in °C and “ y ” in day of year, DOY), (b) the end of the elevated emission season in DOY, and (c) the length of the emission season with mean annual site air temperature ($y = 3.6x + 176.6$, with “ x ” in °C and “ y ” in days). Each point represents a site year of data, and all reported r^2 values are significant to $p < 0.0001$. Tropical sites are discussed separately in Sect. 3.3.3.

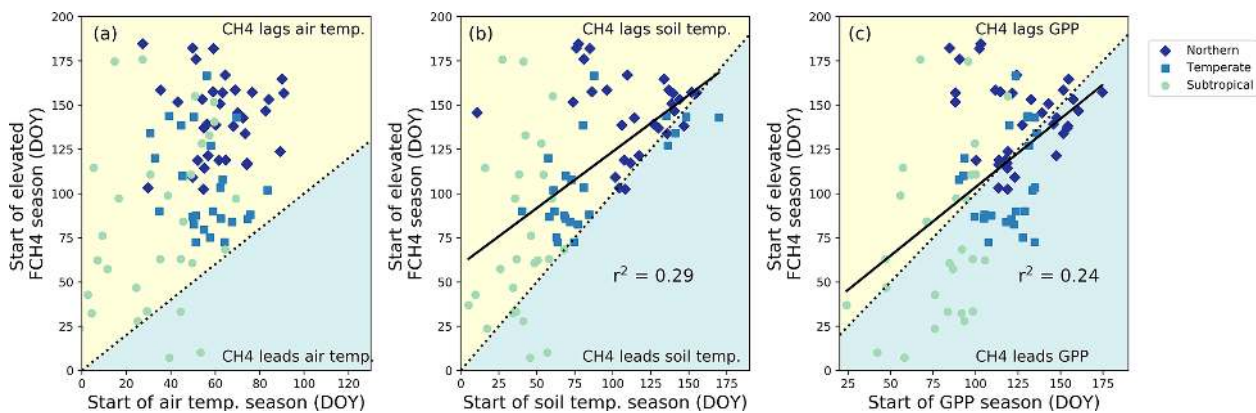


Figure 11. Relationship between the onset of the methane (CH₄) emission season to (a) the beginning of the air warming by day of year (DOY), (b) soil warming at the shallowest probe depth per site by DOY, and (c) gross primary productivity (GPP) increase for the subset of sites with soil temperature data by DOY. Each point represents a site year of data. Dashed lines represent a 1 : 1 relationship, and solid lines are significant ($p < 0.05$) regression fits. On average, the CH₄ emission season lags behind the soil temperature increase by 31 ± 40 d and is more synchronous with GPP.

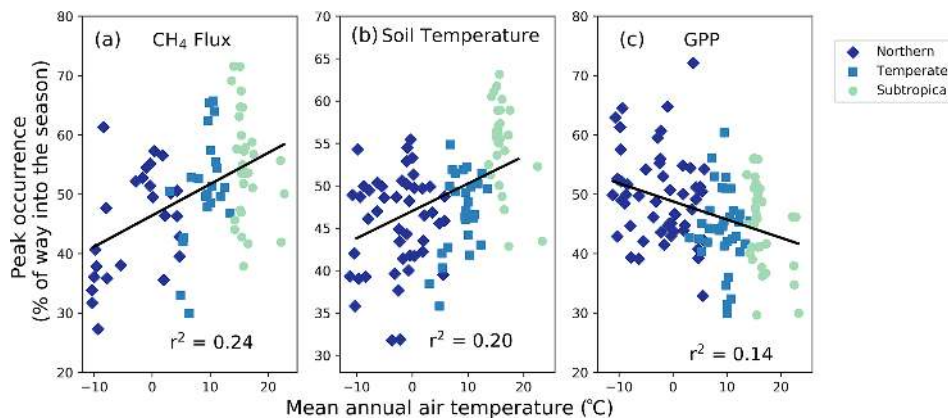


Figure 12. Site-year peak methane (CH₄) emissions (a) and peak soil temperature (b) occur earlier in the season for sites with lower mean annual temperatures. (c) Gross primary productivity (GPP) tends to peak earlier in the season for warmer sites, though the trend is weak. All r^2 values are significant at $p < 0.001$. Each point represents a site year of data.

Table 2. Site identification (SITE_ID), data DOI, and DOI reference for each FLUXNET-CH₄ site.

| SITE_ID | DOI | DOI_REFERENCE |
|---------|---|---------------------------------|
| AT-Neu | https://doi.org/10.18140/FLX/1669365 | Wohlfahrt (2020) |
| BR-Npw | https://doi.org/10.18140/FLX/1669368 | Vourlitis et al. (2020) |
| BW-Gum | https://doi.org/10.18140/FLX/1669370 | Helfter (2020a) |
| BW-Nxr | https://doi.org/10.18140/FLX/1669518 | Helfter (2020b) |
| CA-SCB | https://doi.org/10.18140/FLX/1669613 | Sonnentag and Helbig (2020a) |
| CA-SCC | https://doi.org/10.18140/FLX/1669628 | Sonnentag and Helbig (2020b) |
| CH-Cha | https://doi.org/10.18140/FLX/1669629 | Merbold et al. (2020a) |
| CH-Dav | https://doi.org/10.18140/FLX/1669630 | Merbold et al. (2020b) |
| CH-Oe2 | https://doi.org/10.18140/FLX/1669631 | Maier et al. (2020) |
| CN-Hgu | https://doi.org/10.18140/FLX/1669632 | Niu and Chen (2020) |
| DE-Dgw | https://doi.org/10.18140/FLX/1669633 | Sachs and Wille (2020a) |
| DE-Hte | https://doi.org/10.18140/FLX/1669634 | Koebisch and Jurasinski (2020) |
| DE-SfN | https://doi.org/10.18140/FLX/1669635 | Schmid and Klatt (2020) |
| DE-Zrk | https://doi.org/10.18140/FLX/1669636 | Sachs and Wille (2020b) |
| FI-Hyy | https://doi.org/10.18140/FLX/1669637 | Mammarella et al. (2020) |
| FI-Lom | https://doi.org/10.18140/FLX/1669638 | Lohila et al. (2020) |
| FI-Si2 | https://doi.org/10.18140/FLX/1669639 | Vesala et al. (2020a) |
| FI-Sii | https://doi.org/10.18140/FLX/1669640 | Vesala et al. (2020b) |
| FR-LGt | https://doi.org/10.18140/FLX/1669641 | Jacotot et al. (2020) |
| HK-MPM | https://doi.org/10.18140/FLX/1669642 | Lai (2020) |
| ID-Pag | https://doi.org/10.18140/FLX/1669643 | Sakabe et al. (2020) |
| IT-BCi | https://doi.org/10.18140/FLX/1669644 | Famulari (2020) |
| IT-Cas | https://doi.org/10.18140/FLX/1669645 | Manca and Goded (2020) |
| JP-BBY | https://doi.org/10.18140/FLX/1669646 | Ueyama et al. (2020) |
| JP-Mse | https://doi.org/10.18140/FLX/1669647 | Iwata (2020a) |
| JP-SwL | https://doi.org/10.18140/FLX/1669648 | Iwata (2020b) |
| KR-CRK | https://doi.org/10.18140/FLX/1669649 | Ryu et al. (2020) |
| MY-MLM | https://doi.org/10.18140/FLX/1669650 | Wong et al. (2020) |
| NL-Hor | https://doi.org/10.18140/FLX/1669651 | Dolman et al. (2020a) |
| NZ-Kop | https://doi.org/10.18140/FLX/1669652 | Campbell and Goodrich (2020) |
| PH-RiF | https://doi.org/10.18140/FLX/1669653 | Alberto and Wassmann (2020) |
| RU-Ch2 | https://doi.org/10.18140/FLX/1669654 | Goeckede (2020) |
| RU-Che | https://doi.org/10.18140/FLX/1669655 | Merbold (2020) |
| RU-Cok | https://doi.org/10.18140/FLX/1669656 | Dolman et al. (2020b) |
| RU-Fy2 | https://doi.org/10.18140/FLX/1669657 | Varlagin (2020) |
| SE-Deg | https://doi.org/10.18140/FLX/1669659 | Nilsson and Peichl (2020) |
| UK-LBT | https://doi.org/10.18140/FLX/1670207 | Helfter (2020c) |
| US-A03 | https://doi.org/10.18140/FLX/1669661 | Billesbach and Sullivan (2020a) |
| US-A10 | https://doi.org/10.18140/FLX/1669662 | Billesbach and Sullivan (2020b) |
| US-Atq | https://doi.org/10.18140/FLX/1669663 | Zona and Oechel (2020a) |
| US-Beo | https://doi.org/10.18140/FLX/1669664 | Zona and Oechel (2020b) |
| US-Bes | https://doi.org/10.18140/FLX/1669665 | Zona and Oechel (2020c) |
| US-Bi1 | https://doi.org/10.18140/FLX/1669666 | Rey-Sanchez et al. (2020a) |
| US-Bi2 | https://doi.org/10.18140/FLX/1669667 | Rey-Sanchez et al. (2020b) |
| US-BZB | https://doi.org/10.18140/FLX/1669668 | Euskirchen and Edgar (2020a) |
| US-BZF | https://doi.org/10.18140/FLX/1669669 | Euskirchen and Edgar (2020b) |
| US-BZS | https://doi.org/10.18140/FLX/1669670 | Euskirchen and Edgar (2020c) |
| US-CRT | https://doi.org/10.18140/FLX/1669671 | Chen and Chu (2020a) |
| US-DPW | https://doi.org/10.18140/FLX/1669672 | Hinkle and Bracho (2020) |
| US-EDN | https://doi.org/10.18140/FLX/1669673 | Oikawa (2020) |
| US-EML | https://doi.org/10.18140/FLX/1669674 | Schuur (2020) |
| US-Ho1 | https://doi.org/10.18140/FLX/1669675 | Richardson and Hollinger (2020) |
| US-HRA | https://doi.org/10.18140/FLX/1669676 | Runkle et al. (2020) |
| US-HRC | https://doi.org/10.18140/FLX/1669677 | Reba et al. (2020) |
| US-ICs | https://doi.org/10.18140/FLX/1669678 | Euskirchen et al. (2020) |

Table 2. Continued.

| SITE_ID | DOI | DOI_REFERENCE |
|---------|---|--------------------------------|
| US-Ivo | https://doi.org/10.18140/FLX/1669679 | Zona and Oechel (2020d) |
| US-LA1 | https://doi.org/10.18140/FLX/1669680 | Holm et al. (2020a) |
| US-LA2 | https://doi.org/10.18140/FLX/1669681 | Holm et al. (2020b) |
| US-Los | https://doi.org/10.18140/FLX/1669682 | Desai (2020a) |
| US-MAC | https://doi.org/10.18140/FLX/1669683 | Sparks (2020) |
| US-MRM | https://doi.org/10.18140/FLX/1669684 | Schäfer (2020) |
| US-Myb | https://doi.org/10.18140/FLX/1669685 | Matthes et al. (2020) |
| US-NC4 | https://doi.org/10.18140/FLX/1669686 | Noormets et al. (2020) |
| US-NGB | https://doi.org/10.18140/FLX/1669687 | Torn and Dengel (2020a) |
| US-NGC | https://doi.org/10.18140/FLX/1669688 | Torn and Dengel (2020b) |
| US-ORv | https://doi.org/10.18140/FLX/1669689 | Bohrer and Morin (2020) |
| US-OWC | https://doi.org/10.18140/FLX/1669690 | Bohrer et al. (2020) |
| US-PFa | https://doi.org/10.18140/FLX/1669691 | Desai (2020b) |
| US-Snd | https://doi.org/10.18140/FLX/1669692 | Detto et al. (2020) |
| US-Sne | https://doi.org/10.18140/FLX/1669693 | Shortt et al. (2020) |
| US-Srr | https://doi.org/10.18140/FLX/1669694 | Windham-Myers et al. (2020) |
| US-StJ | https://doi.org/10.18140/FLX/1669695 | Vazquez-Lule and Vargas (2020) |
| US-Tw1 | https://doi.org/10.18140/FLX/1669696 | Valach et al. (2020a) |
| US-Tw3 | https://doi.org/10.18140/FLX/1669697 | Chamberlain et al. (2020) |
| US-Tw4 | https://doi.org/10.18140/FLX/1669698 | Eichelmann et al. (2020) |
| US-Tw5 | https://doi.org/10.18140/FLX/1669699 | Valach et al. (2020b) |
| US-Twt | https://doi.org/10.18140/FLX/1669700 | Knox et al. (2020) |
| US-Uaf | https://doi.org/10.18140/FLX/1669701 | Iwata et al. (2020) |
| US-WPT | https://doi.org/10.18140/FLX/1669702 | Chen and Chu (2020b) |

rounded by grassland (BW-NXR) and the other a permanently flooded lagoon covered in a floating papyrus mat (BW-GUM). The relatively low fluxes found at the two Southeast Asian peat forest sites indicate that these ecosystems may be smaller CH₄ sources than expected given their location in the humid tropics. Even the higher-emitting tropical sites in Brazil and Botswana are still well within the range of annual CH₄ flux typical in cooler latitudes (Fig. 1).

In addition to having highly variable CH₄ flux magnitudes, the tropical sites differ from each other in their seasonality. CH₄ flux hit a minimum around July for two sites (BW-GUM, latitude 18.965° S, and MY-MLM, latitude 1.46° N), while CH₄ flux increased through July and the subsequent months for the other Botswana site, BW-NXR (latitude 19.548° S). Site ID-Pag (latitude 2.32° S) had minimal seasonality, whereas the flooded forest site in Brazil (BR-NPW, latitude 16.49° S) had near-zero fluxes from approximately July to January and consistently high fluxes for the remainder of the year. The rice site PH-RiF (latitude 14.14° N) had two annual CH₄ flux peaks, which is consistent with some other rice sites and likely reflects management practices. Baseline CH₄ flux values also differed, with the two Botswana sites having the highest off-season fluxes (29 and 133 nmol m⁻² s⁻¹ for BW-NXR and BW-GUM, respectively, estimated by TIMESAT), MY-MLM having an intermediate baseline CH₄ flux (16 nmol m⁻² s⁻¹, estimated by TIMESAT), and the remainder of the sites having essen-

tially zero flux at baseline. While more tropical wetland data will be needed to extract broad-scale conclusions about these ecosystems, the six tropical sites in FLUXNET-CH₄ provide an important starting point for synthesis studies and highlight tropical wetland CH₄ variability.

4 Data availability

Half-hourly and daily aggregations are available for download at <https://fluxnet.org/data/fluxnet-ch4-community-product/> (for citations, please cite this study), along with a table containing site metadata compiled from Table B3. Variable descriptions and units are provided in Table B1 and at <https://fluxnet.org/data/fluxnet-ch4-community-product/> (last access: 7 April 2021). Each site has a unique FLUXNET-CH₄ DOI as listed in Table B3. All site data used in this analysis are available under the CC BY 4.0 (<https://creativecommons.org/licenses/by/4.0/>, last access: 6 July 2021) copyright policy (two additional sites in FLUXNET-CH₄ are available under the more restrictive Tier 2 data policy, <https://fluxnet.org/data/data-policy/> (last access: 6 July 2021); these sites are not used in our analysis). The individual site DOIs are provided below in Table 2. All seasonality parameters used in these analyses are available at <https://doi.org/10.5281/zenodo.4672601> (Delwiche et al., 2021).

5 Conclusions

The breadth and scope of CH₄ flux data in the FLUXNET-CH₄ dataset make it possible to study the global patterns of CH₄ fluxes, particularly for global freshwater wetlands which release a substantial fraction of atmospheric CH₄. To help data users understand seasonal patterns within the dataset, we provide the first global estimates of CH₄ flux patterns and predictors in CH₄ seasonality using freshwater wetland data. In the seasonality analysis, we find that, on average, the seasonal increase in CH₄ emissions begins about 3 months earlier and lasts about 4 months longer at the warmest sites compared with the coolest sites. We also find that the beginning of the CH₄ emission season lags behind the beginning of seasonal soil warming by approximately 1 month with almost no instances of CH₄ emissions increasing before temperature increases. Additionally, roughly half the sites have CH₄ emissions increasing prior to GPP increase, highlighting the importance of substrate versus temperature limitations on wetland CH₄ emissions. Furthermore, relative to warmer climates, wetland CH₄ emissions in cooler climates increase faster in the warming season and decrease slower in the cooling season. This phenomenon has previously been noted on a regional scale, and we show that it persists at the global scale. Constraining the seasonality of CH₄ fluxes on a global scale can help improve the accuracy of global wetland models.

FLUXNET-CH₄ is an important new resource for the research community, but critical data gaps and opportunities remain. The current FLUXNET-CH₄ dataset is biased towards sites in boreal and temperate regions, which influence the relationships presented in our analyses. Tropical ecosystems are estimated to account for 64 % of potential natural CH₄ emissions (< 30° N; Saunio et al., 2020) but only account for 13 % of the FLUXNET-CH₄ sites in the dataset. Unsurprisingly, tropical sites in our network do not represent the range of bioclimatic wetland conditions present in the tropics. Therefore, while maintaining flux towers in tropical ecosystems is challenging, it is necessary to further constrain the global CH₄ cycle. Coastal wetlands are also poorly represented in FLUXNET-CH₄ even though there is evidence of substantial CH₄ emissions from these ecosystems, and so better representation across salinity gradients is warranted. Lastly, the average time series for FLUXNET-CH₄ Version 1.0 is relatively short, only 3.7 site years on average compared with 7.2 for CO₂ sites in FLUXNET (Pastorello et al., 2020). Adding additional site years of data from existing sites, as a complement to adding new sites, will increase the community's ability to explain interannual variability in CH₄ emissions and seasonality. Nevertheless, FLUXNET-CH₄ is an important and unprecedented resource with which to diagnose and understand drivers of the global CH₄ cycle.

Appendix A

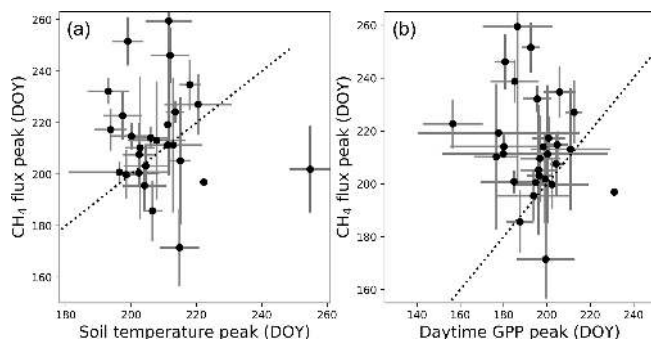


Figure A1. Peak methane (CH₄) flux timing versus peak gross primary productivity (GPP) timing (a) and peak soil temperature timing by day of year (b). Points represent site average, and error bars represent standard deviations. Dotted line represents 1 : 1 relationship.

Appendix B: FLUXNET-CH₄ data variables

This web page describes data variables and file formatting for the FLUXNET-CH₄ Community Product.

B1 Data variable: base names

Base names indicate fundamental quantities that are either measured or calculated/derived. They can also indicate quantified quality information.

B2 Data variable: qualifiers

Qualifiers are suffixes appended to variable base names that provide additional information about the variable. For example, the `_DT` qualifier in the variable label `GPP_DT` indicates that gross primary production (GPP) has been partitioned using the flux partitioning method from Lasslop et al. (2010).

Multiple qualifiers can be added, and they must follow the order in which they are presented here.

B2.1 Qualifiers: general

General qualifiers indicate additional information about a variable.

- `_F`: variable has been gap-filled by the FLUXNET-CH₄ team. Gaps in meteorological variables, including air temperature (TA), incoming shortwave (SW_IN) and longwave (LW_IN) radiation, vapor pressure deficit (VPD), pressure (PA), precipitation (P), and wind speed (WS), were filled with ERA-Interim (ERA-I) reanalysis data (Vuichard and Papale, 2015). Other variables were filled using the multidimensional scaling (MDS)

approach in REdyProc (see Delwiche et al., 2021, for more details).

- `_DT`: variable is acquired using the flux partitioning method from Lasslop et al. (2010), with values estimated by fitting the light-response curve.
- `_NT`: variable is acquired using the flux partitioning method from Reichstein et al. (2005), with values estimated from nighttime data and extrapolated to daytime.
- `_RANDUNC`: random uncertainty is introduced from several different sources including errors associated with the flux measurement system (gas analyzer, sonic anemometer, data acquisition system, flux calculations), errors associated with turbulent transport, and statistical errors relating to the location and activity of the sites of flux exchange (“footprint heterogeneity”) (Hollinger and Richardson, 2005).
- `_ANNOPTLM`: gap-filled variable uses an artificial neural net routine from Matlab with the Levenberg–Marquardt algorithm as the training function and parameters optimized across runs (more detail in Knox et al., 2016, 2019).
- `_UNC`: uncertainty is introduced from ANNOPTLM gap-filling routine, as described in Knox et al. (2016, 2019).
- `_QC`: this reports quality checks on FCH₄ gap-filled data (`_ANNOPTLM`) based on length of data gap: 1 signifies data gap shorter than 2 months, and 3 signifies data gap exceeding 2 months which could lead to poor-quality gap-filled data.

B2.2 Qualifiers: positional (`_V`)

Positional qualifiers are used to indicate relative positions of observations at the site. For FLUXNET-CH₄, positional qualifiers are used to distinguish soil temperature probes for sites with more than one probe. Probe depths for each positional qualifier per site are included in the metadata file included with data download and also in Table B7 of Delwiche et al. (2021). For sites where the original database file release in AmeriFlux, AsiaFlux, or EuroFlux contains multiple probes at the same `_V` depth, we average values and report only the average for each `_V` position. The one exception to this is site US-UAF where the original positional qualifier from the data we downloaded from AmeriFlux had different depths for the same qualifier. We still averaged the probe data, so `_V` qualifiers from US-UAF represent an average of more than one depth.

B3 Missing data

Missing data are reported using `–9999`. Data for all days in a leap year are reported.

Table B1. Data variable names, descriptions, and units.

| Variable | Description | Units |
|-----------------|---|--|
| TIMEKEEPING | | |
| TIMESTAMP_START | ISO time stamp start of averaging period, used in half-hourly data | YYYYMMDDHHMM |
| TIMESTAMP_END | ISO time stamp end of averaging period, used in half-hourly data | YYYYMMDDHHMM |
| TIMESTAMP | ISO time stamp used in daily aggregation files | YYYYMMDD |
| MET_RAD | | |
| SW_IN | Shortwave radiation, incoming | W m ⁻² |
| SW_OUT | Shortwave radiation, outgoing | W m ⁻² |
| LW_IN | Longwave radiation, incoming | W m ⁻² |
| LW_OUT | Longwave radiation, outgoing | W m ⁻² |
| PPFD_IN | Photosynthetic photon flux density, incoming | μmol photon m ⁻² s ⁻¹ |
| PPFD_OUT | Photosynthetic photon flux density, outgoing | μmol photon m ⁻² s ⁻¹ |
| NETRAD | Net radiation | W m ⁻² |
| MET_WIND | | |
| USTAR | Friction velocity | m s ⁻¹ |
| WD | Wind direction | Decimal degrees |
| WS | Wind speed | m s ⁻¹ |
| HEAT | | |
| <i>H</i> | Sensible heat turbulent flux (with storage term if provided by site principal investigator) | W m ⁻² |
| <i>LE</i> | Latent heat turbulent flux (with storage term if provided by site principal investigator) | W m ⁻² |
| <i>G</i> | Soil heat flux | W m ⁻² |
| MET_ATM | | |
| PA | Atmospheric pressure | kPa |
| TA | Air temperature | °C |
| VPD | Vapor pressure deficit | hPa |
| RH | Relative humidity, range 0–100 | % |
| MET_PRECIP | | |
| <i>P</i> | Precipitation | mm |
| PRODUCTS | | |
| NEE | Net ecosystem exchange | μmol CO ₂ m ⁻² s ⁻¹ |
| GPP | Gross primary productivity | μmol CO ₂ m ⁻² s ⁻¹ |
| RECO | Ecosystem respiration | μmol CO ₂ m ⁻² s ⁻¹ |
| GASES | | |
| FCH4 | Methane (CH ₄) turbulent flux (no storage correction) | nmol CH ₄ m ⁻² s ⁻¹ |
| MET_SOIL | | |
| TS | Soil temperature | °C |
| WTD | Water table depth (negative values indicate below the surface) | m |

Table B2. Annual methane flux sum and uncertainty, annual mean soil temperature, and annual mean water table depth. Column headers are explained after the table.

| | SITE_ID | Year | Ann_Flux_g_C_m-2 | Ann_Flux_Uncertainty_g_C_m-2 | Mean_Soil_Temp_C | Mean_Water_Table_Depth_m |
|----|---------|------|------------------|------------------------------|------------------|--------------------------|
| 1 | AT-Neu | 2010 | 0.38 | 0.03 | 8.65 | NaN |
| 2 | AT-Neu | 2011 | 0.25 | 0.02 | 8.61 | NaN |
| 3 | AT-Neu | 2012 | NaN | NaN | 9.39 | NaN |
| 4 | BR-Npw | 2013 | NaN | NaN | NaN | NaN |
| 5 | BR-Npw | 2014 | NaN | NaN | 25.95 | NaN |
| 6 | BR-Npw | 2015 | 20.95 | 1.18 | 26.2 | -0.47 |
| 7 | BR-Npw | 2016 | 17.48 | 1.14 | 25.31 | -0.41 |
| 8 | BW-Gum | 2018 | 51.73 | 10.59 | NaN | NaN |
| 9 | BW-Nxr | 2018 | 47.32 | 3.70 | NaN | NaN |
| 10 | CA-SCB | 2014 | 10.42 | 0.66 | 9.6 | -0.15 |
| 11 | CA-SCB | 2015 | NaN | NaN | 5.58 | -0.1 |
| 12 | CA-SCB | 2016 | 12.12 | 0.31 | 5.38 | -0.15 |
| 13 | CA-SCB | 2017 | 9.48 | 0.27 | 6.32 | -0.21 |
| 14 | CA-SCC | 2013 | NaN | NaN | 7.2 | NaN |
| 15 | CA-SCC | 2014 | 4.94 | 0.12 | 4.38 | NaN |
| 16 | CA-SCC | 2015 | 6.76 | 0.15 | 3.15 | NaN |
| 17 | CA-SCC | 2016 | 6.76 | 0.12 | NaN | NaN |
| 18 | CH-Cha | 2012 | 2.13 | 0.38 | 11.88 | NaN |
| 19 | CH-Cha | 2013 | 2.30 | 0.36 | 10.89 | NaN |
| 20 | CH-Cha | 2014 | 3.46 | 0.40 | 12.2 | NaN |
| 21 | CH-Cha | 2015 | 3.93 | 0.68 | 11.93 | NaN |
| 22 | CH-Cha | 2016 | NaN | NaN | 12.28 | NaN |
| 23 | CH-Dav | 2016 | 1.21 | 0.40 | 4.33 | NaN |
| 24 | CH-Dav | 2017 | NaN | NaN | 4.41 | NaN |
| 25 | CH-Oe2 | 2018 | 0.29 | 0.13 | 12.32 | NaN |
| 26 | CN-Hgu | 2015 | NaN | NaN | NaN | NaN |
| 27 | CN-Hgu | 2016 | 0.81 | 0.16 | 7.26 | NaN |
| 28 | CN-Hgu | 2017 | 0.82 | 0.45 | 7.66 | NaN |
| 29 | DE-Dgw | 2015 | NaN | NaN | NaN | NaN |
| 30 | DE-Dgw | 2016 | 7.51 | 0.22 | NaN | NaN |
| 31 | DE-Dgw | 2017 | 10.42 | 0.16 | NaN | NaN |
| 32 | DE-Dgw | 2018 | NaN | NaN | NaN | NaN |
| 33 | DE-Hte | 2011 | 59.85 | 6.39 | NaN | -0.41 |
| 34 | DE-Hte | 2012 | 36.83 | 3.46 | NaN | -0.21 |
| 35 | DE-Hte | 2013 | 49.72 | 2.34 | NaN | -0.25 |
| 36 | DE-Hte | 2014 | NaN | NaN | 13.26 | -0.19 |
| 37 | DE-Hte | 2015 | 51.37 | 1.75 | 10.78 | -0.26 |
| 38 | DE-Hte | 2016 | 50.77 | 2.09 | 9.8 | -0.25 |
| 39 | DE-Hte | 2017 | 46.61 | 1.40 | 10.39 | -0.4 |
| 40 | DE-Hte | 2018 | 41.62 | 2.52 | 6.12 | -0.22 |
| 41 | DE-SfN | 2012 | NaN | NaN | NaN | -0.08 |
| 42 | DE-SfN | 2013 | 3.62 | 0.93 | 10.32 | -0.05 |
| 43 | DE-SfN | 2014 | NaN | NaN | 8.16 | NaN |
| 44 | DE-Zrk | 2013 | NaN | NaN | 13.03 | NaN |
| 45 | DE-Zrk | 2014 | NaN | NaN | 11.67 | NaN |
| 46 | DE-Zrk | 2015 | 30.76 | 1.00 | 10.85 | NaN |
| 47 | DE-Zrk | 2016 | 31.14 | 1.23 | 11.28 | 0.12 |
| 48 | DE-Zrk | 2017 | 29.10 | 0.87 | 10.84 | 0.31 |
| 49 | DE-Zrk | 2018 | 31.10 | 1.20 | 10.54 | 0.25 |
| 50 | FI-Hyy | 2016 | NaN | NaN | 5.41 | NaN |
| 51 | FI-Lom | 2006 | 13.77 | 0.76 | 4.47 | 0 |
| 52 | FI-Lom | 2007 | 17.22 | 0.25 | 4.33 | 0.04 |
| 53 | FI-Lom | 2008 | 15.52 | 0.22 | 3.79 | 0.06 |
| 54 | FI-Lom | 2009 | 17.63 | 0.27 | 3.98 | 0.02 |
| 55 | FI-Lom | 2010 | 13.78 | 0.29 | 3.71 | 0.03 |
| 56 | FI-Si2 | 2012 | 9.27 | 1.17 | 9.4 | 0.06 |
| 57 | FI-Si2 | 2013 | 10.22 | 1.17 | 10.47 | 0.13 |
| 58 | FI-Si2 | 2014 | NaN | NaN | 7.7 | 0.1 |
| 59 | FI-Si2 | 2015 | NaN | NaN | 8.18 | 0.09 |
| 60 | FI-Si2 | 2016 | NaN | NaN | 7.67 | 0.09 |
| 61 | FI-Sii | 2013 | 14.58 | 0.32 | 6.45 | 0.04 |
| 62 | FI-Sii | 2014 | 12.93 | 0.78 | 6.42 | 0.03 |

Table B2. Continued.

| | SITE_ID | Year | Ann_Flux_g_C_m-2 | Ann_Flux_Uncertainty_g_C_m-2 | Mean_Soil_Temp_C | Mean_Water_Table_Depth_m |
|-----|---------|------|------------------|------------------------------|------------------|--------------------------|
| 63 | FI-Sii | 2015 | NaN | NaN | 6.92 | -0.02 |
| 64 | FI-Sii | 2016 | 16.56 | 0.68 | 5.87 | -0.01 |
| 65 | FI-Sii | 2017 | 8.63 | 0.23 | 8.4 | 0.06 |
| 66 | FI-Sii | 2018 | 9.46 | 1.10 | 6.68 | 0.11 |
| 67 | FR-LGt | 2017 | NaN | NaN | 10.45 | -0.24 |
| 68 | FR-LGt | 2018 | 2.45 | 0.60 | 10.87 | -0.22 |
| 69 | HK-MPM | 2016 | 11.62 | 0.61 | 25.06 | -0.61 |
| 70 | HK-MPM | 2017 | 10.60 | 0.30 | 23.14 | -0.64 |
| 71 | HK-MPM | 2018 | 11.04 | 0.59 | NaN | -0.8 |
| 72 | ID-Pag* | 2016 | 0.09 | 0.07 | NaN | NaN |
| 73 | ID-Pag* | 2017 | 0.09 | 0.09 | NaN | NaN |
| 74 | IT-BCi | 2017 | NaN | NaN | 17.16 | NaN |
| 75 | IT-BCi | 2018 | NaN | NaN | 17.36 | NaN |
| 76 | IT-Cas | 2009 | 25.44 | 1.46 | 9.62 | NaN |
| 77 | IT-Cas | 2010 | 17.80 | 1.26 | 12.37 | NaN |
| 78 | JP-BBY | 2015 | 9.53 | 0.29 | 10.12 | 0 |
| 79 | JP-BBY | 2016 | 16.42 | 0.45 | 10.02 | 0 |
| 80 | JP-BBY | 2017 | 19.61 | 0.65 | 9.33 | -0.03 |
| 81 | JP-BBY | 2018 | NaN | NaN | 9.79 | -0.04 |
| 82 | JP-Mse | 2012 | 9.50 | 1.97 | 14.52 | 0.03 |
| 83 | JP-SwL | 2016 | 66.68 | 4.29 | NaN | 1.91 |
| 84 | KR-CRK | 2015 | NaN | NaN | 14.41 | 0.02 |
| 85 | KR-CRK | 2016 | 29.12 | 0.91 | 12.48 | 0.03 |
| 86 | KR-CRK | 2017 | 25.84 | 0.86 | 13.94 | 0.02 |
| 87 | KR-CRK | 2018 | 28.82 | 1.15 | 11.32 | 0.02 |
| 88 | MY-MLM | 2014 | 9.55 | 0.59 | 26.8 | -0.09 |
| 89 | MY-MLM | 2015 | NaN | NaN | 26.9 | -0.01 |
| 90 | NL-Hor | 2007 | NaN | NaN | 12.4 | NaN |
| 91 | NL-Hor | 2008 | NaN | NaN | 10.37 | NaN |
| 92 | NL-Hor | 2009 | NaN | NaN | 11.61 | NaN |
| 93 | NK-Kop | 2012 | 23.98 | 1.38 | 12.17 | -0.08 |
| 94 | NK-Kop | 2013 | 15.33 | 0.43 | 12.68 | -0.13 |
| 95 | NK-Kop | 2014 | 15.67 | 0.39 | 12.38 | -0.11 |
| 96 | NK-Kop | 2015 | 14.37 | 2.66 | 12.46 | -0.1 |
| 97 | PH-RiF | 2012 | NaN | NaN | 27.78 | NaN |
| 98 | PH-RiF | 2013 | 12.41 | 0.99 | 28.17 | NaN |
| 99 | PH-RiF | 2014 | NaN | NaN | 27.47 | NaN |
| 100 | RU-Ch2 | 2014 | 6.99 | 0.14 | -4.21 | NaN |
| 101 | RU-Ch2 | 2015 | 5.86 | 0.14 | -4.87 | NaN |
| 102 | RU-Ch2 | 2016 | NaN | NaN | -2.88 | NaN |
| 103 | RU-Che | 2014 | 3.84 | 0.14 | -3.31 | NaN |
| 104 | RU-Che | 2015 | 4.19 | 0.22 | -3.28 | NaN |
| 105 | RU-Che | 2016 | 4.24 | 0.19 | -1.65 | NaN |
| 106 | RU-Cok | 2008 | NaN | NaN | NaN | NaN |
| 107 | RU-Cok | 2009 | NaN | NaN | NaN | NaN |
| 108 | RU-Cok | 2010 | NaN | NaN | NaN | NaN |
| 109 | RU-Cok | 2011 | NaN | NaN | NaN | NaN |
| 110 | RU-Cok | 2012 | NaN | NaN | -0.46 | NaN |
| 111 | RU-Cok | 2013 | NaN | NaN | -5.73 | NaN |
| 112 | RU-Cok | 2014 | NaN | NaN | -4.82 | NaN |
| 113 | RU-Cok | 2015 | 4.45 | 0.15 | -4.4 | NaN |
| 114 | RU-Cok | 2016 | NaN | NaN | -11.1 | NaN |
| 115 | RU-Fy2 | 2015 | NaN | NaN | 9.83 | NaN |
| 116 | RU-Fy2 | 2016 | 2.69 | 0.59 | 6.88 | 0.68 |
| 117 | RU-Fy2 | 2017 | 2.17 | 0.52 | 6.1 | 0.19 |
| 118 | RU-Fy2 | 2018 | 5.66 | 1.37 | 6.48 | 0.79 |
| 119 | SE-Deg | 2014 | 11.24 | 1.98 | 5.02 | -0.02 |
| 120 | SE-Deg | 2015 | 11.11 | 0.08 | 5.04 | 0.02 |
| 121 | SE-Deg | 2016 | 11.19 | 0.15 | 5.19 | -0.01 |
| 122 | SE-Deg | 2017 | NaN | NaN | 4.19 | 0 |
| 123 | SE-Deg | 2018 | 9.42 | 0.09 | 5.49 | -0.03 |
| 124 | UK-LBT | 2011 | NaN | NaN | NaN | NaN |
| 125 | UK-LBT | 2012 | NaN | NaN | NaN | NaN |

Table B2. Continued.

| | SITE_ID | Year | Ann_Flux_g_C_m-2 | Ann_Flux_Uncertainty_g_C_m-2 | Mean_Soil_Temp_C | Mean_Water_Table_Depth_m |
|-----|---------|------|------------------|------------------------------|------------------|--------------------------|
| 126 | UK-LBT | 2013 | 50.50 | 0.97 | NaN | NaN |
| 127 | UK-LBT | 2014 | 42.57 | 2.25 | NaN | NaN |
| 128 | US-A03 | 2015 | NaN | NaN | -6.65 | NaN |
| 129 | US-A03 | 2016 | NaN | NaN | -6.14 | NaN |
| 130 | US-A03 | 2017 | 7.26 | 2.58 | -4.48 | NaN |
| 131 | US-A03 | 2018 | 4.35 | 0.62 | -4.93 | NaN |
| 132 | US-A10 | 2012 | NaN | NaN | NaN | NaN |
| 133 | US-A10 | 2013 | NaN | NaN | NaN | NaN |
| 134 | US-A10 | 2014 | NaN | NaN | NaN | NaN |
| 135 | US-A10 | 2015 | NaN | NaN | NaN | NaN |
| 136 | US-A10 | 2016 | NaN | NaN | NaN | NaN |
| 137 | US-A10 | 2017 | NaN | NaN | NaN | NaN |
| 138 | US-A10 | 2018 | NaN | NaN | NaN | NaN |
| 139 | US-Atq | 2013 | NaN | NaN | -5.65 | NaN |
| 140 | US-Atq | 2014 | 1.80 | 0.19 | -4.48 | NaN |
| 141 | US-Atq | 2015 | 1.75 | 0.11 | -0.43 | NaN |
| 142 | US-Atq | 2016 | 1.75 | 0.00 | NaN | NaN |
| 143 | US-Beo | 2013 | NaN | NaN | -2.67 | NaN |
| 144 | US-Beo | 2014 | 2.74 | 0.05 | -4.95 | NaN |
| 145 | US-Bes | 2013 | NaN | NaN | -6.01 | NaN |
| 146 | US-Bes | 2014 | 3.32 | 0.04 | -5.69 | NaN |
| 147 | US-Bes | 2015 | 3.06 | 0.54 | -6.24 | NaN |
| 148 | US-Bil | 2016 | NaN | NaN | 15.62 | NaN |
| 149 | US-Bil | 2017 | NaN | NaN | 17.17 | NaN |
| 150 | US-Bil | 2018 | 0.69 | 0.29 | 16.82 | NaN |
| 151 | US-Bi2 | 2017 | 0.86 | 0.20 | 20.42 | NaN |
| 152 | US-Bi2 | 2018 | 1.69 | 0.29 | 17.12 | NaN |
| 153 | US-BZB | 2014 | 8.02 | 4.61 | 4.03 | NaN |
| 154 | US-BZB | 2015 | 7.52 | 0.82 | 3.9 | NaN |
| 155 | US-BZB | 2016 | 11.61 | 2.25 | 4.89 | NaN |
| 156 | US-BZF | 2014 | 6.61 | 0.63 | 4.32 | NaN |
| 157 | US-BZF | 2015 | 10.82 | 0.90 | 3.99 | NaN |
| 158 | US-BZF | 2016 | NaN | NaN | 5.93 | NaN |
| 159 | US-BZS | 2015 | 0.68 | 0.68 | 0.48 | NaN |
| 160 | US-BZS | 2016 | 0.89 | 0.27 | 0.67 | NaN |
| 161 | US-CRT | 2011 | 2.21 | 0.15 | 11.49 | -0.92 |
| 162 | US-CRT | 2012 | 2.21 | 0.11 | 12.38 | -1.45 |
| 163 | US-DPW | 2013 | NaN | NaN | NaN | NaN |
| 164 | US-DPW | 2014 | 58.91 | 0.69 | NaN | NaN |
| 165 | US-DPW | 2015 | NaN | NaN | NaN | NaN |
| 166 | US-DPW | 2016 | 43.60 | 1.29 | NaN | NaN |
| 167 | US-DPW | 2017 | 43.60 | 0.06 | NaN | NaN |
| 168 | US-EDN | 2018 | -0.04 | 0.06 | NaN | NaN |
| 169 | US-EML | 2015 | NaN | NaN | 5.71 | NaN |
| 170 | US-EML | 2016 | 1.04 | 0.08 | 3.07 | NaN |
| 171 | US-EML | 2017 | 0.36 | 0.27 | 3.8 | NaN |
| 172 | US-EML | 2018 | 0.36 | 0.07 | NaN | NaN |
| 173 | US-Ho1 | 2012 | NaN | NaN | NaN | -0.43 |
| 174 | US-Ho1 | 2013 | -0.05 | 0.02 | NaN | -0.33 |
| 175 | US-Ho1 | 2014 | -0.04 | 0.02 | NaN | -0.38 |
| 176 | US-Ho1 | 2015 | -0.16 | 0.01 | NaN | -0.48 |
| 177 | US-Ho1 | 2016 | -0.22 | 0.01 | NaN | -0.57 |
| 178 | US-Ho1 | 2017 | -0.24 | 0.01 | NaN | -0.56 |
| 179 | US-Ho1 | 2018 | -0.24 | 0.01 | NaN | NaN |
| 180 | US-HRA | 2017 | -0.24 | 0.56 | NaN | NaN |
| 181 | US-HRC | 2017 | -0.24 | 0.81 | NaN | NaN |
| 182 | US-ICs | 2014 | NaN | NaN | -1.55 | NaN |
| 183 | US-ICs | 2015 | NaN | NaN | -0.62 | NaN |
| 184 | US-ICs | 2016 | NaN | NaN | -1.48 | NaN |
| 185 | US-Ivo | 2013 | NaN | NaN | 3.19 | NaN |
| 186 | US-Ivo | 2014 | 5.05 | 0.22 | 0.02 | NaN |
| 187 | US-Ivo | 2015 | 3.89 | 0.27 | 0.47 | NaN |

Table B2. Continued.

| | SITE_ID | Year | Ann_Flux_g_C_m-2 | Ann_Flux_Uncertainty_g_C_m-2 | Mean_Soil_Temp_C | Mean_Water_Table_Depth_m |
|-----|---------|------|------------------|------------------------------|------------------|--------------------------|
| 188 | US-Ivo | 2016 | 5.77 | 0.55 | -1.01 | NaN |
| 189 | US-LA1 | 2011 | NaN | NaN | 18.92 | NaN |
| 190 | US-LA1 | 2012 | 12.68 | 0.63 | 24.23 | NaN |
| 191 | US-LA2 | 2011 | 12.68 | 0.19 | NaN | NaN |
| 192 | US-LA2 | 2012 | 48.42 | 1.57 | 23.09 | NaN |
| 193 | US-LA2 | 2013 | 43.34 | 1.32 | 23.19 | NaN |
| 194 | US-Los | 2014 | 6.66 | 1.48 | 8.3 | -0.06 |
| 195 | US-Los | 2015 | 5.51 | 0.40 | 5.65 | -0.1 |
| 196 | US-Los | 2016 | 8.67 | 0.35 | 6.3 | -0.07 |
| 197 | US-Los | 2017 | 6.00 | 0.33 | 5.5 | -0.09 |
| 198 | US-Los | 2018 | 5.71 | 0.37 | 4.29 | -0.19 |
| 199 | US-MAC | 2013 | 5.71 | 2.68 | NaN | NaN |
| 200 | US-MAC | 2014 | 26.37 | 1.69 | 23.18 | -0.71 |
| 201 | US-MAC | 2015 | 15.40 | 0.85 | 23.29 | -0.55 |
| 202 | US-MRM | 2012 | 0.30 | 0.19 | 11.16 | NaN |
| 203 | US-MRM | 2013 | 0.37 | 0.14 | 8.99 | NaN |
| 204 | US-Myb | 2010 | NaN | NaN | NaN | 0.95 |
| 205 | US-Myb | 2011 | 33.83 | 0.72 | 17.18 | 1.23 |
| 206 | US-Myb | 2012 | 64.20 | 0.58 | 16.25 | 1.12 |
| 207 | US-Myb | 2013 | 59.81 | 0.92 | 15.7 | 1.19 |
| 208 | US-Myb | 2014 | 58.97 | 0.68 | 11.27 | 1.24 |
| 209 | US-Myb | 2015 | 60.85 | 0.55 | NaN | 1.3 |
| 210 | US-Myb | 2016 | 45.72 | 0.48 | NaN | 1.22 |
| 211 | US-Myb | 2017 | 30.32 | 0.84 | 18.5 | 1.35 |
| 212 | US-Myb | 2018 | 29.33 | 0.55 | 17.05 | 1.19 |
| 213 | US-NC4 | 2012 | 38.28 | 1.70 | 17.12 | NaN |
| 214 | US-NC4 | 2013 | 18.60 | 3.88 | NaN | NaN |
| 215 | US-NC4 | 2014 | 26.98 | 0.60 | 18.02 | NaN |
| 216 | US-NC4 | 2015 | 23.37 | 2.30 | 16.27 | NaN |
| 217 | US-NC4 | 2016 | 62.20 | 2.78 | 16.35 | NaN |
| 218 | US-NGB | 2012 | NaN | NaN | NaN | NaN |
| 219 | US-NGB | 2013 | NaN | NaN | NaN | NaN |
| 220 | US-NGB | 2014 | NaN | NaN | NaN | NaN |
| 221 | US-NGB | 2015 | NaN | NaN | NaN | NaN |
| 222 | US-NGB | 2016 | NaN | NaN | NaN | NaN |
| 223 | US-NGB | 2017 | 2.31 | 0.11 | NaN | NaN |
| 224 | US-NGB | 2018 | 2.52 | 0.22 | NaN | NaN |
| 225 | US-NGC | 2017 | 2.52 | 0.06 | NaN | NaN |
| 226 | US-NGC | 2018 | 2.52 | 0.05 | NaN | NaN |
| 227 | US-ORv | 2011 | 3.53 | 0.54 | 16.64 | NaN |
| 228 | US-ORv | 2012 | 9.11 | 0.45 | 14.23 | NaN |
| 229 | US-ORv | 2013 | 7.70 | 0.41 | 13.19 | NaN |
| 230 | US-ORv | 2014 | 8.46 | 0.26 | 12 | NaN |
| 231 | US-ORv | 2015 | NaN | NaN | 13.36 | NaN |
| 232 | US-OWC | 2015 | NaN | NaN | 22.11 | 0.9 |
| 233 | US-OWC | 2016 | 113.99 | 3.25 | 21.19 | 0.54 |
| 234 | US-PFa | 2010 | NaN | NaN | NaN | NaN |
| 235 | US-PFa | 2011 | 0.34 | 0.05 | NaN | NaN |
| 236 | US-PFa | 2012 | 0.30 | 0.04 | NaN | NaN |
| 237 | US-PFa | 2013 | 0.31 | 0.05 | NaN | NaN |
| 238 | US-PFa | 2014 | NaN | NaN | NaN | NaN |
| 239 | US-PFa | 2015 | 0.63 | 0.03 | NaN | NaN |
| 240 | US-PFa | 2016 | 0.85 | 0.02 | NaN | NaN |
| 241 | US-PFa | 2017 | 0.80 | 0.06 | NaN | NaN |
| 242 | US-PFa | 2018 | NaN | NaN | NaN | NaN |
| 243 | US-Snd | 2010 | NaN | NaN | 16.85 | NaN |
| 244 | US-Snd | 2011 | NaN | NaN | 14.96 | NaN |
| 245 | US-Snd | 2012 | 6.34 | 0.25 | 16.06 | NaN |
| 246 | US-Snd | 2013 | 6.04 | 0.48 | 16.59 | -0.65 |
| 247 | US-Snd | 2014 | 3.23 | 0.36 | 17.52 | -0.78 |
| 248 | US-Snd | 2015 | 3.23 | 0.21 | NaN | NaN |
| 249 | US-Sne | 2016 | NaN | NaN | 17.85 | -0.2 |

Table B2. Continued.

| | SITE_ID | Year | Ann_Flux_g_C_m-2 | Ann_Flux_Uncertainty_g_C_m-2 | Mean_Soil_Temp_C | Mean_Water_Table_Depth_m |
|-----|---------|------|------------------|------------------------------|------------------|--------------------------|
| 250 | US-Sne | 2017 | 45.96 | 0.40 | 17.05 | 0.16 |
| 251 | US-Sne | 2018 | 39.63 | 0.66 | 16.83 | 0.09 |
| 252 | US-Srr | 2014 | 0.71 | 0.10 | NaN | NaN |
| 253 | US-Srr | 2015 | 0.88 | 0.11 | NaN | NaN |
| 254 | US-Srr | 2016 | 0.86 | 0.10 | 16.3 | -0.18 |
| 255 | US-Srr | 2017 | 0.86 | 0.11 | NaN | NaN |
| 256 | US-StJ | 2016 | 9.55 | 1.04 | 11.66 | -0.26 |
| 257 | US-Tw1 | 2011 | 26.09 | 2.70 | 14.01 | NaN |
| 258 | US-Tw1 | 2012 | NaN | NaN | 11.58 | 0.24 |
| 259 | US-Tw1 | 2013 | 33.93 | 1.78 | 11.92 | 0.25 |
| 260 | US-Tw1 | 2014 | 49.60 | 1.67 | 13.14 | 0.25 |
| 261 | US-Tw1 | 2015 | 54.80 | 2.58 | 12.79 | 0.33 |
| 262 | US-Tw1 | 2016 | 45.93 | 1.90 | 12.91 | 0.41 |
| 263 | US-Tw1 | 2017 | 38.66 | 2.09 | 12.53 | 0.38 |
| 264 | US-Tw1 | 2018 | 27.60 | 1.64 | 12.1 | 0.24 |
| 265 | US-Tw3 | 2013 | NaN | NaN | 19.63 | NaN |
| 266 | US-Tw3 | 2014 | NaN | NaN | 17.91 | NaN |
| 267 | US-Tw4 | 2013 | NaN | NaN | NaN | NaN |
| 268 | US-Tw4 | 2014 | 16.26 | 0.39 | NaN | 0.48 |
| 269 | US-Tw4 | 2015 | 27.61 | 0.43 | 17.2 | 0.36 |
| 270 | US-Tw4 | 2016 | 33.49 | 0.37 | 14.8 | 0.18 |
| 271 | US-Tw4 | 2017 | 47.95 | 0.58 | 13.78 | 0.07 |
| 272 | US-Tw4 | 2018 | 37.41 | 0.48 | 13.02 | 0.08 |
| 273 | US-Tw5 | 2018 | 59.72 | 1.15 | 16.67 | 0.69 |
| 274 | US-Twt | 2009 | NaN | NaN | 17.66 | -0.01 |
| 275 | US-Twt | 2010 | 9.87 | 1.15 | 15.67 | -0.18 |
| 276 | US-Twt | 2011 | 12.32 | 4.92 | 14.95 | -0.11 |
| 277 | US-Twt | 2012 | 8.12 | 0.51 | 16.05 | -0.04 |
| 278 | US-Twt | 2013 | 12.64 | 0.48 | 15.98 | -0.11 |
| 279 | US-Twt | 2014 | 17.02 | 0.97 | 17.44 | -0.09 |
| 280 | US-Twt | 2015 | 14.43 | 0.38 | 17.04 | -0.14 |
| 281 | US-Twt | 2016 | 11.07 | 0.59 | 16.44 | -0.29 |
| 282 | US-Twt | 2017 | 11.07 | 0.31 | NaN | NaN |
| 283 | US-Uaf | 2011 | 0.32 | 0.04 | -2.14 | -0.17 |
| 284 | US-Uaf | 2012 | NaN | NaN | -2.43 | -0.18 |
| 285 | US-Uaf | 2013 | NaN | NaN | -1.15 | -0.18 |
| 286 | US-Uaf | 2014 | NaN | NaN | -1.18 | -0.13 |
| 287 | US-Uaf | 2015 | NaN | NaN | -0.49 | -0.12 |
| 288 | US-Uaf | 2016 | 0.68 | 0.05 | -0.05 | -0.1 |
| 289 | US-Uaf | 2017 | 0.58 | 0.06 | 1.09 | -0.13 |
| 290 | US-Uaf | 2018 | NaN | NaN | 0.87 | -0.13 |
| 291 | US-WPT | 2011 | 41.05 | 1.57 | 17.22 | 0.43 |
| 292 | US-WPT | 2012 | 54.96 | 1.71 | 14.27 | 0.28 |
| 293 | US-WPT | 2013 | 52.76 | 1.29 | 12.89 | 0.44 |

* Data from ID-Pag spans 365 d from June 2016 to June 2017. Annual methane flux for each year is the sum of these 365 d, with uncertainty being calculated separately for each year.

| Column | Description |
|--|---|
| SITE_ID | Site identification code as assigned by regional flux data network |
| Year | Data year |
| Ann_Flux_g_C_m ⁻² | Total annual methane flux (g C m ⁻²) |
| Ann_Flux_Uncertainty_g_C_m ⁻² | Gap-filling and random uncertainty associated with annual flux (g C m ⁻²) |
| Mean_Soil_Temp_C | Annual mean soil temperature (degree C). For sites with multiple probes, we use the probe closest to the surface. |
| Mean_Water_Table_Depth_m | Annual mean water table depth (m) |

Table B3. Metadata and select data for FLUXNET-CH₄ sites.

| (a) SITE_ID | SITE_NAME | SITE_PERSONNEL | COUNTRY | LAT | LONG | DATA_DOI | YEAR_START | YEAR_END | UTC_OFFSET | ORIGINAL_SOURCE |
|-------------|-----------|------------------------------------|-------------|---------|----------|---|------------|----------|------------|-----------------|
| 1 | AT-Neu | Neustift | Austria | 47.117 | 11.318 | https://doi.org/10.18140/FLX/1669365 | 2010 | 2012 | 1 | EuroFlux |
| 2 | BR-Npw | Northern Pantanal Wetland | Brazil | -16.498 | -56.412 | https://doi.org/10.18140/FLX/1669368 | 2013 | 2016 | -4 | AmeriFlux |
| 3 | BW-Gum | Guma | Botswana | -18.965 | 22.371 | https://doi.org/10.18140/FLX/1669370 | 2018 | 2018 | 2 | EuroFlux |
| 4 | BW-Nxr | Nxaraga | Botswana | -19.548 | 23.179 | https://doi.org/10.18140/FLX/1669518 | 2018 | 2018 | 2 | EuroFlux |
| 5 | CA-SCB | Scotty Creek Bog | Canada | 61.309 | -121.298 | https://doi.org/10.18140/FLX/1669613 | 2014 | 2017 | -7 | AmeriFlux |
| 6 | CA-SCC | Scotty Creek Landscape | Canada | 61.308 | -121.299 | https://doi.org/10.18140/FLX/1669628 | 2013 | 2016 | -7 | AmeriFlux |
| 7 | CH-Cha | Chamau | Switzerland | 47.210 | 8.410 | https://doi.org/10.18140/FLX/1669629 | 2012 | 2016 | 1 | EuroFlux |
| 8 | CH-Dav | Davos | Switzerland | 46.815 | 9.856 | https://doi.org/10.18140/FLX/1669630 | 2016 | 2017 | 1 | EuroFlux |
| 9 | CH-Oe2 | Oensingen crop | Switzerland | 47.286 | 7.734 | https://doi.org/10.18140/FLX/1669631 | 2018 | 2018 | 1 | EuroFlux |
| 10 | CN-Hgu | Hongyuan | China | 32.845 | 102.590 | https://doi.org/10.18140/FLX/1669632 | 2015 | 2017 | 8 | EuroFlux |
| 11 | DE-Dgw | Dagowsee | Germany | 53.151 | 13.054 | https://doi.org/10.18140/FLX/1669633 | 2015 | 2018 | 1 | EuroFlux |
| 12 | DE-Hie | Huetelmoor | Germany | 54.210 | 12.176 | https://doi.org/10.18140/FLX/1669634 | 2011 | 2018 | 1 | EuroFlux |
| 13 | DE-SFN | Schechenfliz Nord | Germany | 47.806 | 11.328 | https://doi.org/10.18140/FLX/1669635 | 2012 | 2014 | 1 | EuroFlux |
| 14 | DE-Zrk | Zamekow | Germany | 53.876 | 12.889 | https://doi.org/10.18140/FLX/1669636 | 2013 | 2018 | 1 | EuroFlux |
| 15 | FI-Hyy | Hyytiälä | Finland | 61.847 | 24.295 | https://doi.org/10.18140/FLX/1669637 | 2016 | 2016 | 2 | EuroFlux |
| 16 | FI-Lom | Lompolojankka | Finland | 67.997 | 24.209 | https://doi.org/10.18140/FLX/1669638 | 2006 | 2010 | 2 | EuroFlux |
| 17 | FI-Si2 | Siikaneva-2 Bog | Finland | 61.837 | 24.197 | https://doi.org/10.18140/FLX/1669639 | 2012 | 2016 | 2 | EuroFlux |
| 18 | FI-Sii | Siikaneva | Finland | 61.833 | 24.193 | https://doi.org/10.18140/FLX/1669640 | 2013 | 2018 | 2 | EuroFlux |
| 19 | FR-LGt | La Guette | France | 47.323 | 2.284 | https://doi.org/10.18140/FLX/1669641 | 2017 | 2018 | 1 | EuroFlux |
| 20 | HK-MPM | Mai Po Mangrove | Hong Kong | 22.498 | 114.029 | https://doi.org/10.18140/FLX/1669642 | 2016 | 2018 | 8 | EuroFlux |
| 21 | ID-Pag | Palangkaraya undrained forest | Indonesia | -2.320 | 113.900 | https://doi.org/10.18140/FLX/1669643 | 2016 | 2017 | 7 | EuroFlux |
| 22 | IT-BCi | Borgo Cioffi | Italy | 40.524 | 14.957 | https://doi.org/10.18140/FLX/1669644 | 2017 | 2018 | 1 | EuroFlux |
| 23 | IT-Cas | Castellaro | Italy | 45.070 | 8.718 | https://doi.org/10.18140/FLX/1669645 | 2009 | 2010 | 1 | EuroFlux |
| 24 | JP-BBY | Bibai bog | Japan | 43.323 | 141.811 | https://doi.org/10.18140/FLX/1669646 | 2015 | 2018 | 9 | AsiaFlux |
| 25 | JP-Mse | Mase rice paddy field | Japan | 36.054 | 140.027 | https://doi.org/10.18140/FLX/1669647 | 2012 | 2012 | 9 | AsiaFlux |
| 26 | JP-SwL | Suwa Lake | Japan | 36.047 | 138.108 | https://doi.org/10.18140/FLX/1669648 | 2016 | 2016 | 9 | AsiaFlux |
| 27 | KR-CKK | Cheorwon Rice paddy | Korea | 38.201 | 127.251 | https://doi.org/10.18140/FLX/1669649 | 2015 | 2018 | 9 | AsiaFlux |
| 28 | MY-MLM | Maludam National Park | Malaysia | 1.454 | 111.149 | https://doi.org/10.18140/FLX/1669650 | 2014 | 2015 | 8 | AsiaFlux |
| 29 | NL-Hor | Horstermeer | Netherlands | 52.240 | 5.071 | https://doi.org/10.18140/FLX/1669651 | 2007 | 2009 | 1 | EuroFlux |
| 30 | NZ-Kop | Kopuaiti | New Zealand | -37.388 | 175.554 | https://doi.org/10.18140/FLX/1669652 | 2012 | 2015 | 13 | OzFlux |
| 31 | PH-RIF | Philippines Rice Institute flooded | Philippines | 14.141 | 121.265 | https://doi.org/10.18140/FLX/1669653 | 2012 | 2014 | 8 | EuroFlux |
| 32 | RU-Ch2 | Chersky reference | Russia | 68.617 | 161.351 | https://doi.org/10.18140/FLX/1669654 | 2014 | 2016 | 11 | EuroFlux |
| 33 | RU-Che | Chersky | Russia | 68.613 | 161.341 | https://doi.org/10.18140/FLX/1669655 | 2014 | 2016 | 11 | EuroFlux |
| 34 | RU-Cok | Chokurdakh | Russia | 70.829 | 147.494 | https://doi.org/10.18140/FLX/1669656 | 2008 | 2016 | 11 | EuroFlux |
| 35 | RU-Fy2 | Fyodorovskoye dry spruce | Russia | 56.448 | 32.902 | https://doi.org/10.18140/FLX/1669657 | 2015 | 2018 | 3 | EuroFlux |
| 36 | SE-Deg | Degero | Sweden | 64.182 | 19.557 | https://doi.org/10.18140/FLX/1669659 | 2014 | 2018 | 1 | EuroFlux |
| 37 | UK-LBT | London_BT | UK | 51.522 | -0.139 | https://doi.org/10.18140/FLX/1670207 | 2011 | 2014 | 0 | EuroFlux |
| 38 | US-A03 | ARM-AMF3-Oliktok | USA | 70.495 | -149.882 | https://doi.org/10.18140/FLX/1669661 | 2015 | 2018 | -9 | AmeriFlux |
| 39 | US-A10 | ARM-NSA-Barrow | USA | 71.324 | -156.615 | https://doi.org/10.18140/FLX/1669662 | 2012 | 2018 | -9 | AmeriFlux |
| 40 | US-Atq | Atkasuk | USA | 70.470 | -157.409 | https://doi.org/10.18140/FLX/1669663 | 2013 | 2016 | -9 | AmeriFlux |
| 41 | US-Beo | Barrow Environmental | USA | 71.281 | -156.612 | https://doi.org/10.18140/FLX/1669664 | 2013 | 2014 | -8 | AmeriFlux |
| 42 | US-Bes | Barrow-Bes (Biocomplexity | USA | 71.281 | -156.597 | https://doi.org/10.18140/FLX/1669665 | 2013 | 2015 | -8 | AmeriFlux |
| 43 | US-B11 | Experiment South tower | USA | 38.099 | -121.499 | https://doi.org/10.18140/FLX/1669666 | 2016 | 2018 | -8 | AmeriFlux |
| 44 | US-B12 | Bouldin Island Alfalfa | USA | 38.109 | -121.535 | https://doi.org/10.18140/FLX/1669667 | 2017 | 2018 | -8 | AmeriFlux |
| 45 | US-BZB | Bonanza Creek Thermokarst Bog | USA | 64.696 | -148.321 | https://doi.org/10.18140/FLX/1669668 | 2014 | 2016 | -9 | AmeriFlux |
| 46 | US-BZF | Bonanza Creek Rich Fen | USA | 64.704 | -148.313 | https://doi.org/10.18140/FLX/1669669 | 2014 | 2016 | -9 | AmeriFlux |
| 47 | US-BZS | Bonanza Creek Black Spruce | USA | 64.696 | -148.324 | https://doi.org/10.18140/FLX/1669670 | 2015 | 2016 | -9 | AmeriFlux |
| 48 | US-CRT | Curtice Walter-Berger cropland | USA | 41.628 | -83.347 | https://doi.org/10.18140/FLX/1669671 | 2011 | 2012 | -5 | AmeriFlux |
| 49 | US-DPW | Disney Wilderness Preserve Wetland | USA | 28.052 | -81.436 | https://doi.org/10.18140/FLX/1669672 | 2013 | 2017 | -5 | AmeriFlux |

Table B3. Continued.

| SITE_ID | SITE_NAME | SITE_PERSONNEL | COUNTRY | LAT | Lon | DATA_DOI | YEAR_START | YEAR_END | UTC_OFFSET | ORIGINAL_DATA_SOURCE |
|---------|--|------------------------------------|---------|--------|----------|---|------------|----------|------------|----------------------|
| 50 | US-EDN Eden Landing Ecological Reserve | Patry Okawa | USA | 37.616 | -122.114 | https://doi.org/10.18140/FLX/1669673 | 2018 | 2018 | -8 | AmeriFlux |
| 51 | US-EML Eight Mile Lake Permafrost thaw gradient, Healy Alaska | Ted Schuur | USA | 63.878 | -149.254 | https://doi.org/10.18140/FLX/1669674 | 2015 | 2018 | -9 | AmeriFlux |
| 52 | US-H01 Howland Forest (main tower) | Andrew Richardson, David Hollinger | USA | 45.204 | -68.740 | https://doi.org/10.18140/FLX/1669675 | 2012 | 2018 | -5 | AmeriFlux |
| 53 | US-HRA Humnoke Farm Rice Field – Field A | Benjamin Runkle | USA | 34.585 | -91.752 | https://doi.org/10.18140/FLX/1669676 | 2017 | 2017 | -6 | AmeriFlux |
| 54 | US-HRC Humnoke Farm Rice Field – Field C | Benjamin Runkle | USA | 34.589 | -91.752 | https://doi.org/10.18140/FLX/1669677 | 2017 | 2017 | -6 | AmeriFlux |
| 55 | US-ICs Imnavat Creek Watershed Wet Sedge Tundra | Eugenie Euskirchen | USA | 68.606 | -149.311 | https://doi.org/10.18140/FLX/1669678 | 2014 | 2016 | -9 | AmeriFlux |
| 56 | US-Iwo Ivotuk | Donatella Zona | USA | 68.487 | -155.750 | https://doi.org/10.18140/FLX/1669679 | 2013 | 2016 | -9 | AmeriFlux |
| 57 | US-LA1 Pointe-aux-Chenes Brackish Marsh | Ken Krauss | USA | 29.501 | -90.445 | https://doi.org/10.18140/FLX/1669680 | 2011 | 2012 | -6 | AmeriFlux |
| 58 | US-LA2 Salvador WMA Freshwater Marsh | Ken Krauss | USA | 29.859 | -90.287 | https://doi.org/10.18140/FLX/1669681 | 2011 | 2013 | -6 | AmeriFlux |
| 59 | US-Los Lost Creek | Ankur Desai | USA | 46.083 | -89.979 | https://doi.org/10.18140/FLX/1669682 | 2014 | 2018 | -6 | AmeriFlux |
| 60 | US-MAC MacArthur Agro-Ecology Marsh Resource Meadowlands | Jed Sparks, Sam Chamberlain | USA | 27.163 | -81.187 | https://doi.org/10.18140/FLX/1669683 | 2013 | 2015 | -5 | AmeriFlux |
| 61 | US-MRM Marsh Resource Meadowlands Mitigation Bank | Karina Schäfer | USA | 40.816 | -74.044 | https://doi.org/10.18140/FLX/1669684 | 2012 | 2013 | 5 | AmeriFlux |
| 62 | US-Myb Mayberry Wetland | Dennis Baldoocchi | USA | 38.050 | -121.765 | https://doi.org/10.18140/FLX/1669685 | 2010 | 2018 | -8 | AmeriFlux |
| 63 | US-NC4 NC_AlligatorRiver | Asko Noormets | USA | 35.788 | -75.904 | https://doi.org/10.18140/FLX/1669686 | 2012 | 2016 | -5 | AmeriFlux |
| 64 | US-NGB NGEE Arctic Barrow | Margaret Tom | USA | 71.280 | -156.609 | https://doi.org/10.18140/FLX/1669687 | 2012 | 2018 | -9 | AmeriFlux |
| 65 | US-NGC NGEE Arctic Council | Margaret Tom | USA | 64.861 | -163.701 | https://doi.org/10.18140/FLX/1669688 | 2017 | 2018 | -9 | AmeriFlux |
| 66 | US-ORv Olenangy River Wetland Research Park | Gil Bohrer | USA | 40.020 | -83.018 | https://doi.org/10.18140/FLX/1669689 | 2011 | 2015 | -5 | AmeriFlux |
| 67 | US-OWC Old Woman Creek | Gil Bohrer | USA | 41.380 | -82.512 | https://doi.org/10.18140/FLX/1669690 | 2015 | 2016 | -5 | AmeriFlux |
| 68 | US-PFA Park Falls/WLEF | Ankur Desai | USA | 45.946 | -90.272 | https://doi.org/10.18140/FLX/1669691 | 2010 | 2018 | -6 | AmeriFlux |
| 69 | US-Snd Sherman Island | Dennis Baldoocchi | USA | 38.037 | -121.754 | https://doi.org/10.18140/FLX/1669692 | 2010 | 2015 | -8 | AmeriFlux |
| 70 | US-Sne Sherman Island Restored Wetland | Dennis Baldoocchi | USA | 38.037 | -121.755 | https://doi.org/10.18140/FLX/1669693 | 2016 | 2018 | -8 | AmeriFlux |
| 71 | US-Srr Suisun marsh – Rush Ranch | Lisamarie Windham-Myers | USA | 38.201 | -122.026 | https://doi.org/10.18140/FLX/1669694 | 2014 | 2017 | -8 | AmeriFlux |
| 72 | US-SU St James Reserve | Rodrigue Vargas | USA | 39.088 | -75.437 | https://doi.org/10.18140/FLX/1669695 | 2016 | 2016 | -5 | AmeriFlux |
| 73 | US-Tw1 Twitchell Wetland West Pond | Dennis Baldoocchi | USA | 38.107 | -121.647 | https://doi.org/10.18140/FLX/1669696 | 2011 | 2018 | -8 | AmeriFlux |
| 74 | US-Tw3 Twitchell Alfalfa | Dennis Baldoocchi | USA | 38.116 | -121.647 | https://doi.org/10.18140/FLX/1669697 | 2013 | 2014 | -8 | AmeriFlux |
| 75 | US-Tw4 Twitchell East End Wetland | Dennis Baldoocchi | USA | 38.103 | -121.641 | https://doi.org/10.18140/FLX/1669698 | 2013 | 2018 | -8 | AmeriFlux |
| 76 | US-Tw5 East Pond Wetland | Dennis Baldoocchi | USA | 38.107 | -121.643 | https://doi.org/10.18140/FLX/1669699 | 2018 | 2018 | -8 | AmeriFlux |
| 77 | US-Twt Twitchell Island | Dennis Baldoocchi | USA | 38.109 | -121.653 | https://doi.org/10.18140/FLX/1669700 | 2009 | 2017 | -8 | AmeriFlux |
| 78 | US-Uaf University of Alaska, Fairbanks | Masahito Ueyama | USA | 64.866 | -147.856 | https://doi.org/10.18140/FLX/1669701 | 2011 | 2018 | -9 | AmeriFlux |
| 79 | US-WPT Winous Point North Marsh | Jiqun Chen, Housen Chu | USA | 41.465 | -82.996 | https://doi.org/10.18140/FLX/1669702 | 2011 | 2013 | -5 | AmeriFlux |

Table B3. Continued.

| (b) SITE_ID | SITE_CLASSIFICATION | UPLAND_CLASS | IGBP | KOP-PEN | MEAN_ANNUAL_TEMP_C_WORLDCLIM | MEAN_ANNUAL_PRECIP_MM_WORLDCLIM | MOSS_BROWN | MOSS_SPHAGNUM | AERENCHYMATOUS | ERI_SHRUB | TREE | DOM_VEG | IN_SEASONALITY_ANALYSIS |
|-------------|---------------------|--------------|------|---------|------------------------------|---------------------------------|------------|---------------|----------------|-----------|------|----------------|-------------------------|
| 1 | AT-Neu | Upland | GRA | Dfb | 7.0 | 1029 | 0 | 0 | 1 | 0 | 0 | 0 | aerenchymatous |
| 2 | BR-Npw | Swamp | WSA | Aw | 25.2 | 1318 | 0 | 0 | 1 | 0 | 1 | tree | 0 |
| 3 | BW-Ginn | Swamp | WET | Bsh | 23.1 | 459 | 0 | 0 | 1 | 0 | 1 | aerenchymatous | 0 |
| 4 | BW-Nxr | Swamp | GRA | Bsh | 23.5 | 433 | 0 | 0 | 1 | 0 | 1 | aerenchymatous | 0 |
| 5 | CA-SCB | Bog | WET | Dfc | -2.8 | 414 | 0 | 1 | 1 | 1 | 0 | moss_sphagnum | 1 |
| 6 | CA-SCC | Upland | ENF | Dfc | -2.9 | 414 | 0 | 1 | 0 | 0 | 0 | tree | 0 |
| 7 | CH-Cha | Upland | GRA | Cfb | 9.6 | 1194 | 0 | 0 | 0 | 0 | 0 | aerenchymatous | 0 |
| 8 | CH-Dav | Upland | ENF | ET | 3.8 | 1053 | 1 | 0 | 0 | 1 | 1 | tree | 0 |
| 9 | CH-Oc2 | Upland | CRO | Cfb | 9.1 | 1122 | 0 | 0 | 0 | 0 | 0 | aerenchymatous | 0 |
| 10 | CN-Hgu | Upland | CRO | Cvc | 2.8 | 702 | 0 | 0 | 1 | 0 | 0 | aerenchymatous | 0 |
| 11 | DE-Dgw | Lake | WAT | Cfb | 8.3 | 567 | 0 | 0 | 0 | 0 | 0 | no vegetation | 0 |
| 12 | DE-Hte | Fen | WET | Dfb | 8.5 | 584 | 0 | 0 | 1 | 0 | 0 | aerenchymatous | 1 |
| 13 | DE-SIN | Bog | WET | Cfb | 8.3 | 1123 | 0 | 1 | 1 | 1 | 1 | tree | 1 |
| 14 | DE-Zrk | Fen | WET | Dfb | 8.3 | 580 | 0 | 0 | 0 | 0 | 0 | aerenchymatous | 1 |
| 15 | FI-Hyy | Upland | ENF | Dfc | 3.1 | 671 | 1 | 1 | 0 | 1 | 1 | tree | 0 |
| 16 | FI-Lom | Fen | WET | Dfc | -1.0 | 512 | 1 | 1 | 1 | 1 | 1 | aerenchymatous | 1 |
| 17 | FI-SI2 | Bog | WET | Dfc | 3.2 | 664 | 0 | 1 | 1 | 1 | 1 | moss_sphagnum | 1 |
| 18 | FI-Sii | Fen | WET | Dfc | 3.2 | 666 | 0 | 1 | 1 | 1 | 1 | moss_sphagnum | 1 |
| 19 | FR-LGt | Fen | WET | Cfb | 11.0 | 707 | 0 | 1 | 1 | 0 | 0 | aerenchymatous | 1 |
| 20 | HK-MPM | Mangrove | EBF | Cfa | 22.7 | 1991 | 0 | 0 | 1 | 0 | 1 | aerenchymatous | 0 |
| 21 | ID-Pag | Swamp | EBF | Af | 27.4 | 2386 | 0 | 0 | 1 | 0 | 1 | tree | 0 |
| 22 | IT-BGt | Upland | CRO | Csa | 16.3 | 1035 | 0 | 0 | 1 | 0 | 0 | aerenchymatous | 0 |
| 23 | IT-Cas | Rice | CRO | Cfa | 12.3 | 773 | 0 | 0 | 1 | 0 | 0 | aerenchymatous | 0 |
| 24 | JP-BBY | Bog | WET | Dfb | 6.7 | 1153 | 0 | 1 | 1 | 1 | 0 | aerenchymatous | 1 |
| 25 | JP-Mse | Rice | CRO | Cfa | 14.1 | 1305 | 0 | 0 | 1 | 0 | 0 | aerenchymatous | 0 |
| 26 | JP-SwL | Lake | WAT | Dfb | 10.2 | 1141 | 0 | 0 | 1 | 0 | 0 | aerenchymatous | 0 |
| 27 | KR-CRK | Rice | EBF | Af | 9.9 | 1234 | 0 | 0 | 1 | 0 | 0 | aerenchymatous | 0 |
| 28 | MY-MLM | Swamp | GRA | Cfb | 26.9 | 3401 | 0 | 0 | 1 | 0 | 1 | tree | 0 |
| 29 | NL-Hor | Drained | GRA | Cfb | 9.7 | 827 | 0 | 0 | 1 | 0 | 0 | aerenchymatous | 0 |
| 30 | NZ-Kop | Bog | EBF | Cfb | 13.9 | 1343 | 0 | 1 | 1 | 0 | 0 | aerenchymatous | 1 |
| 31 | PH-RIF | Rice | CRO | Am | 26.9 | 2010 | 0 | 0 | 1 | 0 | 0 | aerenchymatous | 0 |
| 32 | RU-Ch2 | Wet tundra | WET | Dfc | -12.3 | 172 | 0 | 0 | 1 | 1 | 0 | aerenchymatous | 1 |
| 33 | RU-Che | Drained | WET | Dfc | -12.3 | 172 | 0 | 0 | 1 | 1 | 0 | aerenchymatous | 0 |
| 34 | RU-Cok | Wet tundra | OSH | Dfc | -14.1 | 210 | 0 | 1 | 1 | 1 | 0 | moss_sphagnum | 0 |
| 35 | RU-Fy2 | Upland | ENF | Dfb | 4.3 | 694 | 0 | 1 | 0 | 1 | 1 | tree | 0 |
| 36 | SE-Deg | Fen | GRA | Dfc | 1.7 | 620 | 0 | 1 | 1 | 1 | 0 | moss_sphagnum | 1 |
| 37 | UK-LBT | Upland | URB | Cfb | 11.0 | 646 | 0 | 0 | 0 | 0 | 0 | no vegetation | 0 |
| 38 | US-A03 | Wet tundra | BSV | ET | -11.9 | 144 | 0 | 1 | 1 | 0 | 0 | moss_sphagnum | 0 |
| 39 | US-A10 | Wet tundra | BSV | ET | -12.0 | 107 | 0 | 1 | 1 | 0 | 0 | moss_sphagnum | 0 |
| 40 | US-A1q | Wet tundra | WET | ET | -10.3 | 133 | 1 | 0 | 1 | 1 | 0 | aerenchymatous | 1 |
| 41 | US-Beo | Wet tundra | WET | ET | -11.9 | 109 | 1 | 0 | 1 | 0 | 0 | aerenchymatous | 1 |
| 42 | US-Bes | Wet tundra | WET | ET | -12.0 | 109 | 0 | 1 | 0 | 0 | 0 | aerenchymatous | 1 |
| 43 | US-BI1 | Drained | CRO | Csa | 15.5 | 382 | 0 | 0 | 1 | 0 | 0 | aerenchymatous | 0 |
| 44 | US-BI2 | Drained | CRO | Csa | 15.5 | 380 | 0 | 0 | 1 | 0 | 0 | aerenchymatous | 0 |
| 45 | US-BZB | Bog | WET | Dfd | -2.4 | 292 | 1 | 1 | 1 | 0 | 0 | eri_shrub | 1 |
| 46 | US-BZF | Fen | WET | Dfd | -2.5 | 294 | 1 | 1 | 1 | 0 | 0 | aerenchymatous | 1 |
| 47 | US-BZS | Upland | ENF | Dfd | -2.4 | 292 | 1 | 0 | 0 | 0 | 1 | tree | 0 |
| 48 | US-CRT | Upland | CRO | Dfa | 9.7 | 855 | 0 | 0 | 1 | 0 | 0 | aerenchymatous | 0 |
| 49 | US-DPW | Marsh | WET | Cwa | 22.1 | 1223 | 0 | 0 | 1 | 0 | 0 | aerenchymatous | 1 |
| 50 | US-EDN | Salt marsh | WET | Csa | 14.9 | 403 | 0 | 0 | 1 | 0 | 0 | aerenchymatous | 0 |

Table B3. Continued.

| SITE_ID | SITE_CLASSIFICATION | UPLAND_CLASS | IGBP | KOP-PEN | MEAN_ANNUAL_TEMP_C_WORLDCLIM | MEAN_ANNUAL_PRECIP_MML_WORLDCLIM | MOSS_BROWN | MOSS_SPHAGNUM | AERENCHYMATOUS | ERI_SHRUB | TREE | DOM_VEG | IN_SEASONALITY_ANALYSIS |
|---------|---------------------|--------------|------|---------|------------------------------|----------------------------------|------------|---------------|----------------|-----------|------|---------------|-------------------------|
| 51 | US-EMU | Upland | OSH | ET | -3.3 | 421 | 1 | 0 | 1 | 1 | 0 | aerenchymatus | 0 |
| 52 | US-Hol | Upland | ENF | Dbh | 5.7 | 1069 | 0 | 0 | 0 | 0 | 1 | tree | 0 |
| 53 | US-HRA | Rice | CRO | Cla | 16.8 | 1290 | 0 | 0 | 1 | 0 | 0 | aerenchymatus | 0 |
| 54 | US-HRC | Rice | CRO | Cla | 16.8 | 1290 | 0 | 0 | 1 | 0 | 0 | aerenchymatus | 0 |
| 55 | US-ICs | Wet tundra | WET | ET | -8.9 | 242 | 1 | 0 | 1 | 1 | 0 | aerenchymatus | 1 |
| 56 | US-Iwo | Wet tundra | WET | ET | -8.5 | 247 | 1 | 0 | 1 | 1 | 0 | aerenchymatus | 1 |
| 57 | US-LA1 | Salt marsh | WET | Cla | 20.4 | 1596 | 0 | 0 | 1 | 0 | 0 | aerenchymatus | 0 |
| 58 | US-LA2 | Marsh | WET | Cla | 20.0 | 1616 | 0 | 0 | 1 | 0 | 0 | aerenchymatus | 1 |
| 59 | US-Los | Fen | WET | Dbh | 4.1 | 833 | 0 | 0 | 1 | 1 | 1 | ert_shrub | 1 |
| 60 | US-MAC | Drained | WET | Cwa | 22.7 | 1207 | 0 | 0 | 0 | 0 | 0 | aerenchymatus | 0 |
| 61 | US-MBM | Salt marsh | WET | Cla | 12.0 | 1211 | 0 | 0 | 1 | 0 | 0 | aerenchymatus | 0 |
| 62 | US-Mjb | Marsh | WET | Csa | 15.4 | 346 | 0 | 0 | 1 | 0 | 0 | aerenchymatus | 1 |
| 63 | US-NC4 | Swamp | WET | Cla | 16.5 | 1322 | 0 | 0 | 1 | 0 | 1 | aerenchymatus | 1 |
| 64 | US-NGB | Wet tundra | SNO | ET | -11.9 | 109 | 0 | 1 | 1 | 0 | 0 | moss_sphagnum | 0 |
| 65 | US-NGC | Wet tundra | GRA | ET | -3.1 | 413 | 0 | 1 | 1 | 1 | 0 | ert_shrub | 0 |
| 66 | US-ORv | Marsh | WET | Cla | 11.0 | 954 | 0 | 0 | 1 | 0 | 0 | aerenchymatus | 1 |
| 67 | US-ORw | Marsh | WET | Dbh | 9.9 | 898 | 0 | 0 | 1 | 0 | 0 | aerenchymatus | 1 |
| 68 | US-Pra | Upland | MF | Dbh | 4.3 | 826 | 0 | 0 | 0 | 0 | 1 | tree | 0 |
| 69 | US-Snd | Drained | GRA | Csa | 15.5 | 340 | 0 | 0 | 1 | 0 | 0 | aerenchymatus | 0 |
| 70 | US-Sne | Marsh | GRA | Csa | 15.5 | 340 | 0 | 0 | 1 | 0 | 0 | aerenchymatus | 1 |
| 71 | US-Sr | Salt marsh | WET | Csa | 15.4 | 541 | 0 | 0 | 1 | 0 | 0 | aerenchymatus | 0 |
| 72 | US-SJ1 | Salt marsh | WET | Cla | 13.0 | 1133 | 0 | 0 | 1 | 0 | 0 | aerenchymatus | 0 |
| 73 | US-Tw1 | Marsh | WET | Csa | 15.4 | 371 | 0 | 0 | 1 | 0 | 0 | aerenchymatus | 1 |
| 74 | US-Tw3 | Drained | CRO | Csa | 15.4 | 371 | 0 | 0 | 1 | 0 | 0 | aerenchymatus | 0 |
| 75 | US-Tw4 | Marsh | WET | Csa | 15.4 | 370 | 0 | 0 | 1 | 0 | 0 | aerenchymatus | 1 |
| 76 | US-Tw5 | Marsh | WET | Csa | 15.4 | 371 | 0 | 0 | 1 | 0 | 0 | aerenchymatus | 1 |
| 77 | US-Tw6 | Rice | CRO | Csa | 15.3 | 372 | 0 | 0 | 1 | 0 | 0 | aerenchymatus | 0 |
| 78 | US-Uaf | Bog | ENF | Dwc | -2.8 | 298 | 1 | 1 | 1 | 1 | 1 | moss_sphagnum | 0 |
| 79 | US-WPT | Marsh | WET | Dia | 9.9 | 881 | 0 | 0 | 1 | 0 | 0 | aerenchymatus | 1 |

Table B3. Continued.

| (c) SITE_ID_ID | Mean_Air_Temp_C | Mean_Air_Temp_stddev_C | Ann_Flux_g_CH4-C_m-2 | Ann_Flux_stddev_g_CH4-C_m-2 | JFM_flux_g_CH4-C_m-2 | JFM_flux_stddev_g_CH4-C_m-2 | JFM_flux_stddev_g_CH4-C_m-2 | AMJ_flux_g_CH4-C_m-2 | AMJ_flux_stddev_g_CH4-C_m-2 | JAS_flux_g_CH4-C_m-2 | JAS_flux_stddev_g_CH4-C_m-2 | OND_flux_g_CH4-C_m-2 | OND_flux_stddev_g_CH4-C_m-2 |
|----------------|-----------------|------------------------|----------------------|-----------------------------|----------------------|-----------------------------|-----------------------------|----------------------|-----------------------------|----------------------|-----------------------------|----------------------|-----------------------------|
| 1 | AF-Neu | 6.60 | 0.51 | 0.32 | 0.09 | 0.03 | 0.03 | 0.05 | 0.04 | 0.16 | 0.07 | 0.09 | 0.01 |
| 2 | BR-Npw | 25.44 | 0.73 | 19.21 | 2.45 | 9.68 | 1.46 | 19.32 | 1.15 | 0.01 | 0.16 | 0.15 | |
| 3 | BW-Cum | 22.79 | 51.73 | 47.32 | | | | 8.88 | | 16.90 | | 18.09 | |
| 4 | BW-Nxr | 23.06 | 1.92 | 10.67 | 1.34 | | | 2.96 | 0.70 | 6.58 | 0.77 | 1.16 | 0.11 |
| 5 | CA-SCB | -0.75 | 2.04 | 6.15 | 1.05 | | | 1.79 | 0.45 | 3.41 | 0.67 | | |
| 6 | CA-SCC | -0.24 | 0.54 | 2.95 | 0.88 | | | 0.99 | 0.37 | 0.60 | 0.28 | 0.61 | 0.25 |
| 7 | CH-Chia | 9.74 | 0.09 | 1.21 | | 0.75 | 0.18 | 0.37 | 0.21 | 0.13 | | 0.24 | |
| 8 | CH-Duv | 4.37 | | | | 0.28 | 0.05 | 0.37 | | 0.14 | | 0.13 | |
| 9 | CH-Ose2 | 11.00 | | 0.29 | | | | | | 0.15 | | 0.15 | |
| 10 | CN-Hgu | 3.77 | 1.31 | 0.82 | 0.01 | | | 0.23 | 0.04 | 0.28 | 0.15 | 0.28 | |
| 11 | DE-Dgw | 9.72 | 0.38 | 8.97 | 2.06 | 0.07 | 0.06 | 1.49 | 0.57 | 4.15 | 0.76 | 2.51 | 1.05 |
| 12 | DE-Hte | 10.04 | 0.54 | 48.11 | 7.41 | 2.98 | 0.72 | 17.18 | 3.66 | 24.28 | 4.07 | 6.17 | 1.46 |
| 13 | DE-SIN | 8.28 | 0.72 | 3.62 | | 0.43 | 0.10 | 2.33 | | 1.67 | 0.43 | 0.72 | 0.25 |
| 14 | DE-Zrk | 9.55 | 0.51 | 30.53 | 0.96 | 1.18 | 0.24 | 12.27 | 1.55 | 16.18 | 1.47 | 1.51 | 0.56 |
| 15 | FI-Hyy | 4.36 | | | | | | | | -0.02 | | 0.05 | |
| 16 | FI-Lom | -0.35 | 0.78 | 15.58 | 1.83 | 0.93 | 0.22 | 3.75 | 0.51 | 9.49 | 1.25 | 1.68 | 0.24 |
| 17 | FI-Si2 | 5.14 | 0.84 | 9.74 | 0.67 | 0.68 | 0.11 | 2.71 | 0.59 | 5.83 | 1.15 | 1.19 | 0.08 |
| 18 | FI-Sii | 4.72 | 0.42 | 12.43 | 3.36 | 0.02 | | 3.34 | 0.75 | 6.79 | 2.90 | 1.58 | 0.42 |
| 19 | FR-LGt | 11.07 | 0.37 | 2.45 | | 0.02 | | 1.09 | | 0.85 | | 0.29 | |
| 20 | HK-MPM | 23.75 | 0.10 | 11.09 | 0.51 | 0.97 | | 2.33 | 0.52 | 5.56 | 0.34 | 2.95 | 0.26 |
| 21 | ID-Pag | 26.57 | 0.19 | 0.09 | 0.00 | -5.18 | | 0.13 | | -0.24 | | 0.05 | |
| 22 | IT-BCi | 16.69 | 0.39 | | | | | | | | | -2.69 | |
| 23 | IT-Cas | 12.58 | 0.58 | 21.62 | 5.40 | 0.60 | 0.39 | 5.59 | 3.71 | 15.31 | 2.24 | 0.42 | 0.12 |
| 24 | JP-BBY | 7.11 | 0.44 | 15.19 | 5.15 | 1.60 | | 2.61 | 0.97 | 8.27 | 2.60 | 3.67 | 0.03 |
| 25 | JP-Mse | 13.75 | | 9.50 | | | | 1.59 | | 7.42 | | 0.45 | |
| 26 | JP-SwL | 11.67 | | 66.68 | | | | | | 39.86 | | 18.53 | |
| 27 | KR-CRK | 10.96 | 0.46 | 27.92 | 1.81 | 0.92 | 0.15 | 8.81 | 0.92 | 16.69 | 1.77 | 1.25 | 0.11 |
| 28 | MY-MLM | 27.09 | 0.11 | 9.55 | | 3.28 | | 2.60 | 0.02 | 1.62 | | 2.34 | |
| 29 | NL-Hor | 10.75 | 0.60 | | | | | | | | | | |
| 30 | NZ-Kop | 13.68 | 0.28 | 17.34 | 4.46 | 3.99 | 0.84 | 3.03 | 1.63 | 3.63 | 0.52 | 5.87 | 0.30 |
| 31 | PH-RIF | 26.54 | 0.15 | 12.41 | | 3.57 | 1.02 | 2.58 | 2.66 | 5.53 | 0.01 | 3.34 | 0.28 |
| 32 | RU-Ch2 | -9.88 | 1.26 | 6.43 | 0.79 | 0.29 | | 0.87 | 0.09 | 4.65 | 0.48 | 1.44 | 0.04 |
| 33 | RU-Che | -9.77 | 1.25 | 4.09 | 0.22 | 0.37 | 0.00 | 0.47 | 0.08 | 2.18 | 0.12 | 1.19 | |
| 34 | RU-Cok | -12.38 | 0.92 | 4.45 | | | | 0.74 | 0.09 | 3.42 | | | |
| 35 | RU-Fy2 | 5.80 | 0.53 | 3.50 | 1.88 | 1.65 | 0.58 | -0.27 | 0.04 | -0.39 | 0.10 | 2.36 | 1.32 |
| 36 | SE-Deg | 2.57 | 0.77 | 10.74 | 0.88 | 0.59 | 0.55 | 3.30 | 0.29 | 5.70 | 0.78 | 1.44 | 0.09 |
| 37 | UK-LBT | 10.62 | 0.78 | 46.54 | 5.61 | 13.70 | 1.77 | 12.52 | 0.19 | 12.26 | 1.66 | 14.04 | 1.87 |
| 38 | US-A03 | -7.15 | 0.66 | 5.81 | 2.06 | | | 1.27 | | 3.25 | 0.32 | | |
| 39 | US-A10 | | | | | | | | | 1.08 | | | |
| 40 | US-Atq | -10.88 | 2.23 | 1.77 | 0.03 | 0.00 | | 0.30 | 0.07 | 1.05 | 0.03 | 0.55 | 0.12 |
| 41 | US-Beo | -9.50 | 0.20 | 2.74 | | 0.09 | | 0.58 | | 1.77 | | 0.69 | |
| 42 | US-Bes | -10.46 | 0.21 | 3.19 | 0.18 | 0.09 | | 0.58 | 0.26 | 2.20 | 0.18 | 0.71 | 0.05 |
| 43 | US-Bil | 13.87 | 1.20 | 0.69 | | 0.45 | 0.43 | -0.07 | 0.02 | -0.13 | 0.06 | 0.17 | 0.02 |
| 44 | US-Bi2 | 15.01 | 0.28 | 1.28 | 0.59 | 0.66 | | 0.30 | 0.21 | 0.10 | 0.21 | 0.54 | |
| 45 | US-BZB | -0.62 | 0.55 | 9.05 | 2.23 | | | 2.41 | 0.39 | 6.06 | 1.43 | 6.06 | |
| 46 | US-BZF | -0.31 | 0.55 | 8.72 | 2.98 | | | 3.21 | 2.77 | 6.35 | 2.24 | 2.24 | |
| 47 | US-BZS | 0.26 | 0.68 | | 0.15 | | | 0.23 | 0.01 | 0.53 | 0.11 | 0.59 | |
| 48 | US-CRT | 11.32 | 0.91 | 2.21 | 0.00 | 0.58 | | 0.15 | | 0.26 | | 0.26 | |
| 49 | US-DPW | 22.23 | 0.41 | 48.71 | 8.84 | 1.53 | 1.84 | 11.27 | 2.75 | 27.64 | 7.55 | 12.90 | 2.54 |
| 50 | US-EDN | 14.99 | | -0.04 | | | | -0.19 | | 0.16 | | | |

Table B3. Continued.

| SITE_ID | Mean_Air_Temp_C | Mean_Air_Temp_stddev_C | Ann_Flux_g_CH4-C_m-2 | Ann_Flux_stddev_g_CH4-C_m-2 | JFM_flux_g_CH4-C_m-2 | JFM_flux_stddev_g_CH4-C_m-2 | AMJ_flux_g_CH4-C_m-2 | AMJ_flux_stddev_g_CH4-C_m-2 | JAS_flux_g_CH4-C_m-2 | JAS_flux_stddev_g_CH4-C_m-2 | OND_flux_g_CH4-C_m-2 | OND_flux_stddev_g_CH4-C_m-2 |
|-----------|-----------------|------------------------|----------------------|-----------------------------|----------------------|-----------------------------|----------------------|-----------------------------|----------------------|-----------------------------|----------------------|-----------------------------|
| 51 US-EML | -1.72 | 3.76 | 0.59 | 0.39 | -0.03 | 0.27 | 0.06 | 0.17 | 0.35 | 0.12 | 0.27 | 0.42 |
| 52 US-Ho1 | 6.48 | 1.32 | -0.16 | 0.09 | -0.04 | 0.01 | -0.03 | 0.02 | -0.02 | 0.05 | -0.07 | 0.02 |
| 53 US-HRA | 19.36 | | -0.24 | | | | 1.28 | | 6.08 | | | |
| 54 US-HRC | 20.23 | 0.48 | -0.24 | | | | 3.07 | | 8.38 | | | |
| 55 US-ICS | -6.02 | | | | | | | | 1.23 | 0.30 | | |
| 56 US-Iwo | -8.27 | 0.54 | 4.90 | 0.95 | 0.70 | 0.02 | 0.80 | 0.05 | 2.55 | 0.54 | 1.26 | 0.42 |
| 57 US-LA1 | 24.12 | 0.42 | 12.68 | | 0.68 | | 2.27 | | 7.58 | | 1.39 | 1.08 |
| 58 US-LA2 | 20.34 | 4.43 | 34.81 | 19.34 | 4.27 | | 14.50 | 2.18 | 21.72 | 2.75 | 6.96 | 0.79 |
| 59 US-Los | 5.01 | 1.23 | 6.51 | 1.28 | 0.36 | 0.07 | 1.71 | 0.46 | 3.57 | 0.96 | 0.81 | 0.25 |
| 60 US-MAC | 23.15 | 0.96 | 15.82 | 10.34 | 1.32 | 0.02 | 3.71 | 2.07 | 14.70 | 5.53 | 2.81 | 0.25 |
| 61 US-MRM | 13.14 | 0.88 | 0.34 | 0.05 | 0.09 | 0.02 | 0.07 | 0.01 | 0.11 | 0.01 | 0.01 | |
| 62 US-MvB | 15.53 | 0.58 | 47.88 | 14.90 | 4.51 | 1.99 | 14.12 | 5.54 | 22.04 | 7.87 | 6.52 | 3.17 |
| 63 US-NC4 | 16.74 | 0.85 | 33.89 | 17.41 | 0.80 | 0.18 | 5.70 | 1.62 | 20.41 | 9.80 | 6.77 | 2.19 |
| 64 US-NGB | -9.45 | 0.92 | 2.41 | 0.15 | | | 0.26 | 0.15 | 2.00 | 0.26 | | |
| 65 US-NGC | 1.21 | 0.82 | 2.52 | 0.00 | | | | | 0.86 | 0.41 | | |
| 66 US-ORv | 12.20 | 0.92 | 7.20 | 2.51 | 0.88 | 0.10 | 2.55 | 0.93 | 3.14 | 1.16 | 0.99 | 0.17 |
| 67 US-OWC | 13.02 | 1.72 | 113.99 | | | | 31.03 | | 66.03 | 10.07 | 9.81 | |
| 68 US-Pfa | 5.42 | 1.24 | 0.54 | 0.25 | 0.15 | 0.05 | 0.39 | 0.19 | 0.00 | 0.00 | | |
| 69 US-Snd | 14.76 | 1.16 | 4.71 | 1.71 | 2.00 | 1.79 | 1.11 | 0.74 | 1.35 | 0.61 | 1.74 | 1.14 |
| 70 US-Sne | 15.04 | 0.45 | 42.80 | 4.48 | 2.44 | 0.71 | 14.95 | 5.12 | 12.61 | 10.68 | 4.71 | 3.54 |
| 71 US-Sr | 15.93 | 0.45 | 0.83 | 0.08 | 0.09 | 0.06 | 0.31 | 0.04 | 0.42 | 0.09 | 0.08 | 0.07 |
| 72 US-SU | 13.96 | | 9.55 | | | | 1.40 | | 5.24 | | 2.92 | |
| 73 US-Tw1 | 15.16 | 0.74 | 39.51 | 11.03 | 4.92 | 1.91 | 10.13 | 3.74 | 18.02 | 4.08 | 7.11 | 2.49 |
| 74 US-Tw3 | 16.04 | 0.87 | | | | | | | | | 0.29 | |
| 75 US-Tw4 | 15.52 | 0.56 | 32.54 | 11.74 | 4.39 | 1.75 | 9.49 | 4.83 | 12.78 | 6.07 | 5.89 | 1.83 |
| 76 US-Tw5 | 15.03 | 1.71 | 59.72 | 2.75 | 3.07 | 1.10 | 21.49 | 0.59 | 29.78 | 3.15 | 8.45 | |
| 77 US-Tw | 14.26 | 1.03 | 12.07 | 2.75 | 3.07 | 1.10 | 1.05 | 0.59 | 5.49 | 3.15 | 1.73 | 0.40 |
| 78 US-Ubf | -2.87 | 1.03 | 0.53 | 0.19 | | | 0.07 | | 0.33 | 0.12 | | |
| 79 US-WPT | 11.40 | 0.99 | 49.59 | 7.48 | 1.66 | 0.22 | 16.31 | 3.99 | 28.75 | 3.05 | 3.26 | 0.12 |

Table B3. Continued.

| (d) | SITE_ID | SOIL_TEMP_PROBE_DEPTHS |
|-----|---------|---|
| 1 | AT-Neu | TS_1 = -0.05 cm; TS_2 = -0.1 cm; TS_3 = -0.2 cm |
| 2 | BR-Npw | |
| 3 | BW-Gum | |
| 4 | BW-Nxr | |
| 5 | CA-SCB | TS_1 = 0 cm; TS_2 = -0.02 cm; TS_3 = -0.04 cm; TS_4 = -0.08 cm; TS_5 = -0.16 cm; TS_6 = -0.32 cm; TS_7 = -0.64 cm; TS_8 = -1.28 cm |
| 6 | CA-SCC | TS_1 = -0.1 cm; TS_2 = -0.15 cm; TS_3 = -0.2 cm; TS_4 = -0.25 cm; TS_5 = -0.3 cm; TS_6 = -0.5 cm; TS_7 = -0.6 cm; TS_8 = -0.7 cm |
| 7 | CH-Cha | TS_1 = -0.01 cm; TS_2 = -0.02 cm; TS_3 = -0.04 cm; TS_4 = -0.07 cm; TS_5 = -0.1 cm; TS_6 = -0.15 cm; TS_7 = -0.25 cm; TS_8 = -0.4 cm; TS_9 = -0.95 cm |
| 8 | CH-Dav | TS_1 = -0.05 cm; TS_2 = -0.15 cm; TS_3 = -0.5 cm |
| 9 | CH-Oe2 | TS_1 = -0.05 cm; TS_2 = -0.1 cm; TS_3 = -0.15 cm; TS_5 = -0.3 cm; TS_6 = -0.5 cm |
| 10 | CN-Hgu | |
| 11 | DE-Dgw | |
| 12 | DE-Hte | TS_1 = 0 cm; TS_2 = -0.1 cm; TS_3 = -0.2 cm |
| 13 | DE-SIN | TS_1 = -0.02 cm; TS_3 = -0.1 cm; TS_4 = -0.2 cm; TS_5 = -0.5 cm |
| 14 | DE-Zrk | TS_1 = -0.05 cm; TS_2 = -0.1 cm; TS_3 = -0.2 cm; TS_4 = -0.3 cm; TS_5 = -0.5 cm |
| 15 | FI-Hyy | TS_1 = -0.02 cm; TS_2 = -0.04 cm; TS_3 = -0.12 cm; TS_4 = -0.25 cm; TS_5 = -0.5 cm |
| 16 | FI-Lom | TS_1 = -0.07 cm; TS_2 = -0.3 cm; TS_3 = -0.5 cm |
| 17 | FI-Si2 | TS_1 = -0.05 cm; TS_2 = -0.2 cm; TS_3 = -0.35 cm; TS_4 = -0.5 cm; TS_5 = -0.7 cm; TS_6 = -1.0 cm; TS_7 = -1.5 cm; TS_8 = -2.0 cm; TS_9 = -2.5 cm |
| 18 | FI-Sii | before 2016 (TS_1 = -0.05 cm; TS_2 = -0.2 cm; TS_3 = -0.35 cm; TS_4 = -0.5 cm; TS_5 = -0.7 cm; TS_6 = -1.0 cm; TS_7 = -1.5 cm; TS_8 = -2.0 cm; TS_9 = -2.5 cm) after 2017 (TS_1 = 0 cm; TS_2 = -0.5 cm; TS_3 = -0.35 cm; TS_4 = -0.5 cm; TS_5 = -0.7 cm; TS_6 = -1.0 cm; TS_7 = -1.5 cm; TS_8 = -2.0 cm; TS_9 = -2.5 cm) |
| 19 | FR-LGt | TS_1 = -0.02 cm; TS_2 = -0.05 cm; TS_3 = -0.1 cm; TS_4 = -0.2 cm; TS_5 = -0.4 cm |
| 20 | HK-MPM | |
| 21 | ID-Pag | TS_1 = -0.05 cm |
| 22 | IT-BCi | TS_1 = -0.05 cm; TS_2 = -0.1 cm; TS_3 = -0.3 cm; TS_4 = -0.5 cm; TS_5 = -1 cm |
| 23 | IT-Cas | TS_1 = -0.05 cm; TS_2 = -0.3 cm; TS_3 = -0.5 cm |
| 24 | JP-BBY | TS_1 = -0.183 cm; TS_2 = -0.233 cm; TS_3 = -0.283 cm; TS_4 = -0.383 cm; TS_5 = -0.483 cm |
| 25 | JP-Mse | TS_1 = -0.01 cm; TS_2 = -0.025 cm; TS_3 = -0.05 cm; TS_4 = -0.1 cm; TS_5 = -0.2 cm; TS_6 = -0.4 cm |
| 26 | JP-SwL | |
| 27 | KR-CRK | TS_1 = -0.05 cm; TS_2 = -0.15 cm |
| 28 | MY-MLM | TS_1 = -0.05 cm |
| 29 | NL-Hor | TS_1 = -0.01 cm; TS_2 = -0.02 cm; TS_3 = -0.04 cm; TS_4 = -0.05 cm; TS_5 = -0.1 cm; TS_6 = -0.15 cm; TS_7 = -0.25 cm; TS_8 = -0.4 cm; TS_9 = -0.6 cm |
| 30 | NZ-Kop | TS_1 = -0.5 cm; TS_2 = -0.1 cm; TS_3 = -0.2 cm |
| 31 | PH-RJf | |
| 32 | RU-Ch2 | TS_1 = -0.04 cm; TS_2 = -0.08 cm; TS_3 = -0.16 cm |
| 33 | RU-Che | TS_1 = -0.04 cm; TS_2 = -0.08 cm; TS_3 = -0.16 cm |
| 34 | RU-Cok | |
| 35 | RU-Fy2 | |
| 36 | SE-Deg | TS_1 = -0.02 cm; TS_2 = -0.05 cm; TS_3 = -0.1 cm; TS_4 = -0.15 cm; TS_5 = -0.3 cm; TS_6 = -0.5 cm |
| 37 | UK-LBT | |
| 38 | US-A03 | TS_1 = -0.025 cm; TS_2 = -0.1 cm; TS_3 = -0.3 cm |
| 39 | US-A10 | TS_1 = -0.025 cm; TS_2 = -0.1 cm; TS_3 = -0.3 cm |
| 40 | US-Atq | |
| 41 | US-Beo | |
| 42 | US-Bes | |
| 43 | US-Bil | TS_1 = -0.02 cm; TS_2 = -0.04 cm; TS_3 = -0.08 cm; TS_4 = -0.16 cm; TS_5 = -0.32 cm |
| 44 | US-Bi2 | TS_1 = -0.02 cm; TS_2 = -0.04 cm; TS_3 = -0.08 cm; TS_4 = -0.16 cm; TS_5 = -0.32 cm |
| 45 | US-BZB | TS_1 = -0.075 cm; TS_2 = -0.05 cm |
| 46 | US-BZF | TS_1 = -0.075 cm; TS_2 = -0.05 cm |
| 47 | US-BZS | |
| 48 | US-CRT | |
| 49 | US-DPW | |
| 50 | US-EDN | TS_1 = -0.25 cm; TS_2 = -0.15 cm; TS_3 = -0.05 cm; TS_4 = 0 cm; TS_5 = 0.05 cm; TS_6 = 0.1 cm; TS_7 = 0.2 cm; TS_8 = 0.3 cm |
| 51 | US-EML | TS_1 = -0.05 cm; TS_2 = -0.1 cm; TS_3 = -0.2 cm; TS_4 = -0.4 cm |
| 52 | US-Hol | TS_1 = -0.05 cm; TS_2 = -0.1 cm |
| 53 | US-HRA | |
| 54 | US-HRC | |

Table B3. Continued.

| SITE_ID | SOIL_TEMP_PROBE_DEPTHS |
|---------|---|
| 55 | US-ICs TS_1 = -0.075 cm; TS_2 = -0.05 cm |
| 56 | US-Ivo TS_1 = -0.05 cm; TS_2 = -0.1 cm; TS_3 = -0.15 cm; TS_4 = -0.3 cm; TS_5 = -0.4 cm |
| 57 | US-LA1 TS = -0.1 cm |
| 58 | US-LA2 TS = -0.1 cm |
| 59 | US-Los TS_1 = 0 cm; TS_2 = -0.05 cm; TS_3 = -0.1 cm; TS_4 = -0.2 cm; TS_5 = -0.5 cm |
| 60 | US-MAC |
| 61 | US-MRM |
| 62 | US-Myb TS_1 = -0.02 cm; TS_2 = -0.04 cm; TS_3 = -0.08 cm; TS_4 = -0.16 cm; TS_5 = -0.32 cm |
| 63 | US-NC4 TS_1 = -0.05 cm; TS_2 = -0.2 cm |
| 64 | US-NGB |
| 65 | US-NGC |
| 66 | US-ORv TS_1 = -0.08 cm |
| 67 | US-OWC TS_1 = -0.05 cm; TS_2 = -0.3 cm |
| 68 | US-PFa |
| 69 | US-Shd TS_1 = -0.08 cm; TS_2 = -0.16 cm; TS_3 = nan cm; TS_4 = nan cm; TS_5 = nan cm; TS_6 = nan cm |
| 70 | US-Sne TS_1 = -0.01 cm; TS_2 = -0.02 cm; TS_3 = -0.08 cm; TS_4 = -0.16 cm; TS_5 = -0.32 cm |
| 71 | US-Sr |
| 72 | US-Sd TS_2 = -0.05 cm; TS_3 = -0.1 cm |
| 73 | US-Tw1 TS_1 = -0.02 cm; TS_2 = -0.04 cm; TS_3 = -0.08 cm; TS_4 = -0.16 cm; TS_5 = -0.32 cm |
| 74 | US-Tw3 TS_1 = -0.02 cm; TS_2 = -0.04 cm; TS_3 = -0.08 cm; TS_4 = -0.16 cm; TS_5 = -0.32 cm |
| 75 | US-Tw4 TS_1 = -0.02 cm; TS_2 = -0.04 cm; TS_3 = -0.08 cm; TS_4 = -0.16 cm; TS_5 = -0.32 cm |
| 76 | US-Tw5 TS_1 = -0.02 cm; TS_2 = -0.1 cm; TS_3 = -0.02 cm; TS_4 = -0.08 cm; TS_5 = -0.16 cm |
| 77 | US-Twt TS_1 = -0.02 cm; TS_2 = -0.04 cm; TS_3 = -0.08 cm; TS_4 = -0.16 cm; TS_5 = -0.32 cm |
| 78 | US-Udf TS_1 = -0.09 cm; TS_2 = -0.183 cm; TS_3 = -0.283 cm; TS_4 = -0.367 cm; TS_5 = -0.5 cm; TS_6 = -0.6 cm; TS_7 = -0.75 cm; TS_8 = -0.925 cm; TS_9 = -1 cm |
| 79 | US-WPT TS_1 = -0.1 cm; TS_2 = -0.3 cm |

| Column | Description |
|---------------------------------|---|
| SITE_ID | Site identification code as assigned by regional flux data network |
| SITE_NAME | Site name determined by site personnel |
| SITE_PERSONNEL | People associated with site FLUXNET-CH ₄ data |
| COUNTRY | Site country |
| LAT | Latitude |
| LON | Longitude |
| DATA_DOI | DOI link for site FLUXNET-CH ₄ data |
| YEAR_START | Year data begin |
| YEAR_END | Year data end |
| UTC_OFFSET | Site data offset from coordinated universal time (in hours) |
| ORIGINAL_DATA_SOURCE | Regional network hosting the site's methane data that were incorporated into FLUXNET-CH ₄ |
| SITE_CLASSIFICATION | Site classification based on the literature description of sites |
| UPLAND_CLASS | For upland sites, category of upland type |
| IGBP | International Geosphere–Biosphere Programme (IGBP) ecosystem surface classification |
| KOPPEN | Koppen climate zone abbreviation |
| MEAN_ANNUAL_TEMP_C_WORLDCLIM | Mean annual temperature from WorldClim2 Global Climate Data |
| MEAN_ANNUAL_PRECIP_MM_WORLDCLIM | Mean annual precipitation from WorldClim2 Global Climate Data |
| MOSS_BROWN | Presence/absence (1/0) brown moss. Presence/absence designated by Avni Malhotra using site literature |
| MOSS_SPHAGNUM | Presence/absence (1/0) sphagnum moss. Presence/absence designated by Avni Malhotra using site literature |
| AERENCHYMATOUS | Presence/absence (1/0) aerenchymatous vegetation. Presence/absence designated by Avni Malhotra using site literature |
| ERI_SHRUB | Presence/absence (1/0) ericaceous shrubs. Presence/absence designated by Avni Malhotra using site literature |
| TREE | Presence/absence (1/0) trees. Presence/absence designated by Avni Malhotra using site literature |
| DOM_VEG | Dominant vegetation type in tower footprint. Dom_veg provided to Avni Malhotra by site personnel via survey, except 15 sites where principal investigators did not answer and Avni Malhotra estimated dominant vegetation type based on site literature |
| IN_SEASONALITY_ANALYSIS | Is site in freshwater wetland seasonality analysis? 1 = yes, 0 = no. |
| Mean_Air_Temp_C | Mean annual air temperature (C) |
| Mean_Air_Temp_stdev_C | Standard deviation of annual air temperature (C) |
| Ann_Flux_g_CH4-C_m-2 | Mean annual methane flux (g CH ₄ -C m ⁻² yr ⁻¹) |
| Ann_Flux_stdev_g_CH4-C_m-2 | Standard deviation of annual methane flux (g CH ₄ -C m ⁻² yr ⁻¹) |
| JFM_flux_g_CH4-C_m-2 | Mean methane flux in January, February, March (g CH ₄ -C m ⁻² yr ⁻¹) |
| JFM_flux_stdev_g_CH4-C_m-2 | Standard deviation of methane flux in January, February, March (g CH ₄ -C m ⁻² yr ⁻¹) |
| AMJ_flux_g_CH4-C_m-2 | Mean methane flux in April, May, June (g CH ₄ -C m ⁻² yr ⁻¹) |
| AMJ_flux_stdev_g_CH4-C_m-2 | Standard deviation of methane flux in April, May, June (g CH ₄ -C m ⁻² yr ⁻¹) |
| JAS_flux_g_CH4-C_m-2 | Mean methane flux in July, August, September (g CH ₄ -C m ⁻² yr ⁻¹) |
| JAS_flux_stdev_g_CH4-C_m-2 | Standard deviation of methane flux in July, August, September (g CH ₄ -C m ⁻² yr ⁻¹) |
| OND_flux_g_CH4-C_m-2 | Mean methane flux in October, November, December (g CH ₄ -C m ⁻² yr ⁻¹) |
| OND_flux_stdev_g_CH4-C_m-2 | Standard deviation of methane flux in October, November, December (g CH ₄ -C m ⁻² yr ⁻¹) |
| SOIL_TEMP_PROBE_DEPTHS | Depth of soil temperature probe (m), with negative values being under the surface |

Table B4. Table of bioclimatic predictor data used in the principal component analysis (PCA) of Fig. 6.

| | SITE _ID | Enhanced_Vegetation _Index_(EVI) | Wong_Simple_Ratio _Water_Index_(SRWI) | Latent_Heat _(LE) | Mean_Annual _Temperature_(MAT) |
|----|-------------|-------------------------------------|--|----------------------|-----------------------------------|
| 1 | BR-Npw | 0.31 | 0.86 | 87.6 | 25.3 |
| 2 | BW-Gum | 0.28 | 0.87 | 60.9 | 23 |
| 3 | BW-Nxr | 0.22 | 0.82 | 52.6 | 23.5 |
| 4 | CA-SCB | 0.16 | 1.2 | 27.4 | -2.7 |
| 5 | DE-Hte | 0.28 | 1.01 | 40.2 | 8.6 |
| 6 | DE-SfN | 0.41 | 1.03 | 48.5 | 8.2 |
| 7 | DE-Zrk | 0.33 | 1.05 | 42.5 | 8.2 |
| 8 | FI-Lom | 0.2 | 1.27 | 23.6 | -1.5 |
| 9 | FI-Si2 | 0.27 | 1.12 | 31.6 | 3.3 |
| 10 | FI-Sii | 0.27 | 1.12 | 31.6 | 3.3 |
| 11 | FR-LGt | 0.4 | 0.97 | 50 | 10.8 |
| 12 | ID-Pag | 0.5 | 1.1 | 119.7 | 27.2 |
| 13 | JP-BBY | 0.25 | 1.21 | 45.4 | 6.5 |
| 14 | MY-MLM | 0.42 | 1.17 | 116.6 | 26.9 |
| 15 | NZ-Kop | 0.53 | 1.06 | 71.2 | 13.9 |
| 16 | RU-Ch2 | -0.01 | 1.25 | 20 | -12.1 |
| 17 | RU-Cok | 0.04 | 1.18 | 16.8 | -14.2 |
| 18 | SE-Deg | 0.27 | 1.12 | 29 | 2 |
| 19 | US-A03 | -0.07 | 1.28 | 16.1 | -11.4 |
| 20 | US-Atq | -0.1 | 1.31 | 16.9 | -10.2 |
| 21 | US-BZB | 0.17 | 1.09 | 26 | -2.8 |
| 22 | US-BZF | 0.17 | 1.09 | 26 | -2.8 |
| 23 | US-DPW | 0.32 | 0.88 | 71.8 | 22.2 |
| 24 | US-ICs | -0.04 | 1.3 | 18.5 | -8.8 |
| 25 | US-Ivo | -0.08 | 1.34 | 18.4 | -7.7 |
| 26 | US-LA2 | 0.37 | 0.98 | 69.9 | 20 |
| 27 | US-Los | 0.29 | 1.1 | 46.6 | 4 |
| 28 | US-Myb | 0.23 | 0.86 | 51 | 15.5 |
| 29 | US-NC4 | 0.34 | 0.96 | 68.4 | 16.5 |
| 30 | US-NGC | 0.1 | 1.24 | 22.3 | -3.2 |
| 31 | US-ORv | 0.32 | 0.99 | 50.8 | 10.6 |
| 32 | US-OWC | 0.27 | 1.05 | 55.8 | 9.9 |
| 33 | US-Sne | 0.23 | 0.86 | 51 | 15.5 |
| 34 | US-Tw1 | 0.26 | 0.91 | 51 | 15.5 |
| 35 | US-Tw4 | 0.26 | 0.91 | 51 | 15.5 |
| 36 | US-Tw5 | 0.26 | 0.91 | 51 | 15.5 |

| Column | Description |
|--------------------------------------|--|
| SITE_ID | Site identification code as assigned by regional flux data network |
| Enhanced_Vegetation_Index_(EVI) | Enhanced vegetation index (unitless) from MOD13A3 (Didan, 2015), 2001–2018 monthly data |
| Wong_Simple_Ratio_Water_Index_(SRWI) | Simple ratio water index (unitless) from MOD09A1 (Vermote, 2015), ~ 2001–2018 monthly data |
| Latent_Heat_(LE) | Latent heat (in W m ⁻²) from FLUXCOM (Jung et al., 2019), 2003–2013 monthly data |
| Mean_Annual_Temperature_(MAT) | Mean annual temperature (C) from BioClim (Fick and Hijman, 2017), 2001–2018 monthly data |

Table B5. Seasonality parameters estimated using TIMESAT software for methane flux (FCH₄), gross primary productivity (GPP), air temperature (TA), and soil temperature (TS, for shallowest probe at each site).

| SITE_ID | Year | Start_FCH4_(DOY) | End_FCH4_(DOY) | Base_value_FCH4_(mmol/m ² /s) | Ampl_FCH4_(mmolCH ₄ /m ² /s) | Peak_FCH4_(DOY) | Peak_value_FCH4_(mmolCH ₄ /m ² /s) |
|---------|--------|------------------|----------------|--|--|-----------------|--|
| 1 | AT-Neu | 2010 | NaN | NaN | NaN | NaN | NaN |
| 2 | AT-Neu | 2011 | NaN | NaN | NaN | NaN | NaN |
| 3 | AT-Neu | 2012 | NaN | NaN | NaN | NaN | NaN |
| 4 | BR-Npw | 2014 | NaN | NaN | NaN | NaN | NaN |
| 5 | BR-Npw | 2015 | NaN | NaN | NaN | NaN | NaN |
| 6 | BR-Npw | 2016 | 192.7 | 345.8 | -1.9 | 270 | 152.8 |
| 7 | BW-Gum | 2018 | 34.1 | 151.1 | 132.9 | 89.0 | 319.1 |
| 8 | BW-Gum | 2019 | 230.4 | NaN | 134.2 | 281.9 | 336.3 |
| 9 | BW-Nxr | 2018 | 65.1 | NaN | 29.2 | 287.5 | 237.9 |
| 10 | CA-SCB | 2014 | 138.8 | 299.1 | 17.5 | 222.4 | 89.9 |
| 11 | CA-SCB | 2015 | NaN | NaN | NaN | NaN | NaN |
| 12 | CA-SCB | 2016 | 109.2 | 290.4 | 11.8 | 207.9 | 93.8 |
| 13 | CA-SCB | 2017 | 118.0 | 300.4 | 14.0 | 221.5 | 72.9 |
| 14 | CA-SCC | 2013 | NaN | NaN | NaN | 203.4 | 44.8 |
| 15 | CA-SCC | 2014 | 128.4 | 313.1 | 3.1 | 215.0 | 43.3 |
| 16 | CA-SCC | 2015 | 98.0 | 303.9 | 1.7 | 210.9 | 56.3 |
| 17 | CA-SCC | 2016 | 102.7 | NaN | 1.7 | 208 | 59.6 |
| 18 | DE-Dgw | 2015 | NaN | NaN | NaN | NaN | NaN |
| 19 | DE-Dgw | 2016 | NaN | NaN | NaN | NaN | NaN |
| 20 | DE-Dgw | 2017 | NaN | NaN | NaN | NaN | NaN |
| 21 | DE-Hie | 2011 | NaN | NaN | NaN | NaN | NaN |
| 22 | DE-Hie | 2012 | 82.6 | 330.1 | 20.3 | 205.5 | 222.1 |
| 23 | DE-Hie | 2013 | 101.9 | NaN | 29.9 | 201.1 | 378.7 |
| 24 | DE-Hie | 2014 | NaN | 338.5 | 38.3 | 204.8 | 314.1 |
| 25 | DE-Hie | 2015 | 75.1 | 322.4 | 29.2 | 202 | 306.9 |
| 26 | DE-Hie | 2016 | 83.9 | 289.7 | 21.5 | 202 | 369.3 |
| 27 | DE-Hie | 2017 | 90.0 | 304.5 | 18.2 | 194 | 290.9 |
| 28 | DE-Hie | 2018 | 85.6 | 258.1 | 21.0 | 196.0 | 343.0 |
| 29 | DE-SIN | 2012 | 79.6 | 340.7 | 4.3 | 217.0 | 14.5 |
| 30 | DE-SIN | 2013 | NaN | NaN | 2.7 | 301.9 | 5.7 |
| 31 | DE-SIN | 2014 | NaN | NaN | NaN | NaN | NaN |
| 32 | DE-Zrk | 2013 | NaN | NaN | NaN | NaN | NaN |
| 33 | DE-Zrk | 2014 | NaN | NaN | NaN | NaN | NaN |
| 34 | DE-Zrk | 2015 | 87.0 | 273.0 | 9.3 | 208.7 | 251.9 |
| 35 | DE-Zrk | 2016 | 107.9 | 274.0 | 9.9 | 187.3 | 234.2 |
| 36 | DE-Zrk | 2017 | 110.0 | 270.1 | 11.2 | 190.0 | 214.8 |
| 37 | DE-Zrk | 2018 | 88.1 | 261.0 | 8.5 | 196.0 | 259.2 |
| 38 | FI-Lom | 2006 | 142.81 | 288.8 | 7.8 | 215.1 | 118.9 |
| 39 | FI-Lom | 2007 | 139.3 | 270.6 | 10.9 | 214.5 | 175.9 |
| 40 | FI-Lom | 2008 | 134.0 | 284.8 | 10.8 | 211.5 | 138.5 |
| 41 | FI-Lom | 2009 | 121.5 | 291.0 | 12.1 | 215.0 | 144.4 |
| 42 | FI-Lom | 2010 | 137.1 | 282.8 | 13.4 | 214.0 | 115.0 |
| 43 | FI-Si2 | 2012 | NaN | NaN | NaN | 220.6 | 80.0 |
| 44 | FI-Si2 | 2013 | NaN | NaN | NaN | 211.1 | 77.4 |
| 45 | FI-Si2 | 2014 | NaN | 280.7 | 7.2 | 212.8 | 111.1 |
| 46 | FI-Si2 | 2015 | NaN | 309.5 | 9.5 | 212.0 | 72.15 |
| 47 | FI-Si2 | 2016 | NaN | NaN | NaN | NaN | NaN |
| 48 | FI-Sii | 2013 | 123.8 | 307.6 | 7.2 | 202.5 | 111.5 |
| 49 | FI-Sii | 2014 | 118.8 | NaN | 2.3 | 215.1 | 112.7 |
| 50 | FI-Sii | 2015 | NaN | NaN | NaN | 236.0 | 112.7 |

Table B5. Continued.

| SITE_ID | Year | Start_FCH4_(DOY) | End_FCH4_(DOY) | Base_value_FCH4_FCH4_(nmolCH4/m2/s) | Ampl_FCH4_(nmolCH4/m2/s) | Peak_FCH4_(DOY) | Peak_value_FCH4_(nmolCH4/m2/s) |
|---------|--------|------------------|----------------|-------------------------------------|--------------------------|-----------------|--------------------------------|
| 51 | FI-Sii | 2016 | 114.5 | 311.3 | 8.9 | 214.0 | 130.0 |
| 52 | FI-Sii | 2017 | 118.9 | 300.4 | 6.5 | 203.0 | 63.6 |
| 53 | FI-Sii | 2018 | 116.3 | 295.1 | 7.5 | 187.0 | 61.3 |
| 54 | HK-MPM | 2016 | NaN | NaN | NaN | NaN | NaN |
| 55 | HK-MPM | 2017 | NaN | NaN | NaN | NaN | NaN |
| 56 | HK-MPM | 2018 | NaN | NaN | NaN | NaN | NaN |
| 57 | ID-Pag | 2016 | 274.1 | NaN | -2.8 | NaN | 2.3 |
| 58 | JP-BBY | 2015 | 166.7 | NaN | 18.2 | 237.7 | 71.4 |
| 59 | JP-BBY | 2016 | NaN | 325.0 | 18.3 | 244.3 | 124.0 |
| 60 | JP-BBY | 2017 | 138.5 | 323.1 | 15.2 | 236.0 | 145.3 |
| 61 | JP-BBY | 2018 | NaN | 332.1 | 17.8 | 221.0 | 92.6 |
| 62 | JP-Mse | 2012 | NaN | NaN | NaN | NaN | NaN |
| 63 | KR-CRK | 2015 | NaN | NaN | NaN | NaN | NaN |
| 64 | KR-CRK | 2016 | NaN | NaN | NaN | NaN | NaN |
| 65 | KR-CRK | 2017 | NaN | NaN | NaN | NaN | NaN |
| 66 | KR-CRK | 2018 | NaN | NaN | NaN | NaN | NaN |
| 67 | MY-MLM | 2014 | 229.6 | 562.4 | 15.5 | 64.2 | 35.3 |
| 68 | MY-MLM | 2015 | NaN | NaN | NaN | NaN | NaN |
| 69 | NZ-Kop | 2012 | -94.5 | 227.6 | 36.9 | 176.2 | 65.2 |
| 70 | NZ-Kop | 2013 | 7.2 | 251.5 | 21.1 | 182.0 | 82.8 |
| 71 | NZ-Kop | 2014 | 10.0 | 228.4 | 22.6 | 161 | 65.2 |
| 72 | NZ-Kop | 2015 | -8.5 | NaN | 23.0 | 150.0 | 57.8 |
| 73 | PH-RiF | 2012 | 154.2 | 303.9 | 4.0 | 239.1 | 66.9 |
| 74 | PH-RiF | 2013 | 304.1 | 455.0 | 5.3 | 380.3 | 59.3 |
| 75 | PH-RiF | 2014 | 133.9 | 265.7 | 6.1 | 178.3 | 127.9 |
| 76 | PH-RiF | 2015 | NaN | NaN | 3.8 | NaN | 60.1 |
| 77 | RU-Ch2 | 2014 | 150.8 | 312.2 | 0.7 | 216.5 | 70.9 |
| 78 | RU-Ch2 | 2015 | 153.3 | NaN | 8.0 | 209.0 | 56.1 |
| 79 | RU-Ch2 | 2016 | NaN | NaN | NaN | 218.8 | 68.3 |
| 80 | RU-Che | 2014 | NaN | NaN | NaN | NaN | NaN |
| 81 | RU-Che | 2015 | NaN | NaN | NaN | NaN | NaN |
| 82 | RU-Che | 2016 | NaN | NaN | NaN | NaN | NaN |
| 83 | SE-Deg | 2014 | NaN | NaN | NaN | 204.2 | 91.7 |
| 84 | SE-Deg | 2015 | 103.3 | 318.7 | 5.1 | 211.3 | 78.8 |
| 85 | SE-Deg | 2016 | 102.5 | 324.1 | 4.3 | 205.3 | 78.7 |
| 86 | SE-Deg | 2017 | NaN | NaN | NaN | NaN | NaN |
| 87 | SE-Deg | 2018 | 117.2 | 327.6 | 6.9 | 192.0 | 57.8 |
| 88 | US-Atq | 2013 | NaN | NaN | NaN | NaN | NaN |
| 89 | US-Atq | 2014 | 145.7 | 328.7 | 0.9 | 215.0 | 14.1 |
| 90 | US-Atq | 2015 | 153.3 | 264.0 | 1.0 | 193.2 | 19.6 |
| 91 | US-Beo | 2013 | NaN | NaN | NaN | NaN | NaN |
| 92 | US-Beo | 2014 | 157.0 | 356.3 | 0.4 | 211.4 | 23.4 |
| 93 | US-Bes | 2013 | NaN | NaN | NaN | NaN | NaN |
| 94 | US-Bes | 2014 | 157.3 | 312.6 | 0.6 | 206.5 | 35.0 |
| 95 | US-Bes | 2015 | 146.8 | 283.8 | 0.6 | 193.1 | 35.7 |
| 96 | US-BZB | 2014 | NaN | NaN | NaN | NaN | 67.5 |
| 97 | US-BZB | 2015 | NaN | NaN | NaN | 226.9 | 68.4 |
| 98 | US-BZB | 2016 | NaN | NaN | NaN | 219.4 | 98.4 |
| 99 | US-BZF | 2014 | NaN | NaN | NaN | 226.1 | 57.7 |
| 100 | US-BZF | 2015 | NaN | NaN | NaN | 231.6 | 87.0 |

Table B5. Continued.

| SITE_ID | Year | Start_FCH4_(DOY) | End_FCH4_(DOY) | Base_value_FCH4_(mmolCH ₄ /m ² /s) | Amp_FCH4_(mmolCH ₄ /m ² /s) | Peak_FCH4_(DOY) | Peak_value_FCH4_(mmolCH ₄ /m ² /s) |
|------------|------|------------------|----------------|--|---|-----------------|--|
| 101 US-BZF | 2016 | NaN | NaN | NaN | NaN | 220.1 | 119.1 |
| 102 US-BZS | 2015 | NaN | NaN | NaN | NaN | NaN | NaN |
| 103 US-BZS | 2016 | NaN | NaN | NaN | NaN | NaN | NaN |
| 104 US-DPW | 2013 | 151.7 | 364.0 | 16.4 | 395.0 | 240.7 | 411.4 |
| 105 US-DPW | 2014 | 98.9 | 332.5 | 34.5 | 338.0 | 228.9 | 372.4 |
| 106 US-DPW | 2015 | NaN | 376.3 | 25.0 | NaN | 248.6 | 247.3 |
| 107 US-DPW | 2016 | 84.2 | 389.2 | 23.5 | 184.3 | 237.0 | 207.8 |
| 108 US-HRA | 2017 | NaN | NaN | NaN | NaN | NaN | NaN |
| 109 US-HRC | 2018 | NaN | NaN | NaN | NaN | NaN | NaN |
| 110 US-ICs | 2014 | NaN | NaN | NaN | NaN | NaN | NaN |
| 111 US-ICs | 2015 | NaN | NaN | NaN | NaN | NaN | NaN |
| 112 US-ICs | 2016 | 138.2 | 302.1 | 0.2 | 18.0 | 200.5 | 18.2 |
| 113 US-Ivo | 2013 | NaN | 400.0 | 1.9 | 29.9 | 238.9 | 31.9 |
| 114 US-Ivo | 2014 | 158.5 | 301.8 | 6.7 | 30.0 | 226.8 | 36.7 |
| 115 US-Ivo | 2015 | 156.8 | 278.0 | 6.9 | 19.4 | 231.1 | 26.3 |
| 116 US-Ivo | 2016 | 164.7 | 352.4 | 6.1 | 32.5 | 232.0 | 38.7 |
| 117 US-LAI | 2012 | NaN | NaN | NaN | NaN | NaN | NaN |
| 118 US-LA2 | 2012 | 62.8 | NaN | 38.8 | 225.7 | 229.2 | 264.5 |
| 119 US-LA2 | 2013 | NaN | NaN | 25.1 | 193.2 | 216.2 | 218.3 |
| 120 US-Los | 2014 | 127.1 | 309.8 | 4.0 | 35.1 | 219.3 | 39.1 |
| 121 US-Los | 2015 | 143.4 | 324.4 | 3.2 | 34.6 | 220.7 | 37.8 |
| 122 US-Los | 2016 | 143.8 | 310.1 | 3.3 | 75.8 | 193.6 | 79.1 |
| 123 US-Los | 2017 | 134.1 | 255.2 | 3.6 | 58.3 | 185.0 | 61.9 |
| 124 US-Los | 2018 | 143.0 | 288.8 | 3.0 | 52.4 | 191.0 | 55.4 |
| 125 US-MAC | 2013 | NaN | NaN | NaN | NaN | NaN | NaN |
| 126 US-MAC | 2014 | NaN | NaN | NaN | NaN | NaN | NaN |
| 127 US-MAC | 2015 | NaN | NaN | NaN | NaN | NaN | NaN |
| 128 US-Myb | 2010 | NaN | NaN | NaN | NaN | NaN | NaN |
| 129 US-Myb | 2011 | 72.4 | 369.3 | 18.3 | 174.2 | 253.5 | 192.5 |
| 130 US-Myb | 2012 | 97.2 | 345.3 | 18.9 | 366.6 | 214.7 | 385.5 |
| 131 US-Myb | 2013 | 46.8 | 336.3 | 39.0 | 265.4 | 220.2 | 304.3 |
| 132 US-Myb | 2014 | 57.4 | 334.7 | 37.1 | 276.9 | 206.0 | 314.0 |
| 133 US-Myb | 2015 | 23.7 | 330.0 | 21.6 | 285.7 | 201.0 | 307.3 |
| 134 US-Myb | 2016 | 37.0 | 306.0 | 21.9 | 216.0 | 191.0 | 237.9 |
| 135 US-Myb | 2017 | 175.8 | 332.2 | 30.5 | 191.7 | 235.0 | 222.2 |
| 136 US-Myb | 2018 | 33.1 | 322.6 | 28.8 | 99.3 | 169.0 | 128.1 |
| 137 US-NC4 | 2012 | 132.9 | 307.9 | 9.5 | 323.8 | 232.2 | 333.3 |
| 138 US-NC4 | 2013 | 97.2 | 365.1 | 4.3 | 113.3 | 240.7 | 117.5 |
| 139 US-NC4 | 2014 | 110.6 | 332.3 | -0.1 | 181.8 | 253.9 | 181.6 |
| 140 US-NC4 | 2015 | 68.4 | 414.1 | -0.8 | 122.5 | 245.0 | 121.7 |
| 141 US-NC4 | 2016 | 128.4 | 350.6 | 2.7 | 373.6 | 259.0 | 376.2 |
| 142 US-ORv | 2011 | NaN | 297.3 | 7.3 | 15.2 | 178.5 | 22.4 |
| 143 US-ORv | 2012 | 120.1 | 269.1 | 8.3 | 65.2 | 189.7 | 73.4 |
| 144 US-ORv | 2013 | 72.4 | 308.4 | 9.0 | 27.4 | 189.4 | 36.4 |
| 145 US-ORv | 2014 | 87.6 | 292.2 | 9.1 | 32.4 | 201.0 | 41.5 |
| 146 US-ORv | 2015 | 86.0 | NaN | 9.0 | 38.5 | 170.0 | 47.41 |
| 147 US-OWC | 2015 | NaN | NaN | NaN | NaN | NaN | NaN |
| 148 US-OWC | 2016 | NaN | NaN | NaN | NaN | 219.2 | 883.0 |
| 149 US-Sne | 2016 | NaN | NaN | NaN | NaN | NaN | NaN |

Table B5. Continued.

| SITE_ID | Year | Start_FCH4_(DOY) | End_FCH4_(DOY) | Base_value_FCH4_(nmolCH4/m2/s) | AmpL_FCH4_(nmolCH4/m2/s) | Peak_FCH4_(DOY) | Peak_value_FCH4_(nmolCH4/m2/s) | |
|---------|--------|------------------|----------------|--------------------------------|--------------------------|-----------------|--------------------------------|-------|
| 150 | US-Sne | 2017 | 76.2 | 337.1 | 14.9 | 244.2 | 187.8 | 259.0 |
| 151 | US-Sne | 2018 | 60.6 | 341.6 | 21.4 | 168.3 | 222.6 | 189.8 |
| 152 | US-Srr | 2014 | NaN | NaN | NaN | NaN | NaN | NaN |
| 153 | US-Srr | 2015 | NaN | NaN | NaN | NaN | NaN | NaN |
| 154 | US-Srr | 2016 | NaN | NaN | NaN | NaN | NaN | NaN |
| 155 | US-Srr | 2017 | NaN | NaN | NaN | NaN | NaN | NaN |
| 156 | US-StJ | 2016 | NaN | NaN | NaN | NaN | NaN | NaN |
| 157 | US-Tw1 | 2011 | 140.5 | 352.4 | 36.3 | 104.5 | 233.8 | 140.8 |
| 158 | US-Tw1 | 2012 | NaN | 309.6 | 28.1 | 243.5 | 242.9 | 271.6 |
| 159 | US-Tw1 | 2013 | 33.4 | 307.1 | 42.2 | 114.3 | 218.0 | 156.5 |
| 160 | US-Tw1 | 2014 | 174.6 | 331.5 | 65.3 | 253.2 | 240.0 | 318.5 |
| 161 | US-Tw1 | 2015 | 62.3 | 330.3 | 63.8 | 204.1 | 207.0 | 267.9 |
| 162 | US-Tw1 | 2016 | 32.3 | 323.8 | 48.5 | 160.0 | 221.0 | 208.5 |
| 163 | US-Tw1 | 2017 | 27.8 | 305.0 | 43.0 | 138.1 | 226.0 | 181.1 |
| 164 | US-Tw1 | 2018 | 155.0 | 314.9 | 38.7 | 127.5 | 228.0 | 166.3 |
| 165 | US-Tw4 | 2014 | 93.8 | 461.3 | 27.4 | 36.5 | 226.8 | 63.8 |
| 166 | US-Tw4 | 2015 | 114.5 | 334.1 | 39.8 | 86.5 | 228.2 | 126.3 |
| 167 | US-Tw4 | 2016 | 42.8 | 357.1 | 43.2 | 101.8 | 215.6 | 144.9 |
| 168 | US-Tw4 | 2017 | 110.7 | 318.8 | 55.1 | 201.2 | 222.0 | 256.3 |
| 169 | US-Tw4 | 2018 | 63.0 | 237.3 | 53.0 | 165.1 | 173.0 | 218.1 |
| 170 | US-Tw5 | 2018 | NaN | 331.9 | 26.5 | 339.3 | 196.9 | 365.8 |
| 171 | US-Twt | 2009 | NaN | NaN | NaN | NaN | NaN | NaN |
| 172 | US-Twt | 2010 | NaN | NaN | NaN | NaN | NaN | NaN |
| 173 | US-Twt | 2011 | NaN | NaN | NaN | NaN | NaN | NaN |
| 174 | US-Twt | 2012 | NaN | NaN | NaN | NaN | NaN | NaN |
| 175 | US-Twt | 2013 | NaN | NaN | NaN | NaN | NaN | NaN |
| 176 | US-Twt | 2014 | NaN | NaN | NaN | NaN | NaN | NaN |
| 177 | US-Twt | 2015 | NaN | NaN | NaN | NaN | NaN | NaN |
| 178 | US-Twt | 2016 | NaN | NaN | NaN | NaN | NaN | NaN |
| 179 | US-Uaf | 2011 | 157.6 | NaN | 0.8 | 2.1 | 242.0 | 2.8 |
| 180 | US-Uaf | 2012 | 151.8 | NaN | 0.7 | 1.6 | 265.9 | 2.3 |
| 181 | US-Uaf | 2013 | 167.0 | NaN | 0.8 | 1.4 | 267.0 | 2.2 |
| 182 | US-Uaf | 2014 | 182.2 | NaN | 0.9 | 3.2 | 247.0 | 4.1 |
| 183 | US-Uaf | 2015 | 176.0 | NaN | 0.8 | 3.5 | 245.0 | 4.3 |
| 184 | US-Uaf | 2016 | 184.7 | NaN | 0.9 | 7.3 | 248.0 | 8.2 |
| 185 | US-Uaf | 2017 | 182.0 | NaN | 0.9 | 6.0 | 248.0 | 6.8 |
| 186 | US-Uaf | 2018 | 158.5 | NaN | 0.9 | 4.9 | 250.0 | 5.8 |
| 187 | US-WPT | 2011 | 103.5 | 294.1 | 5.6 | 355.3 | 207.1 | 360.9 |
| 188 | US-WPT | 2012 | 90.0 | 296.5 | 9.0 | 380.5 | 195.6 | 389.5 |
| 189 | US-WPT | 2013 | 72.5 | 296.9 | 7.5 | 343.3 | 220.0 | 350.8 |

Table B5. Continued.

| SITE_ID | Year | Start_GPP_DT_(DOY) | End_GPP_DT_(DOY) | Base_value_GPP_-($\mu\text{molCO}_2/\text{m}^2/\text{s}$) | Ampl_GPP_DT_-($\mu\text{molCO}_2/\text{m}^2/\text{s}$) | Peak_GPP_DT_(DOY) | Peak_value_GPP_-($\mu\text{molCO}_2/\text{m}^2/\text{s}$) | |
|---------|--------|--------------------|------------------|---|--|-------------------|---|------|
| 1 | AT-Neu | 2010 | 61.4 | 332.2 | -0.2 | 9.7 | 175.9 | 9.5 |
| 2 | AT-Neu | 2011 | 76.7 | 303.7 | 0.2 | 11.4 | 167.9 | 11.5 |
| 3 | AT-Neu | 2012 | 84.7 | 305.5 | 0.3 | 9.8 | 179.0 | 10.0 |
| 4 | BR-Npw | 2014 | 59.5 | 367.8 | 2.0 | 5.1 | 242.9 | 7.1 |
| 5 | BR-Npw | 2015 | 61.5 | 385.1 | 2.0 | 5.2 | 228.0 | 7.2 |
| 6 | BR-Npw | 2016 | 83.8 | 375.6 | 2.4 | 4.7 | 203.0 | 7.2 |
| 7 | BW-Gum | 2018 | Nan | Nan | Nan | Nan | Nan | Nan |
| 8 | BW-Gum | 2019 | Nan | Nan | Nan | Nan | Nan | Nan |
| 9 | BW-Nxr | 2018 | Nan | Nan | Nan | Nan | Nan | Nan |
| 10 | CA-SCB | 2014 | 127.5 | 266.1 | 0.1 | 2.7 | 210.0 | 2.8 |
| 11 | CA-SCB | 2015 | 60.2 | 275.2 | 0.1 | 3.4 | 199.4 | 3.5 |
| 12 | CA-SCB | 2016 | 123.0 | 277.1 | 0.0 | 3.7 | 191.9 | 3.7 |
| 13 | CA-SCB | 2017 | 113.8 | 274.6 | 0.0 | 3.0 | 202.0 | 3.0 |
| 14 | CA-SCC | 2013 | 126.4 | 273.7 | 0.2 | 3.2 | 198.8 | 3.4 |
| 15 | CA-SCC | 2014 | 130.1 | 269.3 | 0.3 | 3.2 | 194.3 | 3.5 |
| 16 | CA-SCC | 2015 | 104.4 | 270.0 | 0.3 | 4.5 | 196.9 | 4.8 |
| 17 | CA-SCC | 2016 | 106.9 | 284.8 | 0.1 | 3.7 | 191.0 | 3.8 |
| 18 | DE-Dgw | 2015 | 13.4 | 348.6 | 0.0 | 0.4 | 227.3 | 0.4 |
| 19 | DE-Dgw | 2016 | 31.3 | 294.3 | 0.0 | 0.5 | 167.6 | 0.5 |
| 20 | DE-Dgw | 2017 | 80.6 | 293.5 | 0.0 | 0.5 | 191.0 | 0.5 |
| 21 | DE-Hie | 2011 | 111.7 | 280.5 | 0.1 | 6.9 | 170.1 | 6.9 |
| 22 | DE-Hie | 2012 | 122.6 | 296.5 | 0.3 | 7.1 | 200.1 | 7.4 |
| 23 | DE-Hie | 2013 | 133.5 | 294.0 | 0.3 | 6.1 | 206.4 | 6.4 |
| 24 | DE-Hie | 2014 | 37.5 | 277.7 | 0.3 | 5.5 | 160.0 | 5.8 |
| 25 | DE-Hie | 2015 | 127.8 | 303.3 | 0.3 | 5.3 | 191.0 | 5.6 |
| 26 | DE-Hie | 2016 | 118.0 | 328.5 | 0.2 | 5.4 | 184.0 | 5.6 |
| 27 | DE-Hie | 2017 | 123.8 | 301.6 | 0.1 | 5.7 | 177.0 | 5.8 |
| 28 | DE-Hie | 2018 | 121.0 | 334.1 | 0.1 | 7.0 | 190.0 | 7.0 |
| 29 | DE-SfN | 2012 | -13.8 | 320.9 | 0.4 | 4.3 | 168.1 | 4.7 |
| 30 | DE-SfN | 2013 | 64.4 | 316.6 | 0.3 | 4.0 | 198.0 | 4.3 |
| 31 | DE-SfN | 2014 | 44.0 | 335.8 | 0.4 | 4.1 | 193.0 | 4.5 |
| 32 | DE-Zrk | 2013 | 110.2 | 283.5 | 0.1 | 4.3 | 186.3 | 4.4 |
| 33 | DE-Zrk | 2014 | 86.6 | 309.8 | 0.1 | 3.6 | 180.4 | 3.6 |
| 34 | DE-Zrk | 2015 | 99.4 | 264.2 | 0.1 | 3.5 | 186.6 | 3.6 |
| 35 | DE-Zrk | 2016 | 90.3 | 301.9 | 0.1 | 4.4 | 218.0 | 4.5 |
| 36 | DE-Zrk | 2017 | 92.9 | 303.9 | 0.1 | 4.1 | 180.0 | 4.2 |
| 37 | DE-Zrk | 2018 | 105.2 | 314.6 | 0.1 | 6.9 | 212.0 | 7.0 |
| 38 | FL-Lom | 2006 | 147.8 | 261.4 | 0.1 | 5.9 | 197.4 | 6.0 |
| 39 | FL-Lom | 2007 | 145.8 | 257.6 | 0.1 | 6.4 | 197.9 | 6.4 |
| 40 | FL-Lom | 2008 | 151.6 | 258.9 | 0.1 | 7.2 | 200.0 | 7.3 |
| 41 | FL-Lom | 2009 | 147.6 | 262.6 | 0.0 | 6.5 | 197.0 | 6.6 |
| 42 | FL-Lom | 2010 | 153.9 | 262.6 | 0.0 | 6.4 | 199.0 | 6.4 |
| 43 | FL-Si2 | 2012 | 33.7 | 276.8 | 0.1 | 1.5 | 209.0 | 1.6 |
| 44 | FL-Si2 | 2013 | 106.8 | 338.1 | 0.1 | 1.6 | 182.9 | 1.8 |

Table B5. Continued.

| SITE_ID | Year | Start_GPP_DT_(DOY) | End_GPP_DT_(DOY) | Base_value_GPP_DT_($\mu\text{molCO}_2/\text{m}^2/\text{s}$) | AmpI_GPP_DT_($\mu\text{molCO}_2/\text{m}^2/\text{s}$) | Peak_GPP_DT_(DOY) | Peak_value_GPP_DT_($\mu\text{molCO}_2/\text{m}^2/\text{s}$) | |
|---------|--------|--------------------|------------------|---|---|-------------------|---|------|
| 45 | FI-Si2 | 2014 | 40.9 | 290.0 | 0.1 | 2.2 | 146.0 | 2.3 |
| 46 | FI-Si2 | 2015 | 113.2 | 267.8 | 0.1 | 1.9 | 197.0 | 2.1 |
| 47 | FI-Si2 | 2016 | 43.9 | 284.9 | 0.1 | 1.8 | 166.0 | 2.0 |
| 48 | FI-Sii | 2013 | 119.0 | 282.5 | 0.0 | 3.7 | 185.7 | 3.7 |
| 49 | FI-Sii | 2014 | 100.3 | 294.4 | 0.0 | 2.4 | 199.7 | 2.4 |
| 50 | FI-Sii | 2015 | 84.6 | 321.9 | 0.1 | 2.6 | 204.3 | 2.7 |
| 51 | FI-Sii | 2016 | 118.7 | 284.1 | 0.1 | 3.4 | 200.0 | 3.5 |
| 52 | FI-Sii | 2017 | 117.5 | 290.5 | 0.1 | 3.0 | 206.0 | 3.1 |
| 53 | FI-Sii | 2018 | 113.6 | 295.6 | 0.0 | 2.3 | 185.0 | 2.4 |
| 54 | HK-MPM | 2016 | NaN | NaN | NaN | NaN | NaN | NaN |
| 55 | HK-MPM | 2017 | NaN | NaN | NaN | NaN | NaN | NaN |
| 56 | HK-MPM | 2018 | NaN | NaN | NaN | NaN | NaN | NaN |
| 57 | ID-Pag | 2016 | NaN | NaN | NaN | NaN | NaN | NaN |
| 58 | JP-BBY | 2015 | 123.6 | 304.3 | 0.2 | 5.3 | 203.4 | 5.6 |
| 59 | JP-BBY | 2016 | 114.1 | 302.4 | 0.0 | 7.9 | 203.2 | 8.0 |
| 60 | JP-BBY | 2017 | 119.9 | 300.4 | 0.0 | 7.6 | 199.8 | 7.6 |
| 61 | JP-BBY | 2018 | 96.3 | 311.6 | 0.0 | 5.4 | 217.0 | 5.5 |
| 62 | JP-Mse | 2012 | 144.6 | 266.9 | 0.6 | 9.8 | 209.7 | 10.4 |
| 63 | KR-CRK | 2015 | 135.0 | 267.8 | 0.1 | 10.7 | 202.1 | 10.8 |
| 64 | KR-CRK | 2016 | 137.2 | 262.4 | 0.1 | 12.4 | 198.8 | 12.5 |
| 65 | KR-CRK | 2017 | 143.3 | 266.2 | 0.1 | 12.2 | 193.5 | 12.3 |
| 66 | KR-CRK | 2018 | 139.0 | 263.8 | 0.2 | 11.0 | 198.0 | 11.1 |
| 67 | MY-MLM | 2014 | 180.0 | 437.9 | 8.5 | 2.7 | 272.6 | 11.2 |
| 68 | MY-MLM | 2015 | 194.2 | NaN | 8.8 | 8.3 | 271.1 | 17.1 |
| 69 | NZ-Kop | 2012 | 38.7 | 334.9 | 1.3 | 2.5 | 194.8 | 3.8 |
| 70 | NZ-Kop | 2013 | 58.1 | 351.6 | 1.5 | 2.6 | 190.0 | 4.1 |
| 71 | NZ-Kop | 2014 | 42.2 | 355.0 | 1.4 | 2.8 | 209.0 | 4.2 |
| 72 | NZ-Kop | 2015 | 44.3 | 366.2 | 1.2 | 3.3 | 193.0 | 4.5 |
| 73 | PH-RiF | 2012 | NaN | NaN | NaN | NaN | NaN | NaN |
| 74 | PH-RiF | 2013 | NaN | NaN | NaN | NaN | NaN | NaN |
| 75 | PH-RiF | 2014 | NaN | NaN | NaN | NaN | NaN | NaN |
| 76 | PH-RiF | 2015 | NaN | NaN | NaN | NaN | NaN | NaN |
| 77 | RU-Ch2 | 2014 | 142.9 | 252.8 | 0.0 | 5.1 | 210.3 | 5.1 |
| 78 | RU-Ch2 | 2015 | 157.5 | 247.9 | 0.0 | 5.0 | 202.6 | 5.0 |
| 79 | RU-Ch2 | 2016 | 145.3 | 257.9 | 0.0 | 4.1 | 201.5 | 4.1 |
| 80 | RU-Che | 2014 | 161.7 | 258.8 | 0.1 | 5.5 | 206.9 | 5.6 |
| 81 | RU-Che | 2015 | 157.0 | 250.3 | 0.0 | 5.4 | 203.3 | 5.4 |
| 82 | RU-Che | 2016 | 140.6 | 258.3 | -0.1 | 6.9 | 188.6 | 6.8 |
| 83 | SE-Deg | 2014 | 115.4 | 285.9 | 0.0 | 2.8 | 196.3 | 2.8 |
| 84 | SE-Deg | 2015 | 113.5 | 278.7 | 0.0 | 2.7 | 203.4 | 2.7 |
| 85 | SE-Deg | 2016 | 118.8 | 290.3 | 0.0 | 2.3 | 195.5 | 2.3 |
| 86 | SE-Deg | 2017 | 121.9 | 276.1 | 0.0 | 2.4 | 199.0 | 2.5 |

Table B5. Continued.

| SITE | Year | Start_GPP | End_GPP | Base_value_GPP | Ampl_GPP_DT | Peak_GPP_DT | Peak_value_GPP | |
|------|--------|-----------|-----------|---|--|-------------|---|------|
| _ID | | _DT_(DOY) | _DT_(DOY) | _DT_($\mu\text{molCO}_2/\text{m}^2/\text{s}$) | _($\mu\text{molCO}_2/\text{m}^2/\text{s}$) | _(DOY) | _DT_($\mu\text{molCO}_2/\text{m}^2/\text{s}$) | |
| 87 | SE-Deg | 2018 | 118.5 | 276.6 | 0.0 | 1.7 | 188.0 | 1.7 |
| 88 | US-Atq | 2013 | 33.2 | 256.5 | 0.0 | 3.1 | 161.7 | 3.1 |
| 89 | US-Atq | 2014 | 139.1 | 244.9 | 0.1 | 1.8 | 194.3 | 1.9 |
| 90 | US-Atq | 2015 | 132.8 | 244.0 | 0.1 | 3.4 | 191.0 | 3.5 |
| 91 | US-Bco | 2013 | 39.3 | 285.3 | 0.0 | 0.9 | 159.8 | 0.9 |
| 92 | US-Bco | 2014 | 88.2 | 261.5 | 0.0 | 2.0 | 200.0 | 2.0 |
| 93 | US-Bes | 2013 | 49.4 | 269.4 | 0.0 | 0.8 | 187.9 | 0.9 |
| 94 | US-Bes | 2014 | 174.6 | 262.2 | 0.0 | 1.6 | 220.7 | 1.6 |
| 95 | US-Bes | 2015 | 160.5 | 248.8 | 0.0 | 2.5 | 198.4 | 2.6 |
| 96 | US-BZB | 2014 | NaN | NaN | NaN | NaN | NaN | NaN |
| 97 | US-BZB | 2015 | NaN | NaN | NaN | NaN | NaN | NaN |
| 98 | US-BZB | 2016 | NaN | NaN | NaN | NaN | NaN | NaN |
| 99 | US-BZF | 2014 | 132.7 | 201.3 | 0.2 | 5.8 | 167.5 | 6.0 |
| 100 | US-BZF | 2015 | 129.1 | 258.7 | 0.2 | 6.9 | 187.5 | 7.1 |
| 101 | US-BZF | 2016 | 128.6 | 228.0 | 0.2 | 9.1 | 175.0 | 9.3 |
| 102 | US-BZS | 2015 | NaN | NaN | NaN | NaN | NaN | NaN |
| 103 | US-BZS | 2016 | NaN | NaN | NaN | NaN | NaN | NaN |
| 104 | US-DPW | 2013 | NaN | NaN | NaN | NaN | NaN | NaN |
| 105 | US-DPW | 2014 | 55.7 | 332.1 | 0.6 | 4.6 | 183.5 | 5.2 |
| 106 | US-DPW | 2015 | 53.7 | 372.9 | 0.7 | 4.8 | 174.8 | 5.5 |
| 107 | US-DPW | 2016 | 71.2 | 343.9 | 0.8 | 4.8 | 197.0 | 5.7 |
| 108 | US-HRA | 2017 | 131.3 | 244.8 | 0.4 | 20.1 | 183.1 | 20.5 |
| 109 | US-HRC | 2018 | 135.7 | 237.6 | 1.3 | 18.8 | 182.2 | 20.1 |
| 110 | US-ICs | 2014 | 150.4 | 253.4 | 0.2 | 3.5 | 201.6 | 3.7 |
| 111 | US-ICs | 2015 | 142.8 | 263.2 | 0.2 | 4.4 | 189.9 | 4.6 |
| 112 | US-ICs | 2016 | 154.4 | 245.7 | 0.1 | 3.2 | 192.8 | 3.3 |
| 113 | US-Ivo | 2013 | 149.1 | 258.0 | 0.1 | 3.9 | 201.9 | 3.9 |
| 114 | US-Ivo | 2014 | 151.6 | 257.8 | 0.1 | 3.6 | 199.1 | 3.7 |
| 115 | US-Ivo | 2015 | 121.7 | 248.3 | 0.1 | 4.0 | 187.1 | 4.0 |
| 116 | US-Ivo | 2016 | 154.7 | 254.5 | 0.1 | 5.3 | 194.0 | 5.4 |
| 117 | US-LA1 | 2012 | -8.0 | 216.9 | 0.5 | 2.3 | 142.8 | 2.8 |
| 118 | US-LA2 | 2012 | 47.0 | 334.0 | 0.3 | 5.6 | 146.8 | 6.0 |
| 119 | US-LA2 | 2013 | 93.7 | 335.8 | 0.3 | 6.9 | 166.3 | 7.3 |
| 120 | US-Los | 2014 | 131.4 | 288.1 | 0.0 | 6.7 | 198.2 | 6.6 |
| 121 | US-Los | 2015 | 130.4 | 288.1 | 0.1 | 6.3 | 201.5 | 6.4 |
| 122 | US-Los | 2016 | 130.9 | 291.5 | 0.2 | 7.2 | 198.2 | 7.3 |
| 123 | US-Los | 2017 | 136.0 | 292.4 | 0.1 | 7.4 | 199.0 | 7.5 |
| 124 | US-Los | 2018 | 135.0 | 285.6 | 0.1 | 7.2 | 199.0 | 7.3 |
| 125 | US-MAC | 2013 | NaN | 378.1 | 2.5 | 5.4 | 222.7 | 9.5 |

Table B5. Continued.

| SITE_ID | Year | Start_GPP_DT_(DOY) | End_GPP_DT_(DOY) | Base_value_GPP_DT_(μmolCO2/m2/s) | AmpI_GPP_DT_(μmolCO2/m2/s) | Peak_GPP_DT_(DOY) | DT_(μmolCO2/m2/s) | Peak_value_GPP_DT_(μmolCO2/m2/s) |
|---------|--------|--------------------|------------------|----------------------------------|----------------------------|-------------------|-------------------|----------------------------------|
| 126 | US-MAC | 2014 | 47.0 | 334.2 | 2.5 | 9.2 | 180.7 | 11.7 |
| 127 | US-MAC | 2015 | 46.5 | 356.6 | 2.9 | 5.9 | 154.1 | 8.8 |
| 128 | US-Myb | 2010 | 28.6 | 305.2 | 0.6 | 1.4 | 183.4 | 2.0 |
| 129 | US-Myb | 2011 | 200.4 | 367.3 | 0.3 | 3.6 | 265.5 | 3.9 |
| 130 | US-Myb | 2012 | 88.4 | 331.9 | -0.1 | 13.7 | 204.5 | 13.6 |
| 131 | US-Myb | 2013 | 47.4 | 341.9 | -0.1 | 8.0 | 200.0 | 7.8 |
| 132 | US-Myb | 2014 | 86.8 | 310.7 | 0.2 | 8.2 | 168.0 | 8.4 |
| 133 | US-Myb | 2015 | 76.1 | 323.2 | 0.2 | 7.3 | 202.0 | 7.5 |
| 134 | US-Myb | 2016 | 24.1 | 328.4 | 0.0 | 4.0 | 176.0 | 4.0 |
| 135 | US-Myb | 2017 | 67.5 | 395.2 | -0.2 | 5.8 | 202.0 | 5.5 |
| 136 | US-Myb | 2018 | 83.7 | 331.3 | -0.3 | 10.5 | 201.0 | 10.3 |
| 137 | US-NC4 | 2012 | NaN | NaN | NaN | NaN | NaN | NaN |
| 138 | US-NC4 | 2013 | 94.4 | 304.8 | 0.8 | 7.0 | 181.0 | 7.7 |
| 139 | US-NC4 | 2014 | 97.5 | 354.5 | 0.6 | 6.1 | 173.7 | 6.7 |
| 140 | US-NC4 | 2015 | 92.0 | 315.1 | 0.7 | 9.7 | 185.0 | 10.5 |
| 141 | US-NC4 | 2016 | 99.6 | 327.0 | 0.9 | 8.2 | 183.0 | 9.1 |
| 142 | US-ORv | 2011 | 88.8 | 316.4 | -0.1 | 7.4 | 180.4 | 7.3 |
| 143 | US-ORv | 2012 | 93.5 | 303.4 | 0.3 | 9.3 | 181.0 | 9.6 |
| 144 | US-ORv | 2013 | 107.6 | 305.2 | 0.4 | 10.1 | 192.4 | 10.5 |
| 145 | US-ORv | 2014 | 109.3 | 299.2 | 0.2 | 10.1 | 190.0 | 10.4 |
| 146 | US-ORv | 2015 | 105.0 | 301.6 | 0.3 | 9.6 | 194.0 | 9.9 |
| 147 | US-OWC | 2015 | NaN | 301.4 | 0.3 | 6.7 | 151.3 | 7.0 |
| 148 | US-OWC | 2016 | 116.0 | 309.2 | 0.3 | 6.4 | 204.0 | 6.7 |
| 149 | US-Sne | 2016 | -21.8 | 306.2 | 0.3 | 8.0 | 190.3 | 8.3 |
| 150 | US-Sne | 2017 | NaN | NaN | NaN | NaN | NaN | NaN |
| 151 | US-Sne | 2018 | 84.6 | 370.3 | 0.3 | 2.4 | 202.0 | 2.8 |
| 152 | US-Srr | 2014 | 47.0 | 307.5 | 0.8 | 6.0 | 175.6 | 6.8 |
| 153 | US-Srr | 2015 | 35.5 | 320.9 | 0.3 | 8.0 | 158.6 | 8.3 |
| 154 | US-Srr | 2016 | 44.8 | 318.9 | 0.4 | 8.9 | 170.8 | 9.2 |
| 155 | US-Srr | 2017 | 56.8 | 309.8 | 0.3 | 10.5 | 185.0 | 10.8 |
| 156 | US-StJ | 2016 | 120.7 | 280.7 | 1.3 | 12.0 | 193.8 | 13.3 |
| 157 | US-Tw1 | 2011 | NaN | NaN | NaN | NaN | NaN | NaN |
| 158 | US-Tw1 | 2012 | 102.1 | 325.5 | 0.0 | 12.8 | 216.1 | 12.8 |
| 159 | US-Tw1 | 2013 | 98.3 | 338.0 | -0.2 | 13.1 | 208.4 | 12.9 |
| 160 | US-Tw1 | 2014 | 95.7 | 326.3 | 0.1 | 10.5 | 208.0 | 10.6 |
| 161 | US-Tw1 | 2015 | 105.5 | 344.1 | 0.3 | 9.9 | 215.0 | 10.1 |
| 162 | US-Tw1 | 2016 | 91.8 | 313.1 | 0.0 | 10.1 | 209.0 | 10.1 |
| 163 | US-Tw1 | 2017 | 93.4 | 329.8 | 0.0 | 11.3 | 214.0 | 11.2 |
| 164 | US-Tw1 | 2018 | 119.0 | 363.8 | 0.0 | 12.7 | 217.0 | 12.7 |

Table B5. Continued.

| SITE_ID | Year | Start_GPP_DT_(DOY) | End_GPP_DT_(DOY) | Base_value_GPP_($\mu\text{molCO}_2/\text{m}^2/\text{s}$) | Ampl_GPP_DT_($\mu\text{molCO}_2/\text{m}^2/\text{s}$) | Peak_GPP_DT_(DOY) | Peak_value_GPP_($\mu\text{molCO}_2/\text{m}^2/\text{s}$) |
|---------|--------|--------------------|------------------|--|---|-------------------|--|
| 165 | US-Tw4 | 2014 | 160.0 | 363.2 | 0.0 | 4.7 | 4.7 |
| 166 | US-Tw4 | 2015 | 57.2 | 335.9 | 0.0 | 8.1 | 8.1 |
| 167 | US-Tw4 | 2016 | 76.1 | 311.3 | 0.2 | 8.2 | 8.4 |
| 168 | US-Tw4 | 2017 | 100.2 | 332.9 | 0.1 | 8.8 | 8.9 |
| 169 | US-Tw4 | 2018 | 98.4 | 337.8 | 0.0 | 11.8 | 11.9 |
| 170 | US-Tw5 | 2018 | 115.9 | 321.3 | 1.8 | 6.7 | 8.5 |
| 171 | US-Twt | 2009 | 150.0 | 293.0 | 0.2 | 12.5 | 12.7 |
| 172 | US-Twt | 2010 | 141.1 | 311.9 | 0.1 | 13.7 | 13.8 |
| 173 | US-Twt | 2011 | 158.5 | 288.7 | 0.1 | 14.2 | 14.3 |
| 174 | US-Twt | 2012 | 166.8 | 308.8 | 0.2 | 12.3 | 12.5 |
| 175 | US-Twt | 2013 | 138.2 | 272.4 | 0.3 | 16.7 | 17.0 |
| 176 | US-Twt | 2014 | 148.1 | 281.4 | 0.2 | 15.0 | 15.2 |
| 177 | US-Twt | 2015 | 137.1 | 277.2 | 0.2 | 11.5 | 11.7 |
| 178 | US-Twt | 2016 | 169.1 | 289.9 | 0.3 | 13.8 | 14.1 |
| 179 | US-Uaf | 2011 | 114.6 | 283.5 | 0.1 | 6.0 | 6.2 |
| 180 | US-Uaf | 2012 | 88.0 | 271.2 | 0.2 | 6.6 | 6.8 |
| 181 | US-Uaf | 2013 | 124.1 | 271.6 | 0.2 | 5.8 | 6.0 |
| 182 | US-Uaf | 2014 | 84.6 | 269.3 | 0.1 | 5.3 | 5.5 |
| 183 | US-Uaf | 2015 | 90.5 | 264.3 | 0.1 | 5.2 | 5.3 |
| 184 | US-Uaf | 2016 | 103.1 | 270.8 | 0.1 | 4.7 | 4.8 |
| 185 | US-Uaf | 2017 | 102.3 | 275.6 | 0.1 | 6.1 | 6.2 |
| 186 | US-Uaf | 2018 | 111.6 | 291.5 | 0.0 | 5.6 | 5.6 |
| 187 | US-WPT | 2011 | 135.0 | 285.6 | 0.2 | 7.4 | 7.7 |
| 188 | US-WPT | 2012 | 129.0 | 293.7 | 0.1 | 7.0 | 7.0 |
| 189 | US-WPT | 2013 | 134.9 | 278.1 | 0.0 | 6.2 | 6.2 |

Table B5. Continued.

| SITE_ID | Year | Probe_name | Soil_temp_depth_m | Start_TS_(DOY) | End_TS_(DOY) | Base_value_TS_(C) | Ampl_TS_(C) | Peak_TS_(DOY) | Peak_value_TS_(C) | |
|---------|--------|------------|-------------------|----------------|--------------|-------------------|-------------|---------------|-------------------|------|
| 1 | AT-Neu | 2010 | TS_1 | -0.1 | 61.3 | 339.4 | 0.2 | 17.5 | 200.9 | 17.7 |
| 2 | AT-Neu | 2011 | TS_1 | -0.1 | 51.0 | 328.8 | 0.4 | 16.4 | 201.0 | 16.8 |
| 3 | AT-Neu | 2012 | TS_1 | -0.1 | 61.1 | 341.9 | 0.7 | 17.6 | 202.9 | 18.3 |
| 4 | BR-Npw | 2014 | NaN | NaN | NaN | NaN | NaN | NaN | NaN | NaN |
| 5 | BR-Npw | 2015 | NaN | NaN | NaN | NaN | NaN | NaN | NaN | NaN |
| 6 | BR-Npw | 2016 | NaN | 18.4 | 343.2 | 22.4 | 6.0 | 6.0 | 188.0 | 28.4 |
| 7 | BW-Gum | 2018 | NaN | NaN | NaN | NaN | NaN | NaN | NaN | NaN |
| 8 | BW-Gum | 2019 | NaN | NaN | NaN | NaN | NaN | NaN | NaN | NaN |
| 9 | BW-Nxr | 2018 | NaN | NaN | NaN | NaN | NaN | NaN | NaN | NaN |
| 10 | CA-SCB | 2014 | TS_1 | 0.0 | 105.9 | 292.2 | -0.6 | 20.6 | 196.6 | 20.0 |
| 11 | CA-SCB | 2015 | TS_1 | 0.0 | 106.9 | 287.1 | -0.4 | 17.2 | 186.8 | 16.8 |
| 12 | CA-SCB | 2016 | TS_1 | 0.0 | 101.6 | 284.1 | -0.3 | 19.1 | 193.2 | 18.8 |
| 13 | CA-SCB | 2017 | TS_1 | 0.0 | 107.4 | 289.7 | -0.3 | 17.7 | 198.0 | 17.4 |
| 14 | CA-SCC | 2013 | NaN | NaN | NaN | NaN | NaN | NaN | NaN | NaN |
| 15 | CA-SCC | 2014 | TS_1 | -0.1 | 123.4 | 287.1 | -0.5 | 15.6 | 203.0 | 15.1 |
| 16 | CA-SCC | 2015 | TS_1 | -0.1 | 113.9 | 285.2 | -0.3 | 16.3 | 189.2 | 16.0 |
| 17 | CA-SCC | 2016 | TS_1 | -0.1 | 108.1 | 260.1 | -0.3 | 18.4 | 190.9 | 18.0 |
| 18 | DE-Dgw | 2015 | NaN | NaN | NaN | NaN | NaN | NaN | NaN | NaN |
| 19 | DE-Dgw | 2016 | NaN | NaN | NaN | NaN | NaN | NaN | NaN | NaN |
| 20 | DE-Dgw | 2017 | NaN | NaN | NaN | NaN | NaN | NaN | NaN | NaN |
| 21 | DE-Hte | 2011 | NaN | NaN | NaN | NaN | NaN | NaN | NaN | NaN |
| 22 | DE-Hte | 2012 | TS_3 | -0.2 | 77.0 | 344.0 | 5.0 | 12.3 | 215.5 | 17.2 |
| 23 | DE-Hte | 2013 | TS_3 | -0.2 | 60.9 | 378.0 | 4.0 | 12.0 | 207.9 | 16.0 |
| 24 | DE-Hte | 2014 | TS_1 | 0.0 | NaN | 327.8 | 8.5 | 8.3 | 205.6 | 16.9 |
| 25 | DE-Hte | 2015 | TS_1 | 0.0 | 62.9 | 360.6 | 5.2 | 11.7 | 187.4 | 16.8 |
| 26 | DE-Hte | 2016 | TS_1 | 0.0 | 71.9 | NaN | 4.9 | 12.4 | 175.6 | 17.3 |
| 27 | DE-Hte | 2017 | TS_1 | NaN | 61.6 | 343.3 | 4.5 | 11.8 | 186.0 | 16.3 |
| 28 | DE-Hte | 2018 | NaN | NaN | NaN | NaN | NaN | NaN | NaN | NaN |
| 29 | DE-Sfn | 2012 | TS_1 | 0.0 | NaN | 372.6 | 0.0 | 23.6 | 206.5 | 15.3 |
| 30 | DE-Sfn | 2013 | TS_1 | 0.0 | 55.8 | 381.5 | 0.9 | 13.6 | 216.4 | 14.5 |
| 31 | DE-Sfn | 2014 | NaN | NaN | NaN | NaN | NaN | NaN | NaN | NaN |
| 32 | DE-Zrk | 2013 | NaN | NaN | NaN | NaN | NaN | NaN | NaN | NaN |
| 33 | DE-Zrk | 2014 | TS_1 | -0.1 | 54.8 | 361.6 | 4.4 | 13.9 | 202.3 | 18.3 |
| 34 | DE-Zrk | 2015 | TS_1 | -0.1 | 58.3 | 359.3 | 4.3 | 13.2 | 215.5 | 17.5 |
| 35 | DE-Zrk | 2016 | TS_1 | -0.1 | 72.8 | 332.0 | 4.3 | 14.9 | 200.4 | 19.2 |
| 36 | DE-Zrk | 2017 | TS_1 | -0.1 | 69.1 | 351.4 | 4.4 | 14.7 | 199.0 | 19.1 |
| 37 | DE-Zrk | 2018 | TS_1 | -0.1 | 84.5 | 336.1 | 4.8 | 12.3 | 203.0 | 17.1 |
| 38 | FI-Lom | 2006 | TS_1 | -0.1 | 114.1 | 290.8 | -0.1 | 13.4 | 204.8 | 13.3 |
| 39 | FI-Lom | 2007 | TS_1 | -0.1 | 126.8 | 302.0 | 0.1 | 13.1 | 200.0 | 13.2 |
| 40 | FI-Lom | 2008 | TS_1 | -0.1 | 135.6 | 296.7 | 0.2 | 12.7 | 202.9 | 12.9 |
| 41 | FI-Lom | 2009 | TS_1 | -0.1 | 117.2 | 291.9 | 0.1 | 11.7 | 214.0 | 11.9 |
| 42 | FI-Lom | 2010 | TS_1 | -0.1 | 129.9 | 318.5 | 0.0 | 12.1 | 208.0 | 12.2 |
| 43 | FI-Si2 | 2012 | TS_1 | -0.1 | NaN | 323.5 | 0.0 | 19.9 | 204.6 | 16.0 |
| 44 | FI-Si2 | 2013 | TS_1 | -0.1 | 106.9 | 341.0 | -0.1 | 16.0 | 199.4 | 16.0 |
| 45 | FI-Si2 | 2014 | TS_1 | -0.1 | 104.6 | 331.1 | 0.0 | 17.1 | 208.5 | 17.0 |
| 46 | FI-Si2 | 2015 | TS_1 | -0.1 | 76.5 | 352.3 | -0.9 | 16.3 | 211.0 | 15.4 |

Table B5. Continued.

| SITE_ID | Year | Probe_name | Soil_temp_depth_m | Start_TS_(DOY) | End_TS_(DOY) | Base_value_TS_(C) | Ampl_TS_(C) | Peak_TS_(DOY) | Peak_value_TS_(C) |
|---------|------|------------|-------------------|----------------|--------------|-------------------|-------------|---------------|-------------------|
| 47 | 2016 | TS_1 | -0.1 | 102.6 | 329.4 | -0.9 | 16.5 | 206.0 | 15.6 |
| 48 | 2013 | Nan | Nan | Nan | Nan | Nan | Nan | Nan | Nan |
| 49 | 2014 | Nan | Nan | Nan | Nan | Nan | Nan | Nan | Nan |
| 50 | 2015 | Nan | Nan | Nan | Nan | Nan | Nan | Nan | Nan |
| 51 | 2016 | Nan | Nan | Nan | Nan | Nan | Nan | Nan | Nan |
| 52 | 2017 | Nan | Nan | Nan | Nan | Nan | Nan | Nan | Nan |
| 53 | 2018 | Nan | Nan | Nan | Nan | Nan | Nan | Nan | Nan |
| 54 | 2016 | TS_2 | Nan | Nan | 566.9 | 0.0 | 7.8 | 219.8 | 28.9 |
| 55 | 2017 | TS_2 | Nan | Nan | Nan | 0.0 | 8.7 | 218.5 | 29.1 |
| 56 | 2018 | TS_2 | Nan | Nan | Nan | 0.0 | 7.2 | 204.9 | 28.7 |
| 57 | 2016 | Nan | Nan | Nan | Nan | Nan | Nan | Nan | Nan |
| 58 | 2015 | TS_1 | -0.2 | 87.8 | 340.8 | 0.9 | 21.6 | 218.1 | 22.5 |
| 59 | 2016 | TS_1 | -0.2 | 80.8 | 330.6 | 0.4 | 22.2 | 217.8 | 22.6 |
| 60 | 2017 | TS_1 | -0.2 | 80.4 | 347.8 | 0.2 | 21.8 | 213.8 | 22.0 |
| 61 | 2018 | TS_1 | -0.2 | 78.3 | 355.4 | 0.5 | 20.4 | 222.0 | 20.9 |
| 62 | 2012 | TS_1 | 0.0 | 60.4 | 348.9 | 2.1 | 23.8 | 211.8 | 25.9 |
| 63 | 2015 | Nan | Nan | Nan | Nan | Nan | Nan | Nan | Nan |
| 64 | 2016 | Nan | Nan | Nan | Nan | Nan | Nan | Nan | Nan |
| 65 | 2017 | Nan | Nan | Nan | Nan | Nan | Nan | Nan | Nan |
| 66 | 2018 | Nan | Nan | Nan | Nan | Nan | Nan | Nan | Nan |
| 67 | 2014 | TS | Nan | Nan | 358.4 | 25.1 | 4.0 | 194.5 | 29.0 |
| 68 | 2015 | TS | Nan | 27.3 | Nan | 25.6 | 2.0 | 172.7 | 27.6 |
| 69 | 2012 | TS_1 | -0.5 | 62.5 | 360.3 | 8.3 | 8.4 | 219.8 | 16.7 |
| 70 | 2013 | TS_1 | -0.5 | 45.6 | 367.0 | 8.4 | 7.6 | 210.5 | 16.0 |
| 71 | 2014 | TS_1 | -0.5 | 56.9 | 365.7 | 8.2 | 8.8 | 219.0 | 17.0 |
| 72 | 2015 | TS_1 | -0.5 | 56.5 | 371.8 | 7.7 | 9.4 | 214.0 | 17.1 |
| 73 | 2012 | Nan | Nan | Nan | Nan | Nan | Nan | Nan | Nan |
| 74 | 2013 | Nan | Nan | Nan | Nan | Nan | Nan | Nan | Nan |
| 75 | 2014 | Nan | Nan | Nan | Nan | Nan | Nan | Nan | Nan |
| 76 | 2015 | Nan | Nan | Nan | Nan | Nan | Nan | Nan | Nan |
| 77 | 2014 | TS_1 | 0.0 | 138.8 | 263.8 | -0.1 | 14.4 | 206.6 | 14.3 |
| 78 | 2015 | TS_1 | 0.0 | 143.9 | 269.6 | -0.1 | 14.0 | 193.3 | 13.8 |
| 79 | 2016 | TS_1 | 0.0 | 127.0 | 273.5 | -0.2 | 11.6 | 200.2 | 11.5 |
| 80 | 2014 | TS_1 | 0.0 | 138.0 | 267.6 | -0.1 | 15.0 | 208.0 | 14.9 |
| 81 | 2015 | TS_1 | 0.0 | 143.8 | 274.7 | -0.2 | 14.8 | 193.7 | 14.6 |
| 82 | 2016 | TS_1 | 0.0 | 126.7 | 274.0 | -0.2 | 13.0 | 200.4 | 12.8 |
| 83 | 2014 | TS_1 | 0.0 | 111.8 | 303.6 | -0.5 | 17.2 | 201.6 | 16.7 |
| 84 | 2015 | TS_1 | 0.0 | 104.2 | 310.6 | -0.3 | 15.2 | 207.2 | 14.9 |
| 85 | 2016 | TS_1 | 0.0 | 108.1 | 306.4 | -0.2 | 14.9 | 200.3 | 14.7 |
| 86 | 2017 | TS_1 | 0.0 | 133.4 | 326.9 | -0.2 | 12.4 | 215.0 | 12.2 |
| 87 | 2018 | TS_1 | 0.0 | 111.7 | 310.2 | -0.2 | 14.7 | 198.0 | 14.5 |
| 88 | 2013 | Nan | Nan | Nan | Nan | Nan | Nan | Nan | Nan |
| 89 | 2014 | TS_1 | Nan | 10.7 | 139.5 | -0.2 | 8.1 | 61.0 | 7.9 |
| 90 | 2015 | Nan | Nan | Nan | Nan | Nan | Nan | Nan | Nan |
| 91 | 2013 | Nan | Nan | Nan | Nan | Nan | Nan | Nan | Nan |
| 92 | 2014 | TS_1 | Nan | 155.1 | 270.1 | 0.0 | 4.9 | 211.1 | 4.8 |
| 93 | 2013 | TS_1 | Nan | 143.2 | 262.0 | 0.0 | 5.6 | 201.3 | 5.6 |

Table B5. Continued.

| SITE_ID | Year | Probe_name | Soil_temp_depth_m | Start_TS_(DOY) | End_TS_(DOY) | Base_value_TS_(C) | Ampl_TS_(C) | Peak_TS_(DOY) | Peak_value_TS_(C) |
|---------|--------|------------|-------------------|----------------|--------------|-------------------|-------------|---------------|-------------------|
| 94 | US-Bes | 2014 | TS_1 | 151.8 | 282.3 | -0.1 | 3.9 | 198.5 | 3.8 |
| 95 | US-Bes | 2015 | TS_1 | 140.4 | 271.0 | -0.1 | 4.8 | 195.3 | 4.7 |
| 96 | US-BZB | 2014 | TS_1 | 123.1 | 298.4 | -0.4 | 15.4 | 215.8 | 14.9 |
| 97 | US-BZB | 2015 | TS_1 | 107.8 | 295.6 | -0.4 | 14.0 | 210.2 | 13.7 |
| 98 | US-BZB | 2016 | TS_1 | 125.1 | 292.4 | -0.3 | 16.4 | 214.3 | 16.1 |
| 99 | US-BZF | 2014 | TS_1 | 96.1 | 322.8 | -1.6 | 16.1 | 205.4 | 14.6 |
| 100 | US-BZF | 2015 | TS_1 | 108.4 | 331.1 | -1.2 | 14.9 | 197.5 | 13.7 |
| 101 | US-BZF | 2016 | TS_1 | 95.5 | 315.9 | -1.0 | 17.2 | 205.1 | 16.2 |
| 102 | US-BZS | 2015 | TS_1 | 116.5 | 275.2 | -0.1 | 4.9 | 202.9 | 4.8 |
| 103 | US-BZS | 2016 | TS_1 | 119.1 | 278.9 | 0.0 | 5.6 | 208.4 | 5.5 |
| 104 | US-DPW | 2013 | NaN | NaN | NaN | NaN | NaN | NaN | NaN |
| 105 | US-DPW | 2014 | NaN | NaN | NaN | NaN | NaN | NaN | NaN |
| 106 | US-DPW | 2015 | NaN | NaN | NaN | NaN | NaN | NaN | NaN |
| 107 | US-DPW | 2016 | NaN | NaN | NaN | NaN | NaN | NaN | NaN |
| 108 | US-HRA | 2017 | NaN | NaN | NaN | NaN | NaN | NaN | NaN |
| 109 | US-HRC | 2018 | NaN | NaN | NaN | NaN | NaN | NaN | NaN |
| 110 | US-ICs | 2014 | TS_1 | 147.3 | 263.1 | -0.1 | 5.5 | 205.6 | 5.4 |
| 111 | US-ICs | 2015 | TS_1 | 141.6 | 255.7 | 0.0 | 6.1 | 195.2 | 6.1 |
| 112 | US-ICs | 2016 | TS_1 | 146.7 | 265.9 | 0.0 | 5.7 | 206.2 | 5.6 |
| 113 | US-Ivo | 2013 | NaN | NaN | NaN | NaN | NaN | NaN | NaN |
| 114 | US-Ivo | 2014 | TS_1 | 136.9 | 264.3 | -0.2 | 10.8 | 195.7 | 10.6 |
| 115 | US-Ivo | 2015 | TS_1 | 139.4 | 257.1 | -0.1 | 14.9 | 185.6 | 14.7 |
| 116 | US-Ivo | 2016 | TS_1 | 133.6 | 262.4 | -0.1 | 8.9 | 197.3 | 8.8 |
| 117 | US-LAI | 2012 | TS_1 | 29.1 | 331.4 | 15.6 | 13.5 | 197.2 | 29.1 |
| 118 | US-LA2 | 2012 | TS_1 | 36.6 | 336.1 | 15.0 | 14.4 | 193.2 | 29.4 |
| 119 | US-LA2 | 2013 | TS_1 | 65.8 | 377.9 | 14.7 | 16.1 | 201.5 | 30.8 |
| 120 | US-Los | 2014 | TS_1 | 0.0 | 417.4 | 2.0 | 8.3 | 244.3 | 10.2 |
| 121 | US-Los | 2015 | TS_1 | 0.0 | 422.3 | 2.4 | 7.8 | 258.7 | 10.2 |
| 122 | US-Los | 2016 | TS_1 | 0.0 | 415.7 | 2.5 | 8.1 | 255.1 | 10.6 |
| 123 | US-Los | 2017 | TS_1 | 0.0 | 414.6 | 1.9 | 7.5 | 256.0 | 9.3 |
| 124 | US-Los | 2018 | TS_1 | 0.0 | 421.8 | 1.5 | 7.4 | 260.0 | 8.9 |
| 125 | US-MAC | 2013 | NaN | NaN | NaN | NaN | NaN | NaN | NaN |
| 126 | US-MAC | 2014 | NaN | NaN | NaN | NaN | NaN | NaN | NaN |
| 127 | US-MAC | 2015 | NaN | NaN | NaN | NaN | NaN | NaN | NaN |
| 128 | US-Myb | 2010 | NaN | NaN | NaN | NaN | NaN | NaN | NaN |
| 129 | US-Myb | 2011 | TS_3 | NaN | 329.5 | 12.1 | 8.9 | 231.7 | 21.0 |
| 130 | US-Myb | 2012 | TS_3 | 35.6 | 372.2 | 9.4 | 11.0 | 216.1 | 20.4 |
| 131 | US-Myb | 2013 | TS_3 | 34.4 | 354.7 | 9.2 | 11.3 | 210.9 | 20.5 |
| 132 | US-Myb | 2014 | TS_3 | 26.0 | 365.9 | 9.6 | 12.3 | 210.0 | 21.9 |
| 133 | US-Myb | 2015 | TS_3 | 17.3 | 340.7 | 9.8 | 11.9 | 212.0 | 21.6 |
| 134 | US-Myb | 2016 | TS_3 | 5.1 | 357.8 | 9.6 | 11.2 | 201.0 | 20.8 |
| 135 | US-Myb | 2017 | TS_3 | 27.3 | 352.9 | 9.9 | 13.1 | 214.0 | 23.0 |
| 136 | US-Myb | 2018 | TS_3 | 36.3 | 326.1 | 10.2 | 10.7 | 207.0 | 20.9 |
| 137 | US-NC4 | 2012 | TS_1 | 42.4 | 336.0 | 7.9 | 15.8 | 215.4 | 23.6 |
| 138 | US-NC4 | 2013 | TS_1 | 60.0 | 368.8 | 6.9 | 16.8 | 210.5 | 23.7 |
| 139 | US-NC4 | 2014 | TS_1 | 54.4 | 362.3 | 6.7 | 16.8 | 208.5 | 23.5 |

Table B5. Continued.

| SITE_ID | Year | Probe_name | Soil_temp_depth_m | Start_TS_(DOY) | End_TS_(DOY) | Base_value_TS_(C) | Ampl_TS_(C) | Peak_TS_(DOY) | Peak_value_TS_(C) | |
|---------|--------|------------|-------------------|----------------|--------------|-------------------|-------------|---------------|-------------------|------|
| 140 | US-NC4 | 2015 | TS_1 | -0.1 | 68.1 | 387.3 | 8.3 | 16.1 | 205.0 | 24.3 |
| 141 | US-NC4 | 2016 | TS_1 | -0.1 | 53.0 | 351.4 | 9.4 | 15.0 | 220.0 | 24.5 |
| 142 | US-ORv | 2011 | NAN | NAN | NAN | NAN | NAN | NAN | NAN | NAN |
| 143 | US-ORv | 2012 | TS | NAN | 57.4 | 352.6 | 4.4 | 20.6 | 203.9 | 25.0 |
| 144 | US-ORv | 2013 | TS | NAN | 63.7 | 356.7 | 2.9 | 20.0 | 210.8 | 22.9 |
| 145 | US-ORv | 2014 | TS | NAN | 68.1 | 365.0 | 2.1 | 20.2 | 205.3 | 22.3 |
| 146 | US-ORv | 2015 | TS | NAN | 68.8 | 387.8 | 1.8 | 21.3 | 206.0 | 23.0 |
| 147 | US-OWC | 2015 | NAN | NAN | NAN | NAN | NAN | NAN | NAN | NAN |
| 148 | US-OWC | 2016 | TS_1 | -0.1 | 0.0 | 0.0 | 0.0 | 0.0 | 211.2 | 23.9 |
| 149 | US-Sne | 2016 | NAN | NAN | NAN | NAN | NAN | NAN | NAN | NAN |
| 150 | US-Sne | 2017 | TS_1 | 0.0 | 46.1 | 337.9 | 10.3 | 13.1 | 212.7 | 23.5 |
| 151 | US-Sne | 2018 | TS_1 | 0.0 | 48.4 | 325.1 | 10.3 | 12.2 | 217.3 | 22.4 |
| 152 | US-Srr | 2014 | NAN | NAN | NAN | NAN | NAN | NAN | NAN | NAN |
| 153 | US-Srr | 2015 | NAN | NAN | NAN | NAN | NAN | NAN | NAN | NAN |
| 154 | US-Srr | 2016 | TS_1 | NAN | NAN | 326.3 | 10.0 | 10.7 | 200.5 | 20.7 |
| 155 | US-Srr | 2017 | TS_1 | NAN | 11.3 | 346.8 | 7.2 | 13.7 | 199.5 | 20.9 |
| 156 | US-Srd | 2016 | TS_2 | -0.1 | 68.4 | 347.4 | 4.1 | 16.2 | 213.7 | 20.3 |
| 157 | US-Tw1 | 2011 | NAN | NAN | NAN | NAN | NAN | NAN | NAN | NAN |
| 158 | US-Tw1 | 2012 | TS_1 | 0.0 | 50.5 | 360.0 | 6.0 | 11.5 | 225.2 | 17.5 |
| 159 | US-Tw1 | 2013 | TS_1 | 0.0 | 35.8 | 337.6 | 4.4 | 14.6 | 206.6 | 19.0 |
| 160 | US-Tw1 | 2014 | TS_1 | 0.0 | 41.2 | 395.4 | 6.7 | 10.9 | 208.3 | 17.6 |
| 161 | US-Tw1 | 2015 | TS_1 | 0.0 | 50.7 | 342.5 | 9.0 | 7.8 | 235.0 | 16.9 |
| 162 | US-Tw1 | 2016 | TS_1 | 0.0 | 34.6 | 361.1 | 8.8 | 7.9 | 218.0 | 16.7 |
| 163 | US-Tw1 | 2017 | TS_1 | 0.0 | 41.2 | 343.7 | 7.5 | 10.2 | 228.0 | 17.8 |
| 164 | US-Tw1 | 2018 | TS_1 | 0.0 | 60.5 | 327.4 | 6.7 | 10.4 | 222.0 | 17.1 |
| 165 | US-Tw4 | 2014 | NAN | NAN | NAN | NAN | NAN | NAN | NAN | NAN |
| 166 | US-Tw4 | 2015 | TS_1 | 0.0 | 15.9 | 327.2 | 10.0 | 11.6 | 199.4 | 21.6 |
| 167 | US-Tw4 | 2016 | TS_1 | 0.0 | 9.6 | 358.7 | 8.2 | 11.3 | 201.7 | 19.5 |
| 168 | US-Tw4 | 2017 | TS_1 | 0.0 | 38.3 | 347.3 | 8.1 | 11.5 | 211.9 | 19.6 |
| 169 | US-Tw4 | 2018 | TS_1 | 0.0 | 58.1 | 344.9 | 8.0 | 10.9 | 218.0 | 18.9 |
| 170 | US-Tw5 | 2018 | TS_1 | 0.0 | NAN | 414.8 | 0.0 | 8.9 | 222.2 | 18.4 |
| 171 | US-Twt | 2009 | NAN | NAN | NAN | NAN | NAN | NAN | NAN | NAN |
| 172 | US-Twt | 2010 | NAN | NAN | NAN | NAN | NAN | NAN | NAN | NAN |
| 173 | US-Twt | 2011 | NAN | NAN | NAN | NAN | NAN | NAN | NAN | NAN |
| 174 | US-Twt | 2012 | NAN | NAN | NAN | NAN | NAN | NAN | NAN | NAN |
| 175 | US-Twt | 2013 | NAN | NAN | NAN | NAN | NAN | NAN | NAN | NAN |
| 176 | US-Twt | 2014 | NAN | NAN | NAN | NAN | NAN | NAN | NAN | NAN |
| 177 | US-Twt | 2015 | NAN | NAN | NAN | NAN | NAN | NAN | NAN | NAN |
| 178 | US-Twt | 2016 | NAN | NAN | NAN | NAN | NAN | NAN | NAN | NAN |
| 179 | US-Uaf | 2011 | TS_1 | -0.1 | 86.2 | 372.5 | -12.3 | 22.0 | 199.6 | 9.7 |

Table B5. Continued.

| SITE_ID | Year | Probe_name | Soil_temp_depth_m | Start_TS_(DOY) | End_TS_(DOY) | Base_value_TS_(C) | Ampl_TS_(C) | Peak_TS_(DOY) | Peak_value_TS_(C) |
|---------|--------|------------|-------------------|----------------|--------------|-------------------|-------------|---------------|-------------------|
| 180 | US-Uaf | TS_1 | -0.1 | 73.8 | 338.5 | -11.8 | 20.9 | 202.4 | 9.0 |
| 181 | US-Uaf | TS_1 | -0.1 | 109.6 | 395.5 | -10.1 | 20.5 | 200.4 | 10.4 |
| 182 | US-Uaf | TS_1 | -0.1 | 76.1 | 365.4 | -10.9 | 19.9 | 206.0 | 9.0 |
| 183 | US-Uaf | TS_1 | -0.1 | 81.0 | 423.2 | -9.8 | 19.8 | 190.0 | 10.0 |
| 184 | US-Uaf | TS_1 | -0.1 | 77.4 | 315.8 | -7.7 | 19.1 | 198.0 | 11.4 |
| 185 | US-Uaf | TS_1 | -0.1 | 84.9 | 380.2 | -7.4 | 19.1 | 196.0 | 11.7 |
| 186 | US-Uaf | TS_1 | -0.1 | 96.0 | 333.3 | -5.6 | 17.7 | 199.0 | 12.1 |
| 187 | US-WPT | TS_1 | -0.1 | 81.0 | 342.2 | 5.3 | 19.3 | 202.6 | 24.5 |
| 188 | US-WPT | TS_1 | -0.1 | 40.3 | 345.6 | 3.7 | 21.6 | 197.4 | 25.3 |
| 189 | US-WPT | TS_1 | -0.1 | 74.6 | 340.5 | 3.7 | 18.2 | 207.2 | 22.0 |

Table B5. Continued.

| SITE_ID | Year | Start_TA_(DOY) | End_TA_(DOY) | Base_value_TA_(C) | Ampl_TA_(C) | Peak_TA_(DOY) | Peak_value_TA_(C) | |
|---------|---------|----------------|--------------|-------------------|-------------|---------------|-------------------|------|
| 1 | AT-Neu | 2010 | 43.2 | 351.7 | -4.8 | 20.9 | 195.9 | 16.1 |
| 2 | AT-Neu | 2011 | 18.5 | 359.9 | -5.1 | 20.6 | 198.5 | 15.5 |
| 3 | AT-Neu | 2012 | 38.0 | 366.6 | -5.6 | 22.4 | 197.2 | 16.8 |
| 4 | BR-Npw | 2014 | NaN | NaN | NaN | NaN | NaN | NaN |
| 5 | BR-Npw | 2015 | NaN | NaN | NaN | NaN | NaN | NaN |
| 6 | BR-Npw | 2016 | 7.5 | 348.7 | 19.6 | 7.5 | 211.0 | 27.1 |
| 7 | BW-Gunn | 2018 | NaN | NaN | NaN | NaN | NaN | NaN |
| 8 | BW-Gunn | 2019 | NaN | NaN | NaN | NaN | NaN | NaN |
| 9 | BW-Nxr | 2018 | NaN | NaN | NaN | NaN | NaN | NaN |
| 10 | CA-SCB | 2014 | 60.2 | 335.3 | -23.3 | 41.3 | 197.4 | 18.0 |
| 11 | CA-SCB | 2015 | 45.1 | 360.8 | -21.8 | 39.1 | 186.4 | 17.4 |
| 12 | CA-SCB | 2016 | 49.8 | 335.8 | -18.9 | 37.3 | 193.9 | 18.4 |
| 13 | CA-SCB | 2017 | 64.7 | 327.3 | -18.5 | 36.0 | 201.0 | 17.5 |
| 14 | CA-SCC | 2013 | 67.6 | 338.2 | -21.1 | 39.1 | 203.8 | 18.1 |
| 15 | CA-SCC | 2014 | 54.1 | 337.8 | -22.3 | 41.0 | 196.7 | 18.7 |
| 16 | CA-SCC | 2015 | 46.4 | 359.4 | -20.1 | 37.9 | 187.1 | 17.8 |
| 17 | CA-SCC | 2016 | 47.3 | 350.2 | -18.8 | 37.7 | 194.0 | 18.9 |
| 18 | DE-Dgw | 2015 | 72.5 | 347.6 | 2.2 | 16.3 | 203.8 | 18.4 |
| 19 | DE-Dgw | 2016 | 64.5 | 324.7 | 1.3 | 17.4 | 205.4 | 18.7 |
| 20 | DE-Dgw | 2017 | 43.8 | 375.3 | -0.2 | 18.5 | 202.2 | 18.3 |
| 21 | DE-Hie | 2011 | NaN | NaN | NaN | NaN | NaN | NaN |
| 22 | DE-Hie | 2012 | 50.3 | 352.5 | 0.8 | 17.0 | 207.6 | 17.8 |
| 23 | DE-Hie | 2013 | 83.5 | 365.3 | 1.6 | 17.1 | 202.5 | 18.7 |
| 24 | DE-Hie | 2014 | 48.7 | 352.5 | 2.9 | 15.8 | 213.0 | 18.7 |
| 25 | DE-Hie | 2015 | 57.6 | 366.3 | 2.6 | 15.3 | 211.0 | 17.9 |
| 26 | DE-Hie | 2016 | 67.5 | 323.1 | 2.7 | 16.0 | 211.0 | 18.8 |
| 27 | DE-Hie | 2017 | 58.9 | 370.1 | 1.8 | 16.2 | 212.0 | 18.0 |
| 28 | DE-Hie | 2018 | 74.5 | 368.0 | 0.9 | 19.1 | 203.0 | 20.1 |
| 29 | DE-SfN | 2012 | 54.9 | 355.2 | -2.1 | 20.3 | 196.3 | 18.2 |
| 30 | DE-SfN | 2013 | 64.6 | 344.0 | -0.3 | 18.6 | 202.8 | 18.2 |
| 31 | DE-SfN | 2014 | NaN | NaN | NaN | NaN | NaN | NaN |
| 32 | DE-Zrk | 2013 | NaN | NaN | NaN | NaN | NaN | NaN |
| 33 | DE-Zrk | 2014 | NaN | NaN | NaN | NaN | NaN | NaN |
| 34 | DE-Zrk | 2015 | 49.7 | 355.4 | 2.1 | 15.3 | 203.4 | 17.5 |
| 35 | DE-Zrk | 2016 | 63.3 | 323.8 | 1.9 | 16.5 | 204.0 | 18.3 |
| 36 | DE-Zrk | 2017 | 45.2 | 372.5 | 0.5 | 17.4 | 205.0 | 17.9 |
| 37 | DE-Zrk | 2018 | 75.8 | 358.9 | -0.1 | 18.8 | 190.0 | 18.7 |
| 38 | Fl-Lom | 2006 | 72.5 | 355.6 | -12.2 | 26.7 | 195.0 | 14.5 |
| 39 | Fl-Lom | 2007 | 56.2 | 372.5 | -11.0 | 22.6 | 193.4 | 11.6 |
| 40 | Fl-Lom | 2008 | 73.5 | 348.1 | -10.4 | 22.3 | 200.4 | 12.0 |
| 41 | Fl-Lom | 2009 | 56.7 | 356.3 | -13.6 | 27.1 | 205.0 | 13.5 |
| 42 | Fl-Lom | 2010 | 54.8 | 346.0 | -16.1 | 27.8 | 200.0 | 11.7 |
| 43 | Fl-Si2 | 2012 | 70.4 | 349.7 | -6.9 | 22.7 | 199.1 | 15.8 |
| 44 | Fl-Si2 | 2013 | 88.2 | 369.5 | -6.0 | 23.7 | 188.6 | 17.8 |

Table B5. Continued.

| SITE_ID | Year | Start_TA_(DOY) | End_TA_(DOY) | Base_value_TA_(C) | Ampl_TA_(C) | Peak_TA_(DOY) | Peak_value_TA_(C) | |
|---------|--------|----------------|--------------|-------------------|-------------|---------------|-------------------|------|
| 45 | FI-Si2 | 2014 | 53.3 | 350.4 | -4.4 | 21.5 | 200.3 | 17.1 |
| 46 | FI-Si2 | 2015 | 39.6 | 359.2 | -5.0 | 19.4 | 212.0 | 14.4 |
| 47 | FI-Si2 | 2016 | 42.6 | 345.0 | -6.7 | 23.2 | 199.0 | 16.5 |
| 48 | FI-Sii | 2013 | 89.3 | 363.9 | -5.7 | 22.2 | 189.1 | 16.5 |
| 49 | FI-Sii | 2014 | 52.0 | 339.8 | -4.4 | 21.5 | 200.9 | 17.2 |
| 50 | FI-Sii | 2015 | 34.4 | 357.7 | -5.4 | 19.7 | 209.5 | 14.3 |
| 51 | FI-Sii | 2016 | 55.0 | 320.6 | -5.2 | 20.9 | 195.0 | 15.7 |
| 52 | FI-Sii | 2017 | 61.6 | 377.3 | -6.3 | 20.9 | 208.0 | 14.6 |
| 53 | FI-Sii | 2018 | 74.2 | 378.7 | -9.0 | 27.4 | 195.0 | 18.4 |
| 54 | HK-MPM | 2016 | 53.6 | 378.9 | 16.0 | 13.3 | 198.1 | 29.2 |
| 55 | HK-MPM | 2017 | 49.1 | 357.3 | 16.3 | 13.1 | 215.6 | 29.3 |
| 56 | HK-MPM | 2018 | 42.1 | 383.0 | 15.3 | 14.1 | 199.0 | 29.3 |
| 57 | ID-Pag | 2016 | NaN | NaN | NaN | NaN | NaN | NaN |
| 58 | JP-BBY | 2015 | 56.2 | 355.7 | -5.3 | 25.9 | 209.5 | 20.6 |
| 59 | JP-BBY | 2016 | 46.1 | 348.0 | -7.1 | 28.0 | 212.0 | 20.9 |
| 60 | JP-BBY | 2017 | 44.7 | 361.6 | -7.5 | 28.2 | 208.7 | 20.7 |
| 61 | JP-BBY | 2018 | 45.6 | 367.9 | -7.6 | 27.1 | 210.0 | 19.6 |
| 62 | JP-Mse | 2012 | 54.5 | 351.8 | 1.5 | 24.6 | 219.9 | 26.1 |
| 63 | KR-CRK | 2015 | NaN | NaN | NaN | NaN | NaN | NaN |
| 64 | KR-CRK | 2016 | NaN | NaN | NaN | NaN | NaN | NaN |
| 65 | KR-CRK | 2017 | NaN | NaN | NaN | NaN | NaN | NaN |
| 66 | KR-CRK | 2018 | NaN | NaN | NaN | NaN | NaN | NaN |
| 67 | MY-MLM | 2014 | 17.5 | 365.8 | 26.0 | 1.9 | 179.4 | 27.9 |
| 68 | MY-MLM | 2015 | NaN | NaN | NaN | NaN | NaN | NaN |
| 69 | NZ-Kop | 2012 | 50.8 | 347.1 | 9.1 | 9.7 | 219.9 | 18.8 |
| 70 | NZ-Kop | 2013 | 39.3 | 352.9 | 9.3 | 8.3 | 209.6 | 17.6 |
| 71 | NZ-Kop | 2014 | 53.5 | 352.7 | 9.1 | 9.7 | 215.0 | 18.8 |
| 72 | NZ-Kop | 2015 | 51.0 | 357.8 | 8.5 | 10.4 | 212.0 | 19.0 |
| 73 | PH-RiF | 2012 | NaN | NaN | NaN | NaN | NaN | NaN |
| 74 | PH-RiF | 2013 | NaN | NaN | NaN | NaN | NaN | NaN |
| 75 | PH-RiF | 2014 | NaN | NaN | NaN | NaN | NaN | NaN |
| 76 | PH-RiF | 2015 | NaN | NaN | NaN | NaN | NaN | NaN |
| 77 | RU-Ch2 | 2014 | 62.1 | 339.9 | -31.6 | 46.0 | 208.4 | 14.4 |
| 78 | RU-Ch2 | 2015 | 54.1 | 340.0 | -34.4 | 47.6 | 204.4 | 13.2 |
| 79 | RU-Ch2 | 2016 | 56.4 | 373.2 | -34.4 | 48.4 | 201.9 | 14.0 |
| 80 | RU-Che | 2014 | 61.3 | 340.0 | -31.5 | 45.9 | 208.0 | 14.4 |
| 81 | RU-Che | 2015 | 53.2 | 340.1 | -34.3 | 47.6 | 204.3 | 13.3 |
| 82 | RU-Che | 2016 | 55.9 | 372.3 | -34.3 | 48.4 | 201.7 | 14.1 |
| 83 | SE-Deg | 2014 | 69.6 | 327.7 | -5.2 | 21.4 | 201.0 | 16.2 |
| 84 | SE-Deg | 2015 | 29.7 | 352.2 | -7.4 | 19.3 | 213.9 | 11.9 |
| 85 | SE-Deg | 2016 | 54.7 | 331.3 | -7.3 | 21.0 | 197.1 | 13.7 |
| 86 | SE-Deg | 2017 | 61.9 | 353.2 | -8.3 | 21.3 | 210.0 | 13.0 |
| 87 | SE-Deg | 2018 | 74.4 | 373.7 | -11.3 | 26.5 | 193.0 | 15.2 |
| 88 | US-Atq | 2013 | NaN | NaN | NaN | NaN | NaN | NaN |
| 89 | US-Atq | 2014 | 70.0 | 360.8 | -25.8 | 32.2 | 203.4 | 6.4 |
| 90 | US-Atq | 2015 | 84.1 | 347.2 | -26.1 | 34.7 | 196.7 | 8.6 |
| 91 | US-Beo | 2013 | NaN | NaN | NaN | NaN | NaN | NaN |

Table B5. Continued.

| SITE_ID | Year | Start_TA_(DOY) | End_TA_(DOY) | Base_value_TA_(C) | Ampl_TA_(C) | Peak_TA_(DOY) | Peak_value_TA_(C) | |
|---------|--------|----------------|--------------|-------------------|-------------|---------------|-------------------|------|
| 92 | US-Beo | 2014 | 63.3 | 351.3 | -22.7 | 25.6 | 203.2 | 2.9 |
| 93 | US-Bes | 2013 | NaN | NaN | NaN | NaN | NaN | NaN |
| 94 | US-Bes | 2014 | 76.6 | 357.3 | -24.7 | 26.6 | 208.3 | 1.8 |
| 95 | US-Bes | 2015 | 82.7 | 344.0 | -25.2 | 29.5 | 203.3 | 4.3 |
| 96 | US-BZB | 2014 | 65.0 | 339.3 | -17.1 | 32.1 | 189.6 | 15.0 |
| 97 | US-BZB | 2015 | 52.2 | 340.0 | -17.3 | 33.9 | 181.6 | 16.6 |
| 98 | US-BZB | 2016 | 35.7 | 321.0 | -16.9 | 33.5 | 192.5 | 16.6 |
| 99 | US-BZF | 2014 | 64.6 | 341.5 | -16.8 | 32.0 | 190.5 | 15.2 |
| 100 | US-BZF | 2015 | 52.2 | 341.0 | -16.9 | 33.4 | 181.5 | 16.5 |
| 101 | US-BZF | 2016 | 34.6 | 321.3 | -16.6 | 33.2 | 194.0 | 16.6 |
| 102 | US-BZS | 2015 | 46.2 | 343.6 | -17.4 | 34.6 | 180.2 | 17.2 |
| 103 | US-BZS | 2016 | 32.5 | 320.3 | -15.9 | 33.0 | 193.8 | 17.1 |
| 104 | US-DPW | 2013 | 59.4 | 361.7 | 16.3 | 10.9 | 220.8 | 27.2 |
| 105 | US-DPW | 2014 | 38.7 | 326.8 | 16.0 | 11.8 | 210.3 | 27.8 |
| 106 | US-DPW | 2015 | 33.6 | 381.2 | 15.9 | 10.0 | 211.8 | 25.9 |
| 107 | US-DPW | 2016 | 45.5 | 367.1 | 15.7 | 12.8 | 203.0 | 28.5 |
| 108 | US-HRA | 2017 | NaN | NaN | NaN | NaN | NaN | NaN |
| 109 | US-HRC | 2018 | NaN | NaN | NaN | NaN | NaN | NaN |
| 110 | US-ICs | 2014 | NaN | NaN | NaN | NaN | NaN | NaN |
| 111 | US-ICs | 2015 | NaN | NaN | NaN | NaN | NaN | NaN |
| 112 | US-ICs | 2016 | 68.1 | 328.8 | -16.9 | 26.3 | 196.8 | 9.4 |
| 113 | US-Ivo | 2013 | 93.1 | 360.4 | -23.4 | 36.2 | 193.6 | 12.8 |
| 114 | US-Ivo | 2014 | 69.0 | 341.9 | -21.4 | 30.7 | 193.5 | 9.3 |
| 115 | US-Ivo | 2015 | 90.8 | 326.8 | -21.5 | 31.9 | 188.6 | 10.4 |
| 116 | US-Ivo | 2016 | 90.0 | 340.0 | -21.6 | 31.3 | 197.0 | 9.7 |
| 117 | US-LAI | 2012 | 31.0 | 302.5 | 19.1 | 8.8 | 177.6 | 27.9 |
| 118 | US-LA2 | 2012 | 35.2 | 316.9 | 16.7 | 11.6 | 197.4 | 28.3 |
| 119 | US-LA2 | 2013 | 71.4 | 321.2 | 15.9 | 13.3 | 210.6 | 29.2 |
| 120 | US-Los | 2014 | 58.0 | 365.5 | -14.2 | 33.1 | 195.4 | 18.9 |
| 121 | US-Los | 2015 | 50.4 | 367.6 | -10.8 | 29.4 | 203.5 | 18.6 |
| 122 | US-Los | 2016 | 39.2 | 356.4 | -9.1 | 29.1 | 209.4 | 20.0 |
| 123 | US-Los | 2017 | 30.7 | 345.4 | -9.8 | 28.1 | 212.0 | 18.3 |
| 124 | US-Los | 2018 | 69.6 | 336.0 | -9.7 | 29.8 | 197.0 | 20.0 |
| 125 | US-MAC | 2013 | NaN | NaN | NaN | NaN | NaN | NaN |
| 126 | US-MAC | 2014 | 42.4 | 324.0 | 17.1 | 9.8 | 211.2 | 26.9 |
| 127 | US-MAC | 2015 | 39.5 | 328.0 | 16.9 | 9.6 | 200.6 | 26.6 |
| 128 | US-Myb | 2010 | NaN | NaN | NaN | NaN | NaN | NaN |
| 129 | US-Myb | 2011 | 31.1 | 331.8 | 8.2 | 12.6 | 223.6 | 20.8 |
| 130 | US-Myb | 2012 | 16.5 | 358.5 | 7.2 | 13.5 | 214.9 | 20.7 |
| 131 | US-Myb | 2013 | 24.4 | 342.3 | 7.3 | 13.4 | 197.0 | 20.7 |
| 132 | US-Myb | 2014 | 11.5 | 353.5 | 8.8 | 12.8 | 211.0 | 21.5 |
| 133 | US-Myb | 2015 | -1.0 | 325.6 | 8.9 | 13.1 | 228.0 | 22.0 |
| 134 | US-Myb | 2016 | -3.3 | 351.7 | 8.0 | 13.0 | 208.0 | 20.9 |
| 135 | US-Myb | 2017 | 27.3 | 345.8 | 8.3 | 13.9 | 214.0 | 22.2 |

Table B5. Continued.

| SITE_ID | Year | Start_TA_(DOY) | End_TA_(DOY) | Base_value_TA_(C) | AmpL_TA_(C) | Peak_TA_(DOY) | Peak_value_TA_(C) |
|---------|--------|----------------|--------------|-------------------|-------------|---------------|-------------------|
| 136 | US-Myb | 2018 | 44.4 | 332.6 | 9.0 | 11.5 | 20.5 |
| 137 | US-NC4 | 2012 | 57.3 | 339.3 | 9.0 | 17.5 | 26.5 |
| 138 | US-NC4 | 2013 | 69.3 | 352.4 | 6.8 | 19.0 | 25.8 |
| 139 | US-NC4 | 2014 | 49.2 | 367.7 | 5.4 | 18.3 | 23.7 |
| 140 | US-NC4 | 2015 | 64.4 | 392.2 | 6.9 | 19.4 | 26.3 |
| 141 | US-NC4 | 2016 | 54.0 | 350.6 | 8.1 | 19.1 | 27.2 |
| 142 | US-ORv | 2011 | 64.0 | 358.3 | 0.5 | 25.1 | 25.6 |
| 143 | US-ORv | 2012 | 32.9 | 351.3 | 0.8 | 24.9 | 25.8 |
| 144 | US-ORv | 2013 | 51.2 | 355.8 | -2.4 | 25.9 | 23.5 |
| 145 | US-ORv | 2014 | 51.3 | 370.0 | -4.3 | 28.0 | 23.6 |
| 146 | US-ORv | 2015 | 62.5 | 393.6 | -4.6 | 27.9 | 23.3 |
| 147 | US-OWC | 2015 | NaN | NaN | NaN | NaN | NaN |
| 148 | US-OWC | 2016 | 56.2 | 365.0 | 2.2 | 22.7 | 24.9 |
| 149 | US-Sne | 2016 | NaN | NaN | NaN | NaN | NaN |
| 150 | US-Sne | 2017 | 9.2 | 344.4 | 7.3 | 14.5 | 21.8 |
| 151 | US-Sne | 2018 | 49.6 | 357.4 | 7.1 | 14.0 | 21.1 |
| 152 | US-Srr | 2014 | 50.6 | 337.4 | 10.7 | 10.1 | 20.8 |
| 153 | US-Srr | 2015 | 5.0 | 323.3 | 9.5 | 12.2 | 21.7 |
| 154 | US-Srr | 2016 | -6.2 | 346.2 | 8.3 | 11.7 | 20.0 |
| 155 | US-Srr | 2017 | 17.2 | 346.4 | 7.9 | 13.4 | 21.4 |
| 156 | US-StJ | 2016 | 67.3 | 347.1 | 3.0 | 23.4 | 26.4 |
| 157 | US-Tw1 | 2011 | 59.5 | 328.0 | 7.8 | 13.5 | 21.3 |
| 158 | US-Tw1 | 2012 | 18.5 | 356.8 | 6.7 | 14.9 | 21.6 |
| 159 | US-Tw1 | 2013 | 29.3 | 344.8 | 7.1 | 14.3 | 21.4 |
| 160 | US-Tw1 | 2014 | 14.7 | 349.8 | 8.5 | 13.6 | 22.1 |
| 161 | US-Tw1 | 2015 | 7.0 | 324.1 | 8.2 | 13.5 | 21.6 |
| 162 | US-Tw1 | 2016 | 4.4 | 350.6 | 7.2 | 13.9 | 21.1 |
| 163 | US-Tw1 | 2017 | 25.1 | 343.3 | 7.2 | 15.1 | 22.4 |
| 164 | US-Tw1 | 2018 | 50.8 | 337.8 | 7.4 | 13.4 | 20.8 |
| 165 | US-Tw4 | 2014 | 15.7 | 348.8 | 8.6 | 13.4 | 22.1 |
| 166 | US-Tw4 | 2015 | 5.3 | 324.6 | 8.5 | 13.4 | 21.9 |
| 167 | US-Tw4 | 2016 | 2.7 | 347.6 | 7.6 | 14.1 | 21.6 |
| 168 | US-Tw4 | 2017 | 30.8 | 337.8 | 7.9 | 15.1 | 23.0 |
| 169 | US-Tw4 | 2018 | 44.5 | 331.6 | 8.3 | 13.1 | 21.3 |
| 170 | US-Tw5 | 2018 | 76.3 | 338.5 | 9.2 | 12.6 | 21.8 |
| 171 | US-Twt | 2009 | NaN | NaN | NaN | NaN | NaN |
| 172 | US-Twt | 2010 | NaN | NaN | NaN | NaN | NaN |
| 173 | US-Twt | 2011 | NaN | NaN | NaN | NaN | NaN |
| 174 | US-Twt | 2012 | NaN | NaN | NaN | NaN | NaN |
| 175 | US-Twt | 2013 | NaN | NaN | NaN | NaN | NaN |
| 176 | US-Twt | 2014 | NaN | NaN | NaN | NaN | NaN |
| 177 | US-Twt | 2015 | NaN | NaN | NaN | NaN | NaN |
| 178 | US-Twt | 2016 | NaN | NaN | NaN | NaN | NaN |
| 179 | US-Uaf | 2011 | 59.0 | 330.8 | -23.4 | 38.5 | 15.0 |

Table B5. Continued.

| | SITE_ID | Year | Start_TA_(DOY) | End_TA_(DOY) | Base_value_TA_(C) | Ampl_TA_(C) | Peak_TA_(DOY) | Peak_value_TA_(C) |
|-----|---------|------|----------------|--------------|-------------------|-------------|---------------|-------------------|
| 180 | US-Uaf | 2012 | 43.1 | 317.7 | -23.9 | 38.6 | 192.3 | 14.6 |
| 181 | US-Uaf | 2013 | 64.4 | 344.1 | -22.1 | 39.6 | 195.9 | 17.5 |
| 182 | US-Uaf | 2014 | 49.9 | 343.0 | -20.6 | 34.2 | 190.0 | 13.7 |
| 183 | US-Uaf | 2015 | 51.3 | 346.7 | -19.5 | 34.9 | 182.0 | 15.4 |
| 184 | US-Uaf | 2016 | 27.3 | 325.5 | -20.8 | 36.1 | 193.0 | 15.3 |
| 185 | US-Uaf | 2017 | 59.2 | 357.6 | -22.1 | 38.3 | 191.0 | 16.2 |
| 186 | US-Uaf | 2018 | 35.4 | 354.6 | -21.6 | 36.7 | 196.0 | 15.2 |
| 187 | US-WPT | 2011 | 62.3 | 362.6 | -1.1 | 26.3 | 199.1 | 25.2 |
| 188 | US-WPT | 2012 | 34.9 | 355.2 | -0.4 | 25.5 | 198.4 | 25.1 |
| 189 | US-WPT | 2013 | 64.2 | 341.1 | -1.9 | 24.5 | 205.0 | 22.6 |

| Column | Description |
|--|--|
| SITE_ID | Site identification code as assigned by regional flux data network |
| Year | Data year |
| Start_FCH4_(DOY) | Season start for elevated methane fluxes (DOY), point “f” in Fig. 1 |
| End_FCH4_(DOY) | Season end for elevated methane fluxes (DOY), point “h” in Fig. 1 |
| Base_value_FCH4_(nmolCH ₄ /m ² /s) | Baseline methane flux during non-elevated season (nmol CH ₄ m ⁻² s ⁻¹), average of points “a” and “b” in Fig. 1 |
| Ampl_FCH4_(nmolCH ₄ /m ² /s) | Amplitude of methane flux during elevated flux season (nmol CH ₄ m ⁻² s ⁻¹), difference between point “e” in Fig. 1 and Base_value_FCH4 |
| Peak_FCH4_(DOY) | Day of maximum elevated methane flux (DOY), point “g” in Fig. 1 |
| Peak_value_FCH4_(nmolCH ₄ /m ² /s) | Maximum value of methane flux (nmol CH ₄ m ⁻² s ⁻¹), point “e” in Fig. 1 |
| Start_GPP_DT_(DOY) | Season start for elevated GPP_DT (DOY), point “f” in Fig. 1 |
| End_GPP_DT_(DOY) | Season end for elevated GPP_DT fluxes (DOY), point “h” in Fig. 1 |
| Base_value_GPP_DT_(μmolCO ₂ /m ² /s) | Baseline GPP_DT flux during non-elevated season (μmol CO ₂ m ⁻² s ⁻¹), average of points “a” and “b” in Fig. 1 |
| Ampl_GPP_DT_(μmolCO ₂ /m ² /s) | Amplitude of GPP_DT flux during elevated flux season (μmol CO ₂ m ⁻² s ⁻¹), difference between point “e” in Fig. 1 and Base_value_GPP_DT |
| Peak_GPP_DT_(DOY) | Day of maximum elevated GPP_DT flux (DOY), point “g” in Fig. 1 |
| Peak_value_GPP_DT_(μmolCO ₂ /m ² /s) | Maximum value of GPP_DT flux (μmol CO ₂ m ⁻² s ⁻¹), point “e” in Fig. 1 |
| Probe_name | Temperature probe name as given in data files |
| Soil_temp_depth_m | Depth of soil temperature probe (m), with negative values being under the surface |
| Start_TS_(DOY) | Season start for elevated TS (DOY), point “f” in Fig. 1 |
| End_TS_(DOY) | Season end for elevated TS (DOY), point “h” in Fig. 1 |
| Base_value_TS_(C) | Baseline TS during non-elevated season (C), average of points “a” and “b” in Fig. 1 |
| Ampl_TS_(C) | Amplitude of TS during elevated temperature season (C), difference between point “e” in Fig. 1 and Base_value_TS |
| Peak_TS_(DOY) | Day of maximum elevated TS (DOY), point “g” in Fig. 1 |
| Peak_value_TS_(C) | Maximum value of TS (C), point “e” in Fig. 1 |
| Start_TA_(DOY) | Season start for elevated TA (DOY), point “f” in Fig. 1 |
| End_TA_(DOY) | Season end for elevated TA (DOY), point “h” in Fig. 1 |
| Base_value_TA_(C) | Baseline TA during non-elevated season (C), average of points “a” and “b” in Fig. 1 |
| Ampl_TA_(C) | Amplitude of TA during elevated temperature season (C), difference between point “e” in Fig. 1 and Base_value_TA |
| Peak_TA_(DOY) | Day of maximum elevated TA (DOY), point “g” in Fig. 1 |
| Peak_value_TA_(C) | Maximum value of TA (C), point “e” in Fig. 1 |

Table B6. Seasonality parameters estimated using TIMESAT software for soil temperature (TS, from every probe).

| | SITE_ID | Year | Probe_name | Soil_temp_depth_m | Start_TS_(DOY) | End_TS_(DOY) | Base_value_TS_(C) | Ampl_TS_(C) | Peak_TS_(DOY) | Peak_value_TS_(C) |
|----|---------|------|------------|-------------------|----------------|--------------|-------------------|-------------|---------------|-------------------|
| 1 | AT-Neu | 2010 | TS_1 | -0.05 | 61.3 | 339.4 | 0.15 | 17.54 | 200.9 | 17.7 |
| 2 | AT-Neu | 2011 | TS_1 | -0.05 | 51.0 | 328.8 | 0.40 | 16.37 | 201 | 16.77 |
| 3 | AT-Neu | 2012 | TS_1 | -0.05 | 61.1 | 341.9 | 0.73 | 17.57 | 202.9 | 18.3 |
| 4 | BR-Npw | 2016 | TS_1 | NaN | 18.4 | 343.2 | 22.41 | 5.982 | 188 | 28.4 |
| 5 | CA-SCB | 2014 | TS_1 | 0 | 105.9 | 292.2 | -0.63 | 20.62 | 196.6 | 19.99 |
| 6 | CA-SCB | 2014 | TS_2 | -0.02 | 105.1 | 294.1 | -0.74 | 20.42 | 197.5 | 19.68 |
| 7 | CA-SCB | 2014 | TS_3 | -0.04 | 112.0 | 294.4 | 0.05 | 19.07 | 199.6 | 19.11 |
| 8 | CA-SCB | 2014 | TS_5 | -0.16 | 123.2 | 317.7 | -1.38 | 18.6 | 205.3 | 17.23 |
| 9 | CA-SCB | 2015 | TS_1 | 0 | 106.9 | 287.1 | -0.39 | 17.23 | 186.8 | 16.84 |
| 10 | CA-SCB | 2015 | TS_2 | -0.02 | 107.1 | 287.4 | -0.42 | 17.08 | 187.4 | 16.66 |
| 11 | CA-SCB | 2015 | TS_3 | -0.04 | 107.4 | 289.8 | -0.51 | 16.81 | 188.9 | 16.3 |
| 12 | CA-SCB | 2015 | TS_5 | -0.16 | 114.9 | 305.5 | -0.39 | 15.84 | 195.7 | 15.45 |
| 13 | CA-SCB | 2016 | TS_1 | 0 | 101.6 | 284.1 | -0.31 | 19.07 | 193.2 | 18.77 |
| 14 | CA-SCB | 2016 | TS_2 | -0.02 | 101.8 | 284.1 | -0.30 | 18.96 | 193.5 | 18.66 |
| 15 | CA-SCB | 2016 | TS_3 | -0.04 | 102.2 | 285.2 | -0.30 | 18.6 | 194.3 | 18.3 |
| 16 | CA-SCB | 2016 | TS_5 | -0.16 | 101.2 | 299.0 | -0.24 | 16.99 | 201.1 | 16.74 |
| 17 | CA-SCB | 2017 | TS_1 | 0 | 107.4 | 289.7 | -0.25 | 17.67 | 198 | 17.42 |
| 18 | CA-SCB | 2017 | TS_2 | -0.02 | 107.2 | 288.9 | -0.25 | 17.59 | 198 | 17.33 |
| 19 | CA-SCB | 2017 | TS_3 | -0.04 | 108.6 | 289.3 | -0.26 | 17.28 | 199 | 17.02 |
| 20 | CA-SCB | 2017 | TS_5 | -0.16 | 116.3 | 300.3 | -0.24 | 14.95 | 214 | 14.71 |
| 21 | CA-SCC | 2014 | TS_1 | -0.1 | 123.4 | 287.1 | -0.55 | 15.64 | 203 | 15.09 |
| 22 | CA-SCC | 2014 | TS_2 | -0.15 | 114.9 | 287.7 | -0.83 | 14.49 | 200.8 | 13.66 |
| 23 | CA-SCC | 2014 | TS_3 | -0.2 | 111.4 | 288.6 | -0.69 | 11.52 | 194.9 | 10.84 |
| 24 | CA-SCC | 2014 | TS_4 | -0.25 | 129.5 | 287.2 | -0.22 | 8.612 | 207.4 | 8.391 |
| 25 | CA-SCC | 2014 | TS_5 | -0.3 | 142.4 | 288.0 | -0.10 | 6.329 | 212.1 | 6.225 |
| 26 | CA-SCC | 2015 | TS_1 | -0.1 | 113.9 | 285.2 | -0.28 | 16.26 | 189.2 | 15.98 |
| 27 | CA-SCC | 2015 | TS_2 | -0.15 | 113.1 | 284.2 | -0.24 | 14.56 | 192.8 | 14.32 |
| 28 | CA-SCC | 2015 | TS_3 | -0.2 | 111.8 | 285.4 | -0.22 | 12.71 | 199.1 | 12.48 |
| 29 | CA-SCC | 2015 | TS_4 | -0.25 | 120.8 | 287.1 | -0.16 | 10.08 | 204.8 | 9.922 |
| 30 | CA-SCC | 2015 | TS_5 | -0.3 | 131.9 | 285.4 | -0.09 | 7.705 | 209.2 | 7.616 |
| 31 | CA-SCC | 2016 | TS_1 | -0.1 | 108.1 | 260.1 | -0.33 | 18.37 | 190.9 | 18.04 |
| 32 | CA-SCC | 2016 | TS_2 | -0.15 | 109.0 | 260.2 | -0.30 | 17.31 | 192.1 | 17.01 |
| 33 | CA-SCC | 2016 | TS_3 | -0.2 | 110.5 | 260.4 | -0.26 | 15.4 | 194.1 | 15.14 |
| 34 | CA-SCC | 2016 | TS_4 | -0.25 | 119.2 | 260.3 | -0.20 | 13.38 | 200.2 | 13.18 |
| 35 | CA-SCC | 2016 | TS_5 | -0.3 | 130.8 | 261.7 | -0.12 | 10.03 | 202.2 | 9.906 |
| 36 | DE-Hte | 2012 | TS_3 | -0.2 | 77.0 | 344.0 | 4.98 | 12.26 | 215.5 | 17.23 |
| 37 | DE-Hte | 2013 | TS_3 | -0.2 | 60.9 | 378.0 | 3.96 | 11.99 | 207.9 | 15.95 |
| 38 | DE-Hte | 2014 | TS_1 | 0 | NaN | 327.8 | 8.52 | 8.342 | 205.6 | 16.87 |
| 39 | DE-Hte | 2015 | TS_1 | 0 | 62.9 | 360.6 | 5.17 | 11.67 | 187.4 | 16.84 |
| 40 | DE-Hte | 2016 | TS_1 | 0 | 71.9 | NaN | 4.94 | 12.36 | 175.6 | 17.3 |
| 41 | DE-Hte | 2017 | TS_1 | 0 | 61.6 | 343.3 | 4.50 | 11.76 | 186 | 16.26 |
| 42 | DE-SfN | 2012 | TS_1 | -0.02 | NaN | 372.6 | 0.00 | 23.55 | 206.5 | 15.29 |
| 43 | DE-SfN | 2012 | TS_3 | -0.1 | NaN | 366.7 | 1.64 | 12.91 | 219.7 | 14.55 |
| 44 | DE-SfN | 2012 | TS_4 | -0.2 | NaN | 367.4 | 4.86 | 7.276 | 242.7 | 12.14 |
| 45 | DE-SfN | 2012 | TS_5 | -0.5 | NaN | 367.4 | 4.86 | 7.276 | 242.7 | 12.14 |
| 46 | DE-SfN | 2013 | TS_1 | -0.02 | 55.8 | 381.5 | 0.92 | 13.62 | 216.4 | 14.54 |
| 47 | DE-SfN | 2013 | TS_3 | -0.1 | 60.4 | 384.8 | 1.56 | 12.5 | 221.1 | 14.06 |
| 48 | DE-SfN | 2013 | TS_4 | -0.2 | 83.6 | 394.5 | 3.62 | 8.417 | 243.4 | 12.04 |
| 49 | DE-SfN | 2013 | TS_5 | -0.5 | 83.6 | 394.5 | 3.62 | 8.417 | 243.4 | 12.04 |
| 50 | DE-Zrk | 2014 | TS_1 | -0.05 | 54.8 | 361.6 | 4.36 | 13.93 | 202.3 | 18.29 |
| 51 | DE-Zrk | 2014 | TS_2 | -0.1 | 59.3 | 366.5 | 4.87 | 12.65 | 207.3 | 17.52 |
| 52 | DE-Zrk | 2014 | TS_3 | -0.2 | 62.9 | 371.3 | 5.53 | 11.5 | 211.7 | 17.03 |
| 53 | DE-Zrk | 2014 | TS_4 | -0.3 | 67.4 | 375.1 | 6.05 | 10.4 | 216.5 | 16.45 |
| 54 | DE-Zrk | 2014 | TS_5 | -0.5 | 72.5 | 379.0 | 6.57 | 9.359 | 221 | 15.93 |
| 55 | DE-Zrk | 2015 | TS_1 | -0.05 | 58.3 | 359.3 | 4.28 | 13.24 | 215.5 | 17.52 |

Table B6. Continued.

| | SITE_ID | Year | Probe_name | Soil_temp_depth_m | Start_TS_(DOY) | End_TS_(DOY) | Base_value_TS_(C) | Ampl_TS_(C) | Peak_TS_(DOY) | Peak_value_TS_(C) |
|-----|---------|------|------------|-------------------|----------------|--------------|-------------------|-------------|---------------|-------------------|
| 56 | DE-Zrk | 2015 | TS_2 | -0.1 | 62.6 | 365.0 | 4.79 | 12 | 219.8 | 16.8 |
| 57 | DE-Zrk | 2015 | TS_3 | -0.2 | 66.0 | 369.8 | 5.42 | 10.87 | 223.7 | 16.29 |
| 58 | DE-Zrk | 2015 | TS_4 | -0.3 | 70.5 | 374.4 | 5.93 | 9.771 | 228 | 15.7 |
| 59 | DE-Zrk | 2015 | TS_5 | -0.5 | 74.7 | 378.8 | 6.43 | 8.751 | 232.2 | 15.19 |
| 60 | DE-Zrk | 2016 | TS_1 | -0.05 | 72.8 | 332.0 | 4.28 | 14.93 | 200.4 | 19.2 |
| 61 | DE-Zrk | 2016 | TS_2 | -0.1 | 76.3 | 337.4 | 4.79 | 13.6 | 204.4 | 18.39 |
| 62 | DE-Zrk | 2016 | TS_3 | -0.2 | 79.7 | 343.2 | 5.43 | 12.33 | 208.1 | 17.77 |
| 63 | DE-Zrk | 2016 | TS_4 | -0.3 | 83.6 | 347.6 | 5.94 | 11.14 | 212 | 17.09 |
| 64 | DE-Zrk | 2016 | TS_5 | -0.5 | 87.1 | 354.2 | 6.40 | 10.07 | 216 | 16.47 |
| 65 | DE-Zrk | 2017 | TS_1 | -0.05 | 69.1 | 351.4 | 4.40 | 14.72 | 199 | 19.12 |
| 66 | DE-Zrk | 2017 | TS_2 | -0.1 | 73.3 | 356.5 | 4.91 | 13.33 | 204 | 18.23 |
| 67 | DE-Zrk | 2017 | TS_3 | -0.2 | 77.2 | 362.4 | 5.56 | 12.02 | 208 | 17.58 |
| 68 | DE-Zrk | 2017 | TS_4 | -0.3 | 82.2 | 367.2 | 6.04 | 10.8 | 212 | 16.84 |
| 69 | DE-Zrk | 2017 | TS_5 | -0.5 | 86.2 | 373.0 | 6.48 | 9.675 | 217 | 16.15 |
| 70 | DE-Zrk | 2018 | TS_1 | -0.05 | 84.5 | 336.1 | 4.83 | 12.32 | 203 | 17.14 |
| 71 | DE-Zrk | 2018 | TS_2 | -0.1 | 86.6 | 342.6 | 5.30 | 11.27 | 208 | 16.57 |
| 72 | DE-Zrk | 2018 | TS_3 | -0.2 | 87.7 | 348.1 | 5.89 | 10.25 | 212 | 16.14 |
| 73 | DE-Zrk | 2018 | TS_4 | -0.3 | 89.8 | 354.8 | 6.31 | 9.308 | 217 | 15.61 |
| 74 | DE-Zrk | 2018 | TS_5 | -0.5 | 92.0 | 360.5 | 6.69 | 8.412 | 222 | 15.11 |
| 75 | FI-Lom | 2006 | TS_1 | -0.07 | 114.1 | 290.8 | -0.11 | 13.42 | 204.8 | 13.31 |
| 76 | FI-Lom | 2006 | TS_2 | -0.3 | 117.2 | 307.9 | 0.27 | 12.01 | 214.1 | 12.28 |
| 77 | FI-Lom | 2006 | TS_3 | -0.5 | 128.8 | 329.0 | 1.06 | 9.071 | 225.8 | 10.13 |
| 78 | FI-Lom | 2007 | TS_1 | -0.07 | 126.8 | 302.0 | 0.11 | 13.05 | 200 | 13.16 |
| 79 | FI-Lom | 2007 | TS_2 | -0.3 | 134.0 | 321.0 | 0.42 | 11.5 | 207.5 | 11.92 |
| 80 | FI-Lom | 2007 | TS_3 | -0.5 | 138.4 | 348.0 | 1.06 | 8.873 | 221.1 | 9.936 |
| 81 | FI-Lom | 2008 | TS_1 | -0.07 | 135.6 | 296.7 | 0.16 | 12.73 | 202.9 | 12.88 |
| 82 | FI-Lom | 2008 | TS_2 | -0.3 | 141.5 | 318.7 | 0.58 | 10.62 | 209.6 | 11.2 |
| 83 | FI-Lom | 2008 | TS_3 | -0.5 | 146.7 | 349.2 | 1.17 | 8.214 | 221.2 | 9.382 |
| 84 | FI-Lom | 2009 | TS_1 | -0.07 | 117.2 | 291.9 | 0.14 | 11.73 | 214 | 11.87 |
| 85 | FI-Lom | 2009 | TS_2 | -0.3 | 123.5 | 314.5 | 0.67 | 9.692 | 221 | 10.36 |
| 86 | FI-Lom | 2009 | TS_3 | -0.5 | 133.7 | 336.6 | 1.30 | 7.896 | 233 | 9.193 |
| 87 | FI-Lom | 2010 | TS_1 | -0.07 | 129.9 | 318.5 | 0.05 | 12.13 | 208 | 12.18 |
| 88 | FI-Lom | 2010 | TS_2 | -0.3 | 138.1 | 338.2 | 0.52 | 9.962 | 218 | 10.48 |
| 89 | FI-Lom | 2010 | TS_3 | -0.5 | 147.3 | 359.9 | 1.19 | 7.344 | 231 | 8.532 |
| 90 | FI-Si2 | 2012 | TS_1 | -0.05 | NaN | 323.5 | 0.00 | 19.85 | 204.6 | 16.02 |
| 91 | FI-Si2 | 2012 | TS_2 | -0.2 | 103.6 | 333.5 | -0.04 | 15.75 | 217.5 | 15.71 |
| 92 | FI-Si2 | 2012 | TS_3 | -0.35 | 105.6 | NaN | 0.00 | 19.38 | 230.6 | 15.09 |
| 93 | FI-Si2 | 2012 | TS_4 | -0.5 | 110.9 | NaN | 0.00 | 17.26 | 237.5 | 14.66 |
| 94 | FI-Si2 | 2013 | TS_1 | -0.05 | 106.9 | 341.0 | -0.05 | 16.04 | 199.4 | 15.98 |
| 95 | FI-Si2 | 2013 | TS_2 | -0.2 | 102.6 | 356.1 | 0.23 | 14.91 | 207.3 | 15.14 |
| 96 | FI-Si2 | 2013 | TS_3 | -0.35 | NaN | 376.5 | 0.00 | 18.26 | 209.6 | 14.23 |
| 97 | FI-Si2 | 2013 | TS_4 | -0.5 | NaN | 392.4 | 0.00 | 16.71 | 216.4 | 13.48 |
| 98 | FI-Si2 | 2014 | TS_1 | -0.05 | 104.6 | 331.1 | -0.04 | 17.07 | 208.5 | 17.03 |
| 99 | FI-Si2 | 2014 | TS_2 | -0.2 | 107.8 | 359.8 | 0.59 | 15.33 | 215.3 | 15.92 |
| 100 | FI-Si2 | 2014 | TS_3 | -0.35 | 112.0 | 385.9 | 0.99 | 13.61 | 222.2 | 14.61 |
| 101 | FI-Si2 | 2014 | TS_4 | -0.5 | 118.2 | 400.1 | 1.59 | 12.01 | 229.1 | 13.59 |
| 102 | FI-Si2 | 2015 | TS_1 | -0.05 | 76.5 | 352.3 | -0.87 | 16.31 | 211 | 15.44 |
| 103 | FI-Si2 | 2015 | TS_2 | -0.2 | 80.1 | 364.7 | -0.41 | 14.83 | 218 | 14.42 |
| 104 | FI-Si2 | 2015 | TS_3 | -0.35 | 82.0 | 374.8 | 0.12 | 13.27 | 225 | 13.39 |
| 105 | FI-Si2 | 2015 | TS_4 | -0.5 | 88.2 | 382.4 | 0.84 | 11.7 | 233 | 12.53 |
| 106 | FI-Si2 | 2016 | TS_1 | -0.05 | 102.6 | 329.4 | -0.88 | 16.48 | 206 | 15.6 |
| 107 | FI-Si2 | 2016 | TS_2 | -0.2 | 102.2 | 361.0 | -0.77 | 16.02 | 212 | 15.25 |
| 108 | FI-Si2 | 2016 | TS_3 | -0.35 | 103.1 | 383.8 | -0.63 | 14.7 | 219 | 14.07 |
| 109 | FI-Si2 | 2016 | TS_4 | -0.5 | 104.8 | 399.0 | -0.20 | 13.36 | 227 | 13.16 |
| 110 | HK-MPM | 2016 | TS_2 | NaN | NaN | 566.9 | 0.00 | 7.789 | 219.8 | 28.92 |
| 111 | HK-MPM | 2016 | TS_3 | NaN | NaN | 373.1 | 20.56 | 7.386 | 227.3 | 27.95 |
| 112 | HK-MPM | 2017 | TS_2 | NaN | NaN | NaN | 0.00 | 8.726 | 218.5 | 29.13 |
| 113 | HK-MPM | 2017 | TS_3 | NaN | 69.6 | 364.5 | 19.53 | 8.572 | 233.6 | 28.1 |

Table B6. Continued.

| | SITE_ID | Year | Probe_name | Soil_temp_depth_m | Start_TS_(DOY) | End_TS_(DOY) | Base_value_TS_(C) | Ampl_TS_(C) | Peak_TS_(DOY) | Peak_value_TS_(C) |
|-----|---------|------|------------|-------------------|----------------|--------------|-------------------|-------------|---------------|-------------------|
| 114 | HK-MPM | 2018 | TS_2 | NaN | NaN | NaN | 0.00 | 7.231 | 204.9 | 28.66 |
| 115 | HK-MPM | 2018 | TS_3 | NaN | 64.8 | 383.4 | 19.17 | 8.406 | 221.4 | 27.58 |
| 116 | JP-BBY | 2015 | TS_1 | -0.183 | 87.8 | 340.8 | 0.94 | 21.59 | 218.1 | 22.53 |
| 117 | JP-BBY | 2015 | TS_2 | -0.233 | 90.6 | 341.0 | 1.34 | 20.9 | 219.9 | 22.25 |
| 118 | JP-BBY | 2015 | TS_3 | -0.283 | 90.3 | 341.6 | 1.58 | 20.42 | 221.4 | 22 |
| 119 | JP-BBY | 2015 | TS_4 | -0.383 | 96.0 | 341.3 | 2.39 | 19.09 | 225.1 | 21.48 |
| 120 | JP-BBY | 2015 | TS_5 | -0.483 | 95.8 | 341.5 | 2.91 | 18.09 | 228.9 | 21 |
| 121 | JP-BBY | 2016 | TS_1 | -0.183 | 80.8 | 330.6 | 0.36 | 22.19 | 217.8 | 22.55 |
| 122 | JP-BBY | 2016 | TS_2 | -0.233 | 82.3 | 335.4 | 0.67 | 21.64 | 220.8 | 22.3 |
| 123 | JP-BBY | 2016 | TS_3 | -0.283 | 84.3 | 332.6 | 0.99 | 21.1 | 222 | 22.09 |
| 124 | JP-BBY | 2016 | TS_4 | -0.383 | 89.0 | 332.4 | 1.76 | 19.92 | 225.6 | 21.68 |
| 125 | JP-BBY | 2016 | TS_5 | -0.483 | 94.3 | 331.9 | 2.44 | 18.83 | 228.9 | 21.27 |
| 126 | JP-BBY | 2017 | TS_1 | -0.183 | 80.4 | 347.8 | 0.20 | 21.75 | 213.8 | 21.95 |
| 127 | JP-BBY | 2017 | TS_2 | -0.233 | 84.5 | 347.8 | 0.82 | 21.02 | 214.6 | 21.83 |
| 128 | JP-BBY | 2017 | TS_3 | -0.283 | 86.2 | 347.1 | 1.06 | 20.56 | 216.3 | 21.62 |
| 129 | JP-BBY | 2017 | TS_4 | -0.383 | 92.2 | 346.0 | 1.97 | 19.34 | 218.5 | 21.31 |
| 130 | JP-BBY | 2017 | TS_5 | -0.483 | 98.2 | 345.2 | 2.70 | 18.34 | 221 | 21.03 |
| 131 | JP-BBY | 2018 | TS_1 | -0.183 | 78.3 | 355.4 | 0.50 | 20.38 | 222 | 20.88 |
| 132 | JP-BBY | 2018 | TS_2 | -0.233 | 83.5 | 357.6 | 1.48 | 19.23 | 224 | 20.7 |
| 133 | JP-BBY | 2018 | TS_3 | -0.283 | 85.9 | 355.9 | 1.69 | 18.78 | 225 | 20.47 |
| 134 | JP-BBY | 2018 | TS_4 | -0.383 | 95.9 | 351.3 | 2.81 | 17.25 | 229 | 20.07 |
| 135 | JP-BBY | 2018 | TS_5 | -0.483 | 103.8 | 349.4 | 3.63 | 16.1 | 232 | 19.73 |
| 136 | JP-Mse | 2012 | TS_1 | -0.01 | 60.4 | 348.9 | 2.15 | 23.76 | 211.8 | 25.91 |
| 137 | MY-MLM | 2014 | TS | NaN | NaN | 358.4 | 25.06 | 3.968 | 194.5 | 29.03 |
| 138 | MY-MLM | 2015 | TS | NaN | 27.3 | NaN | 25.57 | 1.973 | 172.7 | 27.55 |
| 139 | NZ-Kop | 2012 | TS_1 | -0.5 | 62.5 | 360.3 | 8.30 | 8.394 | 219.8 | 16.7 |
| 140 | NZ-Kop | 2012 | TS_2 | -0.1 | 65.5 | 362.4 | 8.45 | 8.093 | 222.1 | 16.54 |
| 141 | NZ-Kop | 2012 | TS_3 | -0.2 | 68.8 | 365.6 | 8.73 | 7.243 | 228.2 | 15.98 |
| 142 | NZ-Kop | 2013 | TS_1 | -0.5 | 45.6 | 367.0 | 8.41 | 7.635 | 210.5 | 16.04 |
| 143 | NZ-Kop | 2013 | TS_2 | -0.1 | 47.6 | 371.0 | 8.54 | 7.486 | 212.3 | 16.03 |
| 144 | NZ-Kop | 2013 | TS_3 | -0.2 | 52.7 | 377.2 | 8.82 | 6.87 | 217.8 | 15.69 |
| 145 | NZ-Kop | 2014 | TS_1 | -0.5 | 56.9 | 365.7 | 8.16 | 8.79 | 219 | 16.95 |
| 146 | NZ-Kop | 2014 | TS_2 | -0.1 | 59.4 | 367.5 | 8.29 | 8.512 | 221 | 16.8 |
| 147 | NZ-Kop | 2014 | TS_3 | -0.2 | 62.9 | 372.5 | 8.55 | 7.792 | 226 | 16.34 |
| 148 | NZ-Kop | 2015 | TS_1 | -0.5 | 56.5 | 371.8 | 7.73 | 9.355 | 214 | 17.09 |
| 149 | NZ-Kop | 2015 | TS_2 | -0.1 | 58.3 | 374.7 | 7.87 | 9.063 | 217 | 16.93 |
| 150 | NZ-Kop | 2015 | TS_3 | -0.2 | 62.7 | 378.4 | 8.19 | 8.217 | 222 | 16.4 |
| 151 | RU-Ch2 | 2014 | TS_1 | -0.04 | 138.8 | 263.8 | -0.13 | 14.42 | 206.6 | 14.29 |
| 152 | RU-Ch2 | 2014 | TS_2 | -0.08 | 146.1 | 262.1 | -0.14 | 13.03 | 206.5 | 12.9 |
| 153 | RU-Ch2 | 2014 | TS_3 | -0.16 | 155.9 | 264.5 | -0.05 | 4.581 | 210.5 | 4.535 |
| 154 | RU-Ch2 | 2015 | TS_1 | -0.04 | 143.9 | 269.6 | -0.14 | 13.97 | 193.3 | 13.83 |
| 155 | RU-Ch2 | 2015 | TS_2 | -0.08 | 147.3 | 265.7 | -0.10 | 12.3 | 195.7 | 12.2 |
| 156 | RU-Ch2 | 2015 | TS_3 | -0.16 | 159.9 | 266.6 | -0.04 | 3.995 | 205.2 | 3.96 |
| 157 | RU-Ch2 | 2016 | TS_1 | -0.04 | 127.0 | 273.5 | -0.16 | 11.64 | 200.2 | 11.48 |
| 158 | RU-Ch2 | 2016 | TS_2 | -0.08 | 133.9 | 272.6 | -0.10 | 10.06 | 203.2 | 9.964 |
| 159 | RU-Ch2 | 2016 | TS_3 | -0.16 | 148.0 | 275.5 | -0.04 | 4.042 | 217.7 | 4.001 |
| 160 | RU-Che | 2014 | TS_1 | -0.04 | 138.0 | 267.6 | -0.12 | 15.04 | 208 | 14.92 |
| 161 | RU-Che | 2014 | TS_2 | -0.08 | 149.7 | 263.7 | -0.09 | 8.959 | 206.6 | 8.873 |
| 162 | RU-Che | 2014 | TS_3 | -0.16 | 155.0 | 265.5 | -0.07 | 7.006 | 210.3 | 6.938 |
| 163 | RU-Che | 2015 | TS_1 | -0.04 | 143.8 | 274.7 | -0.17 | 14.81 | 193.7 | 14.64 |
| 164 | RU-Che | 2015 | TS_2 | -0.08 | 149.5 | 267.1 | -0.06 | 8.336 | 197.9 | 8.273 |
| 165 | RU-Che | 2015 | TS_3 | -0.16 | 154.5 | 271.0 | -0.04 | 5.942 | 202.4 | 5.9 |
| 166 | RU-Che | 2016 | TS_1 | -0.04 | 126.7 | 274.0 | -0.19 | 12.95 | 200.4 | 12.76 |
| 167 | RU-Che | 2016 | TS_2 | -0.08 | 137.0 | 273.7 | -0.07 | 7.076 | 205.4 | 7.01 |
| 168 | RU-Che | 2016 | TS_3 | -0.16 | 142.5 | 275.6 | -0.05 | 5.498 | 211.8 | 5.451 |
| 169 | SE-Deg | 2014 | TS_1 | -0.02 | 111.8 | 303.6 | -0.53 | 17.22 | 201.6 | 16.69 |

Table B6. Continued.

| | SITE_ID | Year | Probe_name | Soil_temp_depth_m | Start_TS_(DOY) | End_TS_(DOY) | Base_value_TS_(C) | Ampl_TS_(C) | Peak_TS_(DOY) | Peak_value_TS_(C) |
|-----|---------|------|------------|-------------------|----------------|--------------|-------------------|-------------|---------------|-------------------|
| 286 | US-Sne | 2017 | TS_4 | -0.16 | 46.4 | 346.2 | 11.39 | 11.79 | 211 | 23.18 |
| 287 | US-Sne | 2017 | TS_5 | -0.32 | 50.6 | 350.5 | 11.98 | 10.7 | 216 | 22.67 |
| 288 | US-Sne | 2018 | TS_1 | -0.01 | 48.4 | 325.1 | 10.28 | 12.15 | 217.3 | 22.43 |
| 289 | US-Sne | 2018 | TS_2 | -0.02 | 33.9 | 331.0 | 10.55 | 11.34 | 210.2 | 21.89 |
| 290 | US-Sne | 2018 | TS_3 | -0.08 | 36.8 | 331.5 | 10.87 | 10.63 | 212.1 | 21.5 |
| 291 | US-Sne | 2018 | TS_4 | -0.16 | 35.6 | 335.4 | 11.23 | 10.09 | 220.1 | 21.32 |
| 292 | US-Sne | 2018 | TS_5 | -0.32 | 49.1 | 335.9 | 11.88 | 9.045 | 218 | 20.92 |
| 293 | US-Srr | 2016 | TS_1 | NaN | NaN | 326.3 | 10.03 | 10.71 | 200.5 | 20.74 |
| 294 | US-Srr | 2017 | TS_1 | NaN | 11.3 | 346.8 | 7.22 | 13.71 | 199.5 | 20.93 |
| 295 | US-StJ | 2016 | TS_2 | -0.05 | 68.4 | 347.4 | 4.05 | 16.22 | 213.7 | 20.27 |
| 296 | US-StJ | 2016 | TS_3 | -0.1 | 68.4 | 347.4 | 5.84 | 14.1 | 213.7 | 19.94 |
| 297 | US-Tw1 | 2012 | TS_1 | -0.02 | 50.5 | 360.0 | 5.99 | 11.52 | 225.2 | 17.51 |
| 298 | US-Tw1 | 2012 | TS_2 | -0.04 | 48.0 | 358.8 | 6.14 | 11.32 | 227 | 17.46 |
| 299 | US-Tw1 | 2012 | TS_3 | -0.08 | 50.1 | 367.9 | 5.18 | 12.31 | 222.1 | 17.49 |
| 300 | US-Tw1 | 2012 | TS_4 | -0.16 | 49.0 | 367.5 | 5.31 | 12.19 | 224.5 | 17.5 |
| 301 | US-Tw1 | 2012 | TS_5 | -0.32 | -79.1 | 347.2 | 7.89 | 9.513 | 225.3 | 17.4 |
| 302 | US-Tw1 | 2013 | TS_1 | -0.02 | 35.8 | 337.6 | 4.39 | 14.59 | 206.6 | 18.97 |
| 303 | US-Tw1 | 2013 | TS_2 | -0.04 | 36.1 | 337.7 | 4.39 | 14.57 | 206.8 | 18.96 |
| 304 | US-Tw1 | 2013 | TS_3 | -0.08 | 36.8 | 338.1 | 4.40 | 14.54 | 207.5 | 18.94 |
| 305 | US-Tw1 | 2013 | TS_4 | -0.16 | 37.6 | 338.8 | 4.41 | 14.59 | 208.4 | 19.01 |
| 306 | US-Tw1 | 2013 | TS_5 | -0.32 | 38.6 | 340.1 | 4.46 | 14.62 | 209.6 | 19.07 |
| 307 | US-Tw1 | 2014 | TS_1 | -0.02 | 41.2 | 395.4 | 6.67 | 10.89 | 208.3 | 17.56 |
| 308 | US-Tw1 | 2014 | TS_2 | -0.04 | 41.9 | 397.1 | 6.70 | 10.85 | 208.6 | 17.55 |
| 309 | US-Tw1 | 2014 | TS_3 | -0.08 | 43.5 | 400.0 | 6.78 | 10.72 | 209.8 | 17.49 |
| 310 | US-Tw1 | 2014 | TS_4 | -0.16 | 45.6 | 404.8 | 6.88 | 10.56 | 211.3 | 17.44 |
| 311 | US-Tw1 | 2014 | TS_5 | -0.32 | 49.6 | 416.3 | 7.09 | 10.24 | 213.9 | 17.33 |
| 312 | US-Tw1 | 2015 | TS_1 | -0.02 | 50.7 | 342.5 | 9.02 | 7.831 | 235 | 16.85 |
| 313 | US-Tw1 | 2015 | TS_2 | -0.04 | 52.0 | 342.4 | 9.09 | 7.706 | 235 | 16.8 |
| 314 | US-Tw1 | 2015 | TS_3 | -0.08 | 55.6 | 342.0 | 9.26 | 7.385 | 238 | 16.64 |
| 315 | US-Tw1 | 2015 | TS_4 | -0.16 | 59.6 | 343.0 | 9.51 | 6.972 | 240 | 16.48 |
| 316 | US-Tw1 | 2015 | TS_5 | -0.32 | 69.4 | 345.2 | 10.00 | 6.208 | 246 | 16.21 |
| 317 | US-Tw1 | 2016 | TS_1 | -0.02 | 34.6 | 361.1 | 8.78 | 7.943 | 218 | 16.72 |
| 318 | US-Tw1 | 2016 | TS_2 | -0.04 | 35.5 | 362.2 | 8.86 | 7.837 | 219 | 16.69 |
| 319 | US-Tw1 | 2016 | TS_3 | -0.08 | 38.6 | 363.1 | 9.04 | 7.546 | 221 | 16.59 |
| 320 | US-Tw1 | 2016 | TS_4 | -0.16 | 44.7 | 365.9 | 9.33 | 7.14 | 223 | 16.47 |
| 321 | US-Tw1 | 2016 | TS_5 | -0.32 | 56.2 | 370.5 | 9.86 | 6.35 | 229 | 16.21 |
| 322 | US-Tw1 | 2017 | TS_1 | -0.02 | 41.2 | 343.7 | 7.55 | 10.22 | 228 | 17.77 |
| 323 | US-Tw1 | 2017 | TS_2 | -0.04 | 41.7 | 344.6 | 7.61 | 10.11 | 229 | 17.72 |
| 324 | US-Tw1 | 2017 | TS_3 | -0.08 | 42.6 | 345.0 | 7.75 | 9.803 | 231 | 17.55 |
| 325 | US-Tw1 | 2017 | TS_4 | -0.16 | 45.0 | 347.2 | 7.97 | 9.368 | 234 | 17.34 |
| 326 | US-Tw1 | 2017 | TS_5 | -0.32 | 48.8 | 349.2 | 8.38 | 8.5 | 240 | 16.88 |
| 327 | US-Tw1 | 2018 | TS_1 | -0.02 | 60.5 | 327.4 | 6.70 | 10.42 | 222 | 17.12 |
| 328 | US-Tw1 | 2018 | TS_2 | -0.04 | 61.5 | 327.4 | 6.75 | 10.36 | 223 | 17.1 |
| 329 | US-Tw1 | 2018 | TS_3 | -0.08 | 64.6 | 328.4 | 6.85 | 10.18 | 225 | 17.03 |
| 330 | US-Tw1 | 2018 | TS_4 | -0.16 | 67.7 | 329.4 | 7.01 | 9.925 | 227 | 16.93 |
| 331 | US-Tw1 | 2018 | TS_5 | -0.32 | 75.1 | 331.4 | 7.31 | 9.459 | 230 | 16.77 |
| 332 | US-Tw4 | 2015 | TS_1 | -0.02 | 15.9 | 327.2 | 10.04 | 11.56 | 199.4 | 21.6 |
| 333 | US-Tw4 | 2015 | TS_3 | -0.08 | 20.2 | 329.8 | 10.48 | 10.96 | 202.3 | 21.44 |
| 334 | US-Tw4 | 2015 | TS_4 | -0.16 | 23.9 | 332.5 | 10.86 | 10.42 | 205.7 | 21.28 |
| 335 | US-Tw4 | 2015 | TS_5 | -0.32 | 29.2 | 338.6 | 11.49 | 9.449 | 212.4 | 20.94 |
| 336 | US-Tw4 | 2016 | TS_1 | -0.02 | 9.6 | 358.7 | 8.16 | 11.29 | 201.7 | 19.45 |
| 337 | US-Tw4 | 2016 | TS_3 | -0.08 | 13.2 | 360.1 | 8.67 | 10.58 | 205.7 | 19.25 |
| 338 | US-Tw4 | 2016 | TS_4 | -0.16 | 15.9 | 362.6 | 9.11 | 9.991 | 209.2 | 19.11 |
| 339 | US-Tw4 | 2016 | TS_5 | -0.32 | 21.0 | 367.6 | 9.91 | 8.876 | 216.2 | 18.78 |
| 340 | US-Tw4 | 2017 | TS_1 | -0.02 | 38.3 | 347.3 | 8.07 | 11.52 | 211.9 | 19.59 |
| 341 | US-Tw4 | 2017 | TS_3 | -0.08 | 42.1 | 351.8 | 8.45 | 10.91 | 215.3 | 19.36 |
| 342 | US-Tw4 | 2017 | TS_4 | -0.16 | 46.0 | 354.7 | 8.83 | 10.35 | 218.6 | 19.18 |
| 343 | US-Tw4 | 2017 | TS_5 | -0.32 | 53.5 | 361.4 | 9.52 | 9.275 | 224.9 | 18.79 |

Table B6. Continued.

| | SITE_ID | Year | Probe_name | Soil_temp_depth_m | Start_TS_(DOY) | End_TS_(DOY) | Base_value_TS_(C) | Ampl_TS_(C) | Peak_TS_(DOY) | Peak_value_TS_(C) |
|-----|---------|------|------------|-------------------|----------------|--------------|-------------------|-------------|---------------|-------------------|
| 344 | US-Tw4 | 2018 | TS_1 | -0.02 | 58.1 | 344.9 | 8.00 | 10.93 | 218 | 18.93 |
| 345 | US-Tw4 | 2018 | TS_3 | -0.08 | 63.9 | 349.1 | 8.38 | 10.41 | 222 | 18.79 |
| 346 | US-Tw4 | 2018 | TS_4 | -0.16 | 68.0 | 352.1 | 8.71 | 9.862 | 225 | 18.57 |
| 347 | US-Tw4 | 2018 | TS_5 | -0.32 | 75.3 | 357.9 | 9.33 | 8.8 | 231 | 18.13 |
| 348 | US-Tw5 | 2018 | TS_1 | -0.02 | NaN | 414.8 | 0.00 | 8.894 | 222.2 | 18.37 |
| 349 | US-Tw5 | 2018 | TS_2 | -0.1 | NaN | 401.0 | 0.00 | 12.32 | 204.4 | 22.24 |
| 350 | US-Tw5 | 2018 | TS_3 | -0.02 | NaN | 414.8 | 0.00 | 8.894 | 222.2 | 18.37 |
| 351 | US-Tw5 | 2018 | TS_4 | -0.08 | NaN | 423.4 | 0.00 | 7.898 | 227.3 | 18.14 |
| 352 | US-Tw5 | 2018 | TS_5 | -0.16 | NaN | 430.2 | 0.00 | 7.531 | 230 | 17.94 |
| 353 | US-Uaf | 2011 | TS_1 | -0.09 | 86.2 | 372.5 | -12.29 | 21.95 | 199.6 | 9.667 |
| 354 | US-Uaf | 2012 | TS_1 | -0.09 | 73.8 | 338.5 | -11.83 | 20.86 | 202.4 | 9.028 |
| 355 | US-Uaf | 2013 | TS_1 | -0.09 | 109.6 | 395.5 | -10.08 | 20.52 | 200.4 | 10.44 |
| 356 | US-Uaf | 2014 | TS_1 | -0.09 | 76.1 | 365.4 | -10.94 | 19.94 | 206 | 8.999 |
| 357 | US-Uaf | 2015 | TS_1 | -0.09 | 81.0 | 423.2 | -9.77 | 19.76 | 190 | 9.998 |
| 358 | US-Uaf | 2016 | TS_1 | -0.09 | 77.4 | 315.8 | -7.74 | 19.13 | 198 | 11.39 |
| 359 | US-Uaf | 2017 | TS_1 | -0.09 | 84.9 | 380.2 | -7.39 | 19.08 | 196 | 11.69 |
| 360 | US-Uaf | 2018 | TS_1 | -0.09 | 96.0 | 333.3 | -5.60 | 17.72 | 199 | 12.11 |
| 361 | US-WPT | 2011 | TS_1 | -0.1 | 81.0 | 342.2 | 5.27 | 19.27 | 202.6 | 24.54 |
| 362 | US-WPT | 2011 | TS_2 | -0.3 | NaN | 347.0 | 6.38 | 16.62 | 209.7 | 23.01 |
| 363 | US-WPT | 2012 | TS_1 | -0.1 | 40.3 | 345.6 | 3.70 | 21.6 | 197.4 | 25.3 |
| 364 | US-WPT | 2012 | TS_2 | -0.3 | 44.9 | 355.0 | 4.52 | 19.21 | 203.8 | 23.72 |
| 365 | US-WPT | 2013 | TS_1 | -0.1 | 74.6 | 340.5 | 3.73 | 18.23 | 207.2 | 21.96 |
| 366 | US-WPT | 2013 | TS_2 | -0.3 | 77.6 | 352.3 | 4.32 | 16.69 | 211.7 | 21.01 |

| Column | Description |
|-------------------|--|
| SITE_ID | Site identification code as assigned by regional flux data network |
| Year | Data year |
| Probe_name | Temperature probe name as given in data files |
| Soil_temp_depth_m | Depth of soil temperature probe (m), with negative values being under the surface |
| Start_TS_(DOY) | Season start for elevated TS (DOY), point “f” in Fig. 1 |
| End_TS_(DOY) | Season end for elevated TS (DOY), point “h” in Fig. 1 |
| Base_value_TS_(C) | Baseline TS during non-elevated season (C), average of points “a” and “b” in Fig. 1 |
| Ampl_TS_(C) | Amplitude of TS during elevated temperature season (C), difference between point “e” in Fig. 1 and Base_value_TS |
| Peak_TS_(DOY) | Day of maximum elevated TS (DOY), point “g” in Fig. 1 |
| Peak_value_TS_(C) | Maximum value of TS (C), point “e” in Fig. 1 |

Table B7. Installation depths for soil temperature probes.

| | SITE_ID | Year | Probe name | Soil_temp_depth_m | Additional_notes |
|----|---------|------|------------|-------------------|------------------|
| 1 | AT-NEU | | TS_1 | -0.05 | |
| 2 | AT-NEU | | TS_2 | -0.1 | |
| 3 | AT-NEU | | TS_3 | -0.2 | |
| 4 | BR-NPW | | TS_1 | | |
| 5 | BR-NPW | | TS_2 | | |
| 6 | BW-GUM | | No data | | |
| 7 | BW-NXR | | No data | | |
| 8 | CA-SCB | | TS_1 | 0 | |
| 9 | CA-SCB | | TS_2 | -0.02 | |
| 10 | CA-SCB | | TS_3 | -0.04 | |
| 11 | CA-SCB | | TS_4 | -0.08 | |
| 12 | CA-SCB | | TS_5 | -0.16 | |
| 13 | CA-SCB | | TS_6 | -0.32 | |
| 14 | CA-SCB | | TS_7 | -0.64 | |
| 15 | CA-SCB | | TS_8 | -1.28 | |
| 16 | CA-SCC | | TS_1 | -0.1 | |
| 17 | CA-SCC | | TS_2 | -0.15 | |
| 18 | CA-SCC | | TS_3 | -0.2 | |
| 19 | CA-SCC | | TS_4 | -0.25 | |
| 20 | CA-SCC | | TS_5 | -0.3 | |
| 21 | CA-SCC | | TS_6 | -0.5 | |
| 22 | CA-SCC | | TS_7 | -0.6 | |
| 23 | CA-SCC | | TS_8 | -0.7 | |
| 24 | CH-CHA | | TS_1 | -0.01 | |
| 25 | CH-CHA | | TS_2 | -0.02 | |
| 26 | CH-CHA | | TS_3 | -0.04 | |
| 27 | CH-CHA | | TS_4 | -0.07 | |
| 28 | CH-CHA | | TS_5 | -0.1 | |
| 29 | CH-CHA | | TS_6 | -0.15 | |
| 30 | CH-CHA | | TS_7 | -0.25 | |
| 31 | CH-CHA | | TS_8 | -0.4 | |
| 32 | CH-CHA | | TS_9 | -0.95 | |
| 33 | CH-DAV | | TS_1 | -0.05 | |
| 34 | CH-DAV | | TS_2 | -0.15 | |
| 35 | CH-DAV | | TS_3 | -0.5 | |
| 36 | CH-DAV | | TS_4 | - | |
| 37 | CH-DAV | | TS_5 | - | |
| 38 | CH-DAV | | TS_6 | - | |
| 39 | CH-OE2 | | TS_1 | -0.05 | |
| 40 | CH-OE2 | | TS_2 | -0.1 | |
| 41 | CH-OE2 | | TS_3 | -0.15 | |
| 42 | CH-OE2 | | TS_4 | - | |
| 43 | CH-OE2 | | TS_5 | -0.3 | |
| 44 | CH-OE2 | | TS_6 | -0.5 | |
| 45 | CH-OE2 | | TS_7 | - | |
| 46 | CN-HGU | | TS | | |
| 47 | DE-DGW | | No data | | |
| 48 | DE-HTE | | TS_1 | 0 | |
| 49 | DE-HTE | | TS_2 | -0.1 | |
| 50 | DE-HTE | | TS_3 | -0.2 | |
| 51 | DE-SFN | | TS_1 | -0.02 | |
| 52 | DE-SFN | | TS_3 | -0.1 | |
| 53 | DE-SFN | | TS_4 | -0.2 | |
| 54 | DE-SFN | | TS_5 | -0.5 | |
| 55 | DE-ZRK | | TS_1 | -0.05 | |

Table B7. Continued.

| | SITE_ID | Year | Probe name | Soil_temp_depth_m | Additional_notes |
|-----|---------|------------|------------|-------------------|------------------|
| 56 | DE-ZRK | | TS_2 | -0.1 | |
| 57 | DE-ZRK | | TS_3 | -0.2 | |
| 58 | DE-ZRK | | TS_4 | -0.3 | |
| 59 | DE-ZRK | | TS_5 | -0.5 | |
| 60 | FI-HYY | | TS_1 | -0.02 | |
| 61 | FI-HYY | | TS_2 | -0.04 | |
| 62 | FI-HYY | | TS_3 | -0.12 | |
| 63 | FI-HYY | | TS_4 | -0.25 | |
| 64 | FI-HYY | | TS_5 | -0.5 | |
| 65 | FI-LOM | | TS_1 | -0.07 | |
| 66 | FI-LOM | | TS_2 | -0.3 | |
| 67 | FI-LOM | | TS_3 | -0.5 | |
| 68 | FI-SI2 | | TS_1 | -0.05 | |
| 69 | FI-SI2 | | TS_2 | -0.2 | |
| 70 | FI-SI2 | | TS_3 | -0.35 | |
| 71 | FI-SI2 | | TS_4 | -0.5 | |
| 72 | FI-SII | Pre-2016 | TS_1 | -0.05 | |
| 73 | FI-SII | Pre-2016 | TS_2 | -0.2 | |
| 74 | FI-SII | Pre-2016 | TS_3 | -0.35 | |
| 75 | FI-SII | Pre-2016 | TS_4 | -0.5 | |
| 76 | FI-SII | After 2017 | TS_1 | 0 | |
| 77 | FI-SII | After 2017 | TS_2 | -0.5 | |
| 78 | FI-SII | After 2017 | TS_3 | -0.1 | |
| 79 | FI-SII | After 2017 | TS_4 | -0.15 | |
| 80 | FI-SII | After 2017 | TS_5 | -0.25 | |
| 81 | FI-SII | After 2017 | TS_6 | -0.45 | |
| 82 | FI-SII | After 2017 | TS_7 | -0.95 | |
| 83 | FR-LGT | | TS_1 | -0.02 | |
| 84 | FR-LGT | | TS_2 | -0.05 | |
| 85 | FR-LGT | | TS_3 | -0.1 | |
| 86 | FR-LGT | | TS_4 | -0.2 | |
| 87 | FR-LGT | | TS_5 | -0.4 | |
| 88 | HK-MPM | | TS_1 | | |
| 89 | HK-MPM | | TS_2 | | |
| 90 | HK-MPM | | TS_3 | | |
| 91 | ID-PAG | | TS_1 | -0.05 | |
| 92 | IT-BCI | | TS_1 | -0.05 | |
| 93 | IT-BCI | | TS_2 | -0.1 | |
| 94 | IT-BCI | | TS_3 | -0.3 | |
| 95 | IT-BCI | | TS_4 | -0.5 | |
| 96 | IT-BCI | | TS_5 | -1 | |
| 97 | IT-CAS | | TS_1 | -0.035 | |
| 98 | IT-CAS | | TS_2 | -0.075 | |
| 99 | IT-CAS | | TS_3 | -0.15 | |
| 100 | JP-BBY | | TS_1 | -0.183 | |
| 101 | JP-BBY | | TS_2 | -0.233 | |
| 102 | JP-BBY | | TS_3 | -0.283 | |
| 103 | JP-BBY | | TS_4 | -0.383 | |
| 104 | JP-BBY | | TS_5 | -0.483 | |
| 105 | JP-MSE | | TS_1 | -0.01 | |
| 106 | JP-MSE | | TS_2 | -0.025 | |
| 107 | JP-MSE | | TS_3 | -0.05 | |
| 108 | JP-MSE | | TS_4 | -0.1 | |
| 109 | JP-MSE | | TS_5 | -0.2 | |
| 110 | JP-MSE | | TS_6 | -0.4 | |
| 111 | JP-SWL | | no data | | |

Table B7. Continued.

| | SITE_ID | Year | Probe name | Soil_temp_depth_m | Additional_notes |
|-----|---------|------|------------|-------------------|------------------|
| 112 | KR-CRK | | TS_1 | −0.05 | |
| 113 | KR-CRK | | TS_2 | −0.15 | |
| 114 | MAERC | | TS | | |
| 115 | MY-MLM | | TS_1 | −0.05 | |
| 116 | NL-HOR | | TS_1 | −0.01 | |
| 117 | NL-HOR | | TS_2 | −0.02 | |
| 118 | NL-HOR | | TS_3 | −0.04 | |
| 119 | NL-HOR | | TS_4 | −0.05 | |
| 120 | NL-HOR | | TS_5 | −0.1 | |
| 121 | NL-HOR | | TS_6 | −0.15 | |
| 122 | NL-HOR | | TS_7 | −0.25 | |
| 123 | NL-HOR | | TS_8 | −0.4 | |
| 124 | NL-HOR | | TS_9 | −0.6 | |
| 125 | NZ-KOP | | TS_1 | −0.5 | |
| 126 | NZ-KOP | | TS_2 | −0.1 | |
| 127 | NZ-KOP | | TS_3 | −0.2 | |
| 128 | PH-RIF | | TS_1 | | |
| 129 | RU-CH2 | | TS_1 | −0.04 | |
| 130 | RU-CH2 | | TS_2 | −0.08 | |
| 131 | RU-CH2 | | TS_3 | −0.16 | |
| 132 | RU-CHE | | TS_1 | −0.04 | |
| 133 | RU-CHE | | TS_2 | −0.08 | |
| 134 | RU-CHE | | TS_3 | −0.16 | |
| 135 | RU-COK | | No data | | |
| 136 | RU-FY2 | | TS_1 | | |
| 137 | RU-FY2 | | TS_2 | | |
| 138 | RU-FY2 | | TS_3 | | |
| 139 | RU-FY2 | | TS_4 | | |
| 140 | RU-FY2 | | TS_5 | | |
| 141 | SE-DEG | | TS_1 | −0.02 | |
| 142 | SE-DEG | | TS_2 | −0.05 | |
| 143 | SE-DEG | | TS_3 | −0.1 | |
| 144 | SE-DEG | | TS_4 | −0.15 | |
| 145 | SE-DEG | | TS_5 | −0.3 | |
| 146 | SE-DEG | | TS_6 | −0.5 | |
| 147 | UK-LBT | | No data | | |
| 148 | US-A03 | | TS_1 | −0.025 | |
| 149 | US-A03 | | TS_2 | −0.1 | |
| 150 | US-A03 | | TS_3 | −0.3 | |
| 151 | US-A10 | | TS_1 | −0.025 | |
| 152 | US-A10 | | TS_2 | −0.1 | |
| 153 | US-A10 | | TS_3 | −0.3 | |
| 154 | US-ATQ | | TS_1 | | |
| 155 | US-ATQ | | TS_2 | | |
| 156 | US-ATQ | | TS_3 | | |
| 157 | US-BEO | | TS_1 | | |
| 158 | US-BEO | | TS_2 | | |
| 159 | US-BEO | | TS_3 | | |
| 160 | US-BES | | TS_1 | | |
| 161 | US-BES | | TS_2 | | |
| 162 | US-BES | | TS_3 | | |
| 163 | US-BI1 | | TS_1 | −0.02 | |
| 164 | US-BI1 | | TS_2 | −0.04 | |
| 165 | US-BI1 | | TS_3 | −0.08 | |
| 166 | US-BI1 | | TS_4 | −0.16 | |
| 167 | US-BI1 | | TS_5 | −0.32 | |

Table B7. Continued.

| | SITE_ID | Year | Probe name | Soil_temp_depth_m | Additional_notes |
|-----|---------|------|------------|-------------------|------------------|
| 168 | US-BI2 | | TS_1 | −0.02 | |
| 169 | US-BI2 | | TS_2 | −0.04 | |
| 170 | US-BI2 | | TS_3 | −0.08 | |
| 171 | US-BI2 | | TS_4 | −0.16 | |
| 172 | US-BI2 | | TS_5 | −0.32 | |
| 173 | US-BRW | | | | |
| 174 | US-BZB | | TS_1 | −0.075 | |
| 175 | US-BZB | | TS_2 | −0.05 | |
| 176 | US-BZF | | TS_1 | −0.075 | |
| 177 | US-BZF | | TS_2 | −0.05 | |
| 178 | US-BZS | | TS_1 | | |
| 179 | US-BZS | | TS_2 | | |
| 180 | US-BZS | | TS_3 | | |
| 181 | US-CRT | | TS_1 | | |
| 182 | US-DPW | | No data | | |
| 183 | US-EDN | | TS_1 | −0.25 | |
| 184 | US-EDN | | TS_2 | −0.15 | |
| 185 | US-EDN | | TS_3 | −0.05 | |
| 186 | US-EDN | | TS_4 | 0 | |
| 187 | US-EDN | | TS_5 | 0.05 | |
| 188 | US-EDN | | TS_6 | 0.1 | |
| 189 | US-EDN | | TS_7 | 0.2 | |
| 190 | US-EDN | | TS_8 | 0.3 | |
| 191 | US-EML | | TS_1 | −0.05 | |
| 192 | US-EML | | TS_2 | −0.1 | |
| 193 | US-EML | | TS_3 | −0.2 | |
| 194 | US-EML | | TS_4 | −0.4 | |
| 195 | US-HO1 | | TS_1 | −0.05 | |
| 196 | US-HO1 | | TS_2 | −0.1 | |
| 197 | US-HRA | | No data | −0.02 | |
| 198 | US-HRC | | No data | −0.02 | |
| 199 | US-ICS | | TS_1 | −0.075 | |
| 200 | US-ICS | | TS_2 | −0.05 | |
| 201 | US-IVO | | TS_1 | −0.05 | |
| 202 | US-IVO | | TS_2 | −0.1 | |
| 203 | US-IVO | | TS_3 | −0.15 | |
| 204 | US-IVO | | TS_4 | −0.3 | |
| 205 | US-IVO | | TS_5 | −0.4 | |
| 206 | US-LA1 | | TS | −0.1 | |
| 207 | US-LA2 | | TS | −0.1 | |
| 208 | US-LOS | | TS_1 | 0 | |
| 209 | US-LOS | | TS_2 | −0.05 | |
| 210 | US-LOS | | TS_3 | −0.1 | |
| 211 | US-LOS | | TS_4 | −0.2 | |
| 212 | US-LOS | | TS_5 | −0.5 | |
| 213 | US-MRM | | TS_1 | | |
| 214 | US-MRM | | TS_2 | | |
| 215 | US-MYB | | TS_1 | −0.02 | |
| 216 | US-MYB | | TS_2 | −0.04 | |
| 217 | US-MYB | | TS_3 | −0.08 | |
| 218 | US-MYB | | TS_4 | −0.16 | |
| 219 | US-MYB | | TS_5 | −0.32 | |
| 220 | US-NC4 | | TS_1 | −0.05 | |
| 221 | US-NC4 | | TS_2 | −0.2 | |
| 222 | US-NGB | | No data | | |
| 223 | US-NGC | | No data | | |
| 224 | US-ORV | | TS_1 | −0.08 | |

Table B7. Continued.

| | SITE_ID | Year | Probe name | Soil_temp_depth_m | Additional_notes |
|-----|---------|------|------------|-------------------|---|
| 225 | US-OWC | | TS_1 | -0.05 | |
| 226 | US-OWC | | TS_2 | -0.3 | |
| 227 | US-PFA | | | | |
| 228 | US-SND | | TS_1 | -0.08 | |
| 229 | US-SND | | TS_2 | -0.16 | |
| 230 | US-SND | | TS_3 | | |
| 231 | US-SND | | TS_4 | | |
| 232 | US-SND | | TS_5 | | |
| 233 | US-SND | | TS_6 | | |
| 234 | US-SNE | | TS_1 | -0.01 | |
| 235 | US-SNE | | TS_2 | -0.02 | |
| 236 | US-SNE | | TS_3 | -0.08 | |
| 237 | US-SNE | | TS_4 | -0.16 | |
| 238 | US-SNE | | TS_5 | -0.32 | |
| 239 | US-SRR | | TS_1 | | |
| 240 | US-SRR | | TS_2 | | |
| 241 | US-SRR | | TS_3 | | |
| 242 | US-SRR | | TS_4 | | |
| 243 | US-SRR | | TS_5 | | |
| 244 | US-STJ | | TS_2 | -0.05 | |
| 245 | US-STJ | | TS_3 | -0.1 | |
| 246 | US-TW1 | | TS_1 | -0.02 | |
| 247 | US-TW1 | | TS_2 | -0.04 | |
| 248 | US-TW1 | | TS_3 | -0.08 | |
| 249 | US-TW1 | | TS_4 | -0.16 | |
| 250 | US-TW1 | | TS_5 | -0.32 | |
| 251 | US-TW3 | | TS_1 | -0.02 | |
| 252 | US-TW3 | | TS_2 | -0.04 | |
| 253 | US-TW3 | | TS_3 | -0.08 | |
| 254 | US-TW3 | | TS_4 | -0.16 | |
| 255 | US-TW3 | | TS_5 | -0.32 | |
| 256 | US-TW4 | | TS_1 | -0.02 | |
| 257 | US-TW4 | | TS_2 | -0.04 | |
| 258 | US-TW4 | | TS_3 | -0.08 | |
| 259 | US-TW4 | | TS_4 | -0.16 | |
| 260 | US-TW4 | | TS_5 | -0.32 | |
| 261 | US-TW5 | | TS_1 | -0.02 | |
| 262 | US-TW5 | | TS_2 | -0.1 | |
| 263 | US-TW5 | | TS_3 | -0.02 | |
| 264 | US-TW5 | | TS_4 | -0.08 | |
| 265 | US-TW5 | | TS_5 | -0.16 | |
| 266 | US-TWT | | TS_1 | -0.02 | |
| 267 | US-TWT | | TS_2 | -0.04 | |
| 268 | US-TWT | | TS_3 | -0.08 | |
| 269 | US-TWT | | TS_4 | -0.16 | |
| 270 | US-TWT | | TS_5 | -0.32 | |
| 271 | US-UAF | | TS_1 | -0.09 | average of 3 depths: -0.15, -0.02, -0.1 |
| 272 | US-UAF | | TS_2 | -0.18333 | average of 3 depths: -0.3, -0.05, -0.2 |
| 273 | US-UAF | | TS_3 | -0.28333 | average of 3 depths: -0.3, -0.05, -0.2 |
| 274 | US-UAF | | TS_4 | -0.36667 | average of 3 depths: -0.5, -0.2, -0.4 |
| 275 | US-UAF | | TS_5 | -0.5 | average of 2 depths: -0.7, -0.3 |
| 276 | US-UAF | | TS_6 | -0.6 | average of 2 depths: -0.8, -0.4 |
| 277 | US-UAF | | TS_7 | -0.75 | average of 2 depths: -1, -0.5 |
| 278 | US-UAF | | TS_8 | -0.925 | average of 2 depths: -1.25, 0.6, |
| 279 | US-UAF | | TS_9 | -1 | |
| 280 | US-WPT | | TS_1 | -0.1 | |
| 281 | US-WPT | | TS_2 | -0.3 | |

| Column | Description |
|-------------------|---|
| SITE_ID | Site identification code as assigned by regional flux data network |
| Year | When relevant, information about time span of probe location; if blank, assume constant probe depth |
| Probe_name | Temperature probe name as given in data files |
| Soil_temp_depth_m | Depth of soil temperature probe (m), with negative values being under the surface |
| Additional_notes | When relevant, additional information about site |

Author contributions. KBD oversaw the data release, performed the seasonality analysis, gathered metadata, and prepared the manuscript with contributions from all co-authors. SHK gathered and standardized the data, and gap-filled the CH₄ flux data. AM prepared the manuscript and gathered metadata. EFC did the representativeness analysis and prepared the manuscript. GM gathered data and prepared the manuscript. RBJ oversaw the data collection, processing, analysis, and release. DC and YWC oversaw the FLUXNET-CH₄ dataset release on <https://fluxnet.org> (last access: 6 July 2021). DP, EC, and CT did the data collection, curation, and pre-processing for all of the sites outside North and South America. The remaining co-authors contributed eddy-covariance data to FLUXNET-CH₄ dataset and/or participated in editing the manuscript.

Competing interests. The authors declare that they have no conflict of interest.

Disclaimer. Publisher's note: Copernicus Publications remains neutral with regard to jurisdictional claims in published maps and institutional affiliations.

Acknowledgements. We acknowledge primary support from the Gordon and Betty Moore Foundation (grant GBMF5439, “Advancing Understanding of the Global Methane Cycle”; Stanford University) and from the John Wesley Powell Center for Analysis and Synthesis of the US Geological Survey (“Wetland FLUXNET Synthesis for Methane” working group). Benjamin R. K. Runkle was supported by the US National Science Foundation CBET CAREER Award 1752083. Ankur R. Desai acknowledges support of the DOE AmeriFlux Network Management Project. Masahito Ueyama was supported by ArCS II (JPMXD1420318865) and JSPS KAKENHI (20K21849). Dario Papale and Nina Buchmann acknowledge the support of the RINGO (GA 730944) H2020 EU project. Nina Buchmann and Kathrin Fuchs acknowledge the SNF project M4P (40FA40_154245/1) and InnoFarm (407340_172433). Nina Buchmann acknowledges support from the SNF for ICOS-CH phases 1 and 2 (20FI21_148992, 20FI20_173691). Carlo Trotta acknowledges the support of the E-SHAPE (GA 820852) H2020 EU project. William J. Riley was supported by the US Department of Energy, BER, RGCM, RUBISCO project under contract no. DEAC02–05CH11231. Jessica Turner acknowledges support from NSF GRFP (DGE–1747503) and NTL LTER (DEB–1440297). Minseok Kang was supported by the National Research Foundation of Korea (NRF–2018 R1C1B6002917). Carole Helfter acknowledges the support of the UK Natural Environment Research Council (the Global Methane Budget project, grant number NE/N015746/1). Rodrigo Vargas acknowledges support from the National Science Foundation (1652594). Dennis Baldocchi acknowledges the California Department of Water Resources for a funding contract from the California Department of Fish and Wildlife and the United States Department of Agriculture (NIFA grant #2011-67003-30371), as well as the US Department of Energy's Office of Science (AmeriFlux contract #7079856) for funding the AmeriFlux core sites. US-A03 and US-A10 are operated by the Atmospheric Radiation Measurement (ARM) user facility, a US Department of

Energy's Office of Science user facility managed by the Biological and Environmental Research Program. Work at ANL was supported by the US Department of Energy's Office of Science and Office of Biological and Environmental Research under contract DE-AC02–06CH11357. Any use of trade, firm, or product names is for descriptive purposes only and does not imply endorsement by the US government. The CH-Dav, DE-SfN, FI-Hyy, FI-Lom, FI-Sii, FR-LGt, IT-BCi, SE-Deg, and SE-Sto sites are part of the ICOS European Research Infrastructure. Oliver Sonnentag acknowledges funding by the Canada Research Chairs, Canada Foundation for Innovation Leaders Opportunity Fund, and Natural Sciences and Engineering Research Council Discovery Grant programs for work at CA-SCC and CA-SCB. Benjamin Poulter acknowledges support from the NASA Carbon Cycle and Ecosystems program. Derrick Lai acknowledges the support of the Research Grants Council of the Hong Kong Special Administrative Region, China (project no. CUHK 458913). We thank Nathaniel Goenawan for his help with the representativeness analysis.

Financial support. This research has been supported by the Gordon and Betty Moore Foundation (grant no. GBMF5439), the John Wesley Powell Center for Analysis and Synthesis of the US Geological Survey, the National Science Foundation (grant nos. 1752083, DGE–1747503, and 1652594), the ArCS II (grant no. JPMXD1420318865), the JSPS KAKENHI (grant no. 20K21849), the RINGO (grant no. GA 730944), the SNF (grant nos. 40FA40_154245/1, 20FI21_148992, and 20FI20_173691), the InnoFarm (grant no. 407340_172433), the E-SHAPE (grant no. GA 820852), the US Department of Energy (grant nos. DEAC02–05CH11231, 7079856, and DE-AC02–06CH11357), the NTL LTER (grant no. DEB–1440297), the National Research Foundation of Korea (grant no. NRF–2018 R1C1B6002917), the UK Natural Environment Research Council (grant no. NE/N015746/1), the California Department of Fish and Wildlife (grant no. 2011-67003-30371), the Canada Research Chairs, the Canada Foundation for Innovation Leaders Opportunity Fund, the Natural Sciences and Engineering Research Council Discovery Grant programs, and the NASA Carbon Cycle and Ecosystems program.

Review statement. This paper was edited by David Carlson and reviewed by two anonymous referees.

References

- Abdalla, M., Hastings, A., Truu, J., Espenberg, M., Mander, Ü, and Smith, P.: Emissions of methane from northern peatlands: a review of management impacts and implications for future management options, *Ecol. Evol.*, 6, 7080–7102, <https://doi.org/10.1002/ece3.2469>, 2016.
- Alberto, M. and Wassmann, R.: FLUXNET-CH₄ PH-RiF Philippines Rice Institute flooded, Philippines, FLUXNET-CH₄ Community Product [data set], <https://doi.org/10.18140/FLX/1669653>, 2020.
- Alberto, M. C. R., Wassmann, R., Gummert, M., Buresh, R. J., Quilty, J. R., Correa, T. Q., Centeno, C. A. R., and Oca, G.

- M.: Straw incorporated after mechanized harvesting of irrigated rice affects net emissions of CH₄ and CO₂ based on eddy covariance measurements, *Field Crop. Res.*, 184, 162–175, <https://doi.org/10.1016/j.fcr.2015.10.004>, 2015.
- Anderson, D. E., Verma, S. B., and Rosenberg, N. J.: Eddy correlation measurements of CO₂, latent heat, and sensible heat fluxes over a crop surface, *Bound.-Lay. Meteorol.*, 29, 263–272, <https://doi.org/10.1007/bf00119792>, 1984.
- Anderson, F. E., Bergamaschi, B., Sturtevant, C., Knox, S., Hastings, L., Windham-Myers, L., Detto, M., Hestir, E. L., Drexler, J., Miller, R. L., Matthes, J. H., Verfaillie, J., Baldocchi, D., Snyder, R. L., and Fujii, R.: Variation of energy and carbon fluxes from a restored temperate freshwater wetland and implications for carbon market verification protocols, *J. Geophys. Res.-Biogeo.*, 121, 777–795, <https://doi.org/10.1002/2015JG003083>, 2016.
- Angle, J. C., Morin, T. H., Solden, L. M., Narrowe, A. B., Smith, G. J., Borton, M. A., Rey-Sanchez, C., Daly, R. A., Mirfenderesgi, G., Hoyt, D. W., Riley, W. J., Miller, C. S., Bohrer, G., and Wrighton, K. C.: Methanogenesis in oxygenated soils is a substantial fraction of wetland methane emissions, *Nat. Commun.*, 8, 1567, <https://doi.org/10.1038/s41467-017-01753-4>, 2017.
- Bartlett, K. B., Bartlett, D. S., Harriss, R. C., and Sebacher, D. I.: Methane emissions along a salt marsh salinity gradient, *Biogeochemistry*, 4, 183–202, <https://doi.org/10.1007/bf02187365>, 1987.
- Bastviken, D., Tranvik, L. J., Downing, J. A., Crill, P. M., and Enrich-Prast, A.: Freshwater methane emissions offset the continental carbon sink, *Science*, 331, 6013, <https://doi.org/10.1126/science.1196808>, 2011.
- Billesbach, D. and Sullivan, R.: FLUXNET-CH₄ US-A03 ARM-AMF3-Oliktok, United States, FLUXNET-CH₄ Community Product [data set], <https://doi.org/10.18140/FLX/1669661>, 2020a.
- Billesbach, D. and Sullivan, R.: FLUXNET-CH₄ US-A10 ARM-NSA-Barrow, United States, FLUXNET-CH₄ Community Product [data set], <https://doi.org/10.18140/FLX/1669662>, 2020b.
- Bloom, A. A., Bowman, K. W., Lee, M., Turner, A. J., Schroeder, R., Worden, J. R., Weidner, R., McDonald, K. C., and Jacob, D. J.: A global wetland methane emissions and uncertainty dataset for atmospheric chemical transport models (WetCHARTs version 1.0), *Geosci. Model Dev.*, 10, 2141–2156, <https://doi.org/10.5194/gmd-10-2141-2017>, 2017.
- Bridgman, S. D., Cadillo-Quiroz, H., Keller, J. K., and Zhuang, Q.: Methane emissions from wetlands: biogeochemical, microbial, and modeling perspectives from local to global scales, *Glob. Change Biol.*, 19, 1325–1346, <https://doi.org/10.1111/gcb.12131>, 2013.
- Bohrer, G. and Morin, T. H.: FLUXNET-CH₄ US-ORv Olentangy River Wetland Research Park, United States, FLUXNET-CH₄ Community Product [data set], <https://doi.org/10.18140/FLX/1669689>, 2020.
- Bohrer, G., Kerns, J., Morin, T. H., Rey-Sanchez, A. C., Villa, J., and Ju, Y.: FLUXNET-CH₄ US-OWC Old Woman Creek, United States, FLUXNET-CH₄ Community Product [data set], <https://doi.org/10.18140/FLX/1669690>, 2020.
- Campbell, D. and Goodrich, J.: FLUXNET-CH₄ NZ-Kop Kōpuatai, New Zealand, FLUXNET-CH₄ Community Product [data set], <https://doi.org/10.18140/FLX/1669652>, 2020.
- Castro-Morales, K., Kleinen, T., Kaiser, S., Zaehle, S., Kitzler, F., Kwon, M. J., Beer, C., and Göckede, M.: Year-round simulated methane emissions from a permafrost ecosystem in Northeast Siberia, *Biogeosciences*, 15, 2691–2722, <https://doi.org/10.5194/bg-15-2691-2018>, 2018.
- Chadburn, S. E., Aalto, T., Aurela, M., Baldocchi, D., Biasi, C., Boike, J., Burke, E. J., Comyn-Platt, E., Dolman, A. J., Duran-Rojas, C., Fan, Y., Friborg, T., Gao, Y., Gedney, N., Göckede, M., Hayman, G. D., Holl, D., Hugelius, G., Kutzbach, L., Lee, H., Lohila, A., Parmentier, F. W., Sachs, T., Shurpali, N. J., and Westermann, S.: Modeled microbial dynamics explain the apparent temperature sensitivity of wetland methane emissions, *Global Biogeochem. Cy.*, 34, e2020GB006678, <https://doi.org/10.1029/2020gb006678>, 2020.
- Chamberlain, S. D., Oikawa, P., Sturtevant, C., Szutu, D., Verfaillie, J., and Baldocchi, D.: FLUXNET-CH₄ US-Tw3 Twitchell Alfalfa, United States, FLUXNET-CH₄ Community Product [data set], <https://doi.org/10.18140/FLX/1669697>, 2020.
- Chambers, L. G., Ramesh Reddy, K., and Osborne, T. Z.: Short-Term Response of Carbon Cycling to Salinity Pulses in a Freshwater Wetland, *Soil Sci. Soc. Am. J.*, 75, 2000–2007, <https://doi.org/10.2136/sssaj2011.0026>, 2011.
- Chang, K. Y., Riley, W. J., Knox, S. H., Jackson, R. B., McNicol, G., Poulter, B., Aurela, M., Baldocchi, D., Bansal, S., Bohrer, G., Campbell, D. I., Cescatti, A., Chu, H., Delwiche, K. B., Desai, A., Euskirchen, E., Friborg, T., Göckede, M., Holm, G., Kang, M., Keenan, T., Krauss, K. W., Lohila, A., Mammarella, I., Miyata, A., Nilsson, M. B., Noormets, A., Papale, D., Runkle, B. R. K., Ryu, Y., Sachs, T., Schäfer, K. V. R., Schmid, H. P., Shurpali, N., Sonntag, O., Tang, A. C. I., Torn, M. S., Trotta, C., Ueyama, M., Vargas, R., Vesala, T., Windham-Myers, L., Zhang, Z., and Zona, D.: Global wetland methane emissions have hysteretic responses to seasonal temperature, *Nat. Commun.*, 12, 2266, <https://doi.org/10.1038/s41467-021-22452-1>, 2021.
- Chanton, J. P., Glaser, P. H., Chasar, L. S., Burdige, D. J., Hines, M. E., Siegel, D. I., Tremblay, L. B., and Cooper, W. T.: Radiocarbon evidence for the importance of surface vegetation on fermentation and methanogenesis in contrasting types of boreal peatlands, *Global Biogeochem. Cy.*, 22, GB4022, <https://doi.org/10.1029/2008gb003274>, 2008.
- Chen, J. and Chu, H.: FLUXNET-CH₄ US-CRT Curtice Walter-Berger cropland, United States, FLUXNET-CH₄ Community Product [data set], <https://doi.org/10.18140/FLX/1669671>, 2020a.
- Chen, J. and Chu, H.: FLUXNET-CH₄ US-WPT Winous Point North Marsh, United States, FLUXNET-CH₄ Community Product [data set], <https://doi.org/10.18140/FLX/1669702>, 2020b.
- Chu, H., Chen, J., Gottgens, J. F., Ouyang, Z., John, R., Czajkowski, K., and Becker, R.: Net ecosystem methane and carbon dioxide exchanges in a Lake Erie coastal marsh and a nearby cropland, *J. Geophys. Res.-Biogeo.*, 119, 722–740, <https://doi.org/10.1002/2013JG002520>, 2014.
- Chu, H., Baldocchi, D. D., John, R., Wolf, S., and Reichstein, M.: Fluxes all of the time? A primer on the temporal representativeness of FLUXNET, *J. Geophys. Res.-Biogeo.*, 122, 289–307, <https://doi.org/10.1002/2016JG003576>, 2017.
- Chu, H., Luo, X., Ouyang, Z., Chan, W. S., Dengel, S., Biraud, S. C., Torn, M. S., Metzger, S., Kumar, J., Arain, M. A., Arkebauer, T. J., Baldocchi, D., Bernacchi, C., Billesbach, D., Black,

- T. A., Blanken, P. D., Bohrer, G., Bracho, R., Brown, S., Brunzell, N. A., Chen, J., Chen, X., Clark, K., Desai, A.R., Duman, T., Durden, D., Fares, S., Forbrich, I., Gammon, J. A., Gough, C. M., Griffis, T., Helbig, M., Hollinger, D., Humphreys, E., Ikawa, H., Iwata, H., Ju, Y., Knowles, J. F., Knox, S. H., Kobayashi, H., Kolb, T., Law, B., Lee, X., Litvak, M., Liu, H., Munger, J. W., Noormets, A., Novick, K., Oberbauer, S. F., Oechel, W., Oikawa, P., Papuga, S. A., Pendall, E., Prajapati, P., Prueger, J., Quinton, W. L., Richardson, A. D., Russel, E. S., Scott, R. L., Starr, G., Staebler, R., Stoy, P., Stuart-Haentjens, E., Sonnentag, O., Sullivan, R. C., Suyker, A., Ueyama, M., Vargas, R., Wood, J. D., and Zona, D.: Representativeness of Eddy-Covariance flux footprints for areas surrounding AmeriFlux sites, *Agr. Forest Meteorol.*, 301-302, 108350, <https://doi.org/10.1016/j.agrformet.2021.108350>, 2021.
- Dalcin Martins, P., Hoyt, D. W., Bansal, S., Mills, C. T., Tfaily, M., Tangen, B. A., Finocchiaro, R. G., Johnston, M. D., McAdams, B. C., Solensky, M. J., Smith, G. J., Chin, Y.-P., and Wilkins, M. J.: Abundant carbon substrates drive extremely high sulfate reduction rates and methane fluxes in Prairie Pothole Wetlands, *Glob. Change Biol.*, 23, 3107–3120, <https://doi.org/10.1111/gcb.13633>, 2017.
- Dean, J. F., Middelburg, J. J., Röckmann, T., Aerts, R., Blauw, L. G., Egger, M., Jetten, M. S. M., de Jong, A. E. E., Meisel, O. H., Rasigraf, O., Slomp, C. P., in't Zandt, M. H., and Dolman, A. J.: Methane Feedbacks to the Global Climate System in a Warmer World, *Rev. Geophys.*, 56, 207–250, <https://doi.org/10.1002/2017rg000559>, 2018.
- Deemer, B. R., Harrison, J. A., Li, S., Beaulieu, J. J., DelSontro, T., Barros, N., Bezerra-Neto, J. F., Powers, S. M., Dos Santos, M. A., and Vonk, J. A.: Greenhouse Gas Emissions from Reservoir Water Surfaces: A New Global Synthesis, *Bioscience*, 66, 949–964, <https://doi.org/10.1093/biosci/biw117>, 2016.
- Dengel, S., Zona, D., Sachs, T., Aurela, M., Jammert, M., Parmentier, F. J. W., Oechel, W., and Vesala, T.: Testing the applicability of neural networks as a gap-filling method using CH₄ flux data from high latitude wetlands, *Biogeosciences*, 10, 8185–8200, <https://doi.org/10.5194/bg-10-8185-2013>, 2013.
- Delwiche, K. B., Knox, S. H., Malhotra, A., Fluet-Chouinard, E., McNicol, G., Feron, S., Ouyang, Z., Papale, D., Trotta, C., Canfora, E., Cheah, Y.-W., Christianson, D., Alberto, M. C. R., Alekseychik, P., Aurela, M., Baldocchi, D., Bansal, S., Billesbach, D. P., Bohrer, G., Bracho, R., Buchmann, N., Campbell, D. I., Celis, G., Chen, J., Chen, W., Chu, H., Dalmagro, H.J., Dengel, S., Desai, A. R., Detto, M., Dolman, H., Eichelmann, E., Euskirchen, E., Famulari, D., Friborg, T., Fuchs, K., Goeckede, M., Gogo, S., Gondwe, M. J., Goodrich, J. P., Gottschalk, P., Graham, S. L., Heimann, M., Helbig, M., Helfter, C., Hemes, K. S., Hirano, T., Hollinger, D., Hörtnagl, L., Iwata, H., Jacobot, A., Jansen, J., Jurasinski, G., Kang, M., Kasak, K., King, J., Klatt, J., Koebisch, F., Krauss, K. W., Lai, D. Y. F., Mammarella, I., Manca, G., Marchesini, L. B., Matthes, J. H., Maximon, T., Merbold, L., Mitra, B., Morin, T. H., Nemitz, E., Nilsson, M. B., Niu, S., Oechel, W.C., Oikawa, P. Y., Ono, K., Peichl, M., Peltola, O., Reba, M. L., Richardson, A. D., Riley, W., Runkle, B. R. K., Ryu, Y., Sachs, T., Sakabe, A., Sanchez, C. R., Schuur, E. A., Schäfer, K. V. R., Sonnentag, O., Sparks, J. P., Stuart-Haentjens, E., Sturtevant, C., Sullivan, R. C., Szutu, D. J., Thom, J. E., Torn, M. S., Tuittila, E.-S., Turner, J., Ueyama, M., Valach, A. C., Vargas, R., Varlagin, A., Vazquez-Lule, A., Verfaillie, J. G., Vesala, T., Vourlitis, G. L., Ward, E. J., Wille, C., Wohlfahrt, G., Wong, G. X., Zhang, Z., Zona, D., Windham-Myers, L., Poulter, B., and Jackson, R. B.: FLUXNET-CH₄: A global, multi-ecosystem dataset and analysis of methane seasonality from freshwater wetlands (Appendix B and Figure 3), Zenodo [data set], <https://doi.org/10.5281/zenodo.4672601>, 2021.
- Deshmukh, C. S., Julius, D., Evans, C. D., Nardi, Susanto, A. P., Page, S. E., Gauci, V., Laurén, A., Sabiham, S., Agus, F., Asyhari, A., Kurnianto, S., Suardiwerianto, Y., and Desai, A. R.: Impact of forest plantation on methane emissions from tropical peatland, *Glob. Change Biol.*, 26, 2477–2495, <https://doi.org/10.1111/gcb.15019>, 2020.
- Desai, A. R.: FLUXNET-CH₄ US-Los Lost Creek, United States, FLUXNET-CH₄ Community Product [data set], <https://doi.org/10.18140/FLX/1669682>, 2020a.
- Desai, A. R.: FLUXNET-CH₄ US-PfA Park Falls/WLEF, United States, FLUXNET-CH₄ Community Product [data set], <https://doi.org/10.18140/FLX/1669691>, 2020b.
- Desjardins, R. L.: A technique to measure CO₂ exchange under field conditions, *Int. J. Biometeorol.*, 18, 76–83, <https://doi.org/10.1007/bf01450667>, 1974.
- Detto, M., Sturtevant, C., Oikawa, P., Verfaillie, J., and Baldocchi, D.: FLUXNET-CH₄ US-Snd Sherman Island, United States, FLUXNET-CH₄ Community Product [data set], <https://doi.org/10.18140/FLX/1669692>, 2020.
- Didan, K.: MOD13A3 MODIS/Terra vegetation Indices Monthly L3 Global 1km SIN Grid V006, NASA EOSDIS Land Processes DAAC [data set], <https://doi.org/10.5067/MODIS/MOD13A3.006>, 2015.
- Dise, N.: Winter fluxes of methane from Minnesota peatlands, *Biogeochemistry*, 17, 17–83, <https://doi.org/10.1007/bf00002641>, 1992.
- Dolman, H., Hendriks, D., van Huissteden, K., and Belelli, L.: FLUXNET-CH₄ NL-Hor Horstermeer, Netherlands, FLUXNET-CH₄ Community Product [data set], <https://doi.org/10.18140/FLX/1669651>, 2020a.
- Dolman, H., Maximov, T., Parmentier, F., Budishev, A., and Marchesini, L. B.: FLUXNET-CH₄ RU-Cok Chokurdakh, Russian Federation, FLUXNET-CH₄ Community Product [data set], <https://doi.org/10.18140/FLX/1669656>, 2020b.
- Eichelmann, E., Knox, S., Rey Sanchez, C., Valach, A., Sturtevant, C., Szutu, D., Verfaillie, J., and Baldocchi, D.: FLUXNET-CH₄ US-Tw4 Twitchell East End Wetland, United States, FLUXNET-CH₄ Community Product [data set], <https://doi.org/10.18140/FLX/1669698>, 2020.
- Eklundh, L. and Jönsson, P.: TIMESAT: A Software Package for Time-Series Processing and Assessment of Vegetation Dynamics, Remote Sensing Time Series, Springer International Publishing, 141–158, https://doi.org/10.1007/978-3-319-15967-6_7, 2015.
- Etheridge, D. M., Steele, L. P., Francey, R. J., and Langenfelds, R. L.: Atmospheric methane between 1000 A.D. and present: Evidence of anthropogenic emissions and climatic variability, *J. Geophys. Res.-Atmos.*, 103, 15979–15993, <https://doi.org/10.1029/98jd00923>, 1998.
- Etminan, M., Myhre, G., Highwood, E. J., and Shine, K. P.: Radiative forcing of carbon dioxide, methane, and nitrous oxide: A significant revision of the methane radiative forcing, *Geophys. Res.*

- Lett., 43, 12614–12623, <https://doi.org/10.1002/2016gl071930>, 2016.
- Euskirchen, E. and Edgar, C.: FLUXNET-CH₄ US-BZB Bonanza Creek Thermokarst Bog, United States, FLUXNET-CH₄ Community Product [data set], <https://doi.org/10.18140/FLX/1669668>, 2020a.
- Euskirchen, E. and Edgar, C.: FLUXNET-CH₄ US-BZF Bonanza Creek Rich Fen, United States, FLUXNET-CH₄ Community Product [data set], <https://doi.org/10.18140/FLX/1669669>, 2020b.
- Euskirchen, E. and Edgar, C.: FLUXNET-CH₄ US-BZS Bonanza Creek Black Spruce, United States, FLUXNET-CH₄ Community Product [data set], <https://doi.org/10.18140/FLX/1669670>, 2020c.
- Euskirchen, E., Bret-Harte, M., and Edgar, C.: FLUXNET-CH₄ US-ICs Imnavait Creek Watershed Wet Sedge Tundra, United States, FLUXNET-CH₄ Community Product [data set], <https://doi.org/10.18140/FLX/1669678>, 2020.
- Famulari, D.: FLUXNET-CH₄ IT-BCi Borgo Cioffi, Italy, FLUXNET-CH₄ Community Product [data set], <https://doi.org/10.18140/FLX/1669644>, 2020.
- Fick, S. E. and Hijmans, R. J.: WorldClim: 2: new 1km spatial resolution climate surfaces for global land areas, *Int. J. Climatol.*, 37, 4302–4315, 2017.
- Friborg, T., Christensen, T. R., and Sørensen, H.: Rapid response of greenhouse gas emission to early spring thaw in a subarctic mire as shown by micrometeorological techniques, *Geophys. Res. Lett.*, 24, 3061–3064, <https://doi.org/10.1029/97gl03024>, 1997.
- Gallant, A.: The Challenges of Remote Monitoring of Wetlands, *Remote Sensing*, 7, 10938–10950, <https://doi.org/10.3390/rs70810938>, 2015.
- Göckede, M., Kittler, F., and Schaller, C.: Quantifying the impact of emission outbursts and non-stationary flow on eddy-covariance CH₄ flux measurements using wavelet techniques, *Biogeosciences*, 16, 3113–3131, <https://doi.org/10.5194/bg-16-3113-2019>, 2019.
- Goeckede, M.: FLUXNET-CH₄ RU-Ch2 Chersky reference, Russian Federation, FLUXNET-CH₄ Community Product [data set], <https://doi.org/10.18140/FLX/1669654>, 2020.
- Gu, L., Post, W. M., Baldocchi, D. D., Andrew Black, T., Suyker, A. E., Verma, S. B., Vesala, T., and Wofsy, S. C.: Characterizing the Seasonal Dynamics of Plant Community Photosynthesis Across a Range of Vegetation Types, in: *Phenology of Ecosystem Processes*, edited by: Noormets, A., Springer, New York, NY, 35–58, https://doi.org/10.1007/978-1-4419-0026-5_2, 2009.
- Hargreaves, K. J., Fowler, D., Pitcairn, C. E. R., and Aurela, M.: Annual methane emission from Finnish mires estimated from eddy covariance campaign measurements, *Theor. Appl. Climatol.*, 70, 203–213, <https://doi.org/10.1007/s007040170015>, 2001.
- Hargrove, W. W., Hoffman, F. M., and Law, B. E.: New analysis reveals representativeness of the AmeriFlux network, *Eos T. Am. Geophys.*, 84, 529, <https://doi.org/10.1029/2003EO480001>, 2003.
- Hatala, J. A., Detto, M., and Baldocchi, D. D.: Gross ecosystem photosynthesis causes a diurnal pattern in methane emission from rice, *Geophys. Res. Lett.*, 39, L06409m <https://doi.org/10.1029/2012gl051303>, 2012.
- Helbig, M., Quinton, W. L., and Sonntag, O.: Warmer spring conditions increase annual methane emissions from a boreal peat landscape with sporadic permafrost, *Environ. Res. Lett.*, 12, 115009, <https://doi.org/10.1088/1748-9326/aa8c85>, 2017.
- Helfter, C.: FLUXNET-CH₄ BW-Gum Guma, Botswana, FLUXNET-CH₄ Community Product [data set], <https://doi.org/10.18140/FLX/1669370>, 2020a.
- Helfter, C.: FLUXNET-CH₄ BW-Nxr Nxrara, Botswana, FLUXNET-CH₄ Community Product [data set], <https://doi.org/10.18140/FLX/1669518>, 2020b.
- Helfter, C.: FLUXNET-CH₄ UK-LBT London_BT, United Kingdom, FLUXNET-CH₄ Community Product [data set], <https://doi.org/10.18140/FLX/1670207>, 2020c.
- Helfter, C., Tremper, A. H., Halios, C. H., Kotthaus, S., Björkgrén, A., Grimmond, C. S. B., Barlow, J. F., and Nemitz, E.: Spatial and temporal variability of urban fluxes of methane, carbon monoxide and carbon dioxide above London, UK, *Atmos. Chem. Phys.*, 16, 10543–10557, <https://doi.org/10.5194/acp-16-10543-2016>, 2016.
- Hinkle, C. R. and Bracho, R.: FLUXNET-CH₄ US-DPW Disney Wilderness Preserve Wetland, United States, FLUXNET-CH₄ Community Product [data set], <https://doi.org/10.18140/FLX/1669672>, 2020.
- Hoffman, F. M., Kumar, J., Mills, R. T., and Hargrove, W. W.: Representativeness-based sampling network design for the State of Alaska, *Landscape Ecol.*, 28, 1567–1586, <https://doi.org/10.1007/s10980-013-9902-0>, 2013.
- Hollinger, D. Y. and Richardson, A. D.: Uncertainty in Eddy Covariance Measurements and Its Application to Physiological Models, *Tree Physiol.*, 25, 873–885, <https://doi.org/10.1093/treephys/25.7.873>, 2005.
- Holm, G. O., Perez, B. C., McWhorter, D. E., Krauss, K. W., Raynie, R. C., and Killebrew, C. J.: FLUXNET-CH₄ US-LA1 Pointe-aux-Chenes Brackish Marsh, United States, FLUXNET-CH₄ Community Product [data set], <https://doi.org/10.18140/FLX/1669680>, 2020a.
- Holm, G. O., Perez, B. C., McWhorter, D. E., Krauss, K. W., Raynie, R. C., and Killebrew, C. J.: FLUXNET-CH₄ US-LA2 Salvador WMA Freshwater Marsh, United States, FLUXNET-CH₄ Community Product [data set], <https://doi.org/10.18140/FLX/1669681>, 2020b.
- Hwang, Y., Ryu, Y., Huang, Y., Kim, J., Iwata, H., and Kang, M.: Comprehensive assessments of carbon dynamics in an intermittently-irrigated rice paddy, *Agr. Forest Meteorol.*, 285–286, 107933, <https://doi.org/10.1016/j.agrformet.2020.107933>, 2020.
- Iwata, H.: FLUXNET-CH₄ JP-Mse Mase rice paddy field, Japan, FLUXNET-CH₄ Community Product [data set], <https://doi.org/10.18140/FLX/1669647>, 2020a.
- Iwata, H.: FLUXNET-CH₄ JP-SwL Suwa Lake, Japan, FLUXNET-CH₄ Community Product [data set], <https://doi.org/10.18140/FLX/1669648>, 2020b.
- Iwata, H., Mano, M., Ono, K., Tokida, T., Kawazoe, T., Kosugi, Y., Sakabe, A., Takahashi, K., and Miyata, A.: Exploring sub-daily to seasonal variations in methane exchange in a single-crop rice paddy in central Japan, *Atmos. Environ.*, 179, 156–165, <https://doi.org/10.1016/j.atmosenv.2018.02.015>, 2018.
- Iwata, H., Ueyama, M., and Harazono, Y.: FLUXNET-CH₄ US-Uaf University of Alaska, Fairbanks, United States, FLUXNET-CH₄ Community Product [data set], <https://doi.org/10.18140/FLX/1669701>, 2020.

- Jacotot, A., Gogo, S., and Laggoun-Défarge, F.: FLUXNET-CH₄ FR-LGt La Guette, France, FLUXNET-CH₄ Community Product [data set], <https://doi.org/10.18140/FLX/1669641>, 2020.
- Jönsson, P. and Eklundh, L.: Seasonality extraction by function fitting to time-series of satellite sensor data, *IEEE T. Geosci. Remote*, 40, 1824–1832, <https://doi.org/10.1109/tgrs.2002.802519>, 2002.
- Jönsson, P. and Eklundh, L.: TIMESAT – a program for analyzing time-series of satellite sensor data. *Comput. Geosci.*, 30, 833–845, <https://doi.org/10.1016/j.cageo.2004.05.006>, 2004.
- Jung, M., Reichstein, M., and Bondeau, A.: Towards global empirical upscaling of FLUXNET eddy covariance observations: validation of a model tree ensemble approach using a biosphere model, *Biogeosciences*, 6, 2001–2013, <https://doi.org/10.5194/bg-6-2001-2009>, 2009.
- Jung, M., Schwalm, C., Migliavacca, M., Walther, S., Camps-Valls, G., Koirala, S., Anthoni, P., Besnard, S., Bodesheim, P., Carvalhais, N., Chevallier, F., Gans, F., Goll, D. S., Haverd, V., Köhler, P., Ichii, K., Jain, A. K., Liu, J., Lombardozzi, D., Nabel, J. E. M. S., Nelson, J. A., O’Sullivan, M., Pallandt, M., Papale, D., Peters, W., Pongratz, J., Rödenbeck, C., Sitch, S., Tramontana, G., Walker, A., Weber, U., and Reichstein, M.: Scaling carbon fluxes from eddy covariance sites to globe: synthesis and evaluation of the FLUXCOM approach, *Biogeosciences*, 17, 1343–1365, <https://doi.org/10.5194/bg-17-1343-2020>, 2020.
- Kim, Y., Johnson, M. S., Knox, S. H., Andrew Black, T., Dalma-gro, H. J., Kang, M., Kim, J., and Baldocchi, D.: Gap-filling approaches for eddy covariance methane fluxes: A comparison of three machine learning algorithms and a traditional method with principal component analysis, *Glob. Change Biol.*, 26, 1499–1518, <https://doi.org/10.1111/gcb.14845>, 2020.
- Kittler, F., Heimann, M., Kolle, O., Zimov, N., Zimov, S., and Göckede, M.: Long-Term Drainage Reduces CO₂ Uptake and CH₄ Emissions in a Siberian Permafrost Ecosystem: Drainage impact on Arctic carbon cycle, *Global Biogeochem. Cy.*, 31, 1704–1717, <https://doi.org/10.1002/2017GB005774>, 2017.
- Knox, S., Matthes, J. H., Verfaillie, J., and Baldocchi, D.: FLUXNET-CH₄ US-Twt Twitchell Island, United States, FLUXNET-CH₄ Community Product [data set], <https://doi.org/10.18140/FLX/1669700>, 2020.
- Knox, S. H., Sturtevant, C., Matthes, J. H., Koteen, L., Verfaillie, J., and Baldocchi, D.: Agricultural peatland restoration: effects of land-use change on greenhouse gas (CO₂ and CH₄) fluxes in the Sacramento-San Joaquin Delta, *Glob. Change Biol.*, 21, 750–765, <https://doi.org/10.1111/gcb.12745>, 2015.
- Knox, S. H., Matthes, J. H., Sturtevant, C., Oikawa, P. Y., Verfaillie, J., and Baldocchi, D.: Biophysical controls on interannual variability in ecosystem-scale CO₂ and CH₄ exchange in a California rice paddy, *J. Geophys. Res.-Biogeo.*, 121, 978–1001, <https://doi.org/10.1002/2015jg003247>, 2016.
- Knox, S. H., Jackson, R. B., Poulter, B., McNicol, G., Fluet-Chouinard, E., Zhang, Z., Hugelius, G., Bousquet, P., Canadell, J. G., Saunio, M., Papale, D., Chu, H., Keenan, T. F., Baldocchi, D., Torn, M. S., Mammarella, I., Trotta, C., Aurela, M., Bohrer, G., Campbell, D. I., Cescatti, A., Chamberlain, S., Chen, J., Chen, W., Dengel, S., Desai, A. R., Euskirchen, E., Friborg, T., Gasbarra, D., Goded, I., Goeckede, M., Heimann, M., Helbig, M., Hirano, T., Hollinger, D. Y., Iwata, H., Jurasinski, G., Kang, M., Koebisch, F., Mammarella, I., Nilsson, M. B., Ono, K., Peichl, M., Peltola, O., Ryu, Y., Sachs, T., Sakabe, A., Sparks, J., Tuittila, E.-S., Vourlitis, G. L., Wong, G. X., Windham-Myers, L., Poulter, B., and Jackson, R. B.: FLUXNET-CH₄ Synthesis Activity: Objectives, Observations, and Future Directions, *B. Am. Meteorol. Soc.*, 100, 2607–2632, <https://doi.org/10.1175/bams-d-18-0268.1>, 2019.
- Koebisch, F. and Jurasinski, G.: FLUXNET-CH₄ DE-Hte Huetelmoor, Germany, FLUXNET-CH₄ Community Product [data set], <https://doi.org/10.18140/FLX/1669634>, 2020.
- Koebisch, F., Jurasinski, G., Koch, M., Hofmann, J., and Glatzel, S.: Controls for multi-scale temporal variation in ecosystem methane exchange during the growing season of a permanently inundated fen, *Agr. Forest Meteorol.*, 204, 94–105, <https://doi.org/10.1016/j.agrformet.2015.02.002>, 2015.
- Koebisch, F., Winkel, M., Liebner, S., Liu, B., Westphal, J., Schmiedinger, I., Spitz, A., Gehre, M., Jurasinski, G., Köhler, S., Unger, V., Koch, M., Sachs, T., and Böttcher, M. E.: Sulfate deprivation triggers high methane production in a disturbed and rewetted coastal peatland, *Biogeosciences*, 16, 1937–1953, <https://doi.org/10.5194/bg-16-1937-2019>, 2019.
- Kuznetsova, A., Brockhoff, P. B., and Christensen, R. H. B.: lmerTest Package: Tests in Linear Mixed Effects Models, *J. Stat. Softw.*, 82, 1–26, <https://doi.org/10.18637/jss.v082.i13>, 2017.
- Kwon, M. J., Beulig, F., Ilie, I., Wildner, M., Küsel, K., Merbold, L., Mahecha, M. D., Zimov, N., Zimov, S. A., Heimann, M., Schuur, E. A. G., Kostka, J. E., Kolle, O., Hilke, I., and Göckede, M.: Plants, microorganisms, and soil temperatures contribute to a decrease in methane fluxes on a drained Arctic floodplain, *Glob. Change Biol.*, 23, 2396–2412, <https://doi.org/10.1111/gcb.13558>, 2017.
- Lai, D. Y. F.: Methane Dynamics in Northern Peatlands: A Review, *Pedosphere*, 19, 409–421, [https://doi.org/10.1016/s1002-0160\(09\)00003-4](https://doi.org/10.1016/s1002-0160(09)00003-4), 2009.
- Lai, D. Y. F., Roulet, N. T., and Moore, T. R.: The spatial and temporal relationships between CO₂ and CH₄ exchange in a temperate ombrotrophic bog, *Atmos. Environ.*, 89, 249–259, <https://doi.org/10.1016/j.atmosenv.2014.02.034>, 2014.
- Lai, D. Y. F.: FLUXNET-CH₄ HK-MPM Mai Po Mangrove, Hong Kong, FLUXNET-CH₄ Community Product [data set], <https://doi.org/10.18140/FLX/1669642>, 2020.
- Lasslop, G., Reichstein, M., Papale, D., Richardson, A. D., Arneth, A., Barr, A., Stoy, P., and Wohlfahrt, G.: Separation of net ecosystem exchange into assimilation and respiration using a light response curve approach: critical issues and global evaluation, *Glob. Change Biol.*, 16, 187–208, <https://doi.org/10.1111/j.1365-2486.2009.02041.x>, 2010.
- Liu, J., Zhou, Y., Valach, A., Shortt, R., Kasak, K., Rey-Sanchez, C., Hemes, K. S., Baldocchi, D., and Lai, D. Y. F.: Methane emissions reduce the radiative cooling effect of a subtropical estuarine mangrove wetland by half, *Glob. Change Biol.*, 26, 4998–5016, <https://doi.org/10.1111/gcb.15247>, 2020.
- Lohila, A., Aurela, M., Tuovinen, J.-P., Laurila, T., Hatakka, J., Rainne, J., and Mäkelä, T.: FLUXNET-CH₄ FI-Lom Lompolojankka, Finland, FLUXNET-CH₄ Community Product [data set], <https://doi.org/10.18140/FLX/1669638>, 2020.
- Madsen, K., Nielsen, H. B., and Tingleff, O.: Methods for non-linear least squares problems, *Informatics and Mathematical Modelling*, Technical University of Denmark, 2nd Edn., 2004.

- Maier, R., Hörtnagl, L., and Buchmann, N.: FLUXNET-CH₄ CH₂Oe2 Oensingen crop, FLUXNET-CH₄ Community Product [data set], Switzerland, <https://doi.org/10.18140/FLX/1669631>, 2020.
- Mahecha, M. D., Gans, F., Sippel, S., Donges, J. F., Kaminski, T., Metzger, S., Migliavacca, M., Papale, D., Rammig, A., and Zscheischler, J.: Detecting impacts of extreme events with ecological in situ monitoring networks, *Biogeosciences*, 14, 4255–4277, <https://doi.org/10.5194/bg-14-4255-2017>, 2017.
- Malhotra, A. and Roulet, N. T.: Environmental correlates of peatland carbon fluxes in a thawing landscape: do transitional thaw stages matter?, *Biogeosciences*, 12, 3119–3130, <https://doi.org/10.5194/bg-12-3119-2015>, 2015.
- Mammarella, I., Rannik, Ü., Kolari, P., Levula, J., and Vesala, T.: FLUXNET-CH₄ FI-Hyy Hyytiala, Finland, FLUXNET-CH₄ Community Product [data set], <https://doi.org/10.18140/FLX/1669637>, 2020.
- Manca, G. and Goded, I. FLUXNET-CH₄ IT-Cas Castellarlo, Italy, FLUXNET-CH₄ Community Product [data set], <https://doi.org/10.18140/FLX/1669645>, 2020.
- Mastepanov, M., Sigsgaard, C., Tagesson, T., Ström, L., Tamstorf, M. P., Lund, M., and Christensen, T. R.: Revisiting factors controlling methane emissions from high-Arctic tundra, *Biogeosciences*, 10, 5139–5158, <https://doi.org/10.5194/bg-10-5139-2013>, 2013.
- Matthes, J. H., Sturtevant, C., Oikawa, P., Chamberlain, S. D., Szutu, D., Ortiz, A. A., Verfaillie, J., and Baldocchi, D.: FLUXNET-CH₄ US-Myb Mayberry Wetland, United States, FLUXNET-CH₄ Community Product [data set], <https://doi.org/10.18140/FLX/1669685>, 2020.
- Matthews, E., Johnson, M. S., Genovese, V., Du, J., and Bastviken, D.: Methane emission from high latitude lakes: methane-centric lake classification and satellite-driven annual cycle of emissions. *Sci. Rep.-UK*, 10, 12465, <https://doi.org/10.1038/s41598-020-68246-1>, 2020.
- Megonigal, J. P., Whalen, S. C., Tissue, D. T., Bovard, B. D., Allen, A. S., and Albert, D. B.: A Plant-Soil-Atmosphere Microcosm for Tracing Radiocarbon from Photosynthesis through Methanogenesis, *Soil Sci. Soc. Am. J.*, 63, 665–671, <https://doi.org/10.2136/sssaj1999.03615995006300030033x>, 1999.
- Meijide, A., Manca, G., Goded, I., Magliulo, V., di Tommasi, P., Seufert, G., and Cescatti, A.: Seasonal trends and environmental controls of methane emissions in a rice paddy field in Northern Italy, *Biogeosciences*, 8, 3809–3821, <https://doi.org/10.5194/bg-8-3809-2011>, 2011.
- Melloh, R. A. and Crill, P. M.: Winter methane dynamics in a temperate peatland, *Global Biogeochem. Cy.*, 10, 247–254, <https://doi.org/10.1029/96gb00365>, 1996.
- Melton, J. R., Wania, R., Hodson, E. L., Poulter, B., Ringeval, B., Spahni, R., Bohn, T., Avis, C. A., Beerling, D. J., Chen, G., Eliseev, A. V., Denisov, S. N., Hopcroft, P. O., Lettenmaier, D. P., Riley, W. J., Singarayer, J. S., Subin, Z. M., Tian, H., Zürcher, S., Brovkin, V., van Bodegom, P. M., Kleinen, T., Yu, Z. C., and Kaplan, J. O.: Present state of global wetland extent and wetland methane modelling: conclusions from a model inter-comparison project (WETCHIMP), *Biogeosciences*, 10, 753–788, <https://doi.org/10.5194/bg-10-753-2013>, 2013.
- Merbold, L.: FLUXNET-CH₄ RU-Che Cherski, Russian Federation, FLUXNET-CH₄ Community Product [data set], <https://doi.org/10.18140/FLX/1669655>, 2020.
- Merbold, L., Fuchs, K., Buchmann, N., and Hörtnagl, L.: FLUXNET-CH₄ CH-Cha Chamau, Switzerland, FLUXNET-CH₄ Community Product [data set], <https://doi.org/10.18140/FLX/1669629>, 2020a.
- Merbold, L., Hörtnagl, L., and Buchmann, N.: FLUXNET-CH₄ CH-Dav Davos, Switzerland, FLUXNET-CH₄ Community Product [data set], <https://doi.org/10.18140/FLX/1669630>, 2020b.
- Meyer, H. and Pebesma, E.: Predicting into unknown space? Estimating the area of applicability of spatial prediction models, *arXiv [preprint]*, arXiv:2005.07939, 2020.
- Mishra, S. R., Pattnaik, P., Sethunathan, N., and Adhya, T. K.: Anion-Mediated Salinity Affecting Methane Production in a Flooded Alluvial Soil. *Geomicrobiol. J.*, 20, 579–586, <https://doi.org/10.1080/713851167>, 2003.
- Moffat, A. M., Papale, D., Reichstein, M., Hollinger, D. Y., Richardson, A. D., Barr, A. G., Beckstein, C., Braswell, B. H., Churkina, G., Desai, A. R., Falge, E., Gove, J. H., Heimann, M., Hui, D., Jarvis, A. J., Kattge, J., Noormets, A., and Stauch, V. J.: Comprehensive comparison of gap-filling techniques for eddy covariance net carbon fluxes, *Agr. Forest Meteorol.*, 147, 209–232, <https://doi.org/10.1016/j.agrformet.2007.08.011>, 2007.
- Myhre, G., Shindell, D., Bréon, F.-M., Collins, W., Fuglestedt, J., Huang, J., Koch, D., Lamarque, J.-F., Lee, D., Mendoza, B., Nakajima, T., Robock, A., Stephens, G., Takemura, T., and Zhang, H.: Anthropogenic and Natural Radiative Forcing Supplementary Material, in: *Climate Change 2013: The Physical Science Basis, Contribution of Working Group I to the Fifth Assessment Report of the Intergovernmental Panel on Climate Change*, edited by: Stocker, T. F., Qin, D., Plattner, G.-K., Tignor, M., Allen, S. K., Boschung, J., Nauels, A., Xia, Y., Bex, V., and Midgley, P. M., 2013.
- Nemitz, E., Mammarella, I., Ibrom, A., Aurela, M., Burba, G. G., Dengel, S., Gielen, B., Grelle, A., Heinesch, B., Herbst, M., Hörtnagl, L., Klemedtsson, L., Lindroth, A., Lohila, A., McDermitt, D. K., Meier, P., Merbold, L., Nelson, D., Nicolini, G., Nilsson, M. B., Peltola, O., Rinne, J., and Zahniser, M.: Standardisation of eddy-covariance flux measurements of methane and nitrous oxide, *Int. Agroph.*, 32, 517–549, <https://doi.org/10.1515/intag-2017-0042>, 2018.
- Nielsen, H. B.: Damping parameter in Marquardt’s method, Department of Mathematical Modeling, IMM, Technical University of Denmark, Technical Report, IMM-REP-1999-05, 1999.
- Nilsson, M. B. and Peichl, M.: FLUXNET-CH₄ SE-Deg Degero, Sweden, FLUXNET-CH₄ Community Product [data set], <https://doi.org/10.18140/FLX/1669659>, 2020.
- Niu, S. and Chen, W.: FLUXNET-CH₄ CN-Hgu Hongyuan, China, FLUXNET-CH₄ Community Product [data set], <https://doi.org/10.18140/FLX/1669632>, 2020.
- Noormets, A., King, J., Mitra, B., Miao, G., Aguilos, W., Minick, W., Prajapati, P., and Domec, J.-C.: FLUXNET-CH₄ US-NC4 NC_AlligatorRiver, United States, FLUXNET-CH₄ Community Product [data set], <https://doi.org/10.18140/FLX/1669686>, 2020.
- Oikawa, P. Y., Jenerette, G. D., Knox, S. H., Sturtevant, C., Verfaillie, J., Dronova, I., Poindexter, C. M., Eichelmann, E., and Baldocchi, D. D.: Evaluation of a hierarchy of models reveals

- importance of substrate limitation for predicting carbon dioxide and methane exchange in restored wetlands, *J. Geophys. Res.-Biogeo.*, 122, 145–167, <https://doi.org/10.1002/2016JG003438>, 2017.
- Oikawa, P.: FLUXNET-CH₄ US-EDN Eden Landing Ecological Reserve, United States, FLUXNET-CH₄ Community Product [data set], <https://doi.org/10.18140/FLX/1669673>, 2020.
- Olefeldt, D., Turetsky, M. R., Crill, P. M., and McGuire, A. D.: Environmental and physical controls on northern terrestrial methane emissions across permafrost zones, *Glob. Change Biol.*, 19, 589–603, <https://doi.org/10.1111/gcb.12071>, 2013.
- Papale, D., Andrew Black, T., Carvalhais, N., Cescatti, A., Chen, J., Jung, M., Kiely, G., Lasslop, G., Mahecha, M. D., Margolis, H., Merbold, L., Montagnani, L., Moors, E., Olesen, J. E., Reichstein, M., Tramontana, G., van Gorsel, E., Wohlfahrt, G., and Ráduly, B.: Effect of spatial sampling from European flux towers for estimating carbon and water fluxes with artificial neural networks, *J. Geophys. Res.-Biogeo.*, 120, 1941–1957, <https://doi.org/10.1002/2015jg002997>, 2015.
- Parmentier, F. J. W., van Huissteden, J., van der Molen, M. K., Schaepman-Strub, G., Karsanaev, S. A., Maximov, T. C., and Dolman, A. J.: Spatial and temporal dynamics in eddy covariance observations of methane fluxes at a tundra site in northeastern Siberia, *J. Geophys. Res.*, 116, 1368, <https://doi.org/10.1029/2010JG001637>, 2011.
- Pastorello, G., Trotta, C., Canfora, E., Chu, H., Christianson, D., Cheah, Y.-W., Poindexter, C., Chen, J., Elbashandy, A., Humphrey, M., Isaac, P., Polidori, D., Ribeca, A., van Ingen, C., Zhang, L., Amiro, B., Ammann, C., Arain, M. A., Ardö, J., et al.: The FLUXNET2015 dataset and the ONEFlux processing pipeline for eddy covariance data, *Sci. Data*, 7, 225, <https://doi.org/10.1038/s41597-020-0534-3>, 2020.
- Pattanaik, P., Mishra, S. R., Bharati, K., Mohanty, S. R., Sethunathan, N., and Adhya, T. K.: Influence of salinity on methanogenesis and associated microflora in tropical rice soils, *Microbiol. Res.*, 155, 215–220, [https://doi.org/10.1016/S0944-5013\(00\)80035-X](https://doi.org/10.1016/S0944-5013(00)80035-X), 2000.
- Poffenbarger, H. J., Needelman, B. A., and Patrick Megonigal, J.: Salinity Influence on Methane Emissions from Tidal Marshes, *Wetlands*, 31, 831–842, <https://doi.org/10.1007/s13157-011-0197-0>, 2011.
- Poulter, B., Bousquet, P., Canadell, J. G., Ciais, P., Peregon, A., Saunio, M., Arora, V. K., Beerling, D. J., Brovkin, V., Jones, C. D., Joos, F., Gedney, N., Ito, A., Kleinen, T., Koven, C. D., McDonald, K., Melton, J. R., Peng, C., Peng, S., Prigent, C., Schroeder, R., Riley, W. J., Saito, M., Spahni, R., Tian, H., Taylor, L., Viovy, N., Wilton, D., Wiltshire, A., Xu, X., Zhang, B., Zhang, Z., and Zhu, Q.: Global wetland contribution to 2000–2012 atmospheric methane growth rate dynamics, *Environ. Res. Lett.*, 12, 094013, <https://doi.org/10.1088/1748-9326/aa8391>, 2017.
- R Core Team: R: A Language and Environment for Statistical Computing. R Foundation for Statistical Computing, Vienna, 2018.
- Reba, M., Runkle, B., and Suvocarev, K.: FLUXNET-CH₄ US-HRC Humnoke Farm Rice Field – Field C, United States, FLUXNET-CH₄ Community Product [data set], <https://doi.org/10.18140/FLX/1669677>, 2020.
- Reichstein, M., Falge, E., Baldocchi, D., Papale, D., Aubinet, M., Berbigier, P., Bernhofer, C., Buchmann, N., Gilmanov, T., Granier, A., Grunwald, T., Havrankova, K., Ilvesniemi, H., Janous, D., Knohl, A., Laurila, T., Lohila, A., Loustau, D., Matteucci, G., Meyers, T., Miglietta, F., Ourcival, J.-M., Pumpanen, J., Rambal, S., Rotenberg, E., Sanz, M., Tenhunen, J., Seufert, G., Vaccari, F., Vesala, T., Yakir, D., and Valentini, R.: On the separation of net ecosystem exchange into assimilation and ecosystem respiration: review and improved algorithm, *Glob. Change Biol.*, 11, 1424–1439, <https://doi.org/10.1111/j.1365-2486.2005.001002.x>, 2005.
- Rey-Sanchez, C., Szutu, D., Shortt, R., Chamberlain, S. D., Verfaillie, J., and Baldocchi, D.: FLUXNET-CH₄ US-Bi1 Bouldin Island Alfalfa, United States, FLUXNET-CH₄ Community Product [data set], <https://doi.org/10.18140/FLX/1669666>, 2020a.
- Rey-Sanchez, C., Szutu, D., Hemes, K., Verfaillie, J., and Baldocchi, D.: FLUXNET-CH₄ US-Bi2 Bouldin Island corn, United States, FLUXNET-CH₄ Community Product [data set], <https://doi.org/10.18140/FLX/1669667>, 2020b.
- Richardson, A. D. and Hollinger, D. Y.: A method to estimate the additional uncertainty in gap-filled NEE resulting from long gaps in the CO₂ flux record, *Agr. Forest Meteorol.*, 147, 199–208, <https://doi.org/10.1016/j.agrformet.2007.06.004>, 2007.
- Richardson, A. D. and Hollinger, D. Y.: FLUXNET-CH₄ US-Ho1 Howland Forest (main tower), United States, FLUXNET-CH₄ Community Product [data set], <https://doi.org/10.18140/FLX/1669675>, 2020.
- Richardson, A. D., Hollinger, D. Y., Burba, G. G., Davis, K. J., Flanagan, L. B., Katul, G. G., William Munger, J., Ricciuto, D. M., Stoy, P. C., Suyker, A. E., Verma, S. B., and Wofsy, S. C.: A multi-site analysis of random error in tower-based measurements of carbon and energy fluxes, *Agr. Forest Meteorol.*, 136, 1–18, <https://doi.org/10.1016/j.agrformet.2006.01.007>, 2006.
- Richardson, A. D., Mahecha, M. D., Falge, E., Kattge, J., Moffat, A. M., Papale, D., Reichstein, M., Stauch, V. J., Braswell, B. H., Churkina, G., Kruijt, B., and Hollinger, D. Y.: Statistical properties of random CO₂ flux measurement uncertainty inferred from model residuals, *Agr. Forest Meteorol.*, 148, 38–50, <https://doi.org/10.1016/j.agrformet.2007.09.001>, 2008.
- Richardson, A. D., Aubinet, M., Barr, A. G., Hollinger, D. Y., Ibrom, A., Lasslop, G., and Reichstein, M.: Uncertainty quantification, Eddy Covariance: A Practical Guide to Measurement and Data Analysis, edited by: Aubinet, M., Vesala, T., and Papale, D.: Springer Atmospheric Sciences, 2012.
- Rinne, J., Riutta, T., Pihlatie, M., Aurela, M., Haapanala, S., Tuovinen, J.-P., Tuittila, E.-S., and Vesala, T.: Annual cycle of methane emission from a boreal fen measured by the eddy covariance technique, *Tellus B*, 59, 449–457, <https://doi.org/10.1111/j.1600-0889.2007.00261.x>, 2007.
- Runkle, B., Reba, M., and Suvocarev, K.: FLUXNET-CH₄ US-HRA Humnoke Farm Rice Field – Field A, United States, FLUXNET-CH₄ Community Product [data set], <https://doi.org/10.18140/FLX/1669676>, 2020.
- Runkle, B. R. K., Suvočarev, K., Reba, M. L., Reavis, C. W., Smith, S. F., Chiu, Y.-L., and Fong, B.: Methane Emission Reductions from the Alternate Wetting and Drying of Rice Fields Detected Using the Eddy Covariance Method, *Environ. Sci. Technol.*, 53, 671–681, <https://doi.org/10.1021/acs.est.8b05535>, 2019.
- Ryu, Y., Kang, M., and Kim, J.: FLUXNET-CH₄ KR-CRK Cheorwon Rice paddy, Korea, Republic of, FLUXNET-CH₄ Commu-

- nity Product [data set], <https://doi.org/10.18140/FLX/1669649>, 2020.
- Sachs, T. and Wille, C.: FLUXNET-CH₄ DE-Dgw Dagowsee, Germany, FLUXNET-CH₄ Community Product [data set], <https://doi.org/10.18140/FLX/1669633>, 2020a.
- Sachs, T. and Wille, C.: FLUXNET-CH₄ DE-Zrk Zarnekow, Germany, FLUXNET-CH₄ Community Product [data set], <https://doi.org/10.18140/FLX/1669636>, 2020b.
- Sachs, T., Giebels, M., Boike, J., and Kutzbach, L.: Environmental controls on CH₄ emission from polygonal tundra on the microsite scale in the Lena river delta, Siberia: controls on tundra CH₄ flux and scaling, *Glob. Change Biol.*, 16, 3096–3110, <https://doi.org/10.1111/j.1365-2486.2010.02232.x>, 2010.
- Sakabe, A., Itoh, M., Hirano, T., and Kusin, K.: FLUXNET-CH₄ ID-Pag Palangkaraya undrained forest, Indonesia, FLUXNET-CH₄ Community Product [data set], <https://doi.org/10.18140/FLX/1669643>, 2020.
- Saunois, M., Bousquet, P., Poulter, B., Peregon, A., Ciais, P., Canadell, J. G., Dlugokencky, E. J., Etiope, G., Bastviken, D., Houweling, S., Janssens-Maenhout, G., Tubiello, F. N., Castaldi, S., Jackson, R. B., Alexe, M., Arora, V. K., Beerling, D. J., Bergamaschi, P., Blake, D. R., Brailsford, G., Brovkin, V., Bruhwiler, L., Crevoisier, C., Crill, P., Covey, K., Curry, C., Frankenberg, C., Gedney, N., Höglund-Isaksson, L., Ishizawa, M., Ito, A., Joos, F., Kim, H.-S., Kleinen, T., Krummel, P., Lamarque, J.-F., Langenfelds, R., Locatelli, R., Machida, T., Maksyutov, S., McDonald, K. C., Marshall, J., Melton, J. R., Morino, I., Naik, V., O'Doherty, S., Parmentier, F.-J. W., Patra, P. K., Peng, C., Peng, S., Peters, G. P., Pison, I., Prigent, C., Prinn, R., Ramonet, M., Riley, W. J., Saito, M., Santini, M., Schroeder, R., Simpson, I. J., Spahni, R., Steele, P., Takizawa, A., Thornton, B. F., Tian, H., Tohjima, Y., Viovy, N., Voulgarakis, A., van Weele, M., van der Werf, G. R., Weiss, R., Wiedinmyer, C., Wilton, D. J., Wiltshire, A., Worthy, D., Wunch, D., Xu, X., Yoshida, Y., Zhang, B., Zhang, Z., and Zhu, Q.: The global methane budget 2000–2012, *Earth Syst. Sci. Data*, 8, 697–751, <https://doi.org/10.5194/essd-8-697-2016>, 2016.
- Saunois, M., Stavert, A. R., Poulter, B., Bousquet, P., Canadell, J. G., Jackson, R. B., Raymond, P. A., Dlugokencky, E. J., Houweling, S., Patra, P. K., Ciais, P., Arora, V. K., Bastviken, D., Bergamaschi, P., Blake, D. R., Brailsford, G., Bruhwiler, L., Carlson, K. M., Carrol, M., Castaldi, S., Chandra, N., Crevoisier, C., Crill, P. M., Covey, K., Curry, C. L., Etiope, G., Frankenberg, C., Gedney, N., Hegglin, M. I., Höglund-Isaksson, L., Hugelius, G., Ishizawa, M., Ito, A., Janssens-Maenhout, G., Jensen, K. M., Joos, F., Kleinen, T., Krummel, P. B., Langenfelds, R. L., Laruelle, G. G., Liu, L., Machida, T., Maksyutov, S., McDonald, K. C., McNorton, J., Miller, P. A., Melton, J. R., Morino, I., Müller, J., Murguía-Flores, F., Naik, V., Niwa, Y., Noce, S., O'Doherty, S., Parker, R. J., Peng, C., Peng, S., Peters, G. P., Prigent, C., Prinn, R., Ramonet, M., Regnier, P., Riley, W. J., Rosentretter, J. A., Segers, A., Simpson, I. J., Shi, H., Smith, S. J., Steele, L. P., Thornton, B. F., Tian, H., Tohjima, Y., Tubiello, F. N., Tsuruta, A., Viovy, N., Voulgarakis, A., Weber, T. S., van Weele, M., van der Werf, G. R., Weiss, R. F., Worthy, D., Wunch, D., Yin, Y., Yoshida, Y., Zhang, W., Zhang, Z., Zhao, Y., Zheng, B., Zhu, Q., Zhu, Q., and Zhuang, Q.: The Global Methane Budget 2000–2017, *Earth Syst. Sci. Data*, 12, 1561–1623, <https://doi.org/10.5194/essd-12-1561-2020>, 2020.
- Schäfer, K.: FLUXNET-CH₄ US-MRM Marsh Resource Meadowlands Mitigation Bank, United States, FLUXNET-CH₄ Community Product [data set], <https://doi.org/10.18140/FLX/1669684>, 2020.
- Schmid, H. P. and Klatt, J.: FLUXNET-CH₄ DE-SfN Schechenfilz Nord, Germany, FLUXNET-CH₄ Community Product [data set], <https://doi.org/10.18140/FLX/1669635>, 2020.
- Schuur, E. A.: FLUXNET-CH₄ US-EML Eight Mile Lake Permafrost thaw gradient, Healy Alaska, United States, FLUXNET-CH₄ Community Product [data set], <https://doi.org/10.18140/FLX/1669674>, 2020.
- Seyfferth, A. L., Bothfeld, F., Vargas, R., Stuckey, J. W., Wang, J., Kearns, K., Michael, H. A., Guimond, J., Yu, X., and Sparks, D. L.: Spatial and temporal heterogeneity of geochemical controls on carbon cycling in a tidal salt marsh, *Geochim. Cosmochim. Ac.*, 282, 1–18, <https://doi.org/10.1016/j.gca.2020.05.013>, 2020.
- Shortt, R., Hemes, K., Szutu, D., Verfaillie, J., and Baldocchi, D.: FLUXNET-CH₄ US-Sne Sherman Island Restored Wetland, United States, FLUXNET-CH₄ Community Product [data set], <https://doi.org/10.18140/FLX/1669693>, 2020.
- Sims, D. A., Rahman, A. F., Cordova, V. D., El-Masri, B. Z., Baldocchi, D. D., Flanagan, L. B., Goldstein, A. H., Hollinger, D. Y., Misson, L., Monson, R. K., Oechel, W. C., Schmid, H. P., Wofsy, S. C., and Xu, L.: On the use of MODIS EVI to assess gross primary productivity of North American ecosystems, *J. Geophys. Res.-Biogeo.*, 111, G04015, <https://doi.org/10.1029/2006jg000162>, 2006.
- Sonnentag, O. and Helbig, M.: FLUXNET-CH₄ CA-SCB Scotty Creek Bog, Canada, FLUXNET-CH₄ Community Product [data set], <https://doi.org/10.18140/FLX/1669613>, 2020a.
- Sonnentag, O. and Helbig, M.: FLUXNET-CH₄ CA-SCC Scotty Creek Landscape, Canada, FLUXNET-CH₄ Community Product [data set], <https://doi.org/10.18140/FLX/1669628>, 2020b.
- Spahni, R., Wania, R., Neef, L., van Weele, M., Pison, I., Bousquet, P., Frankenberg, C., Foster, P. N., Joos, F., Prentice, I. C., and van Velthoven, P.: Constraining global methane emissions and uptake by ecosystems, *Biogeosciences*, 8, 1643–1665, <https://doi.org/10.5194/bg-8-1643-2011>, 2011.
- Sparks, J. P.: FLUXNET-CH₄ US-MAC MacArthur Agro-Ecology, United States, FLUXNET-CH₄ Community Product [data set], <https://doi.org/10.18140/FLX/1669683>, 2020.
- Sturtevant, C. S., Ruddell, B. L., Knox, S. H., Verfaillie, J. G., Matthes, J. H., Oikawa, P. Y., and Baldocchi, D. D.: Identifying scale-emergent, nonlinear, asynchronous processes of wetland methane exchange, *J. Geophys. Res.-Biogeo.*, 121, 188–204, <https://doi.org/10.1002/2015JG003054>, 2016.
- Tagesson, T., Mölder, M., Mastepanov, M., Sigsgaard, C., Tamstorf, M. P., Lund, M., Falk, J. M., Lindroth, A., Christensen, T. R., and Ström, L.: Land-atmosphere exchange of methane from soil thawing to soil freezing in a high-Arctic wet tundra ecosystem, *Glob. Change Biol.*, 18, 1928–1940, <https://doi.org/10.1111/j.1365-2486.2012.02647.x>, 2012.
- Taoka, T., Iwata, H., Hirata, R., Takahashi, Y., Miyabara, Y., and Itoh, M.: Environmental Controls on Diffusive and Ebullitive Methane Emission at a Sub-Daily Time Scale in the Littoral Zone of a Mid-Latitude Shallow Lake, *J. Geophys. Res.-Biogeo.*, 125, e2020JG005753, <https://doi.org/10.1029/2020JG005753>, 2020.
- Torn, M. and Dengel, S.: FLUXNET-CH₄ US-NGB NGEE Arctic Barrow, United States, FLUXNET-CH₄ Community Prod-

- uct [data set], <https://doi.org/10.18140/FLX/1669687>, 2020a.
- Torn, M. and Dengel, S.: FLUXNET-CH₄ US-NGC NGEE Arctic Council, United States, FLUXNET-CH₄ Community Product [data set], <https://doi.org/10.18140/FLX/1669688>, 2020b.
- Treat, C. C., Anthony Bloom, A., and Marushchak, M. E.: Non-growing season methane emissions—a significant component of annual emissions across northern ecosystems, *Glob. Change Biol.*, 24, 3331–3343, <https://doi.org/10.1111/gcb.14137>, 2018.
- Turetsky, M. R., Kotowska, A., Bubier, J., Dise, N. B., Crill, P., Hornibrook, E. R. C., Minkinen, K., Moore, T. R., Myers-Smith, I. H., Nykänen, H., Olefeldt, D., Rinne, J., Saarnio, S., Shurpali, N., Tuittila, E.-S., Waddington, J. M., White, J. R., Wickland, K. P., and Wilkening, M.: A synthesis of methane emissions from 71 northern, temperate, and subtropical wetlands, *Glob. Change Biol.*, 20, 2183–2197, <https://doi.org/10.1111/gcb.12580>, 2014.
- Ueyama, M., Hirano, T., and Kominami, Y.: FLUXNET-CH₄ JP-BBY Bibai bog, Japan, FLUXNET-CH₄ Community Product [data set], <https://doi.org/10.18140/FLX/1669646>, 2020.
- Valach, A., Szutu, D., Eichelmann, E., Knox, S., Verfaillie, J., and Baldocchi, D.: FLUXNET-CH₄ US-Tw1 Twitchell Wetland West Pond, United States, FLUXNET-CH₄ Community Product [data set], <https://doi.org/10.18140/FLX/1669696>, 2020a.
- Valach, A., Kasak, K., Szutu, D., Verfaillie, J., and Baldocchi, D.: FLUXNET-CH₄ US-Tw5 East Pond Wetland, United States, FLUXNET-CH₄ Community Product [data set], <https://doi.org/10.18140/FLX/1669699>, 2020b.
- Varlagin, A.: FLUXNET-CH₄ RU-Fy2 Fyodorovskoye dry spruce, Russian Federation, FLUXNET-CH₄ Community Product [data set], <https://doi.org/10.18140/FLX/1669657>, 2020.
- Vazquez-Lule, A. and Vargas, R.: FLUXNET-CH₄ US-StJ St Jones Reserve, United States, FLUXNET-CH₄ Community Product [data set], <https://doi.org/10.18140/FLX/1669695>, 2020.
- Vázquez-Lule, A. and Vargas, R.: Biophysical drivers of net ecosystem and methane exchange across phenological phases in a tidal salt marsh, *Agr. Forest Meteorol.*, 300, 108309, <https://doi.org/10.1016/j.agrformet.2020.108309>, 2021.
- Verma, S. B., Ullman, F. G., Billesbach, D., Clement, R. J., Kim, J., and Verry, E. S.: Eddy correlation measurements of methane flux in a northern peatland ecosystem, *Bound.-Lay. Meteorol.*, 58, 289–304, <https://doi.org/10.1007/BF02033829>, 1992.
- Vermote, E.: MOD09A1 MODIS Surface Reflectance 8-Day L3 Global 500m SIN Grid V006, NASA EOSDIS Land Processes DAAC [data set], <https://doi.org/10.5067/MODIS/MOD09A1.006> (Terra), 2015.
- Vesala, T., Tuittila, E.-S., Mammarella, I., and Alekseychik, P.: FLUXNET-CH₄ FI-Si2 Siikaneva-2 Bog, Finland, FLUXNET-CH₄ Community Product [data set], <https://doi.org/10.18140/FLX/1669639>, 2020a.
- Vesala, T., Tuittila, E.-S., Mammarella, I., and Rinne, J.: FLUXNET-CH₄ FI-Sii Siikaneva, Finland, FLUXNET-CH₄ Community Product [data set], <https://doi.org/10.18140/FLX/1669640>, 2020b.
- Villarreal, S., Guevara, M., Alcaraz-Segura, D., Brunzell, N. A., Hayes, D., Loescher, H. W., and Vargas, R.: Ecosystem functional diversity and the representativeness of environmental networks across the conterminous United States, *Agr. Forest Meteorol.*, 262, 423–433, <https://doi.org/10.1016/j.agrformet.2018.07.016>, 2018.
- Villarreal, S., Guevara, M., Alcaraz-Segura, D., and Vargas, R.: Optimizing an Environmental Observatory Network Design Using Publicly Available Data, *J. Geophys. Res.-Biogeo.*, 124, 1812–1826, <https://doi.org/10.1029/2018JG004714>, 2019.
- Vourlitis, G., Dalmagro, H., de Nogueira, J. S., Johnson, M., and Arruda, P. FLUXNET-CH₄ BR-Npw Northern Pantanal Wetland, Brazil, FLUXNET-CH₄ Community Product [data set], <https://doi.org/10.18140/FLX/1669368>, 2020.
- Vuichard, N. and Papale, D.: Filling the gaps in meteorological continuous data measured at FLUXNET sites with ERA-Interim reanalysis, *Earth Syst. Sci. Data*, 7, 157–171, <https://doi.org/10.5194/essd-7-157-2015>, 2015.
- Weston, N. B., Dixon, R. E., and Joye, S. B.: Ramifications of increased salinity in tidal freshwater sediments: Geochemistry and microbial pathways of organic matter mineralization, *J. Geophys. Res.*, 111, G01009, <https://doi.org/10.1029/2005jg000071>, 2006.
- Weston, N. B., Vile, M. A., Neubauer, S. C., and Velinsky, D. J.: Accelerated microbial organic matter mineralization following salt-water intrusion into tidal freshwater marsh soils, *Biogeochemistry*, 102, 135–151, <https://doi.org/10.1007/s10533-010-9427-4>, 2011.
- Wik, M., Crill, P. M., Varner, R. K., and Bastviken, D.: Multiyear measurements of ebullitive methane flux from three subarctic lakes, *J. Geophys. Res.-Biogeo.*, 118, 1307–1321, <https://doi.org/10.1002/jgrg.20103>, 2013.
- Windham-Myers, L., Stuart-Haëntjens, E., Bergamaschi, B., and Knox, S.: FLUXNET-CH₄ US-Srr Suisun marsh – Rush Ranch, United States, FLUXNET-CH₄ Community Product [data set], <https://doi.org/10.18140/FLX/1669694>, 2020.
- Windsor, J., Moore, T. R., and Roulet, N. T.: Episodic fluxes of methane from subarctic fens, *Can. J. Soil Sci.*, 72, 441–452, <https://doi.org/10.4141/cjss92-037>, 1992.
- Wohlfahrt, G.: FLUXNET-CH₄ AT-Neu Neustift, Austria, FLUXNET-CH₄ Community Product [data set], <https://doi.org/10.18140/FLX/1669365>, 2020.
- Wong, G. X., Melling, L., Tang, A. C. I. Aeries, E. B., Waili, J. W., Musin, K. K., Lo, K. S., and Kiew, F.: FLUXNET-CH₄ MY-MLM Maludam National Park, Malaysia, FLUXNET-CH₄ Community Product [data set], <https://doi.org/10.18140/FLX/1669650>, 2020.
- Wutzler, T., Lucas-Moffat, A., Migliavacca, M., Knauer, J., Sickel, K., Šigut, L., Menzer, O., and Reichstein, M.: Basic and extensible post-processing of eddy covariance flux data with REddyProc, *Biogeosciences*, 15, 5015–5030, <https://doi.org/10.5194/bg-15-5015-2018>, 2018.
- Xu, X., Riley, W. J., Koven, C. D., Billesbach, D. P., Chang, R. Y.-W., Commane, R., Euskirchen, E. S., Hartery, S., Harazono, Y., Iwata, H., McDonald, K. C., Miller, C. E., Oechel, W. C., Poulter, B., Raz-Yaseef, N., Sweeney, C., Torn, M., Wofsy, S. C., Zhang, Z., and Zona, D.: A multi-scale comparison of modeled and observed seasonal methane emissions in northern wetlands, *Biogeosciences*, 13, 5043–5056, <https://doi.org/10.5194/bg-13-5043-2016>, 2016.
- Yvon-Durocher, G., Allen, A. P., Bastviken, D., Conrad, R., Gudasz, C., St-Pierre, A., Thanh-Duc, N., and del Giorgio, P. A.: Methane fluxes show consistent temperature dependence

- across microbial to ecosystem scales, *Nature*, 507, 488–491, <https://doi.org/10.1038/nature13164>, 2014.
- Zhang, Z., Fluet-Choinard, E., Jensen, K., McDonald, K., Hugelius, G., Gumbrecht, T., Carrol, M., Prigent, C., Bartsch, A., and Poulter, B.: Development of a global dataset of Wetland Area and Dynamics for Methane Modeling (WAD2M), Zenodo [data set], <https://doi.org/10.5281/zenodo.3998454>, 2020.
- Zhang, Z., Fluet-Chouinard, E., Jensen, K., McDonald, K., Hugelius, G., Gumbrecht, T., Carroll, M., Prigent, C., Bartsch, A., and Poulter, B.: Development of the global dataset of Wetland Area and Dynamics for Methane Modeling (WAD2M), *Earth Syst. Sci. Data*, 13, 2001–2023, <https://doi.org/10.5194/essd-13-2001-2021>, 2021.
- Zona, D. and Oechel, W. C.: FLUXNET-CH₄ US-Atq Atqasuk, United States, FLUXNET-CH₄ Community Product [data set], <https://doi.org/10.18140/FLX/1669663>, 2020a.
- Zona, D. and Oechel, W. C.: FLUXNET-CH₄ US-Beo Barrow Environmental Observatory (BEO) tower, United States, FLUXNET-CH₄ Community Product [data set], <https://doi.org/10.18140/FLX/1669664>, 2020b.
- Zona, D. and Oechel, W. C.: FLUXNET-CH₄ US-Bes Barrow-Bes (Biocomplexity Experiment South tower), United States, FLUXNET-CH₄ Community Product [data set], <https://doi.org/10.18140/FLX/1669665>, 2020c.
- Zona, D. and Oechel, W. C.: FLUXNET-CH₄ US-Ivo Ivotuk, United States, FLUXNET-CH₄ Community Product [data set], <https://doi.org/10.18140/FLX/1669679>, 2020d.
- Zona, D., Gioli, B., Commane, R., Lindaas, J., Wofsy, S. C., Miller, C. E., Dinardo, S. J., Dengel, S., Sweeney, C., Karion, A., Chang, R. Y.-W., Henderson, J. M., Murphy, P. C., Goodrich, J. P., Moreaux, V., Liljedahl, A., Watts, J. D., Kimball, J. S., Lipson, D. A., and Oechel, W. C.: Cold season emissions dominate the Arctic tundra methane budget, *P. Natl. Acad. Sci. USA*, 113, 40–45, <https://doi.org/10.1073/pnas.1516017113>, 2016.